NASA TECHNICAL NOTE

NASA TN D-3438

LONGITUDINAL STABILITY AND CONTROL CHARACTERISTICS OF A POWERED MODEL OF A TWIN-PROPELLER DEFLECTED-SLIPSTREAM STOL AIRPLANE CONFIGURATION

by Richard J. Margason, Alexander D. Hammond, and Garl L. Gentry

Langley Research Center
Langley Station, Hampton, Va.

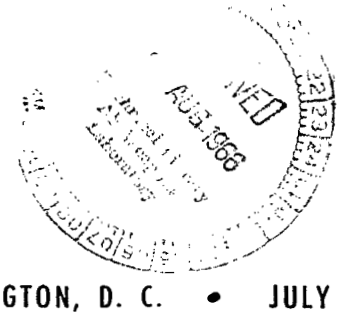

NATIONAL AERONAUTICS AND SPACE ADMINISTRATION • WASHINGTON, D. C. • JULY 1966

LONGITUDINAL STABILITY AND CONTROL CHARACTERISTICS OF A POWERED MODEL OF A TWIN-PROPELLER DEFLECTED-SLIPSTREAM STOL AIRPLANE CONFIGURATION

By Richard J. Margason, Alexander D. Hammond, and Garl L. Gentry

Langley Research Center
Langley Station, Hampton, Va.

NATIONAL AERONAUTICS AND SPACE ADMINISTRATION

For sale by the Clearinghouse for Federal Scientific and Technical Information
Springfield, Virginia 22151 – Price $4.00

LONGITUDINAL STABILITY AND CONTROL CHARACTERISTICS OF A POWERED MODEL OF A TWIN-PROPELLER DEFLECTED-SLIPSTREAM STOL AIRPLANE CONFIGURATION

By Richard J. Margason, Alexander D. Hammond,
and Garl L. Gentry
Langley Research Center

SUMMARY

Results are presented of a wind-tunnel investigation of the static longitudinal stability and control capabilities of a twin-propeller deflected-slipstream STOL airplane in the take-off and landing speed range through the post-stall region at angles of attack up to 44°.

The results of this investigation show that the magnitudes of the pitching moments of the wing-body combination for the flaps-retracted (0° flap deflection) configuration were small. The tail-on data show that any of the tail configurations with the flaps-retracted configuration provide an adequate stability contribution and are capable of trimming the airplane. The wing-body combination for the flaps-deflected (45° flap deflection) configuration had a large tail lift requirement for longitudinal trim, particularly for the highest power setting of the investigation. The small tail in the high position had the capability of trimming the airplane for the low power conditions (thrust coefficients of 0 and 0.70). At higher power conditions the tail stalled before trim was achieved. The large tail in either position had the capability of trimming the airplane up to the angle of attack corresponding to the maximum lift coefficient for all but the highest power condition (thrust coefficient of 2.42). This tail stalled before trim was achieved for the highest power condition.

INTRODUCTION

Recent interest in developing a small deflected-slipstream short take-off and landing (STOL) airplane has led to a need for stability and control data on this type of configuration. A static wind-tunnel investigation of a powered model of a twin-propeller deflected-slipstream STOL aircraft configuration was conducted to provide some of this information. The lateral control characteristics of this model have been presented in reference 1. The longitudinal stability and control characteristics are presented in the present report. This investigation was undertaken to determine the longitudinal stability and control characteristics through the angle-of-attack range from -4° into the post-stall region (to 44°).

The investigation was conducted in the 17-foot (5.18 meter) test section of the Langley 300-MPH 7- by 10-foot tunnel and covered two flap deflections and several power conditions.

SYMBOLS

The units used for the physical quantities defined in this paper are given both in the U.S. Customary Units and in the International System of Units (SI). Factors relating these two systems of units are presented in reference 2. The symbols used are defined as follows:

c wing chord, 1.29 feet (0.39 meter)

C_D drag coefficient, $\frac{\text{Drag}}{qS}$

C_L lift coefficient, $\frac{\text{Lift}}{qS}$

$C_{L,max}$ maximum trimmed lift coefficient

C_{L_α} lift-curve slope, per degree

C_m pitching-moment coefficient referred to model moment center at wing quarter-chord (c/4), $\frac{\text{Pitching moment}}{qSc}$ (see fig. 1)

C_T propeller thrust coefficient based on free-stream velocity and wing area, $\frac{T}{qS}$ (often designated in literature as T_c)

$C_{T,s}$ propeller thrust coefficient based on slipstream velocity and propeller disk area, $\frac{T}{q_s N S_p}$

D propeller diameter, feet (meters)

h_t height of the horizontal-tail chord above the wing chord, feet (meters)

i_t tail incidence, degrees

l_t tail length measured horizontally from the wing quarter-chord to the horizontal-tail quarter-chord, feet (meters)

N number of propellers

q dynamic pressure, $\frac{\rho}{2}V^2$, pounds/foot^2 (newtons/meter^2)

q_s slipstream dynamic pressure, $q + \frac{T}{NS_p}$, pounds/foot^2 (newtons/meter^2)

S_p propeller disk area, $\frac{\pi D^2}{4}$, foot^2 (meter^2)

S_t tail area, foot^2 (meter^2)

S_w wing area, 9.04 foot^2 (0.84 meter^2)

T total propeller thrust, pounds (newtons)

V free-stream velocity, feet/second (meters/second)

V_H nondimensional horizontal-tail volume, $\frac{S_t}{S_w}\frac{l_t}{c}$

x distance measured along airfoil chord line from the leading edge, feet (meters)

y_l distance measured perpendicular from airfoil chord line to airfoil lower surface, feet (meters)

y_u distance measured perpendicular from airfoil chord line to airfoil upper surface, feet (meters)

α angle of attack, degrees

δ deflection of movable surface (with subscript to denote surface deflected), degrees

ϵ downwash angle at the horizontal tail, degrees

ϵ_o downwash angle at the horizontal tail when wing angle of attack is zero, degrees

ρ air density, slugs/foot^3 (kilogram/meter^3)

Subscripts:

f flap (see fig. 3)

t tail

v vane (see fig. 3)

MODEL AND APPARATUS

A three-view drawing of the model is presented in figure 1 and photographs are presented in figure 2. The wing had an NACA 4415 airfoil section, a 15.50-inch (0.39 meter) chord, was unswept, and had a span of 7.00 feet (2.13 meters) with an aspect ratio of 5.42. The wing contour was formed with faired wooden blocks fastened to a metal spar which supported the two motor nacelles and the fuselage strongback as well as the brackets which held the flap system.

The double-slotted high-lift flap system consisted of a 20-percent-wing-chord vane with a St. Cyr 156 airfoil section and a 40-percent-wing-chord flap with a modified Rhode St. Genese 35 airfoil section over the forward 30 percent of its chord faired into the wing airfoil section over the rear 70 percent of its chord. The flap and vane ordinates, as well as the flap and vane positions when deflected, are given in figure 3.

Two different horizontal tails were tested. Both had an aspect ratio of 3.13 and an NACA 4415 airfoil section whose profile was modified to give a 9 percent maximum thickness and were mounted inverted to provide an inverse camber. The two tails had different areas, spans, and chords. (See fig. 1.) The small tail was tested in a high position (h_t = 0.94c) only; the large tail was tested in both the high and the low position (h_t = 0.15c). Both tail positions were above the wing-chord plane. For the tail configurations tested, the nondimensional horizontal-tail volumes V_H are the following: small tail in the high position, 0.85; large tail in the high position, 1.15; large tail in the low position, 1.04. Additional data on the geometric characteristics are also presented in figure 1.

Since no directional stability tests were included in the investigation, the vertical tail served only as a support for the horizontal tail. The vertical surface consisted of a sheet of 1/2-inch (1.27 centimeters) aluminum with a rounded leading edge and a beveled trailing edge.

The three-blade propellers were made of balsa covered with glass-fiber cloth and were driven by water-cooled variable-frequency electric motors operated in parallel from a variable-frequency power supply, which kept the motor speeds matched within 20 revolutions per minute. The speed of rotation of each propeller was determined by a stroboscopic indicator which received the output frequency of small alternators connected to each motor shaft. For all the tests the right propeller rotated in a clockwise direction and the left propeller rotated in a counterclockwise direction when viewed from the rear of the model. During the tests the speed of rotation was maintained at 6000 rpm. The thrust coefficient was varied by changing the wind-tunnel speed.

The motors were mounted inside aluminum-alloy nacelles by means of strain-gage beams so that the propeller thrust could be measured. The total lift, longitudinal force, pitching moment, rolling moment, yawing moment, and side force were measured by a strain-gage balance mounted to the fuselage at the wing quarter-chord. Only longitudinal components of the data are presented in

this report. The results of lateral control tests of this model are presented in reference 1.

TESTS AND CORRECTIONS

The investigation was made in the 17-foot (5.18 meter) test section of the Langley 300-MPH 7- by 10-foot tunnel. For the powered tests the free-stream dynamic pressure was varied from about 1.5 to 5.3 pounds/foot^2 (72 to 254 newtons/meter^2), depending on the desired thrust coefficient. The slipstream dynamic pressure was relatively constant at about 7.5 pounds/foot^2 (359 newtons/meter^2) for all thrust coefficients. A free-stream dynamic pressure of about 6.0 pounds/foot^2 (287 newtons/meter^2) was used for the propeller-off tests. For the powered tests the Reynolds number, based on wing chord, of the flow in the slipstream averaged about 0.65×10^6; for the propeller-off tests the Reynolds number in the free stream averaged about 0.58×10^6. Since errors due to blockage, slipstream contraction, and tunnel-wall effects have been found to be small for models of this size in the 17-foot test section (ref. 3), no corrections for these types of error have been applied to the data.

The propeller thrust data have been presented as the conventional thrust coefficient, that is, thrust nondimensionalized by free-stream dynamic pressure times wing area $(C_T = T/qS)$. In all cases a thrust coefficient of zero was obtained by removing the propellers from the model. For the propeller-on data the thrust was measured by strain-gage beams at the motors. The thrust coefficients based on these measurements are presented with the basic data. Although the motor rotation speed was held constant, the thrust increased as the angle of attack of the model increased; as a result, the thrust coefficients are not constant for a particular test. For convenience the average values of thrust coefficients near zero angle of attack for the data presented in this report (used as reference values throughout the report) are listed in the following table:

δ_f, deg	Reference value of -	
	$C_{T,s}$	C_T
0	0	0
	.20	.17
	.39	.44
45	0	0
	.50	.70
	.64	1.25
	.78	2.42

It is often desirable to use the propeller thrust coefficient based on slipstream velocity and propeller disk area. Figure 4 is a plot of the relation between these two thrust coefficients for the model tested.

RESULTS AND DISCUSSION

The results of a wind-tunnel investigation of the longitudinal control and stability characteristics of a model of a twin-propeller deflected-slipstream STOL airplane are presented in the following figures:

Basic Data

The basic data figures present the variation of the lift and pitching-moment coefficients with angle of attack and the variation of drag and pitching-moment coefficients with lift coefficient. In addition, the variation of thrust coefficient with angle of attack is presented for the propeller-on tests. The pitching-moment coefficients for all the data are presented about the wing quarter-chord line. The angle of attack used in this investigation ranged from -4° to 44°.

The basic data for the configuration with the horizontal tail off are presented in figure 5 for the flaps-retracted ($\delta_f = 0^\circ$) configuration and in figure 15 for the flaps-deflected ($\delta_f = 45^\circ$) configuration. The lift-curve slope C_{L_α} as well as the maximum lift increases with increasing power. The following table gives a summary of the lift-curve slope and of the maximum lift coefficients (model with the horizontal tail off) for both of the flap deflections:

δ_f, deg	C_T	$C_{L,max}$	C_{L_α}
0	0	1.12	0.067
	.17	1.83	.075
	.44	2.11	.085
45	0	2.47	0.068
	.70	4.40	.107
	1.25	5.35	.130
	2.42	6.48	.150

The tail-off pitching moments for the flaps-retracted ($\delta_f = 0^\circ$) configuration are unstable for angles of attack up to wing stall and are generally neutral beyond that angle of attack (fig. 5). The small magnitude of the pitching moments for this configuration shows that the horizontal tail is required mainly to provide stability for the flaps-retracted ($\delta_f = 0^\circ$) configurations. The tail-on data (figs. 6 to 14) show that any of the tail configurations tested with the flaps-retracted configuration provide an adequate stability contribution and, in addition, are capable of trimming the airplane throughout the lift-coefficient range of the investigation.

In contrast to the flaps-retracted ($\delta_f = 0^\circ$) configuration, the flaps-deflected ($\delta_f = 45^\circ$) configuration requires a large increment of pitching moment for trim. The tail-off data of figure 15 show that nose-up increments of pitching-moment coefficient ranging from approximately 0.5 to 1.1 are needed, depending on the power condition; therefore, a large down load is required at the tail position. In order to satisfy this requirement, a normal-force coefficient as large as -0.95 must be developed by the large horizontal tail in the high position, assuming no loss in dynamic pressure at the tail. This value approaches the maximum normal-force coefficient for this tail. The requirement for tail normal-force coefficient is even more severe for the other two tail configurations tested because of their smaller tail volumes.

The data for the flaps-deflected ($\delta_f = 45^\circ$) configuration with each of the several horizontal tails are presented in figures 16 to 27. The configuration with the small tail in the high position (figs. 16 to 19) is stable (at $C_T = 0$, $\partial C_m/\partial C_L = -0.32$) and can be trimmed at low power settings ($C_T = 0$ and $C_T = 0.70$) through the angle of attack for wing stall. Some tail stall is present at low angles of attack for the tail incidence of -10.4°. At higher power settings ($C_T = 1.25$ and $C_T = 2.42$) the tail is beginning to stall at more positive tail incidences. When $C_T = 2.42$, the tail with an incidence of -10.4° is completely stalled. The configuration can no longer be stably trimmed for any of the tail incidences used for these tests with the center-of-gravity position corresponding to the wing quarter-chord.

The data for the flaps-deflected configuration with the large tail in the high position (figs. 20 to 23) are similar to those for the configuration with the small tail but with a larger trim increment due to the additional area. At $C_T = 1.25$ the model is trimmed at an angle of attack of 8° with the tail

incidence of -5.5° but the stability is reduced from that with more positive tail incidences. This indicates that the tail is partially stalled at this incidence. The tail with an incidence of -10.4° is completely stalled in the low range of angle of attack. At $C_T = 2.42$ the model is not trimmed below the angle of attack for wing stall.

The large tail in the low position (figs. 24 to 27) will trim the flap-deflected model for all but the highest power setting $(C_T = 2.42)$. This tail, however, is in a higher field of downwash and is stalled for more of the tail incidences than it is in the high position.

Downwash Analysis

The data for all the configurations tested were analyzed to determine the downwash angle and the dynamic pressure at the horizontal tail. For the cases where both the wing and the tail are unstalled it was possible to obtain the variation of downwash angle $(\epsilon_o$ and $\partial\epsilon/\partial\alpha)$ and an average value of q/q_t over the range of angles of attack where the variation of the parameters with angle of attack is linear. These results are shown in the following table for all the tail configurations tested with the flaps-retracted $(\delta_f = 0°)$ configuration.

Horizontal-tail configuration	C_T	ϵ_o, deg	$\partial\epsilon/\partial\alpha$	q/q_t
Small tail, high position	0	1.02	0.29	1.16
	.17	1.05	.33	1.16
	.44	1.09	.34	1.15
Large tail, high position	0	0.60	0.28	1.18
	.17	.65	.30	1.19
	.44	.80	.34	1.19
Large tail, low position	0	1.06	0.28	1.33
	.17	1.10	.48	1.24
	.44	1.58	.56	1.11

For the configurations with the flaps deflected to 45° it was not possible to determine corresponding information for the highest power setting $(C_T = 2.25)$ or for the large tail in the low position because the tail was stalled for most of the tail incidences used in these tests. The results for the other tail configurations are as follows:

Horizontal-tail configuration	C_T	ϵ_o, deg	$\partial\epsilon/\partial\alpha$	q/q_t
Small tail, high position	0	5.66	0.37	1.08
	.70	8.30	.63	1.10
	1.25	9.28	.74	1.16
Large tail, high position	0	5.67	0.39	1.17
	.70	7.55	.66	1.17
	1.25	8.37	.78	1.16

Effect of Tail Area

The effect of tail area on a stability contribution for the tail at 0° incidence in the high position is presented in figure 28 for $\delta_f = 0°$ and in figure 29 for $\delta_f = 45°$. Over the entire range of angle of attack for the flaps-retracted $(\delta_f = 0°)$ configuration, the data for the large tail show the expected increase in the tail contribution to stability due to the additional area. However, the wing angle of attack for zero lift on the tail is different for each tail because the average downwash angle is different. The data for the flaps-deflected $(\delta_f = 45°)$ configuration are similar to those for the flaps-retracted $(\delta_f = 0°)$ configuration up to the wing angle of attack corresponding to zero tail lift for all but the highest power setting. Beyond this wing angle of attack the tail lift becomes nonlinear for both horizontal tail areas.

When the flaps are retracted $(\delta_f = 0°)$ both horizontal tails are capable of trimming the model up to the angle of attack of wing stall for the thrust coefficients of the tests. As shown in the basic data, the flaps-deflected $(\delta_f = 45°)$ configuration presents a trim problem. The effect of tail area on the maximum trimmed lift coefficient is presented in figure 30 as a function of thrust coefficient. This figure shows the increased trim capability of the large tail due to the additional area. The data for the small tail in the high position are based on the same moment center, 0.25c, as the rest of the data in this report. The data for the large tail have the moment center adjusted to 0.31c so that the static stability at zero thrust coefficient is the same $(C_m/C_L = 0.36)$ as that for the small tail. Also presented as the dashed curve in figure 30 is the maximum attainable lift coefficient for the tail-off configuration. Comparison of this curve with the maximum-trimmed-lift-coefficient curves for the two tails indicates that the small tail is capable of trimming up to the maximum attainable lift coefficient (tail-off values of $C_{L,max}$) for thrust coefficients approaching 0.70 and that the large tail is adequate for thrust coefficients up to 1.25. Neither of the tails is adequate in size to trim the airplane up to the maximum attainable lift coefficients (tail off) at the highest thrust coefficient $(C_T = 2.42)$.

Effect of Tail Height

The effect of tail height for the large tail at zero incidence is presented in figure 31 for $\delta_f = 0^\circ$ and in figure 32 for $\delta_f = 45^\circ$. For the flaps-retracted $(\delta_f = 0^\circ)$ configuration the results with the tail in the two positions are generally similar. The tail in the high position generally produces a greater change of pitching moment with change of angle of attack than it does in the low position. For the flaps-deflected $(\delta_f = 45^\circ)$ configuration (fig. 32) the tail in the low position produces a larger increment of pitching moment. At the highest thrust coefficient $(C_T = 2.42)$ the tail in the low position is stalled throughout the angle-of-attack range and the tail in the high position is stalled above 8° angle of attack. The model with the tail in the high position shows a tendency to pitch up at low power settings at angles of attack above about 20°.

CONCLUSIONS

The results of a wind-tunnel investigation of the static longitudinal stability and control characteristics of a model of a twin-propeller deflected-slipstream STOL airplane configuration indicate the following conclusions:

1. The magnitudes of the pitching moments of the wing-body combination for the flaps-retracted (0° flap deflection) configuration were small. The tail-on data show that any of the tail configurations with the flaps-retracted configuration provide adequate stability contribution and are capable of trimming the airplane.

2. The wing-body combination for the flaps-deflected (flap deflection 45°) configuration had a large tail lift requirement for longitudinal trim, particularly for the highest power setting of the investigation.

3. The small tail in the high position had the capability of trimming the airplane for the low power conditions (thrust coefficients of 0 and 0.70). At higher power conditions the tail stalled before trim was achieved.

4. The large tail in either position had the capability of trimming the airplane up to the angle of attack corresponding to the maximum lift coefficient for all but the highest power condition (thrust coefficient 2.42). This tail stalled before trim was achieved for the highest power condition.

Langley Research Center,
National Aeronautics and Space Administration,
Langley Station, Hampton, Va., February 16, 1966.

REFERENCES

1. Margason, Richard J.; and Hammond, Alexander D.: Lateral Control Characteristics of a Powered Model of a Twin-Propeller Deflected Slipstream STOL Airplane Configuration. NASA TN D-1585, 1964.

2. Mechtly, E. A.: The International System of Units - Physical Constants and Conversion Factors. NASA SP-7012, 1964.

3. Staff of Powered-Lift Aerodynamics Section, NASA Langley Res. Center: Wall Effects and Scale Effects in V/STOL Model Testing. AIAA Aerodynamic Testing Conf., Mar. 1964, pp. 8-16.

Wing:			
Airfoil section			NACA 4415
Chord, ft (m)			1.29 (.39)
Area, ft^2 (m^2)			9.04 (.84)
Span, ft (m)			7.00 (2.13)
Aspect ratio			5.42
Horizontal tail		Large tail	Small tail
Area, ft^2 (m^2)		3.86 (.36)	2.88 (.27)
Span, ft (m)		3.48 (1.06)	3.00 (.91)
Chord, ft (m)		1.11 (.34)	.96 (.29)
Aspect ratio		3.13	3.13
l_t/wing chord	High position	2.70	2.67
	Low position	2.44	2.41
h_t/wing chord	High position	.94	.94
	Low position	.15	.15
Propellers:			
Diameter, ft (m)			2.00 (.61)
Nacelle diameter, ft (m)			.33 (.10)
Number of blades (each)			3

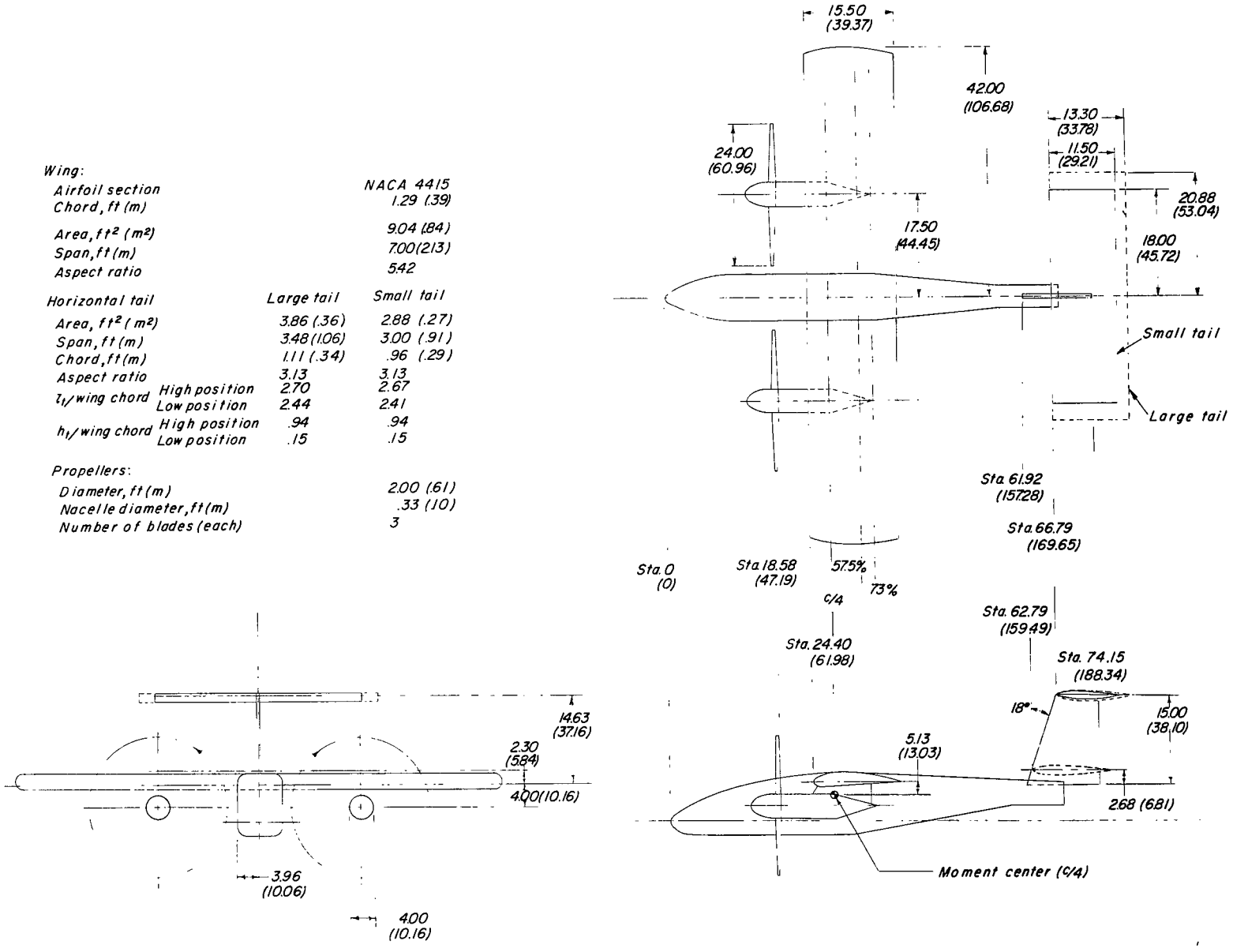

Figure 1.- Three-view drawing of 1/5-scale model and table of geometric characteristics. All dimensions are in inches (centimeters) unless otherwise noted.

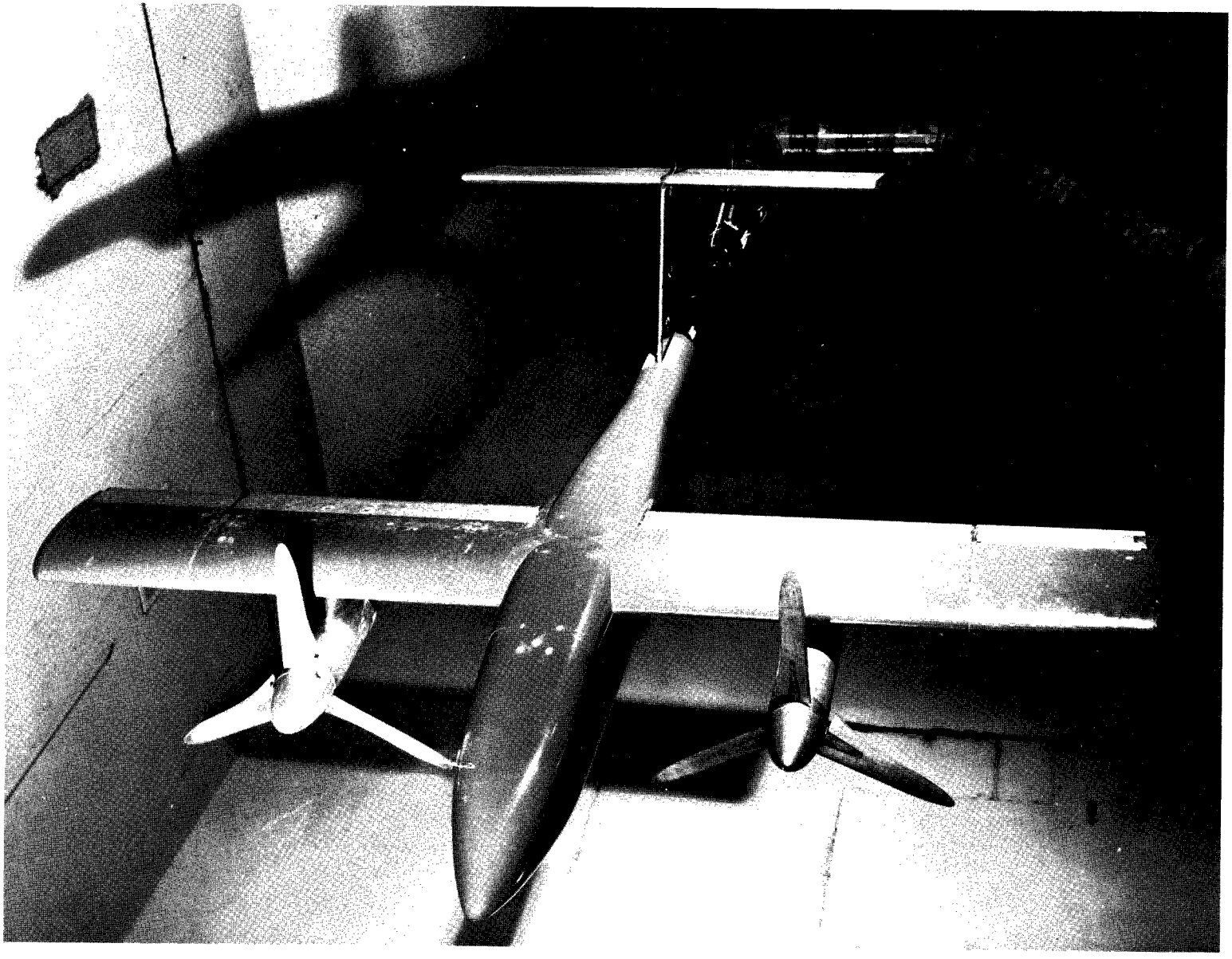

(a) Top quarter front view.

L-63-9676

Figure 2.- Model in wind tunnel.

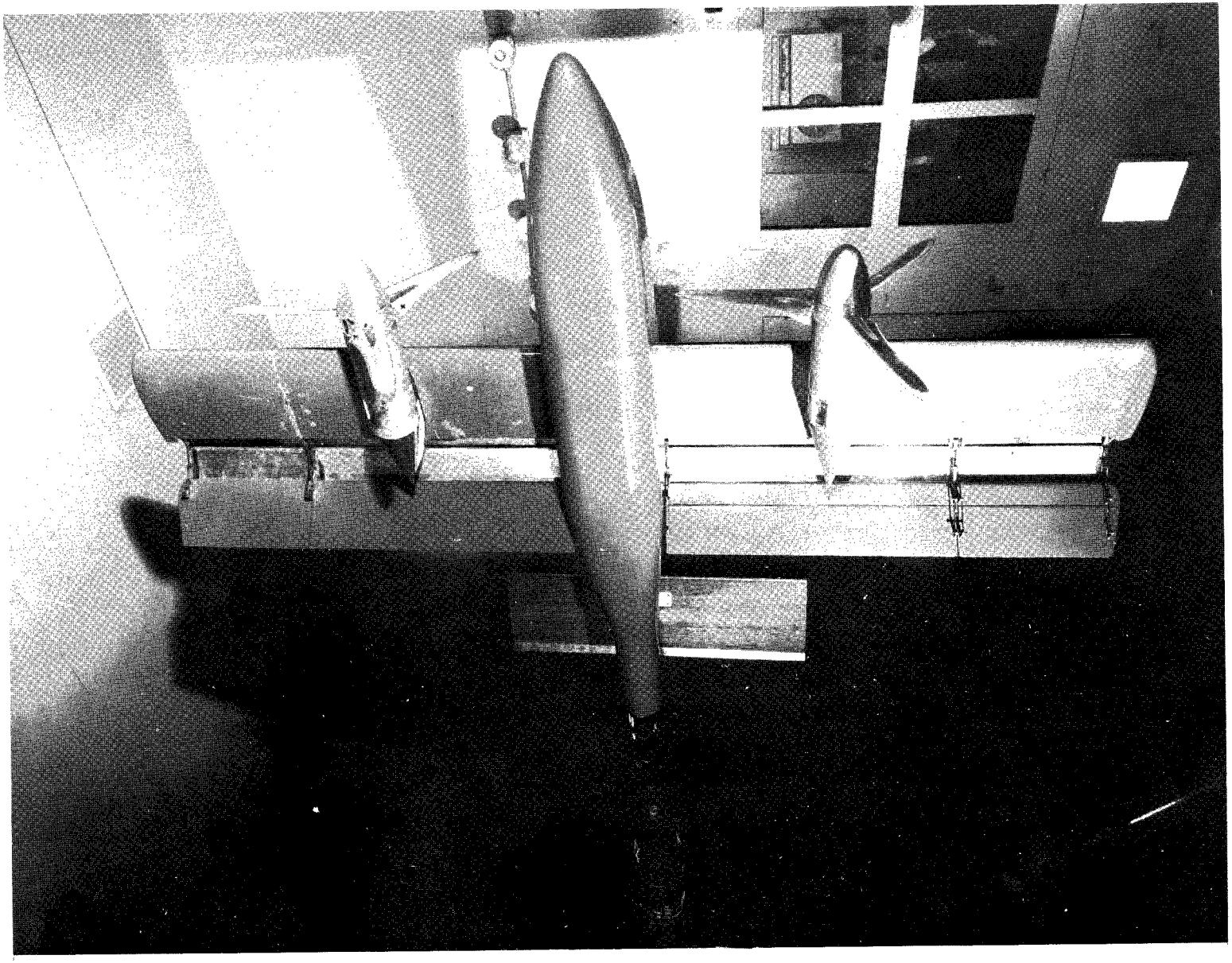

(b) Lower quarter front view. L-63-9677

Figure 2.- Concluded.

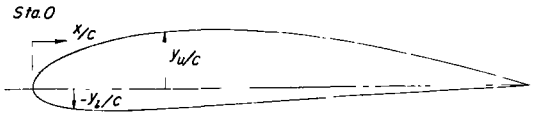

(a) Plain wing (NACA 4415 airfoil).

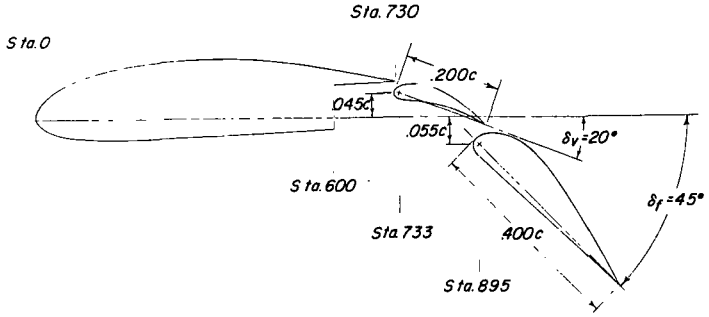

(b) Flap deflected 45°

VANE ORDINATES ST. CYR 156 SECTION		
x/c	y_u/c	y_l/c
0	0	0
.0125	.0381	-.0268
.0250	.0522	-.0339
.0500	.0739	-.0409
.0750	.0905	-.0446
.1000	.1039	-.0448
.1500	.1269	-.0409
.2000	.1440	-.0300
.3000	.1630	-.0140
.4000	.1660	.0010
.5000	.1600	.0180
.6000	.1440	.0300
.7000	.1170	.0320
.8000	.0830	.0300
.9000	.0484	.0180
.9500	.0274	.0107
1.0000	.0065	0

FLAP ORDINATES		
x/c	y_u/c	y_l/c
0	0	0
.0125	.0460	-.0290
.0250	.0645	-.0387
.0500	.0919	-.0435
.0750	.1145	-.0460
.1000	.1306	-.0468
.1500	.1516	-.0444
.2000	.1621	-.0420
.3000	.1677	-.0373
.4275	.1532	-.0312
.5000	.1387	-.0278
.6275	.1065	-.0217
.7500	.0769	-.0159
.8750	.0435	-.0100
1.0000	.0040	-.0040

Figure 3.- Geometric characteristics of wing section and flap deflection. All dimensions given in fraction of wing chord unless otherwise noted.

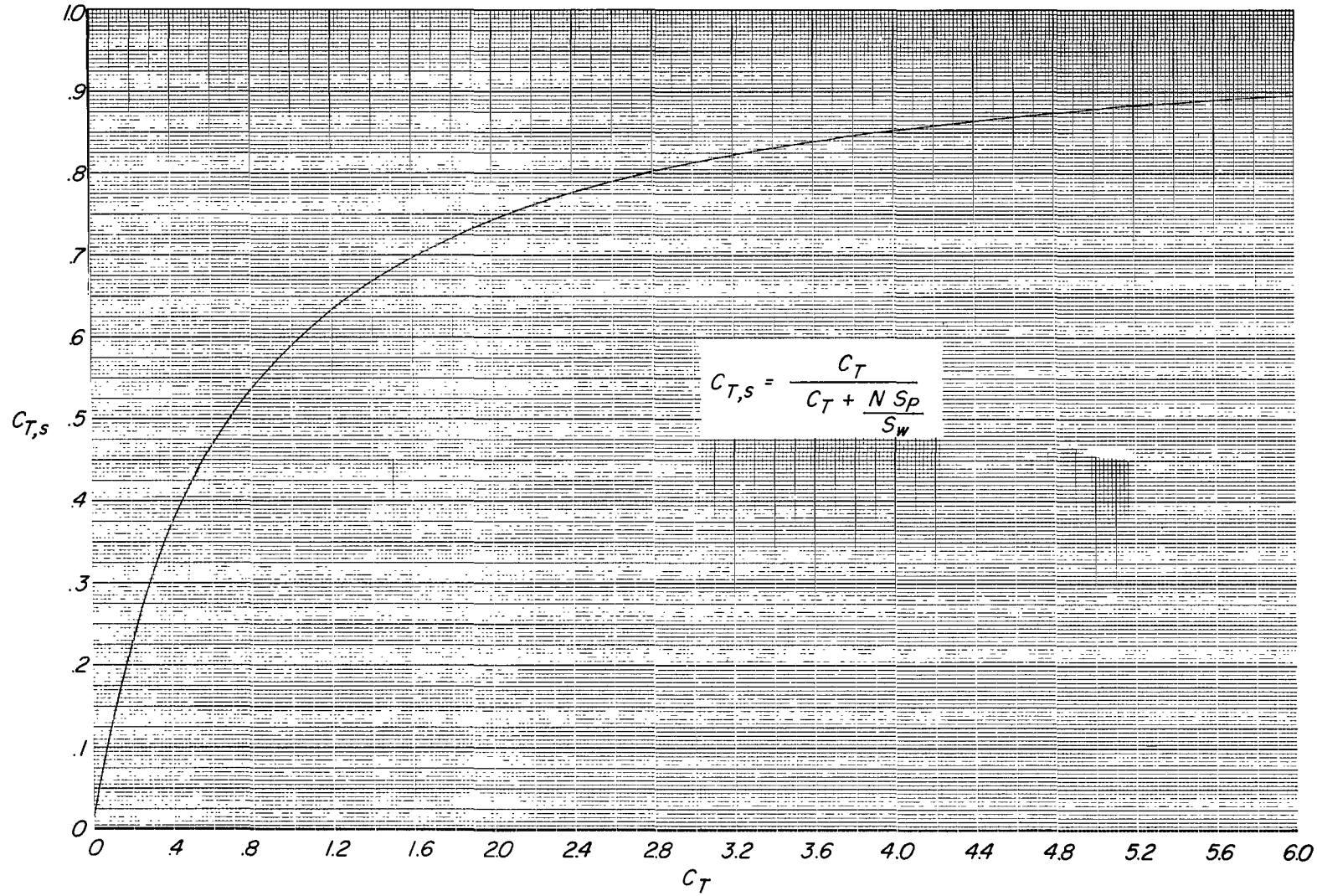

Figure 4.- Slipstream thrust coefficient plotted as a function of free-stream thrust coefficient.

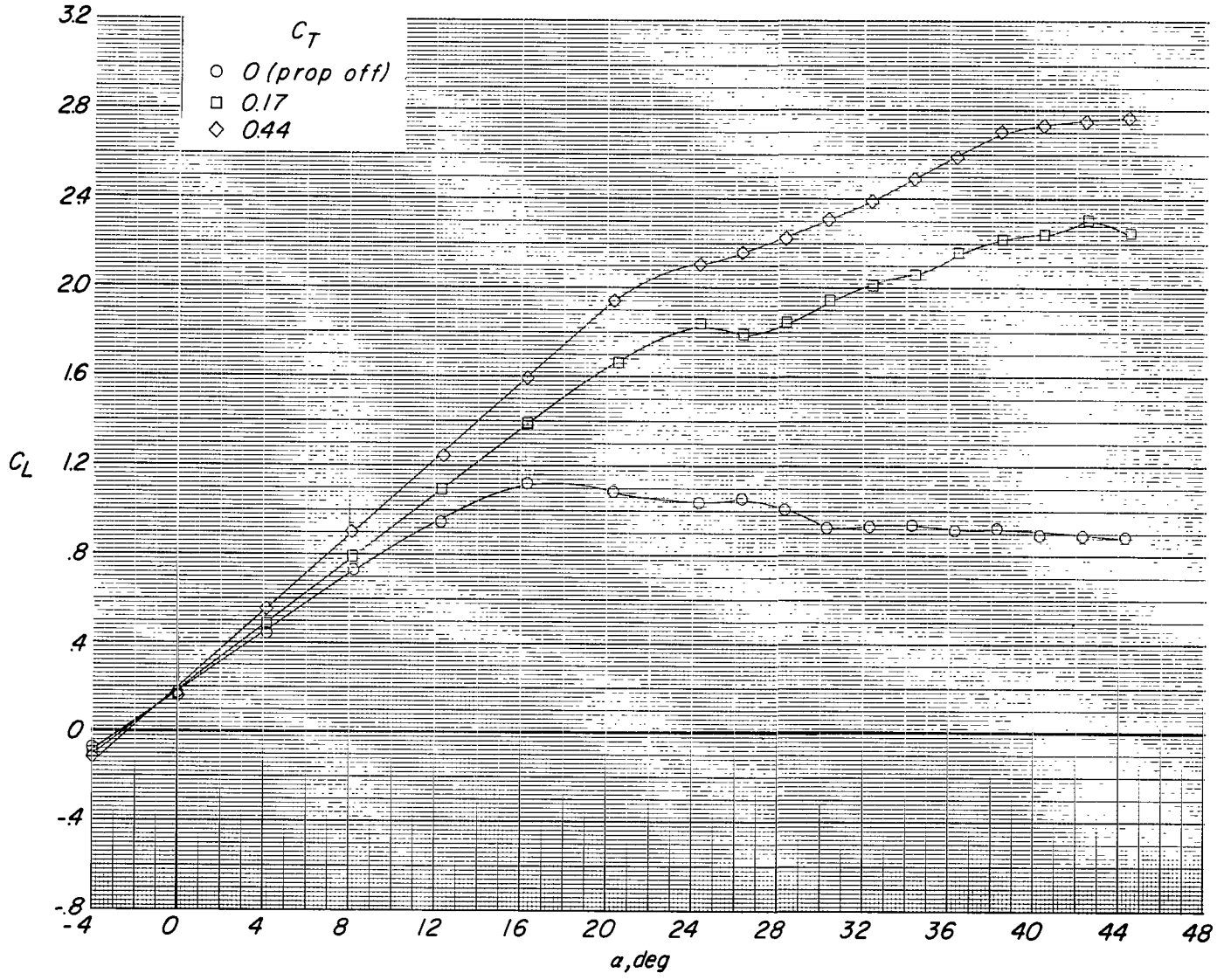

(a) Variation of C_L with α.

Figure 5.- Effect of propeller thrust coefficient (in terms of reference C_T) on longitudinal aerodynamic characteristics of flaps-retracted ($\delta_f = 0^0$) configuration with tail off.

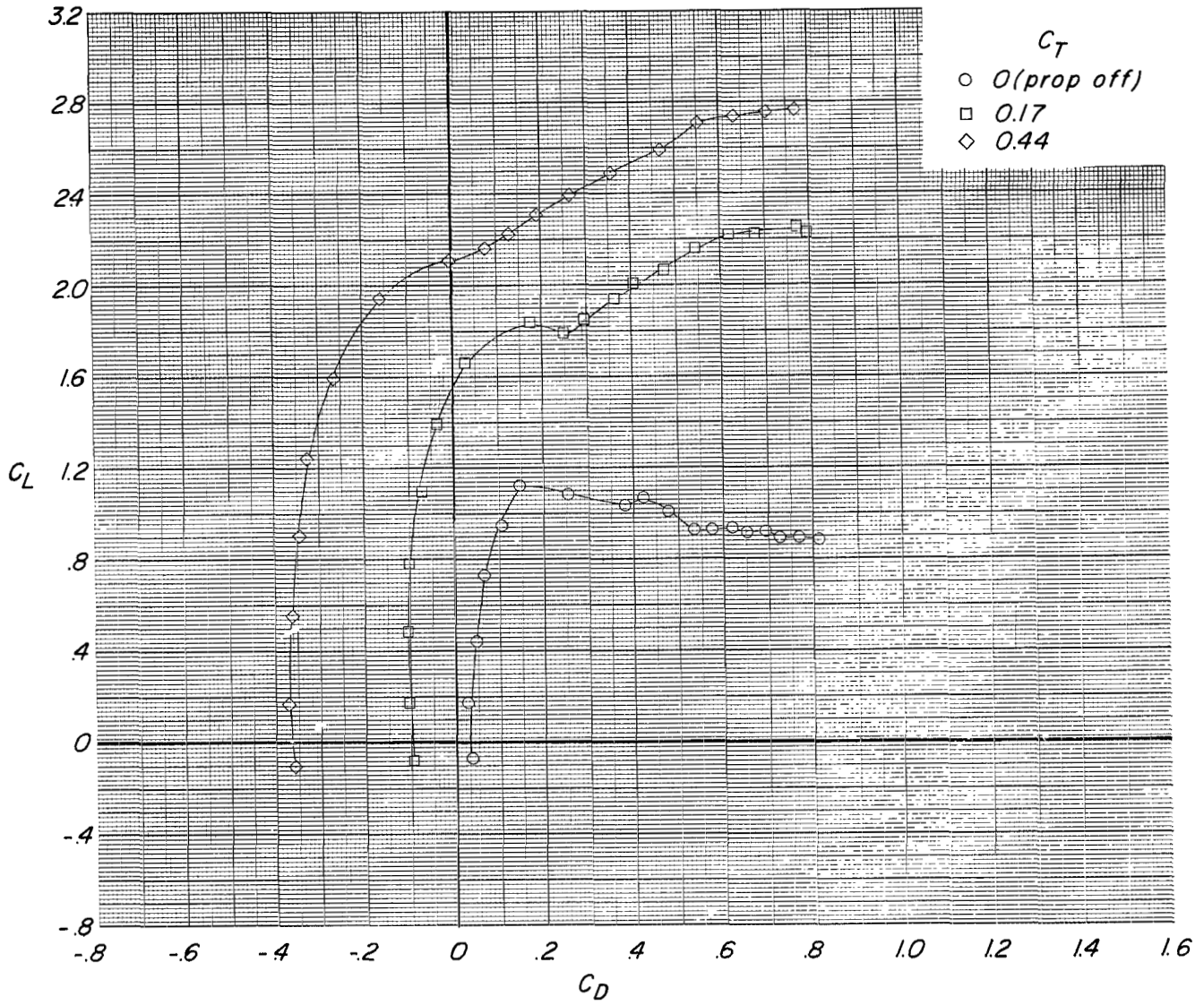

(b) Variation of C_L with C_D.

Figure 5.- Continued.

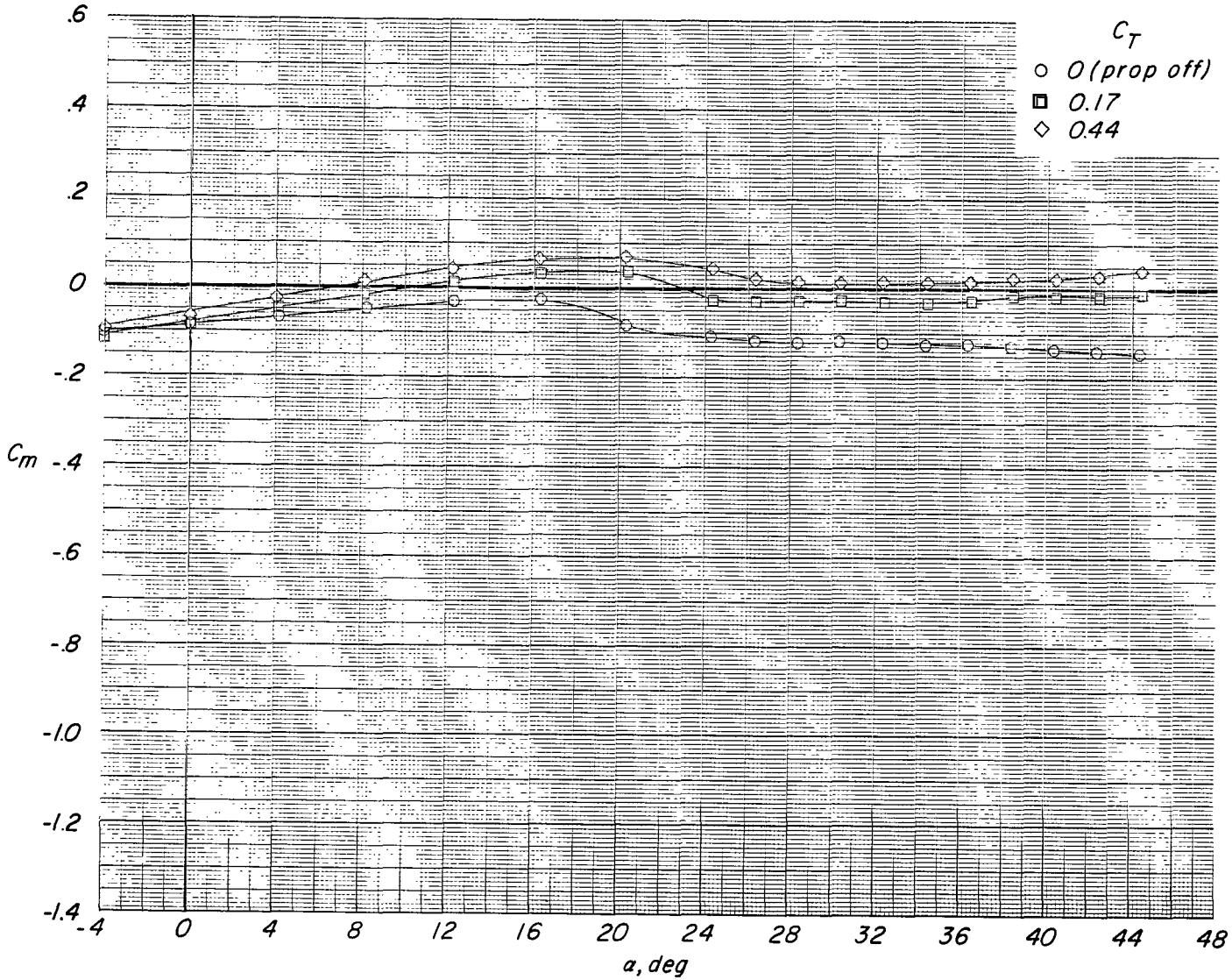

(c) Variation of C_m with α.

Figure 5.- Continued.

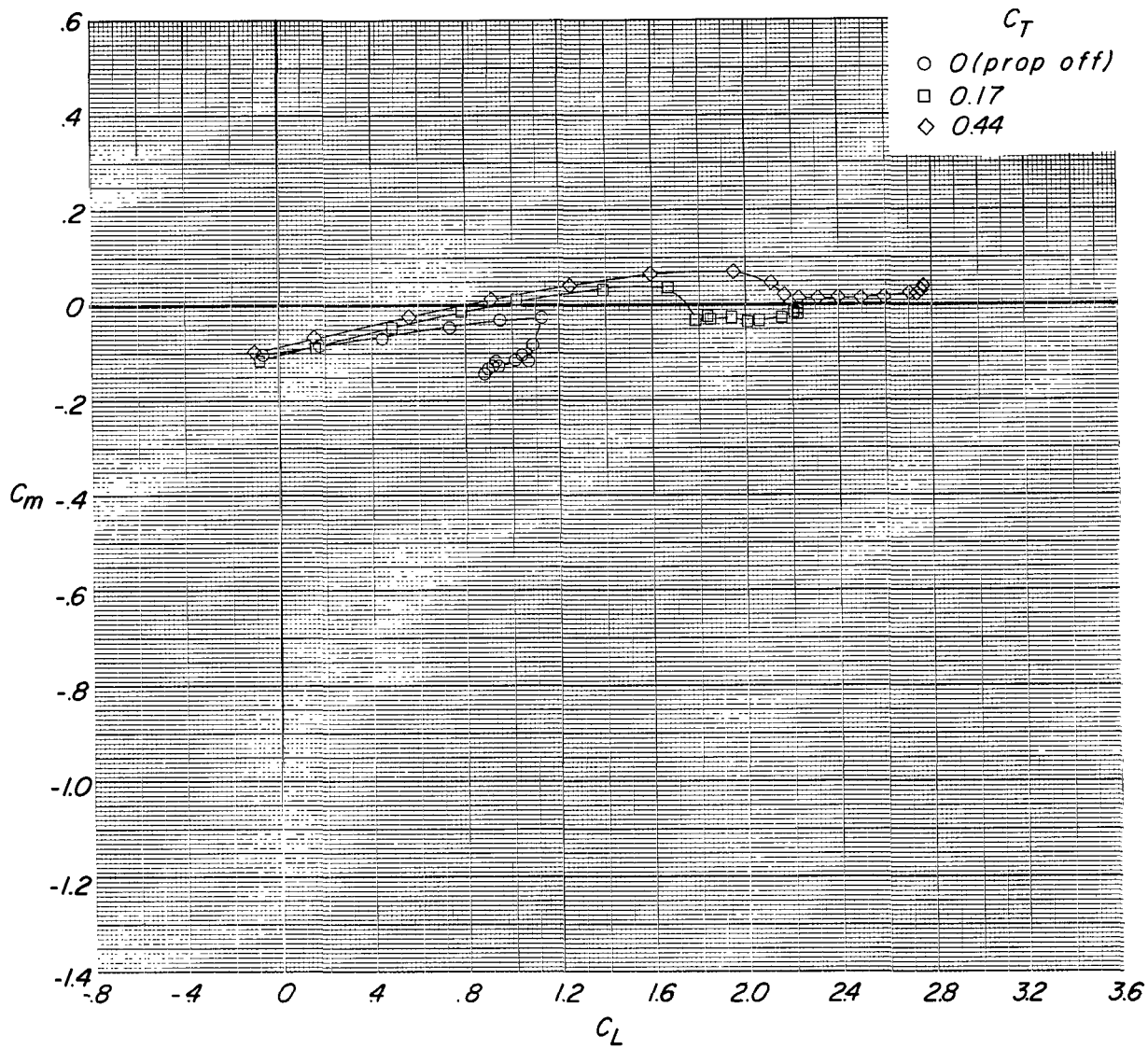

(d) Variation of C_m with C_L.

Figure 5.- Continued.

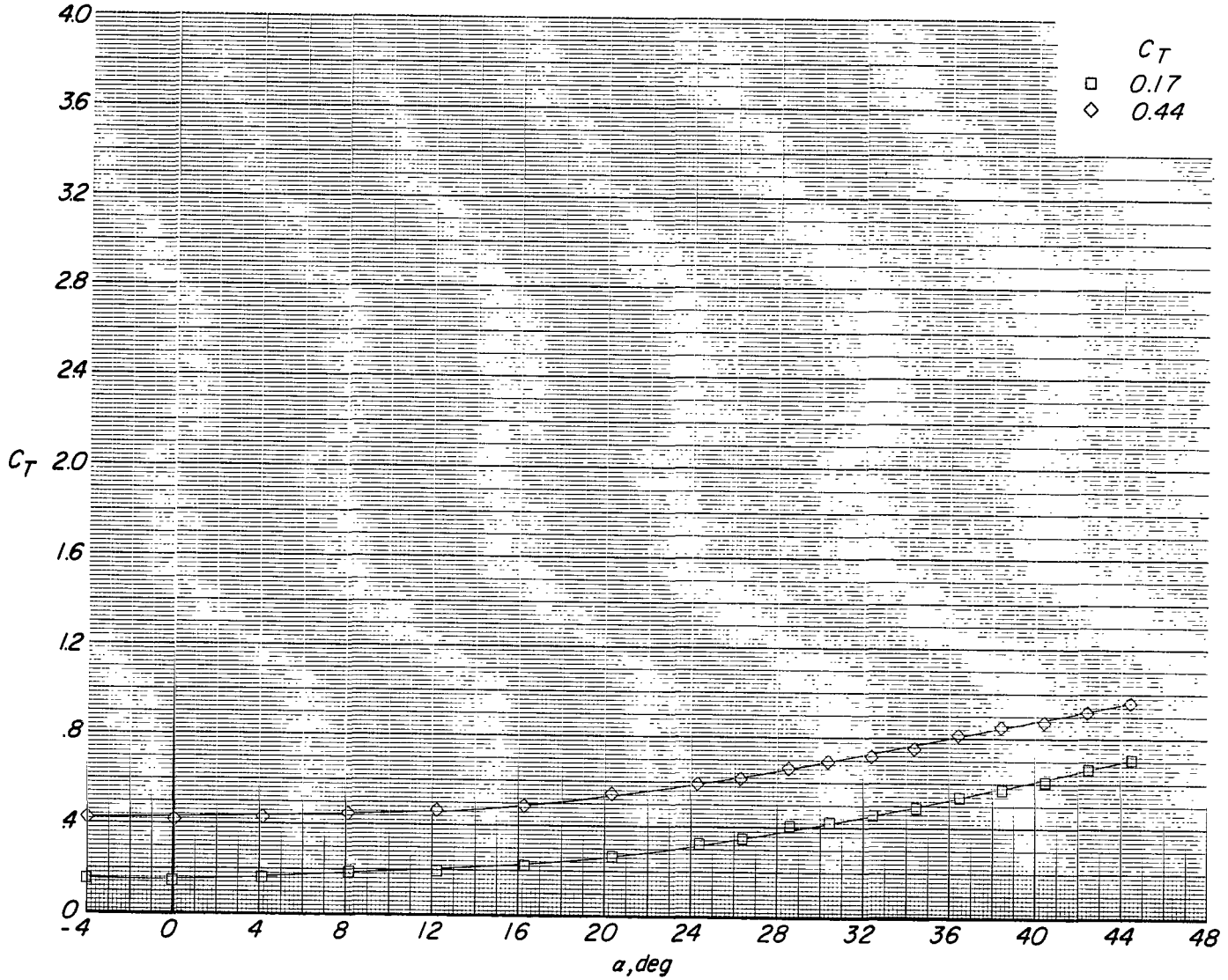

(e) Variation of C_T with α.

Figure 5.- Concluded.

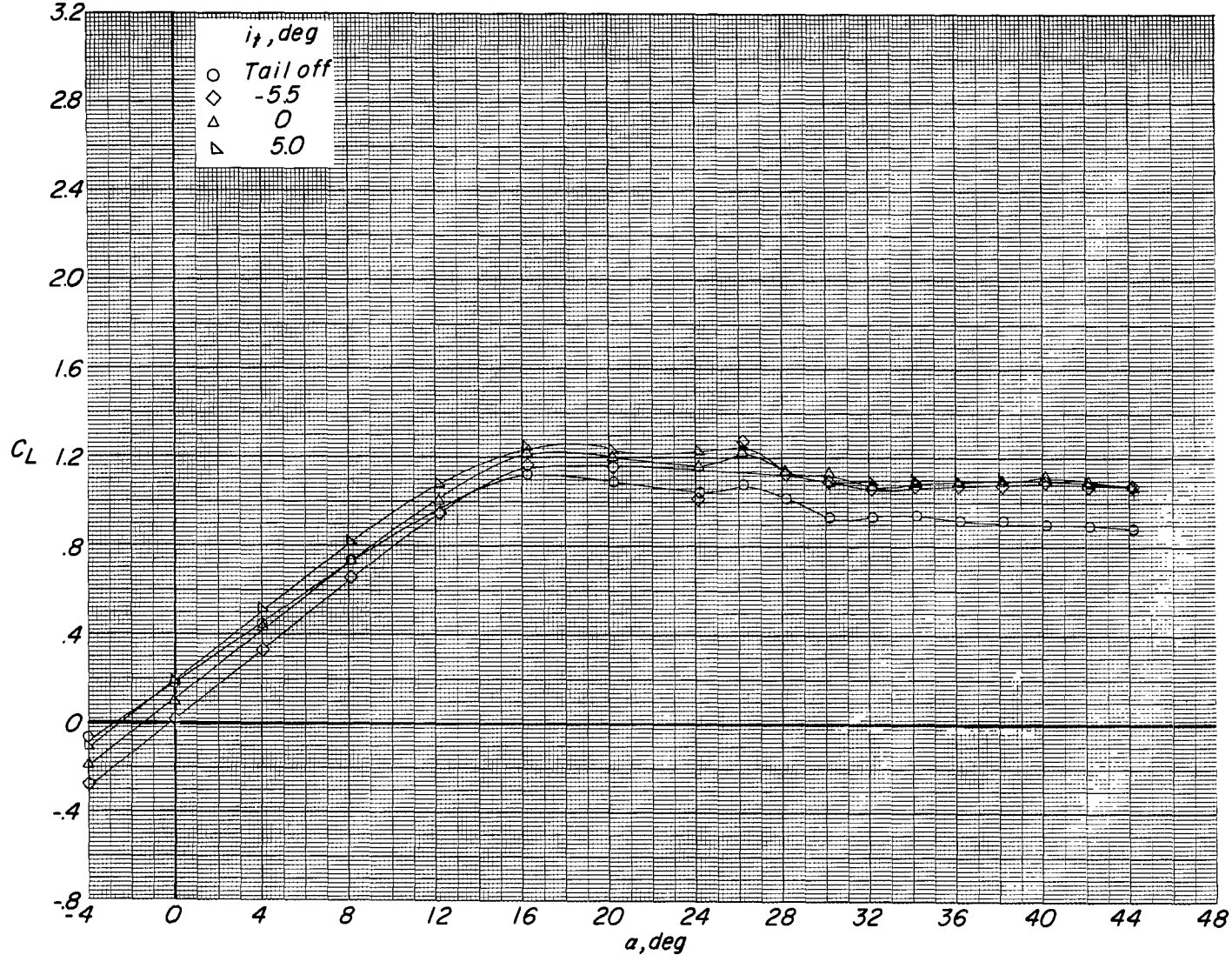

(a) Variation of C_L with α.

Figure 6.- Effect of tail incidence on longitudinal aerodynamic characteristics of configuration with small tail in high position. $\delta_f = 0^o$; $C_T = 0$.

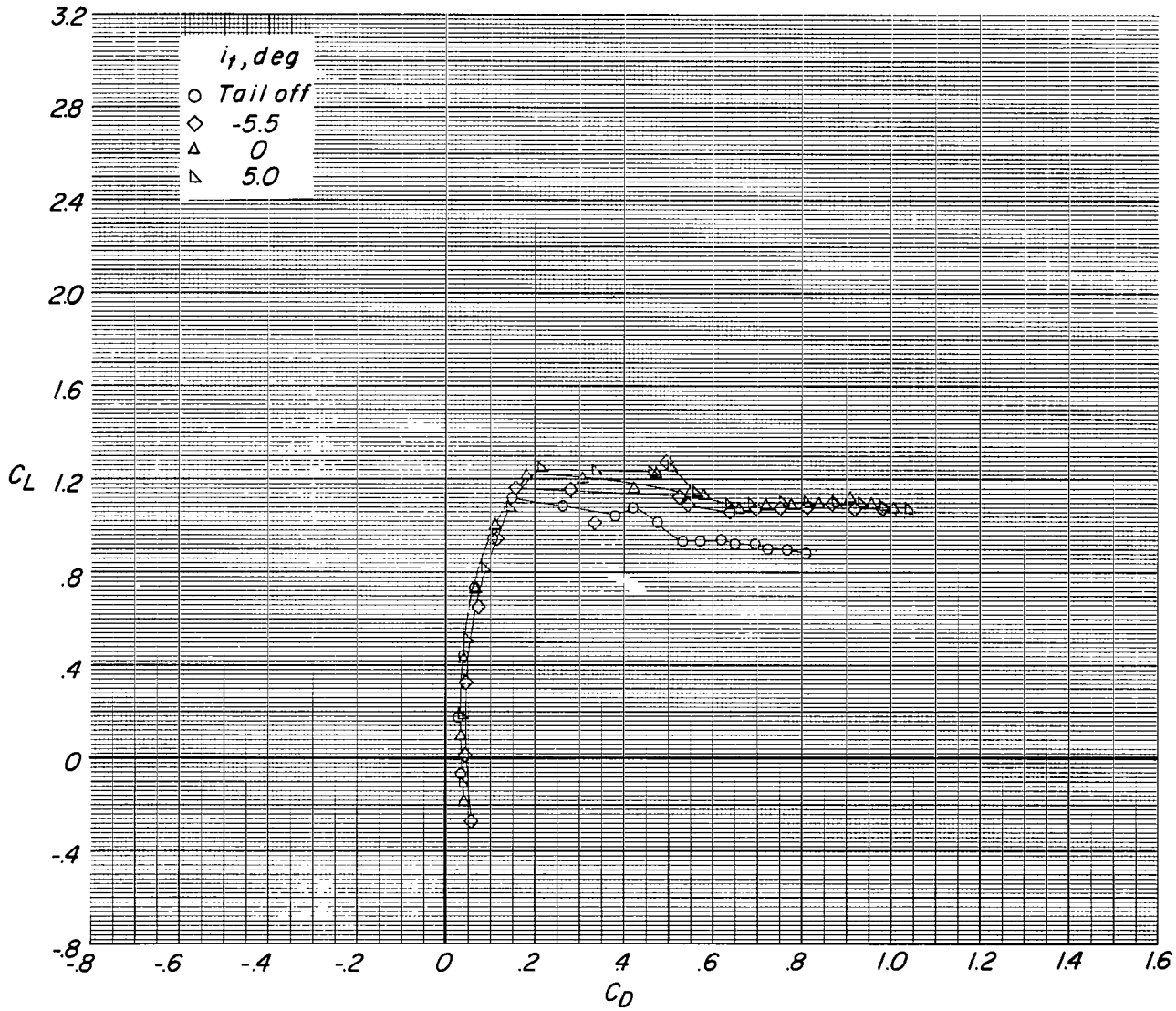

(b) Variation of C_L with C_D.

Figure 6.- Continued.

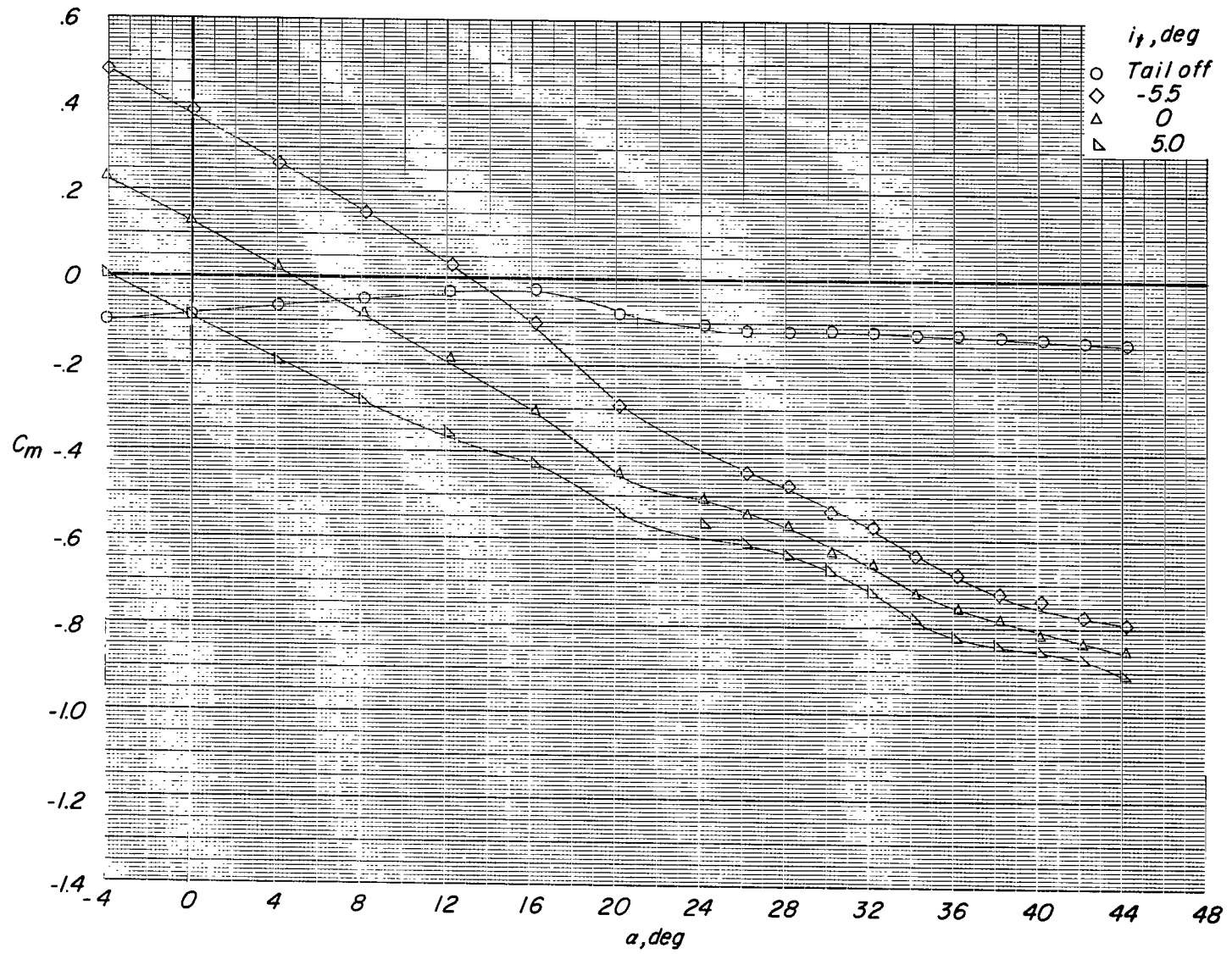

(c) Variation of C_m with α.

Figure 6.- Continued.

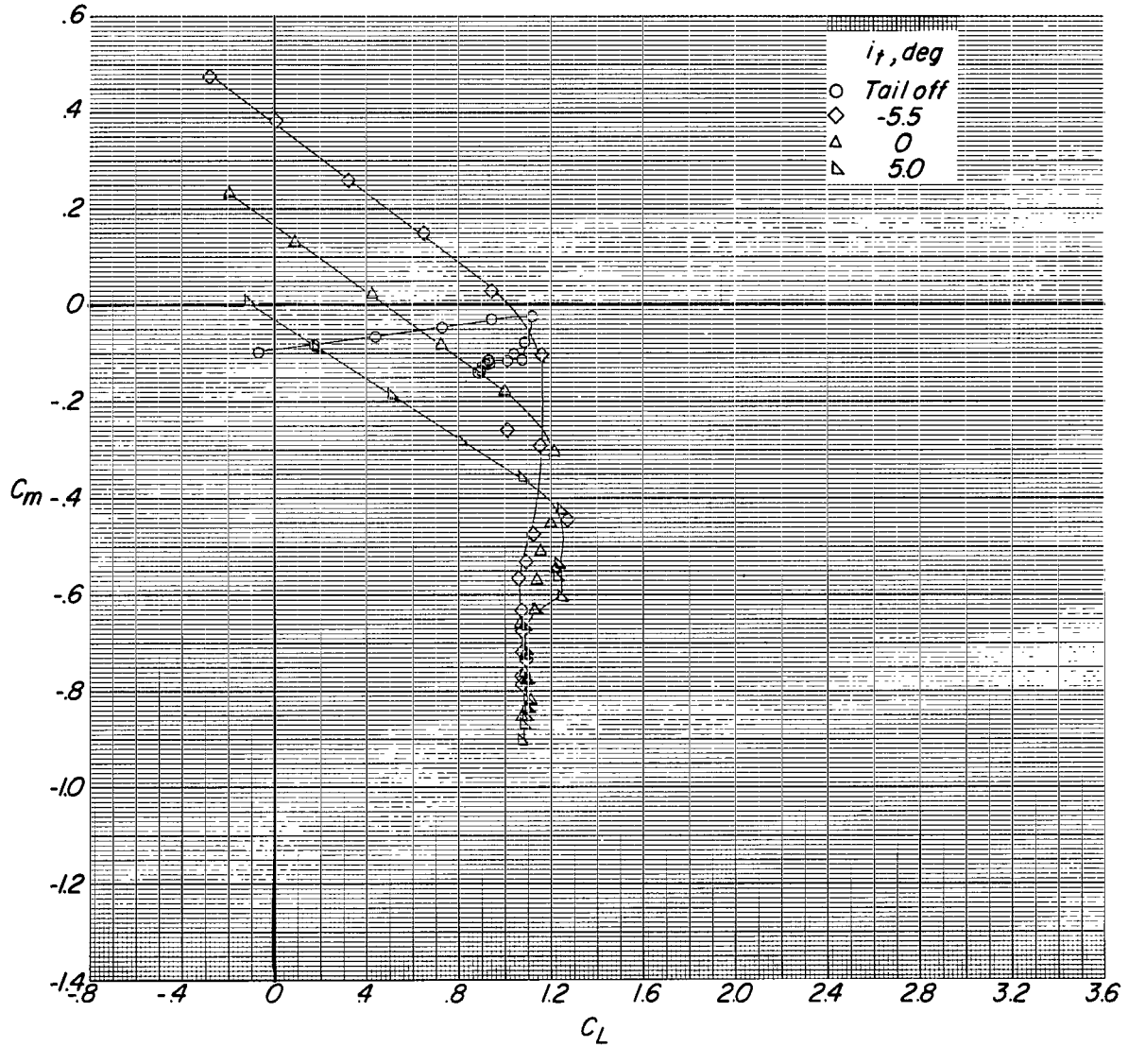

(d) Variation of C_m with C_L.

Figure 6.- Concluded.

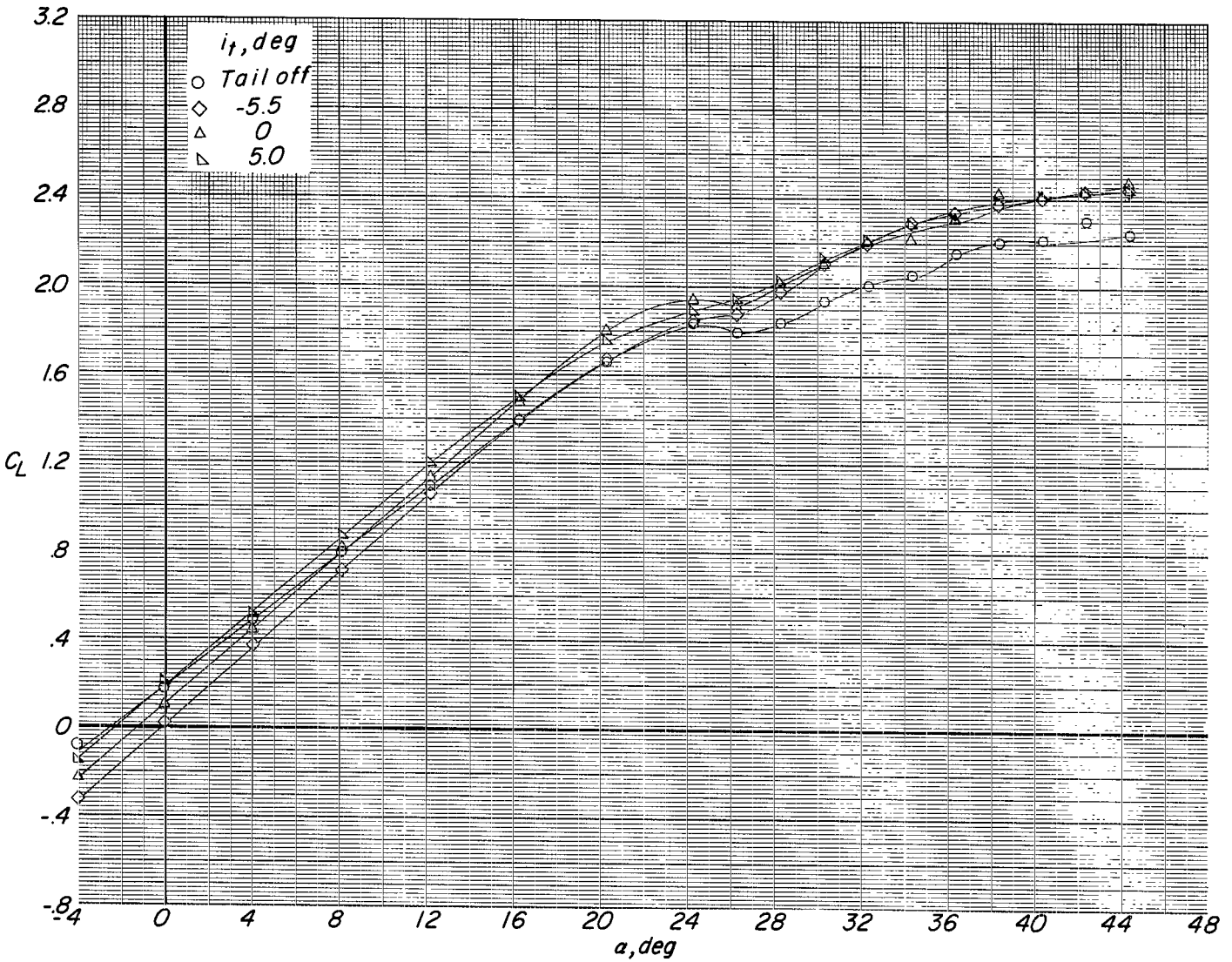

(a) Variation of C_L with α.

Figure 7.- Effect of tail incidence on longitudinal aerodynamic characteristics of configuration with small tail in high position. $\delta_f = 0^o$; reference $C_T = 0.17$.

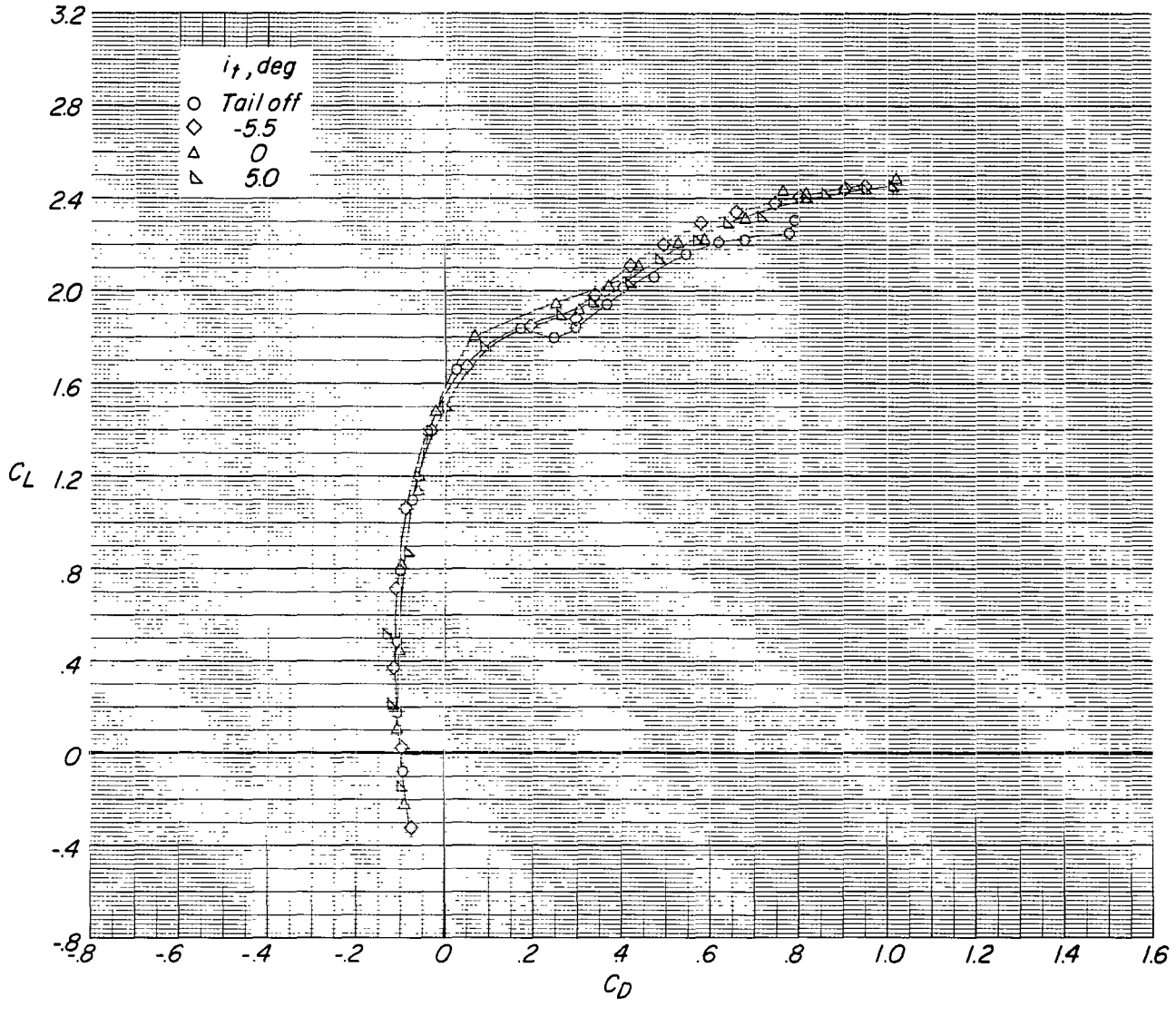

(b) Variation of C_L with C_D.

Figure 7.- Continued.

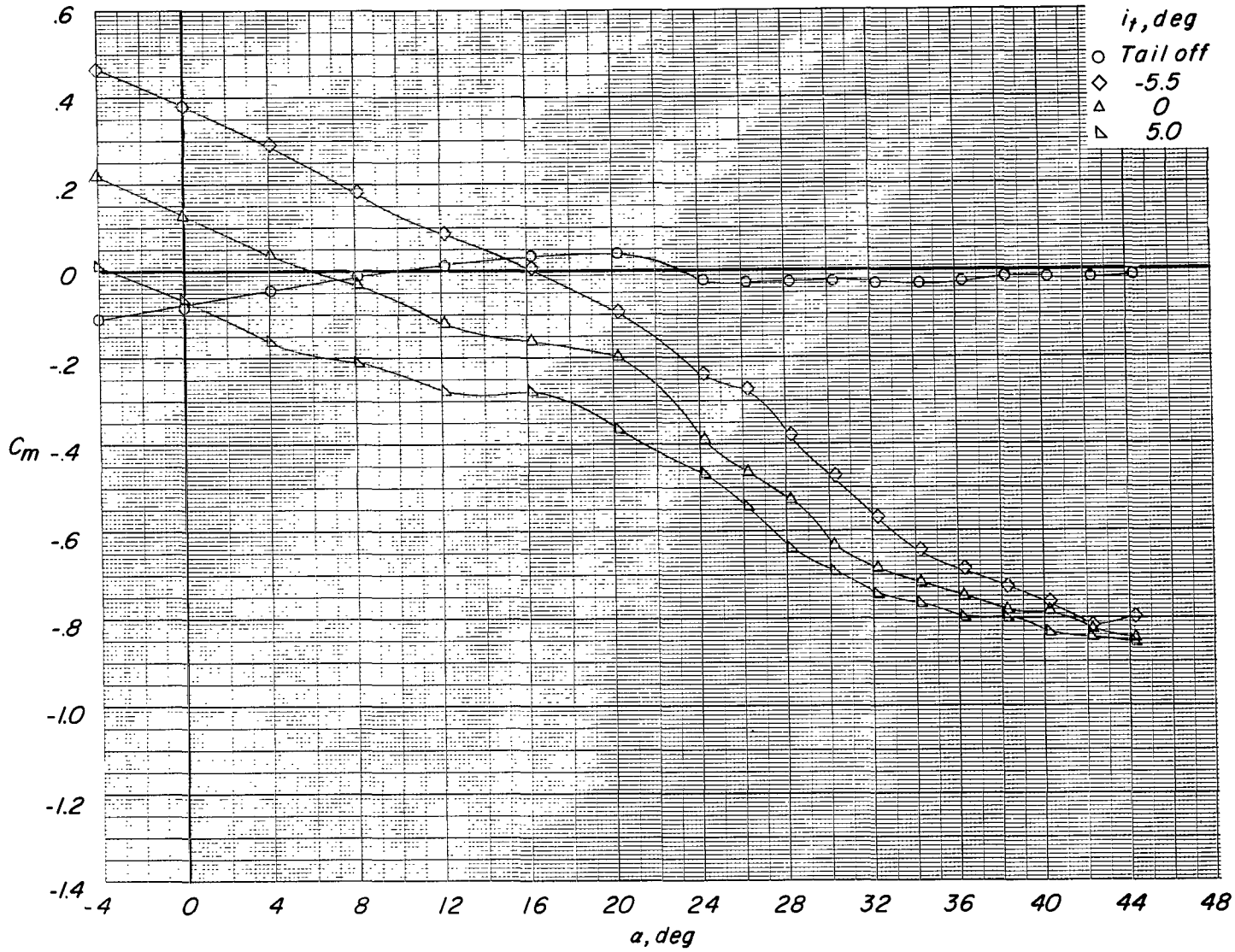

(c) Variation of C_m with α.

Figure 7.- Continued.

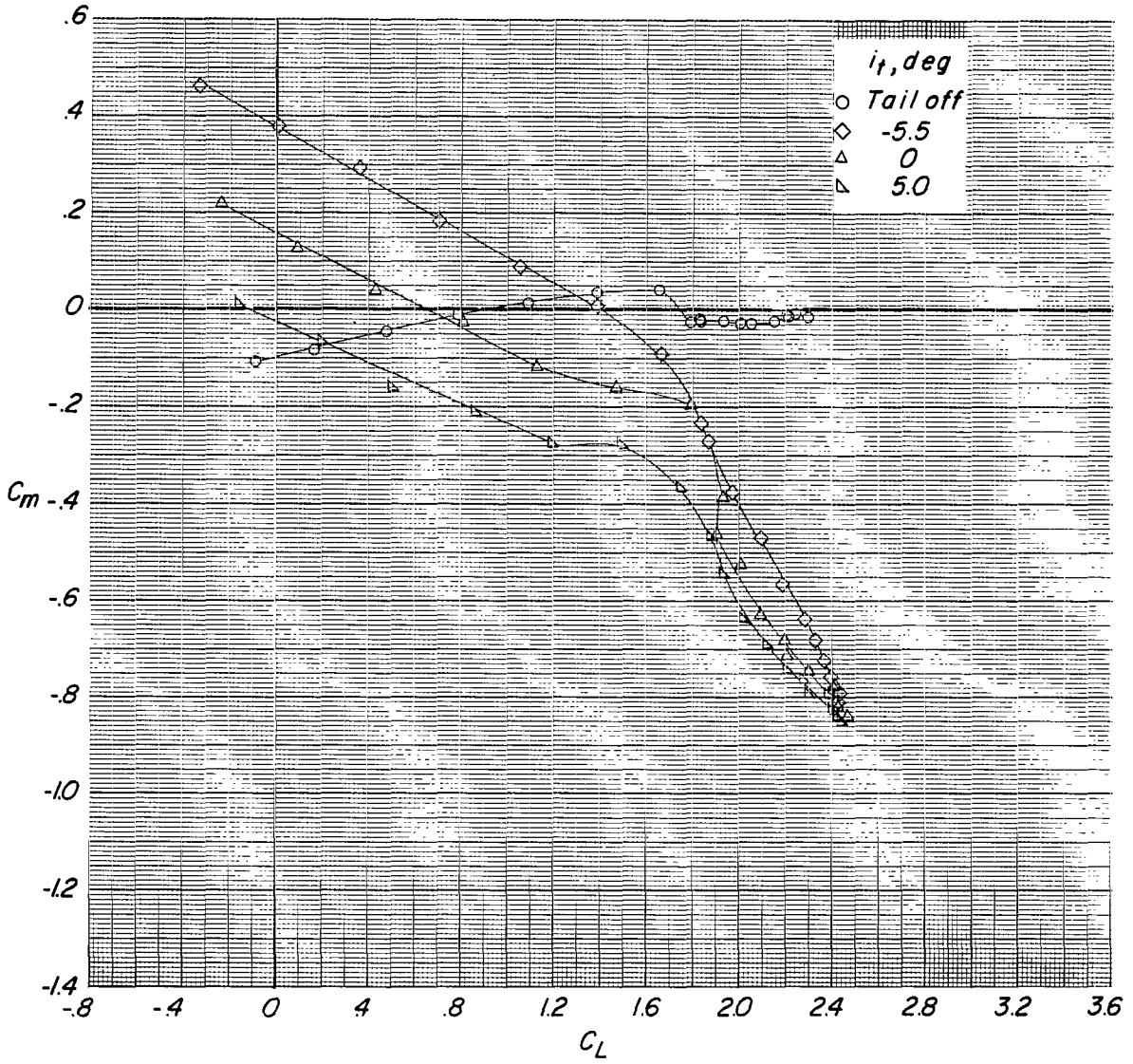

(d) Variation of C_m with C_L.

Figure 7.- Continued.

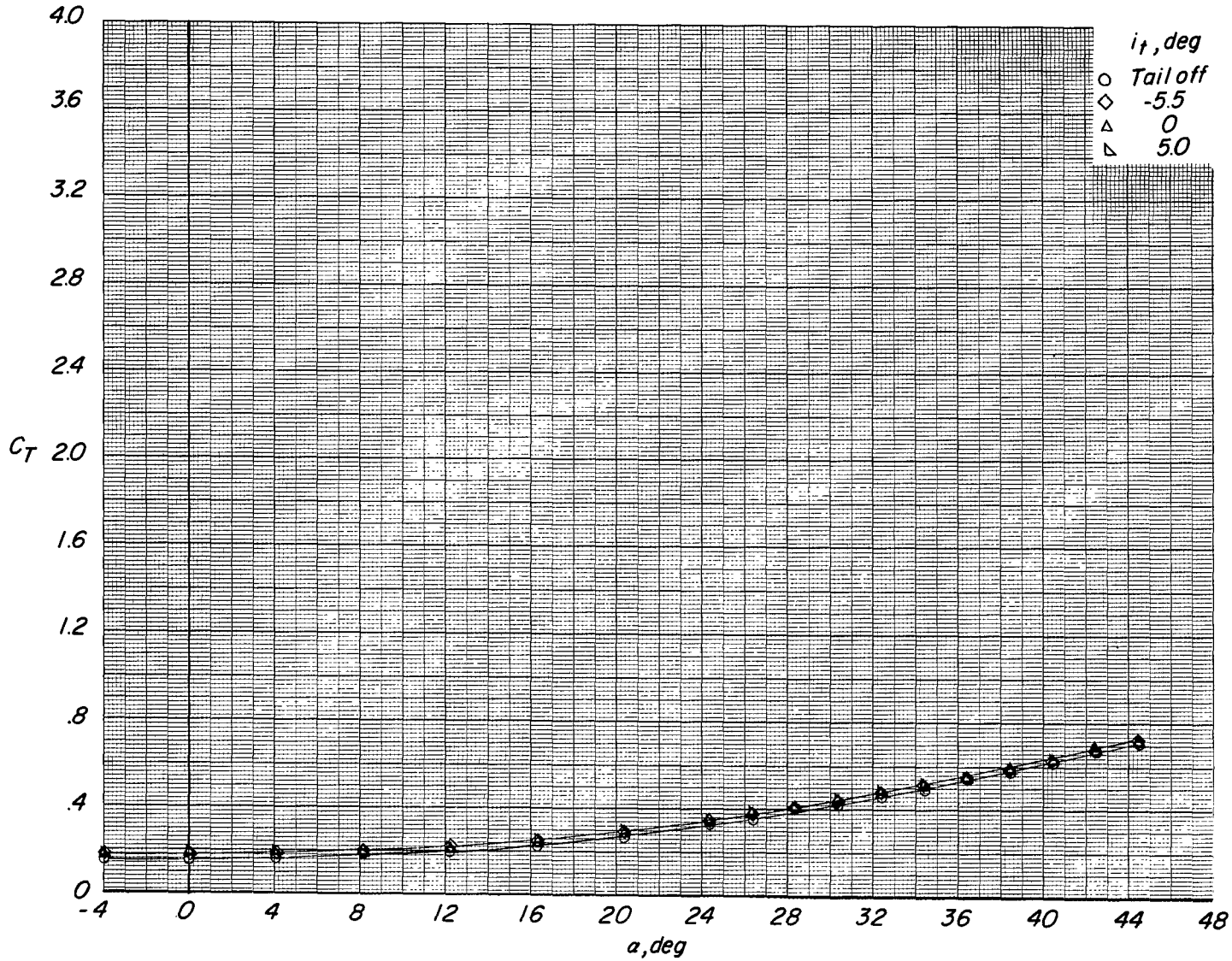

(e) Variation of C_T with α.

Figure 7.- Concluded.

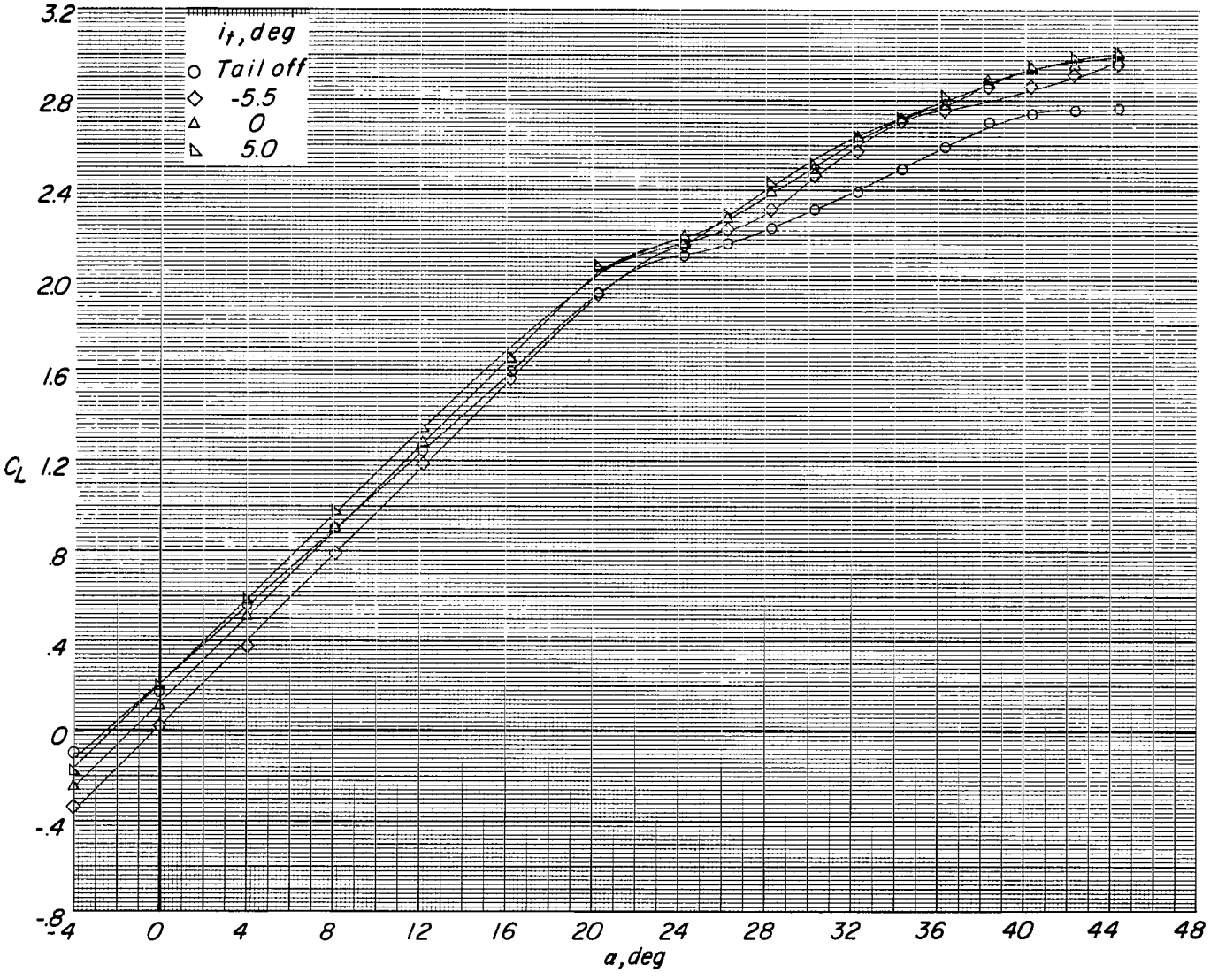

(a) Variation of C_L with α.

Figure 8.- Effect of tail incidence on longitudinal aerodynamic characteristics of configuration with small tail in high position. $\delta_f = 0^o$; reference $C_T = 0.44$.

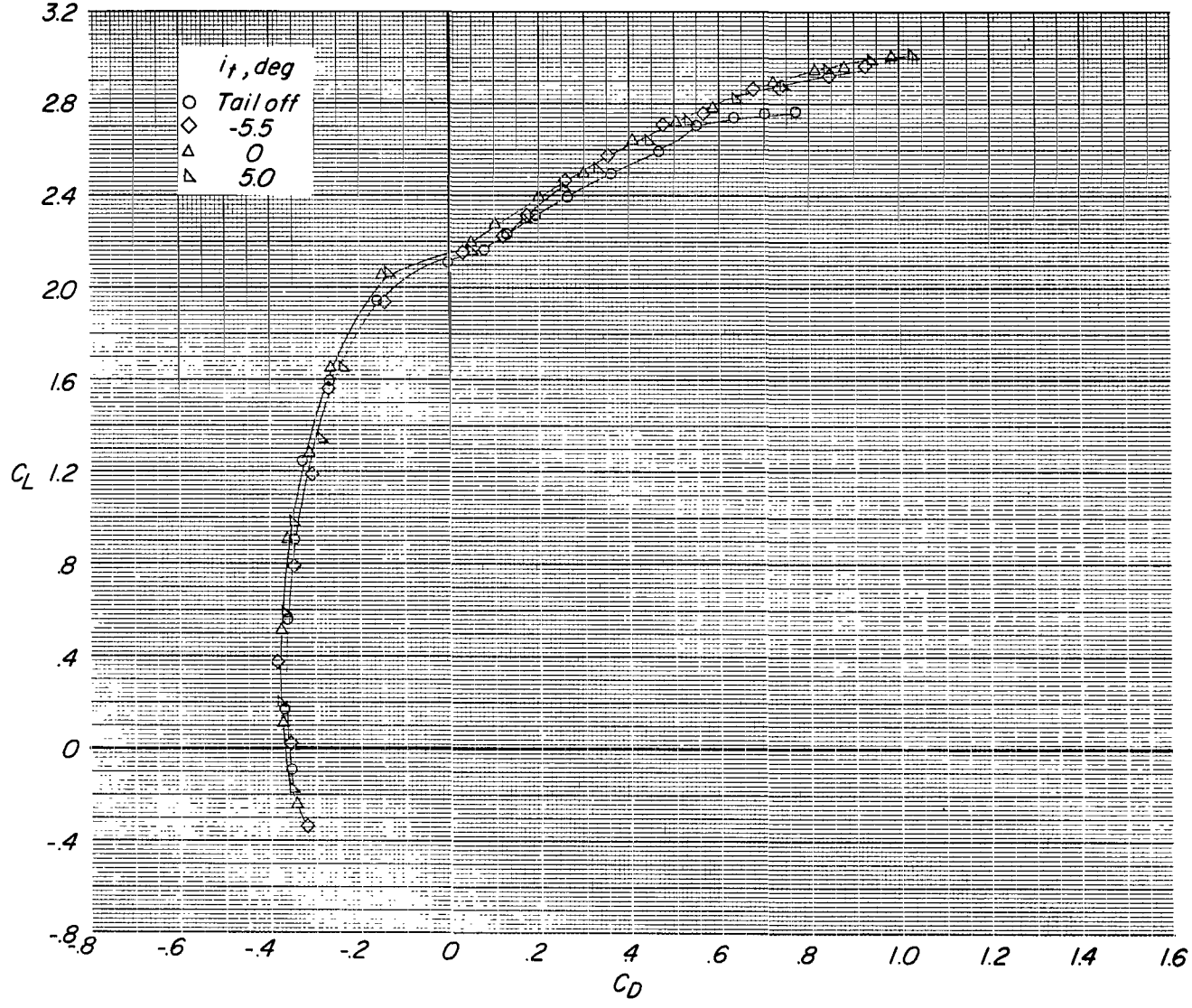

(b) Variation of C_L with C_D.

Figure 8.- Continued.

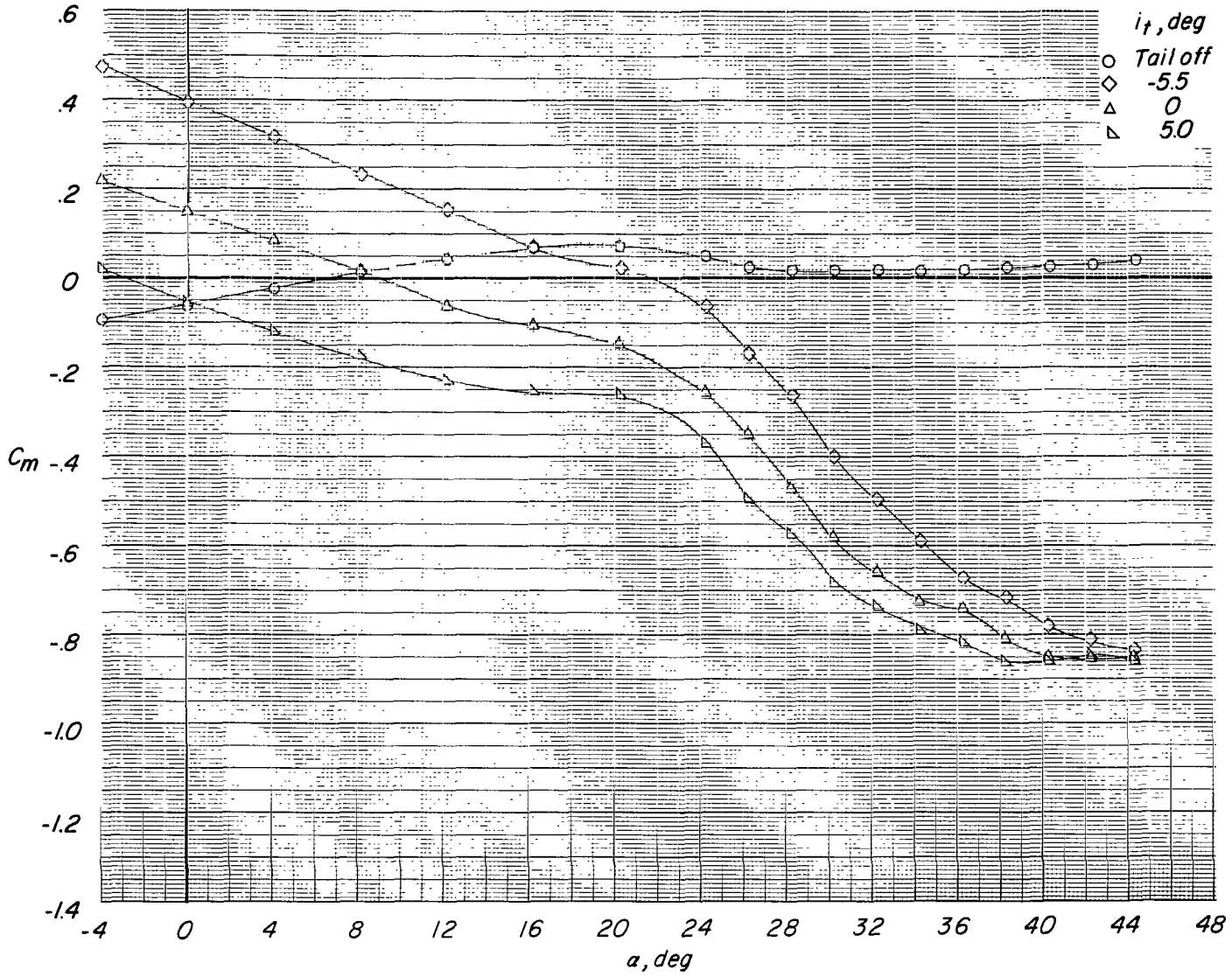

(c) Variation of C_m with α.

Figure 8.- Continued.

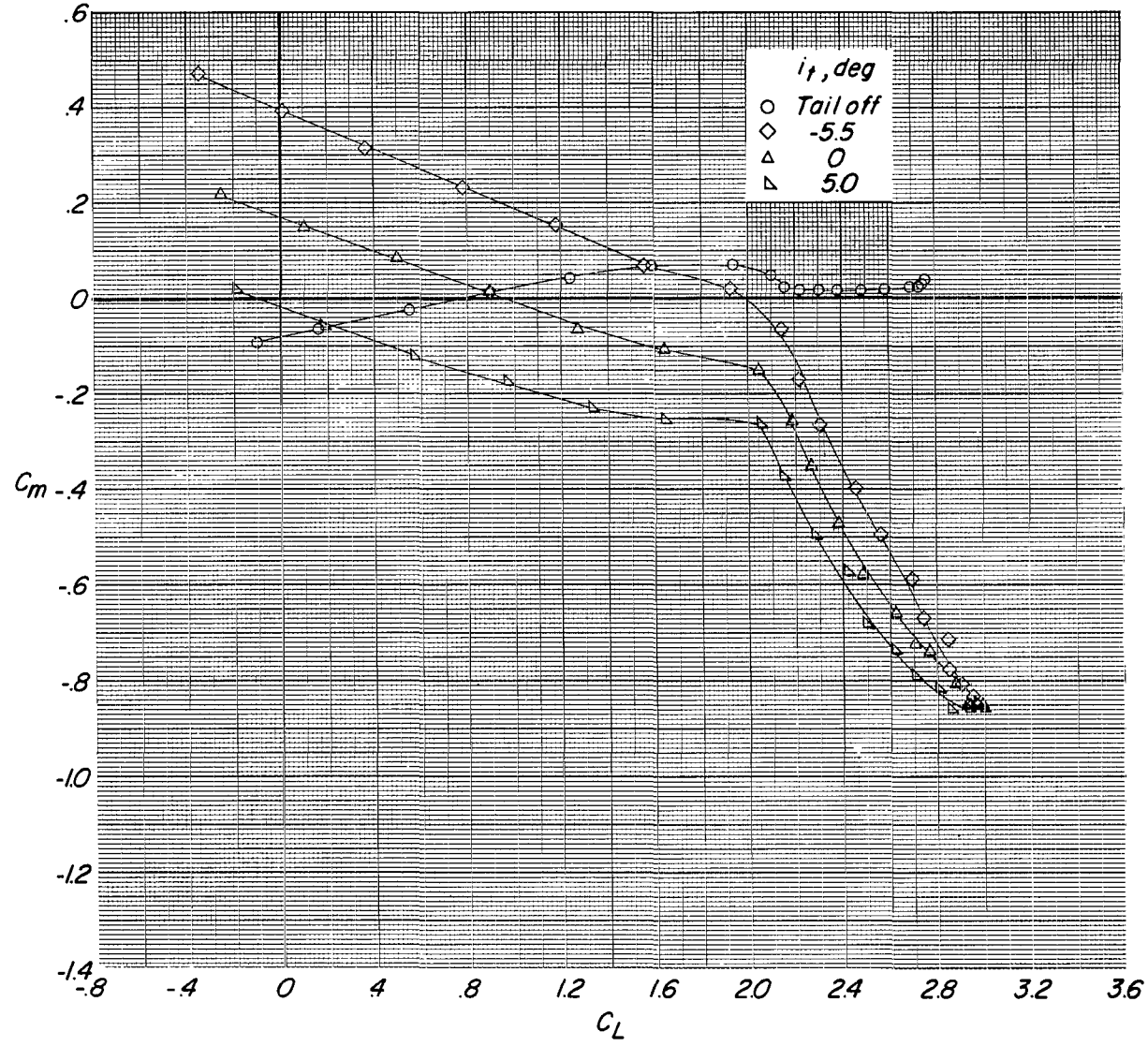

(d) Variation of C_m with C_L.

Figure 8.- Continued.

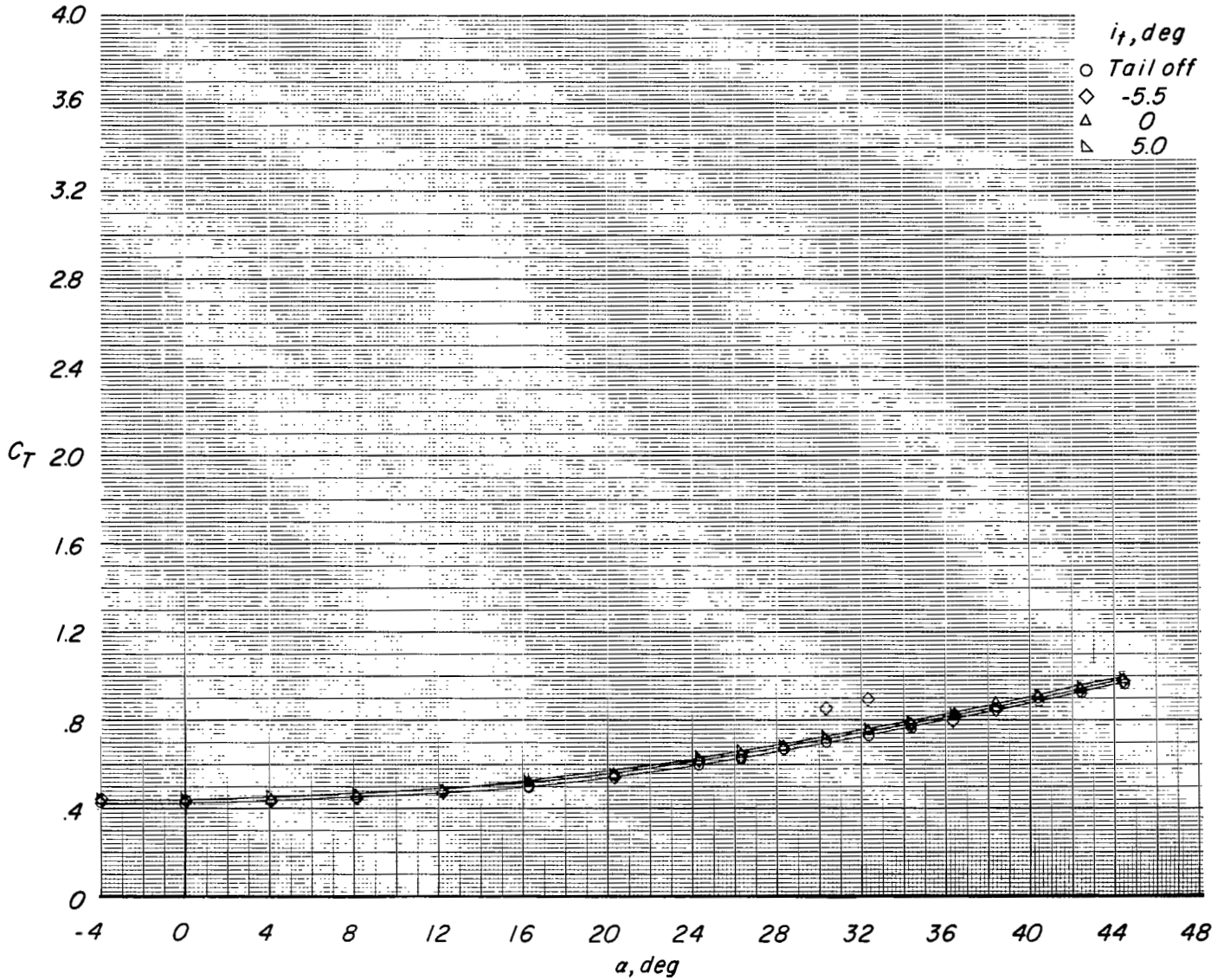

(e) Variation of C_T with α.

Figure 8.- Concluded.

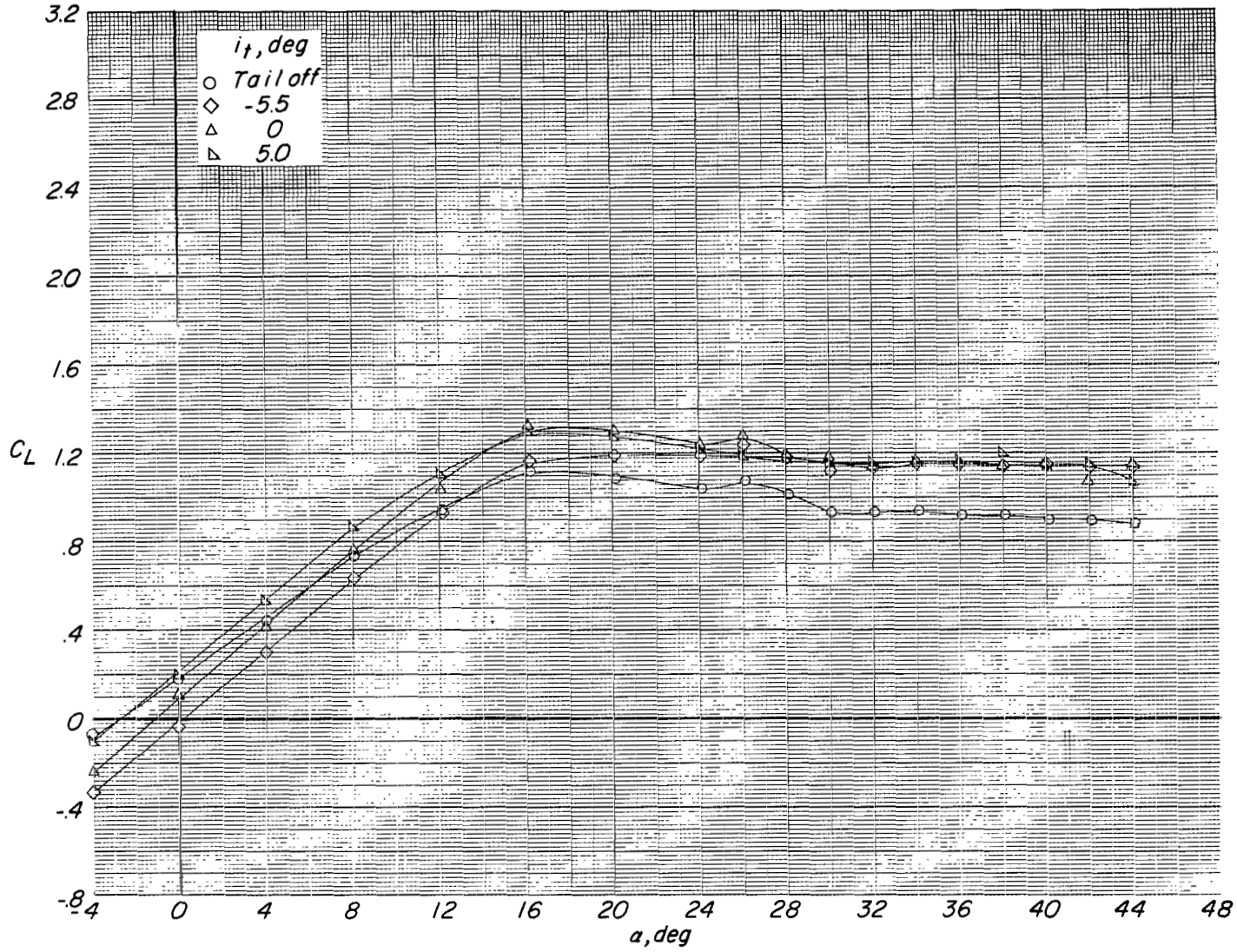

(a) Variation of C_L with α.

Figure 9.- Effect of tail incidence on longitudinal aerodynamic characteristics of configuration with large tail in high position. $\delta_f = 0^o$; $C_T = 0$.

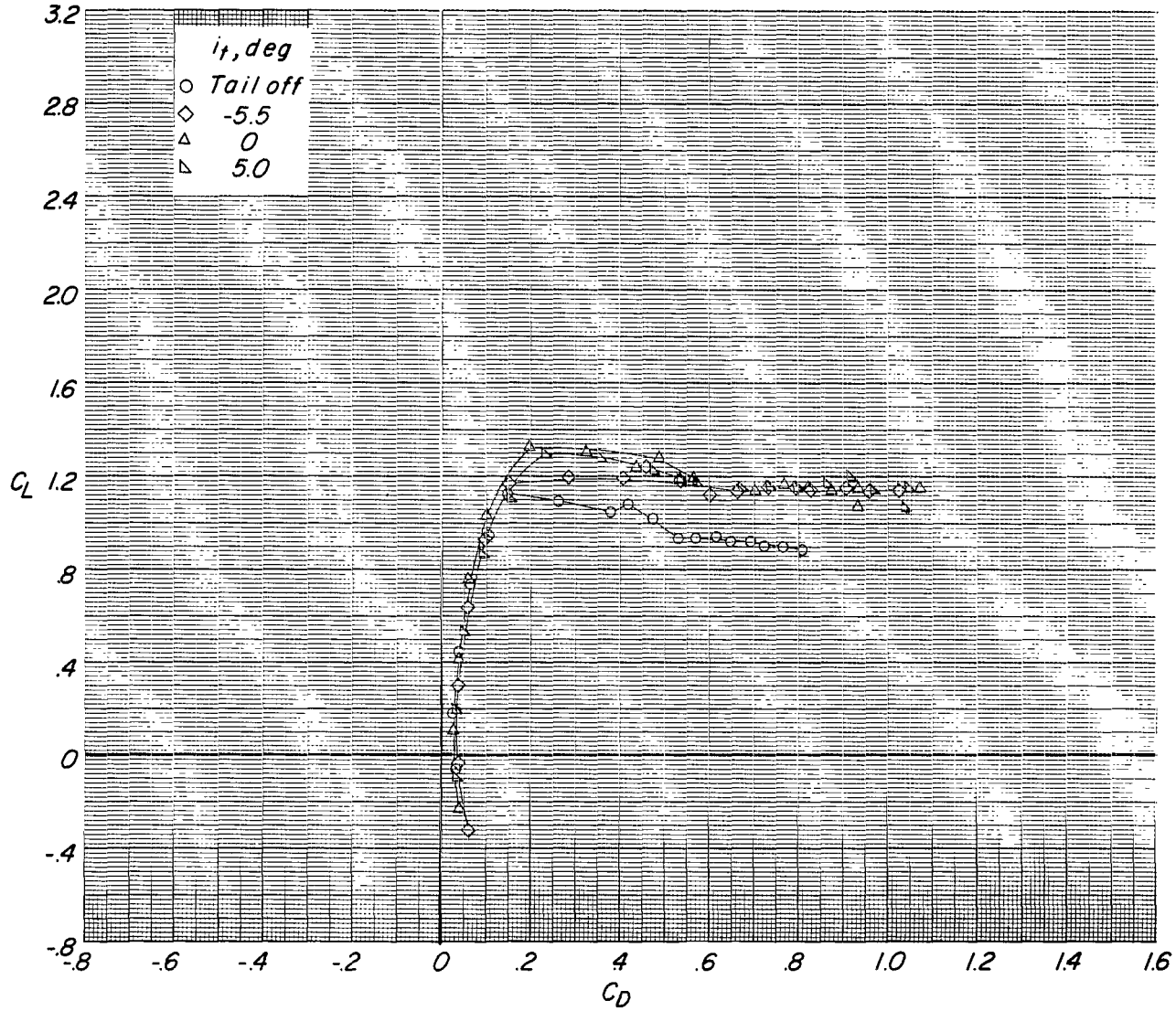

(b) Variation of C_L with C_D.

Figure 9.- Continued.

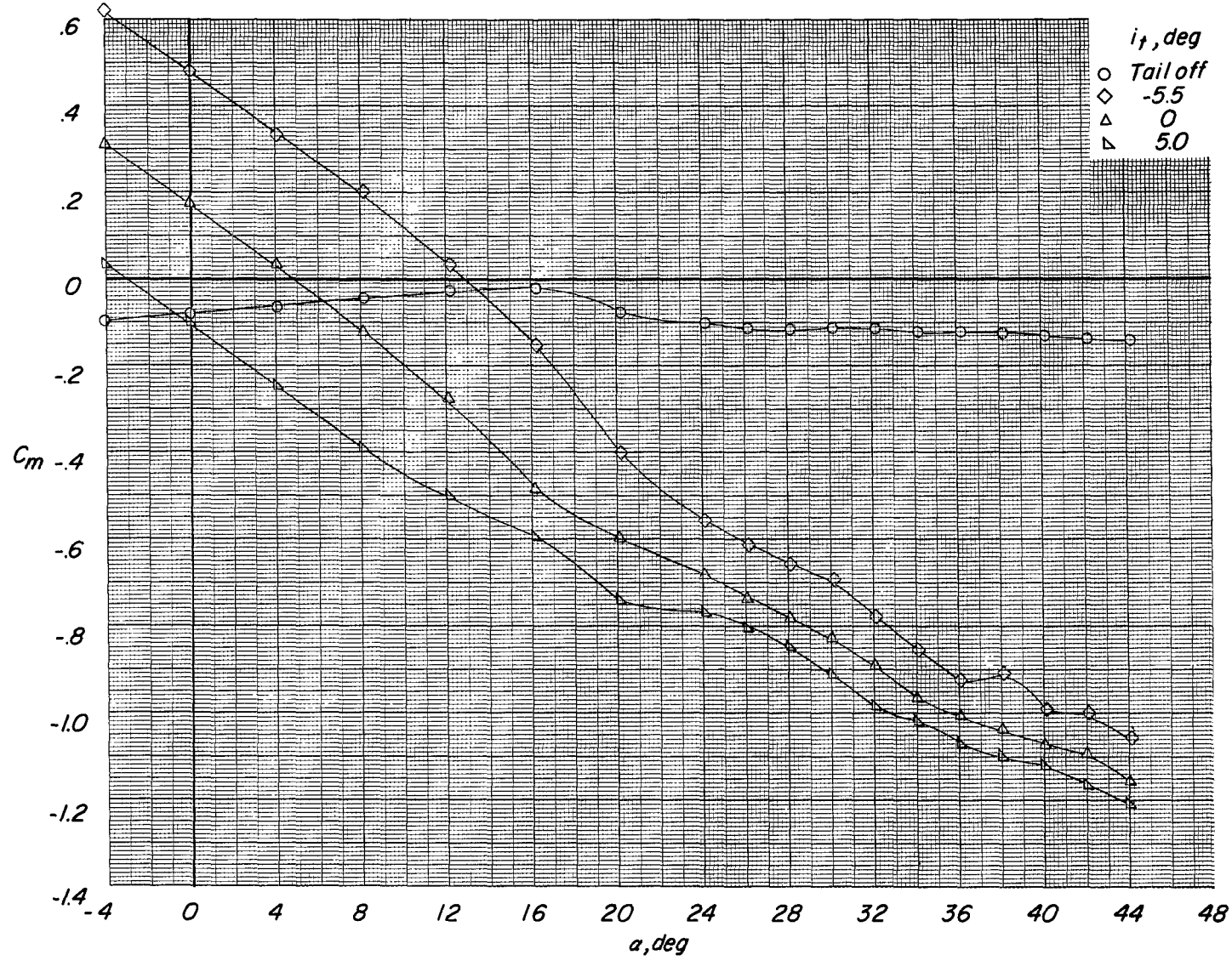

(c) Variation of C_m with α.

Figure 9.- Continued.

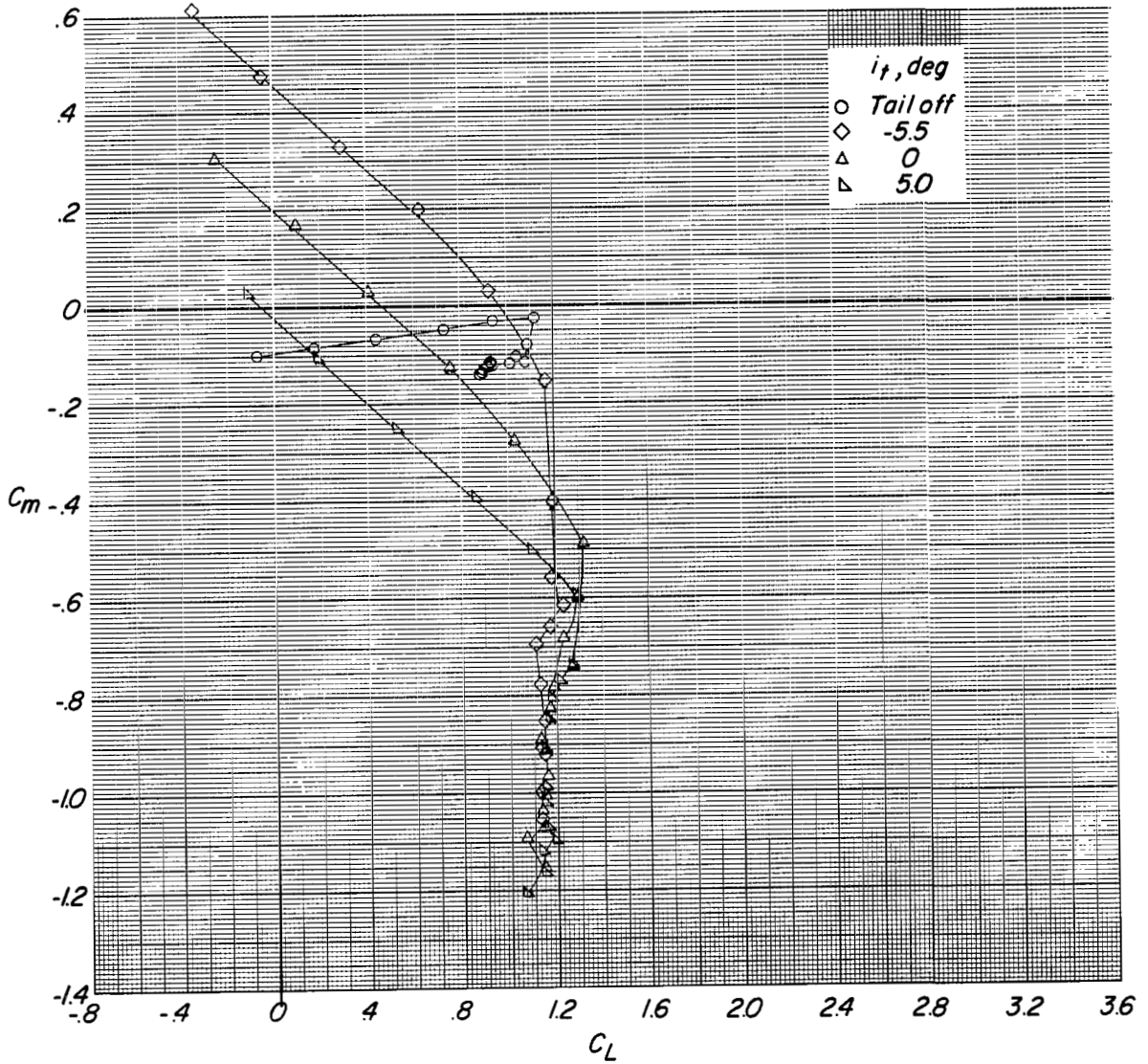

(d) Variation of C_m with C_L.

Figure 9.- Concluded.

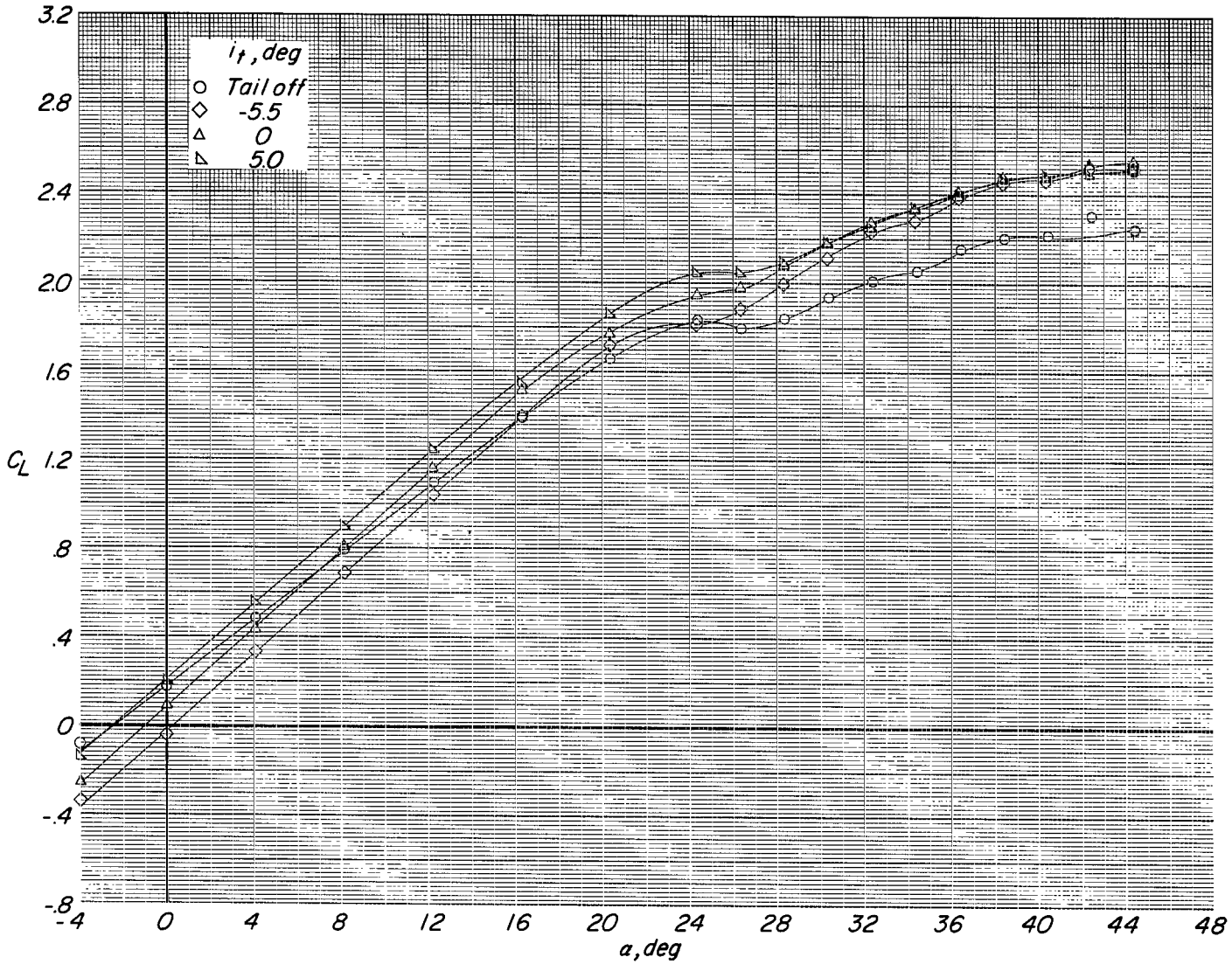

(a) Variation of C_L with α.

Figure 10.- Effect of tail incidence on longitudinal aerodynamic characteristics of configuration with large tail in high position. $\delta_f = 0^0$; reference $C_T = 0.17$.

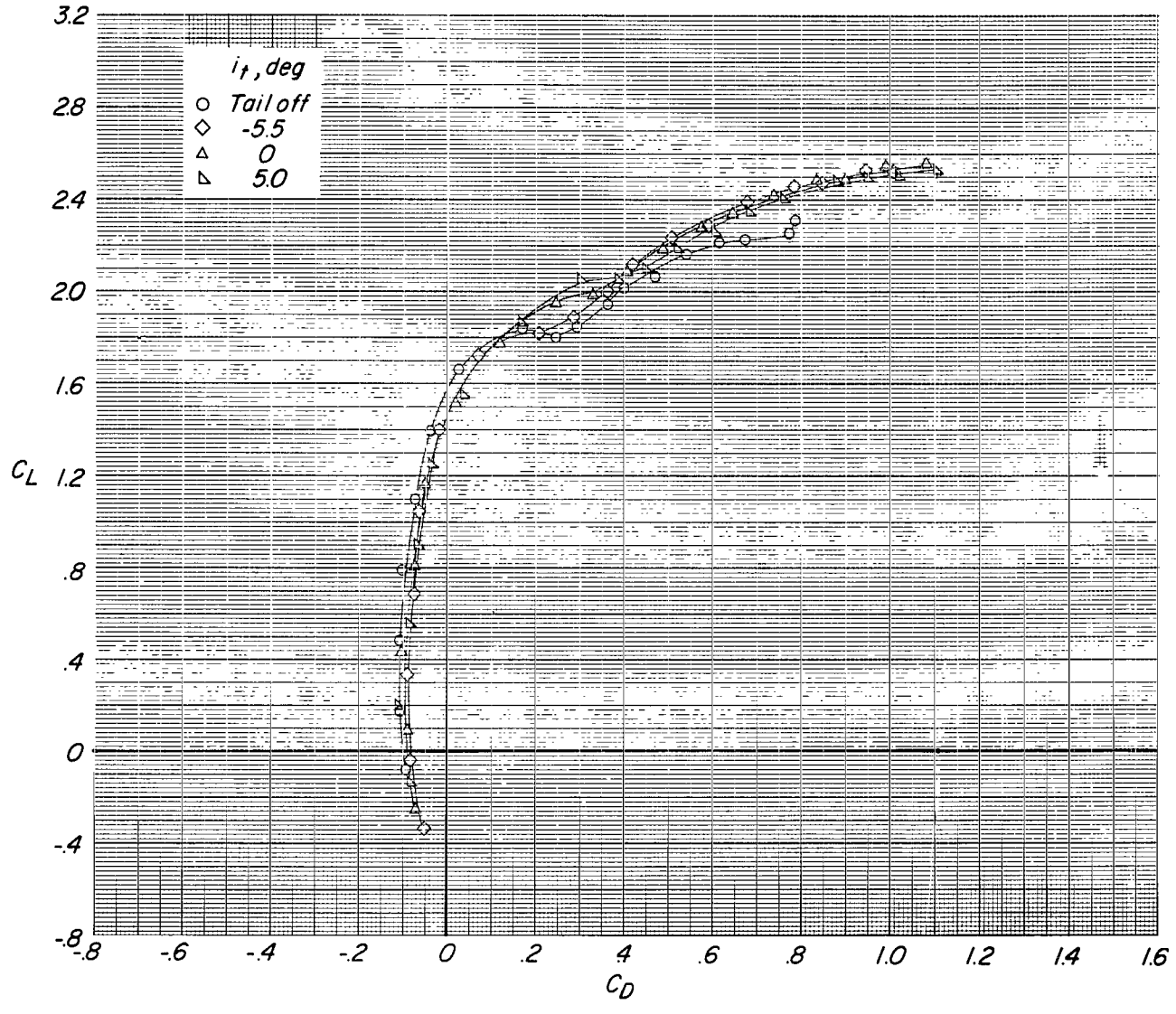

(b) Variation of C_L with C_D.

Figure 10.- Continued.

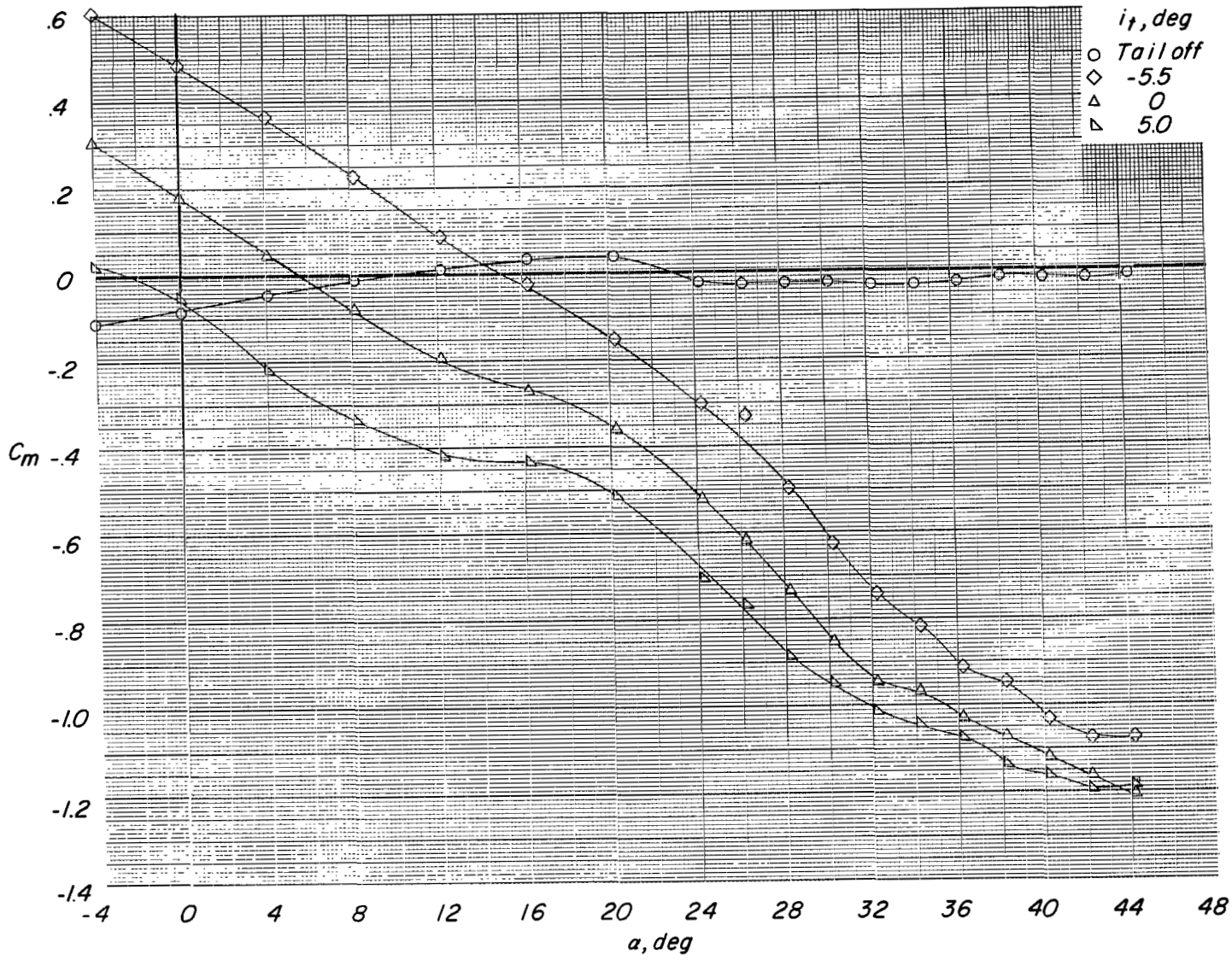

(c) Variation of C_m with α.

Figure 10.- Continued.

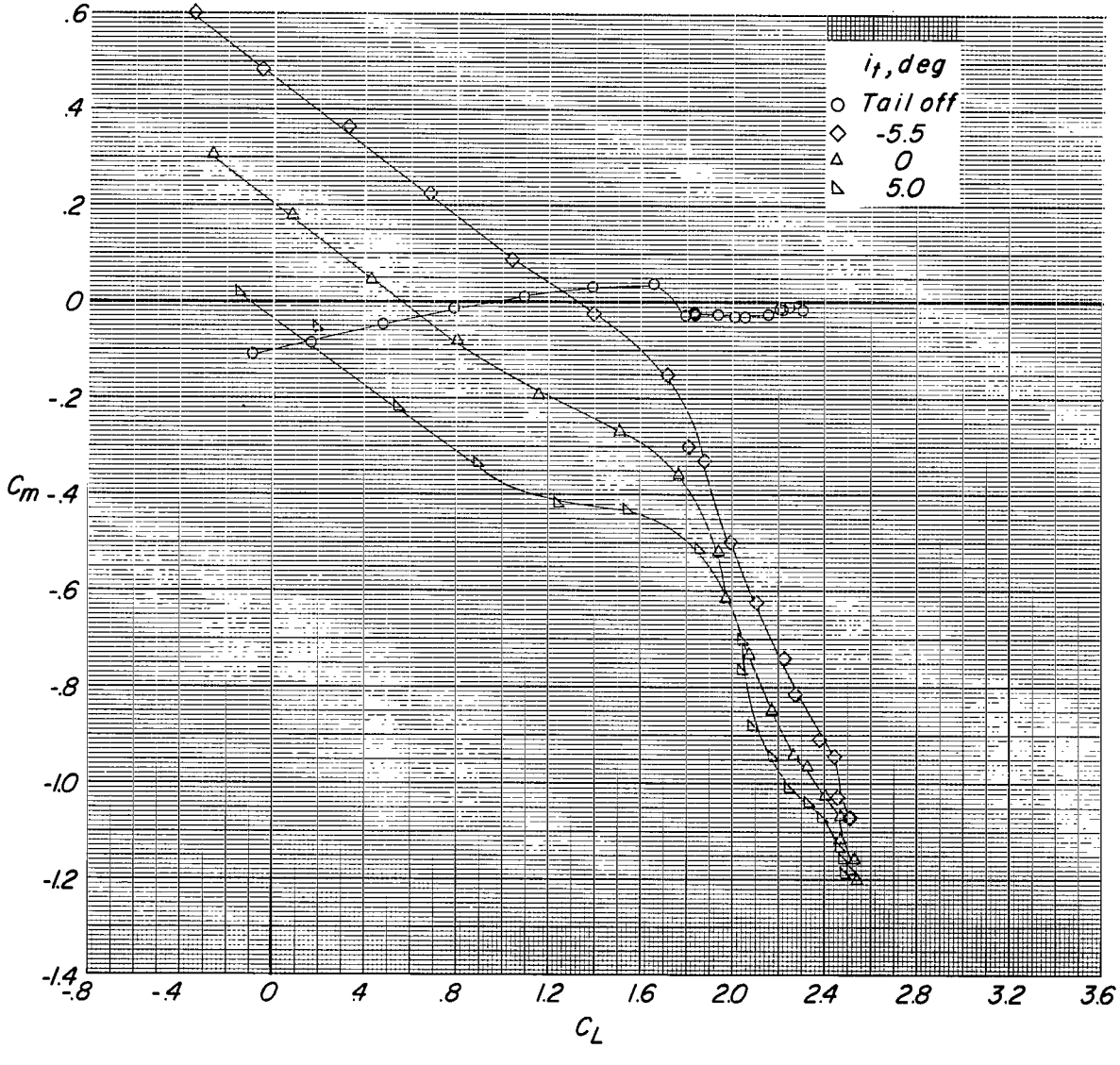

(d) Variation of C_m with C_L.

Figure 10.- Continued.

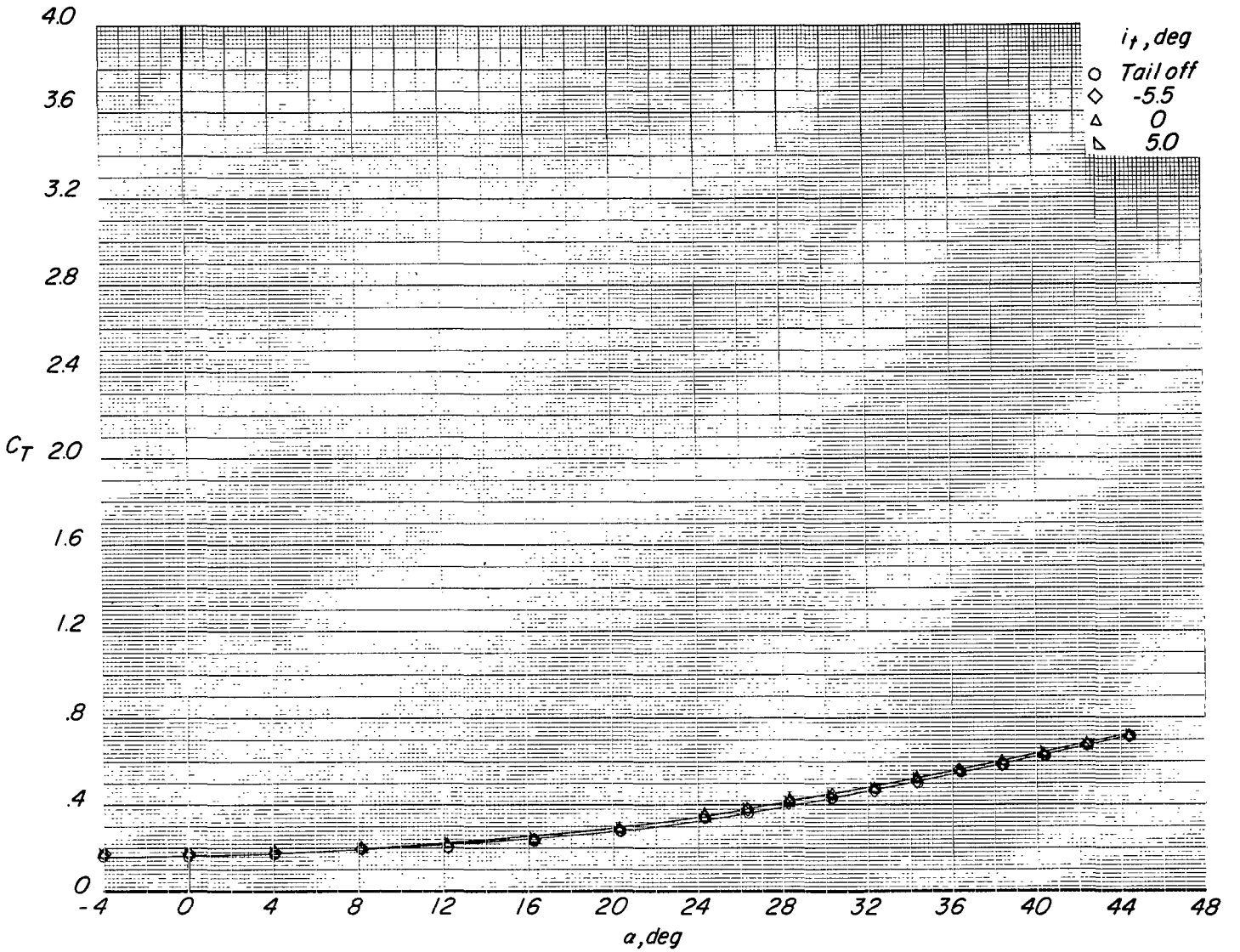

(e) Variation of C_T with α.

Figure 10.- Concluded.

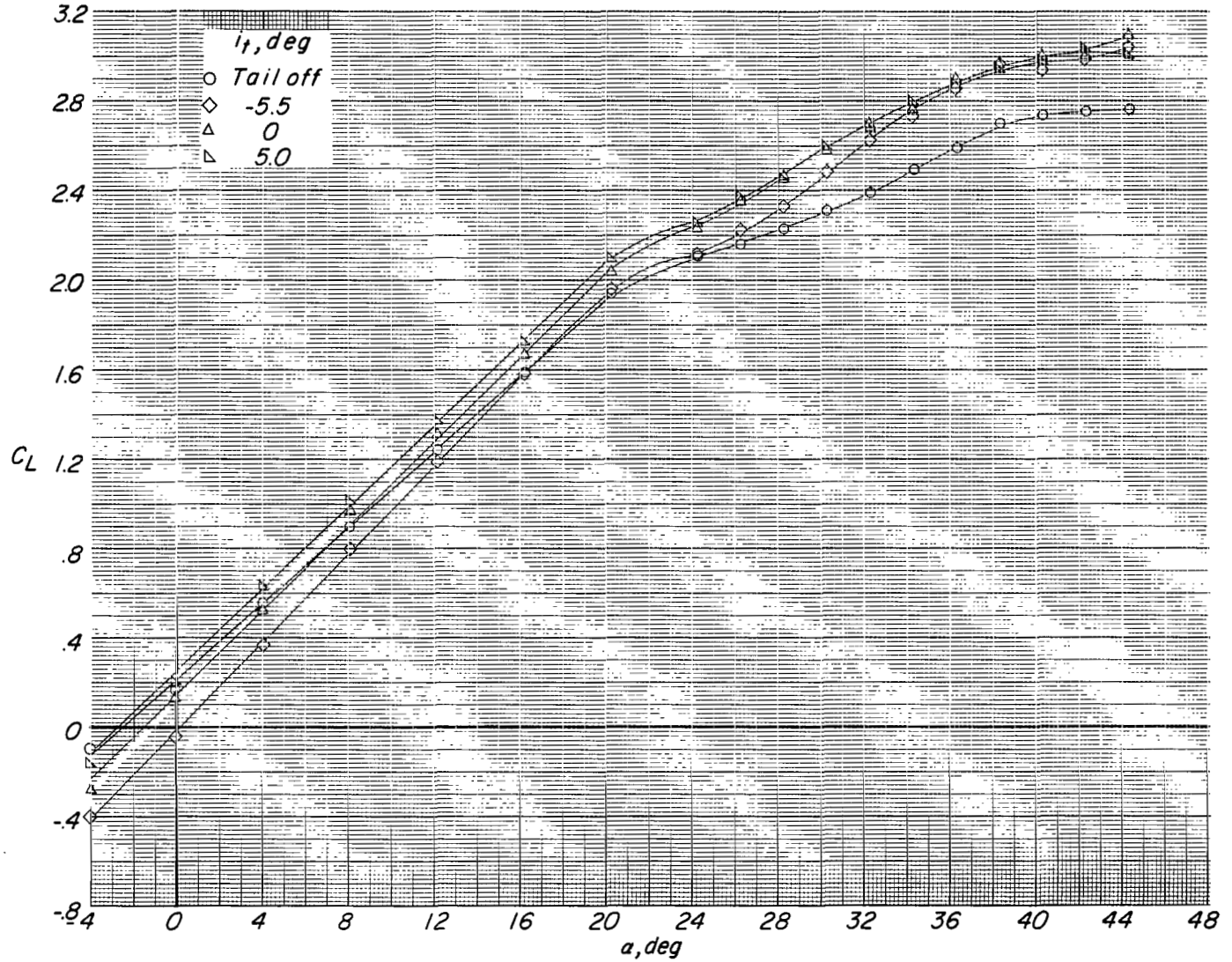

(a) Variation of C_L with α.

Figure 11.- Effect of tail incidence on longitudinal aerodynamic characteristics of configuration with large tail in high position. $\delta_f = 0^0$; reference $C_T = 0.44$.

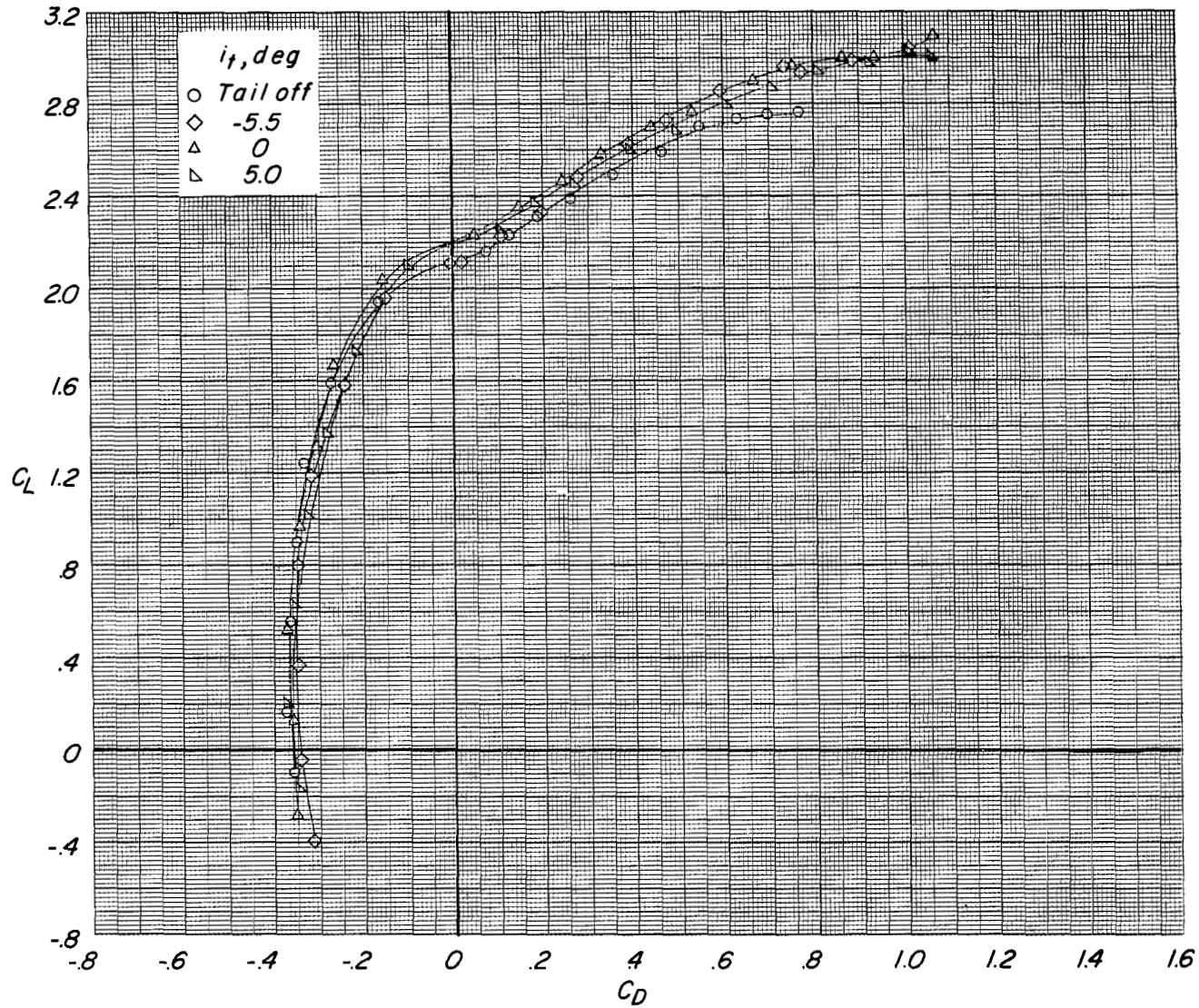

(b) Variation of C_L with C_D.

Figure 11.- Continued.

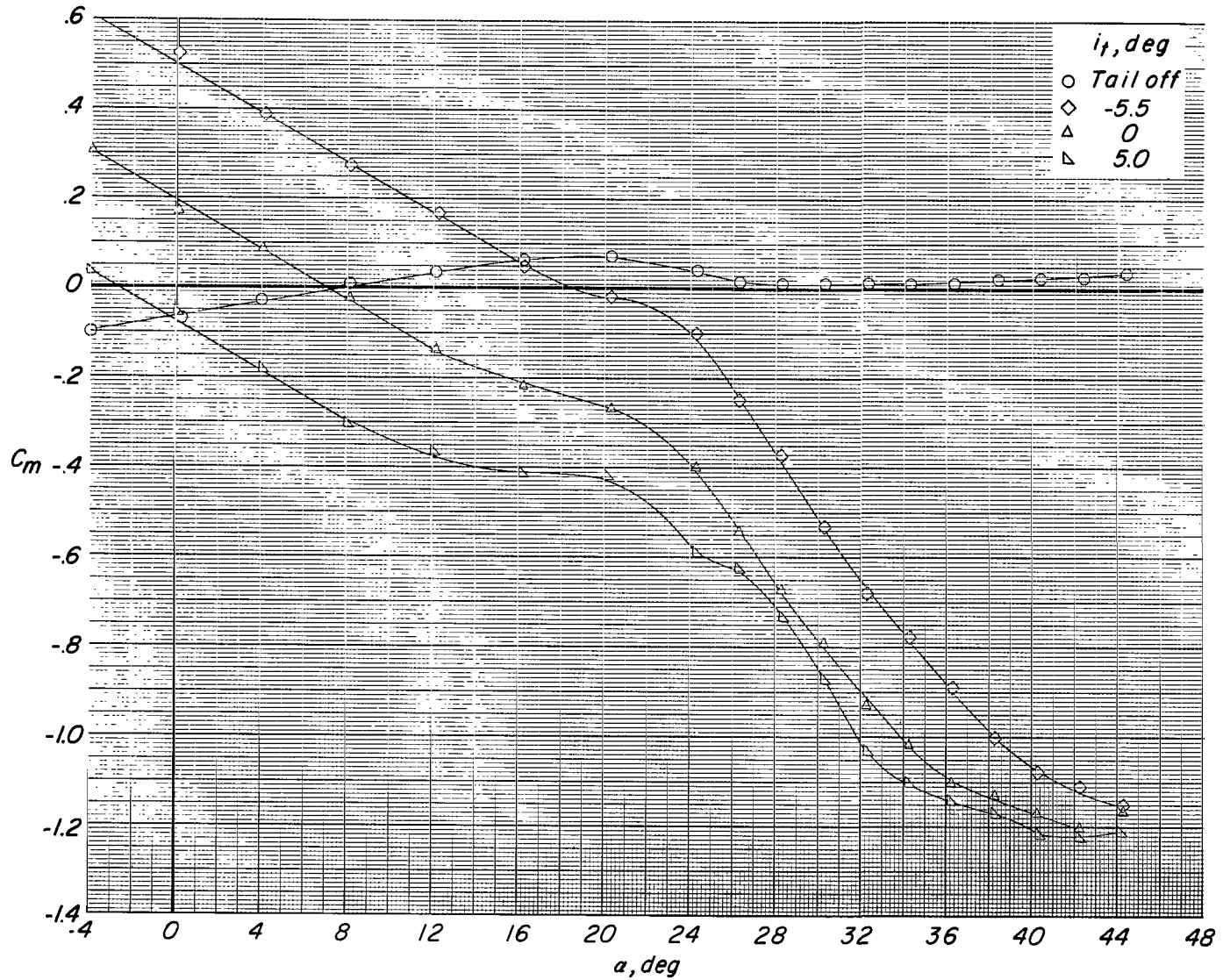

(c) Variation of C_m with α.

Figure 11.- Continued.

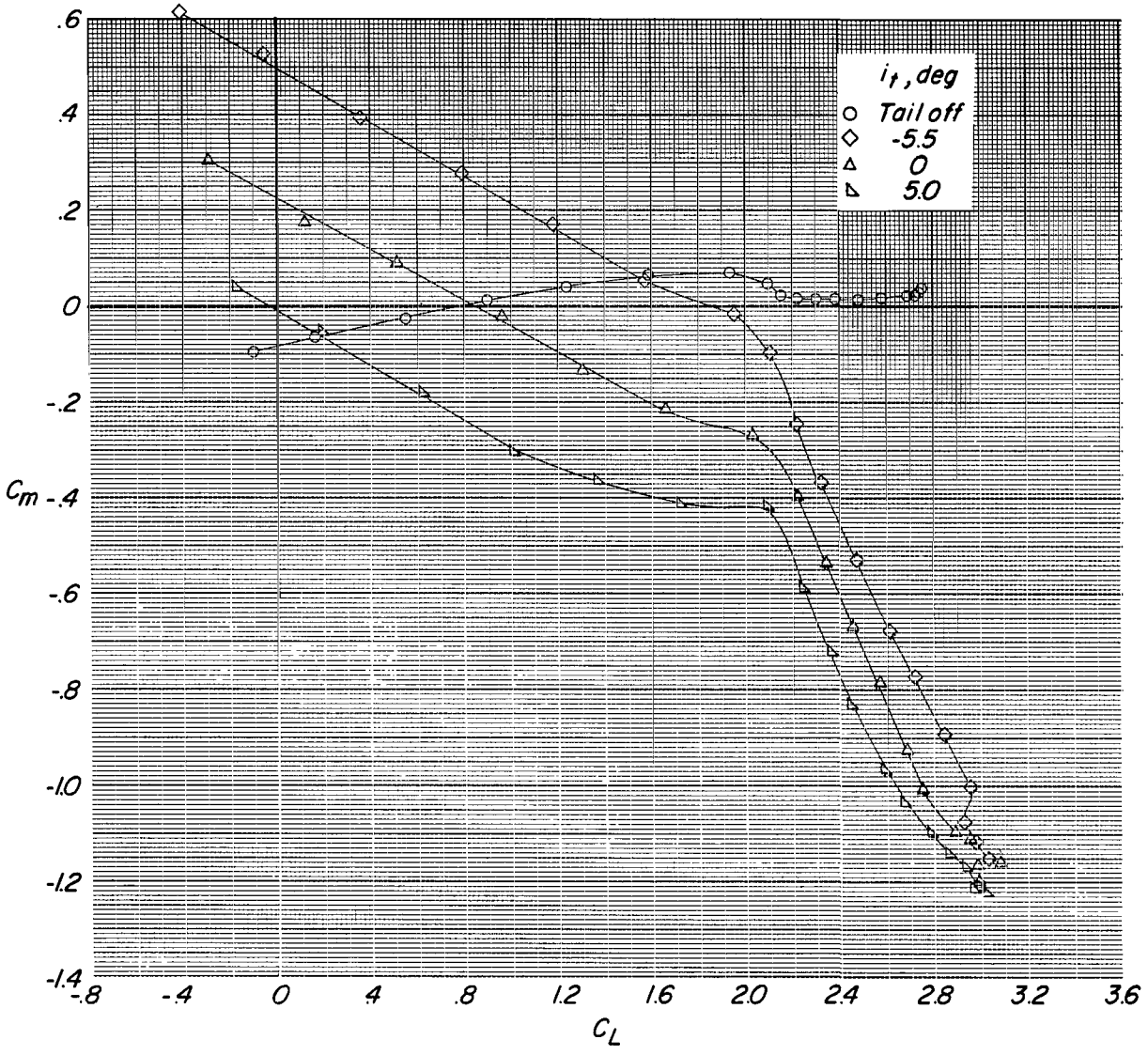

(d) Variation of C_m with C_L.

Figure 11.- Continued.

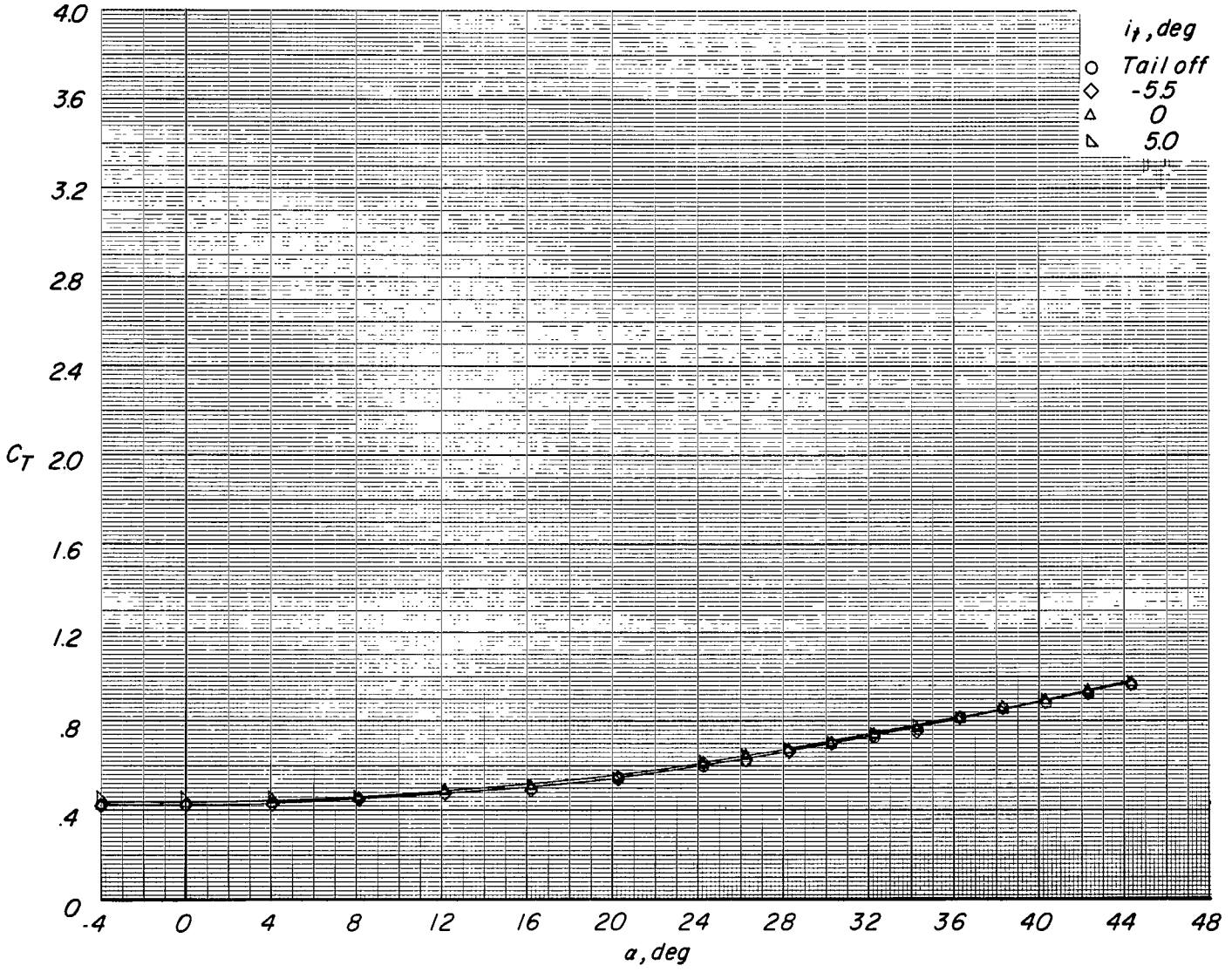

(e) Variation of C_T with α.

Figure 11.- Concluded.

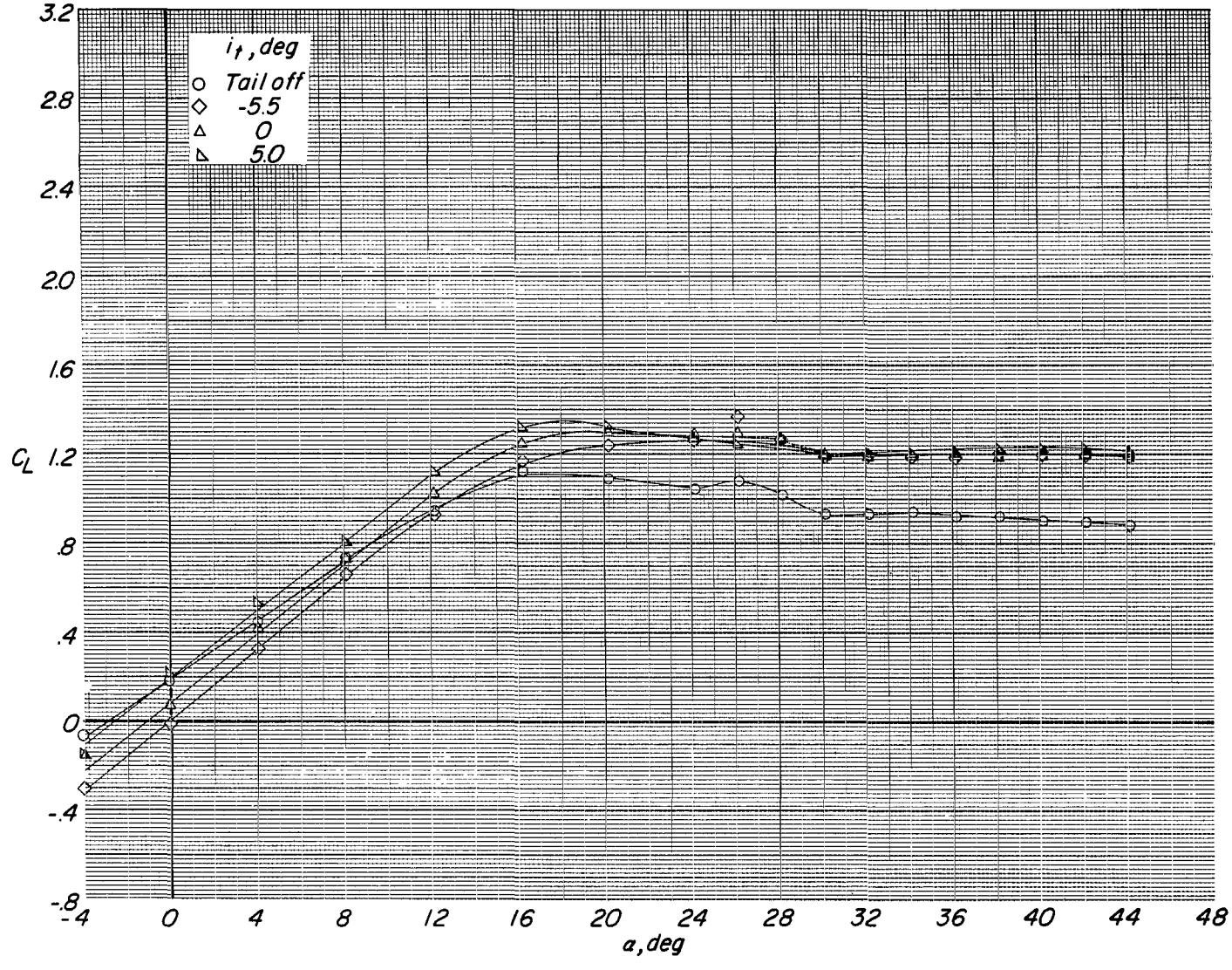

(a) Variation of C_L with α.

Figure 12.- Effect of tail incidence on longitudinal aerodynamic characteristics of configuration with large tail in low position. $\delta_f = 0^0$; $C_T = 0$.

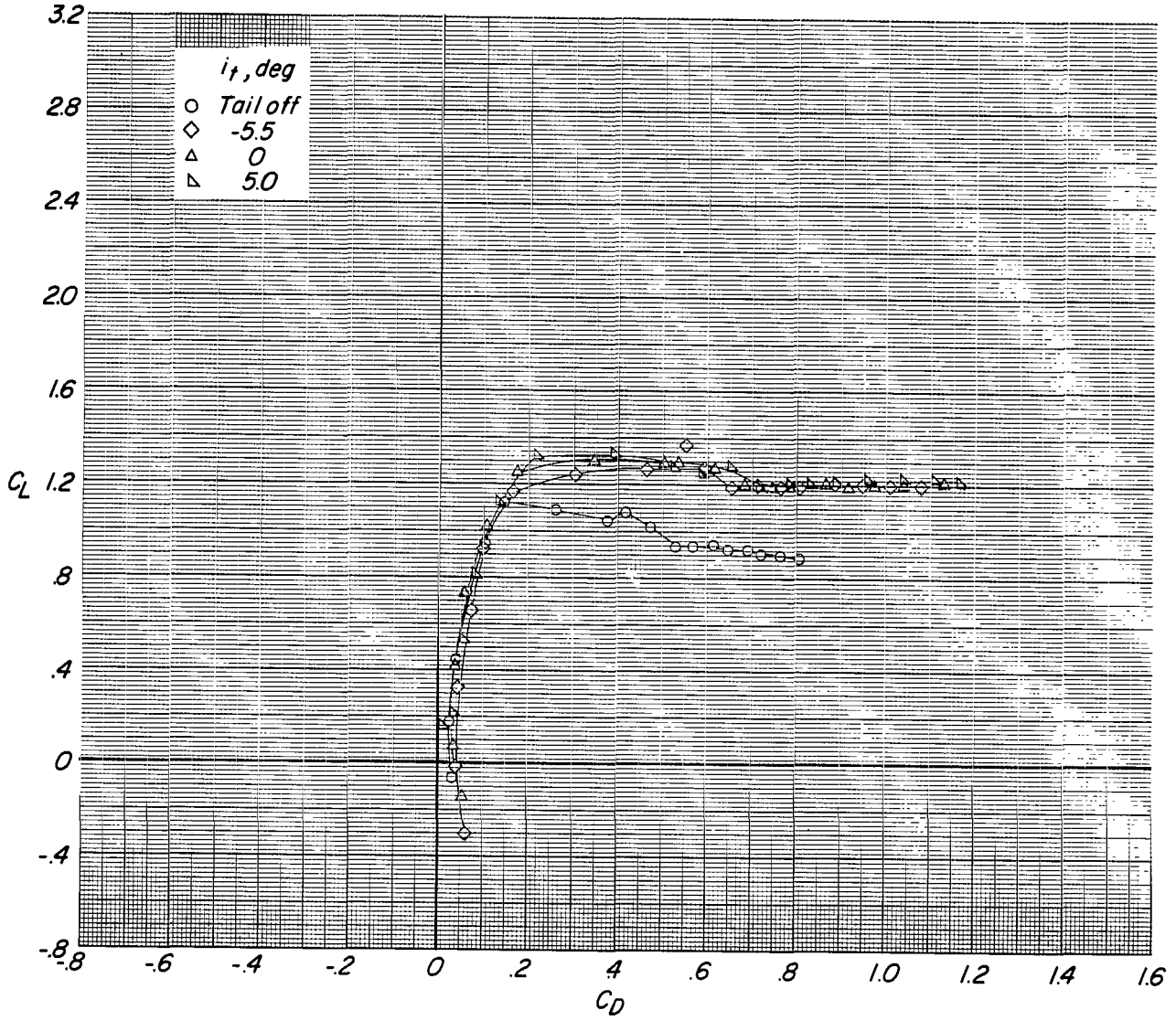

(b) Variation of C_L with C_D.

Figure 12.- Continued.

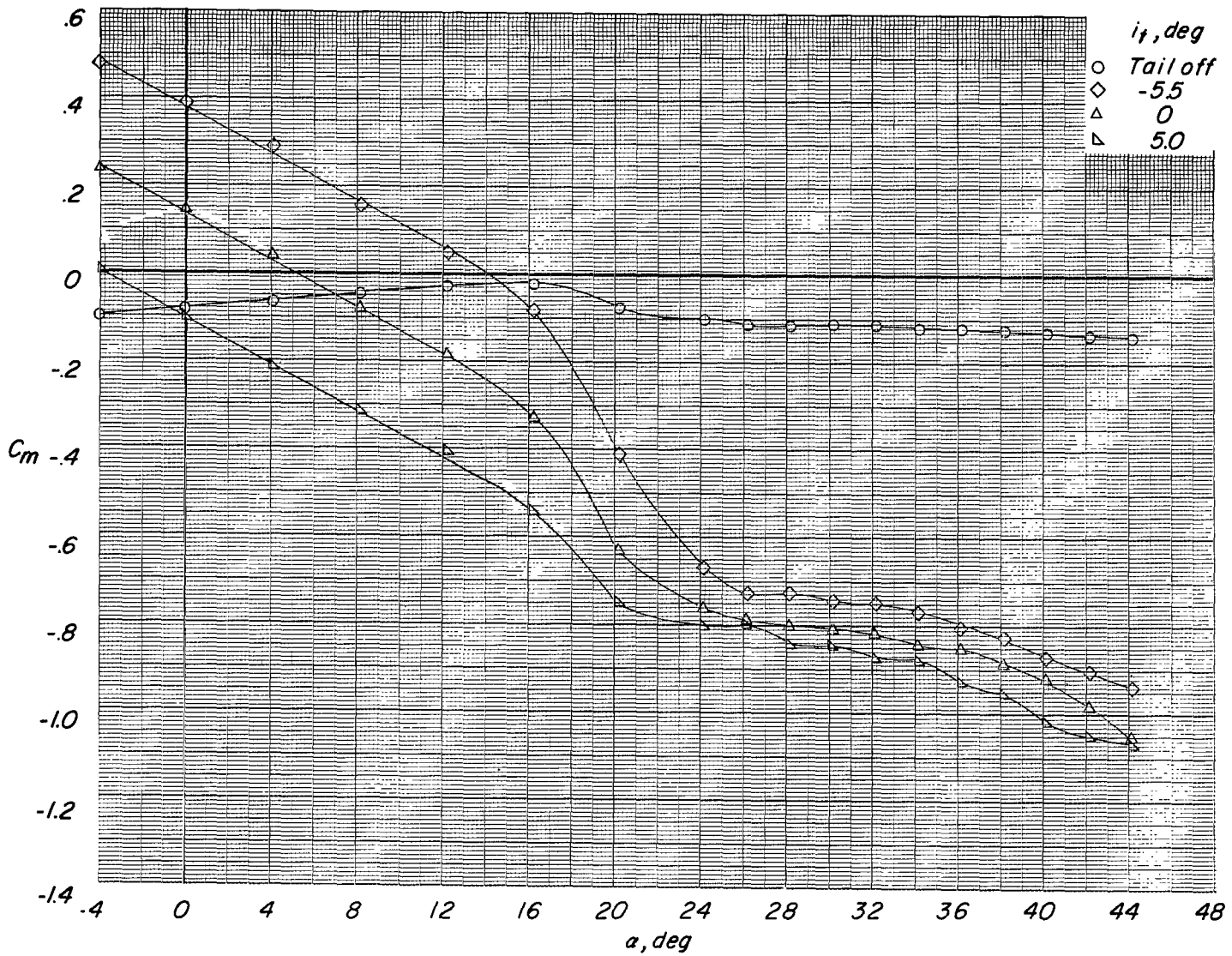

(c) Variation of C_m with α.

Figure 12.- Continued.

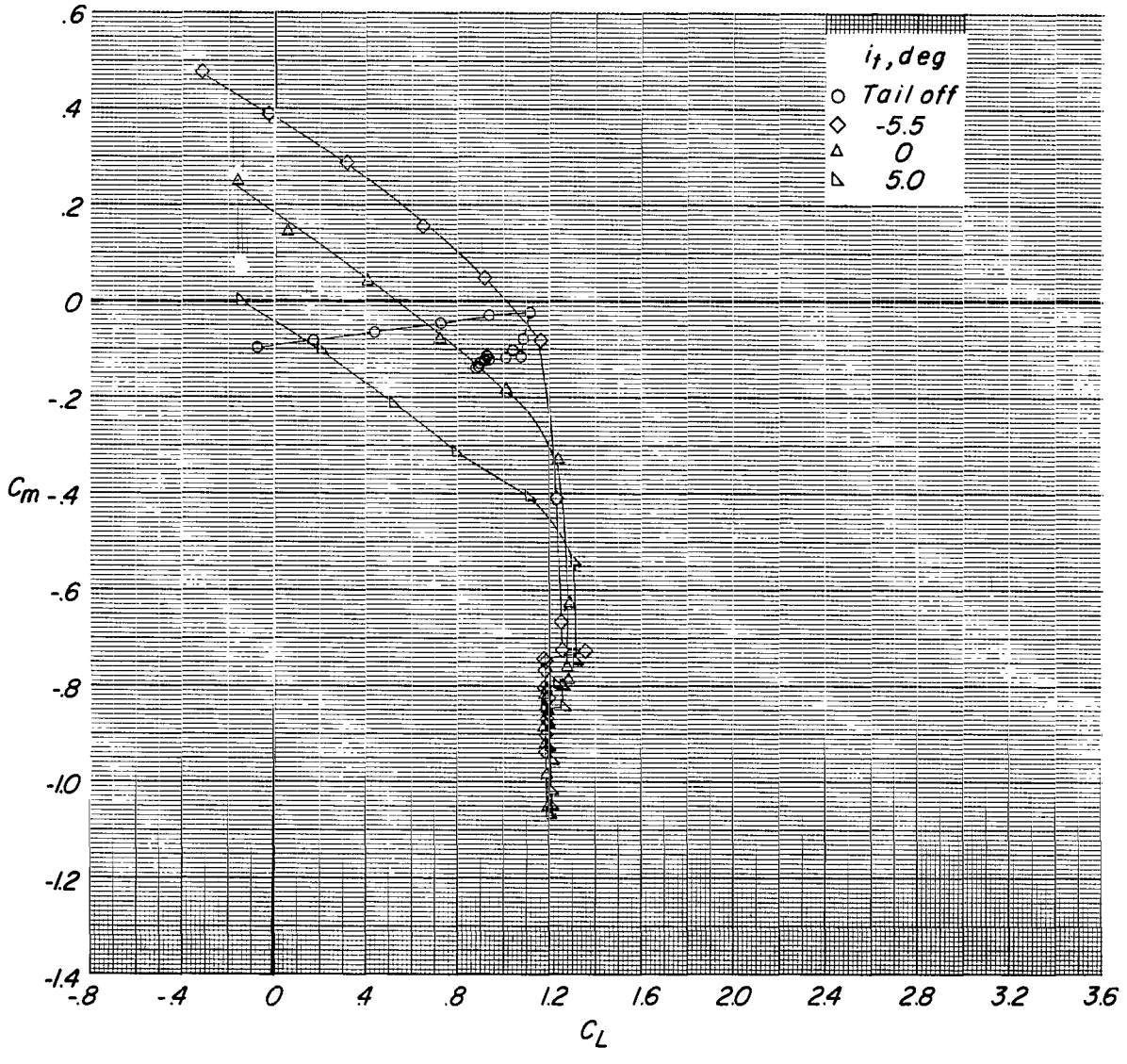

(d) Variation of C_m with C_L.

Figure 12.- Concluded.

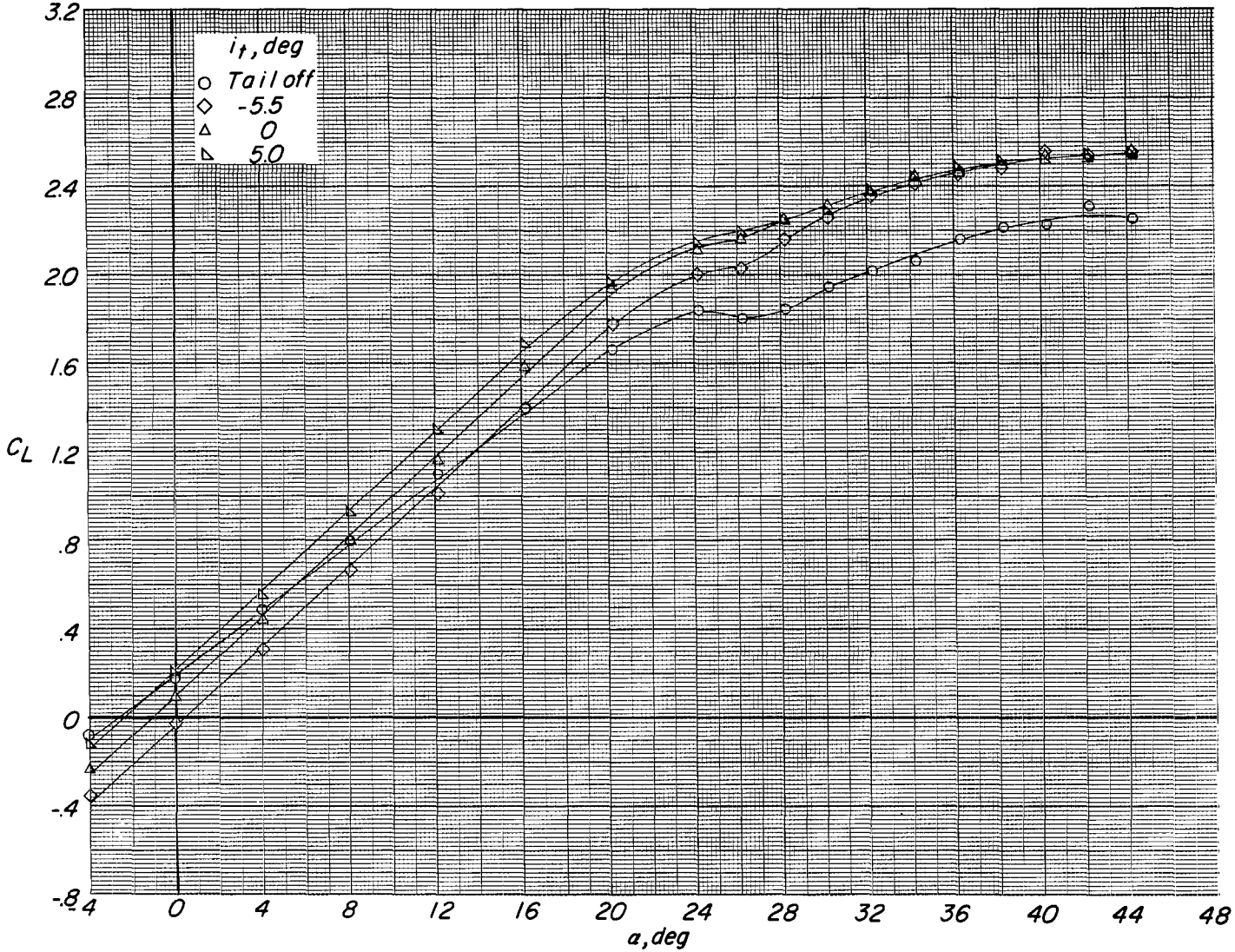

(a) Variation of C_L with α.

Figure 13.- Effect of tail incidence on longitudinal aerodynamic characteristics of configuration with large tail in low position. $\delta_f = 0^o$; reference $C_T = 0.17$.

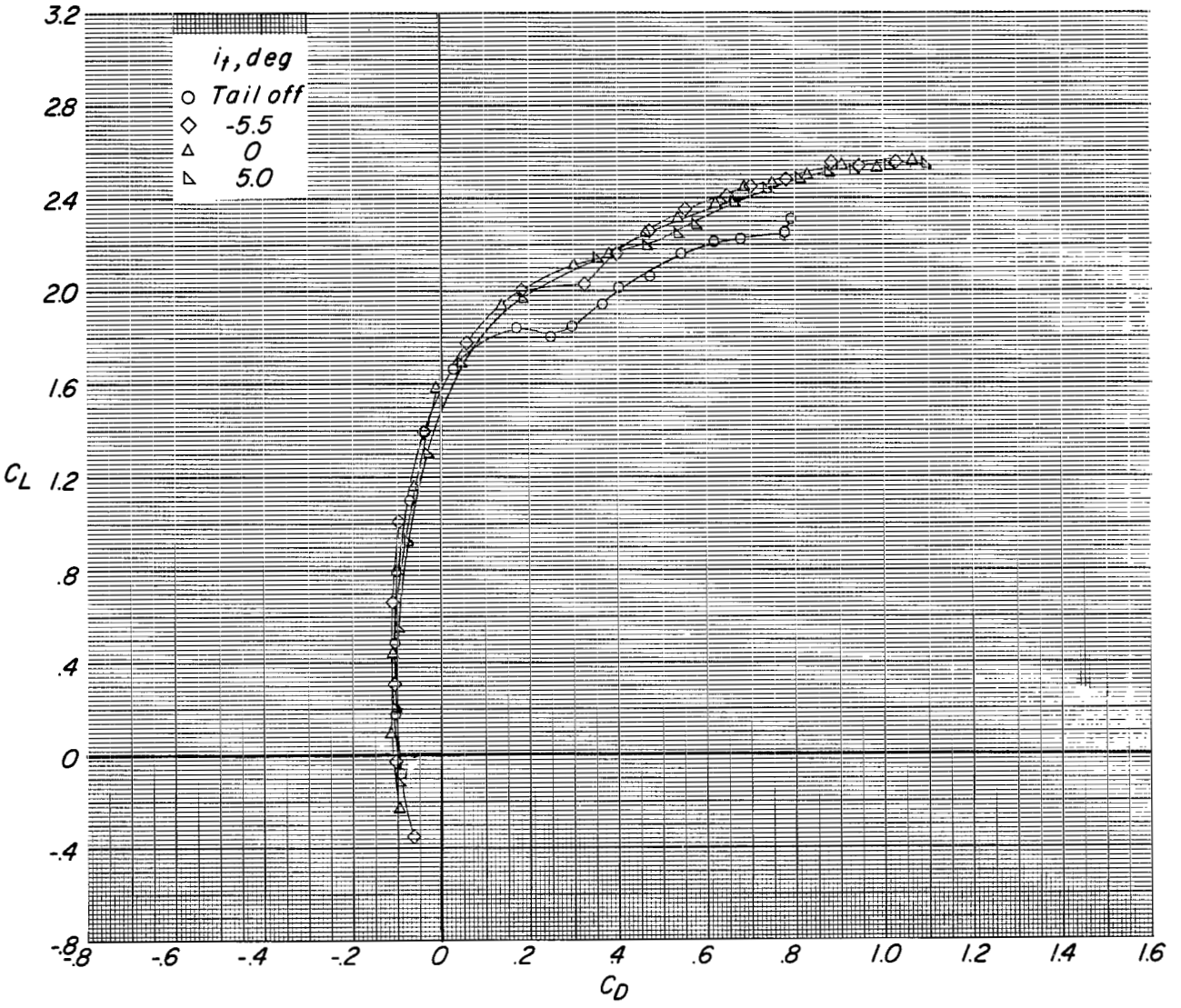

(b) Variation of C_L with C_D.

Figure 13.- Continued.

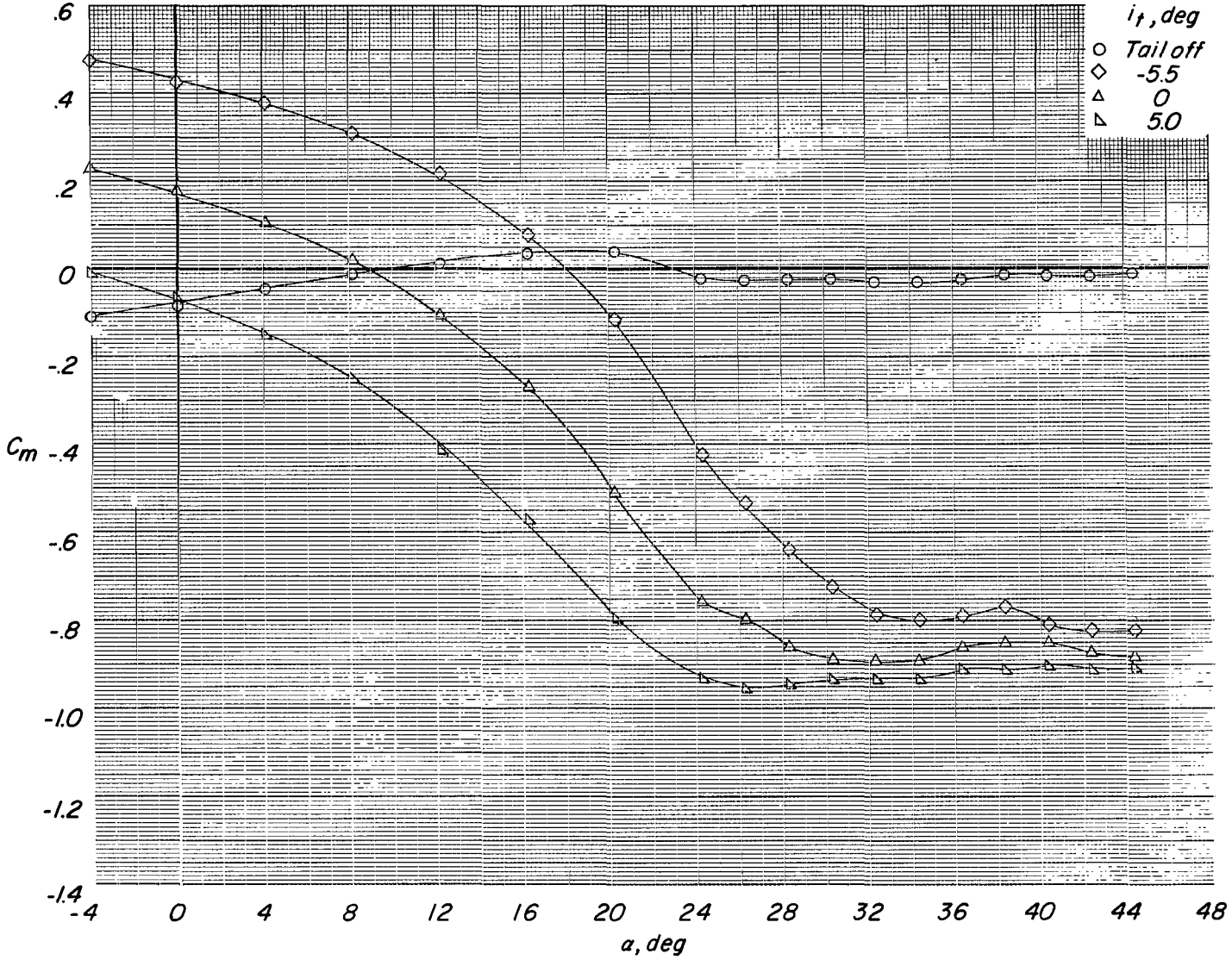

(c) Variation of C_m with α.

Figure 13.- Continued.

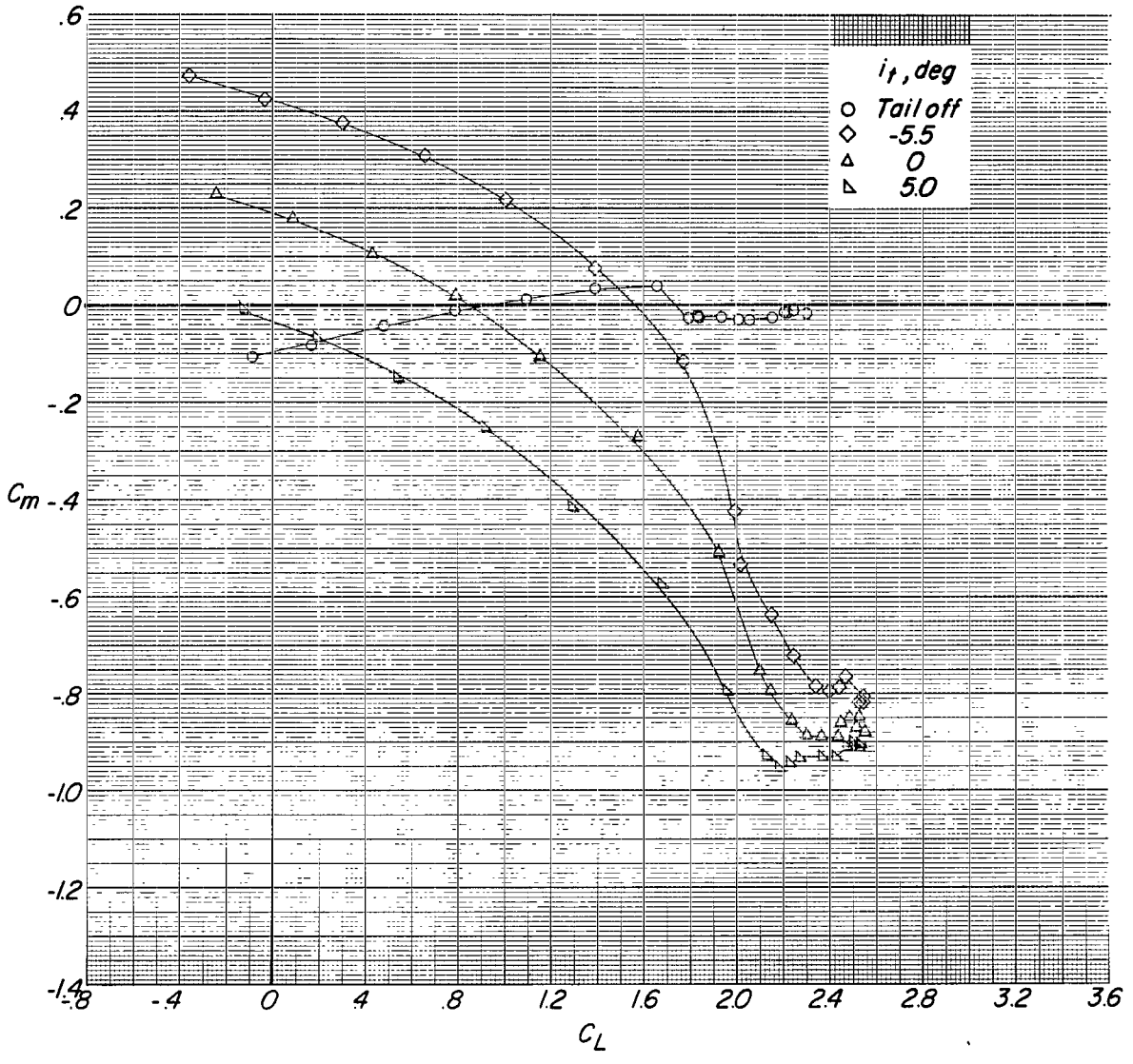

(d) Variation of C_m with C_L.

Figure 13.- Continued.

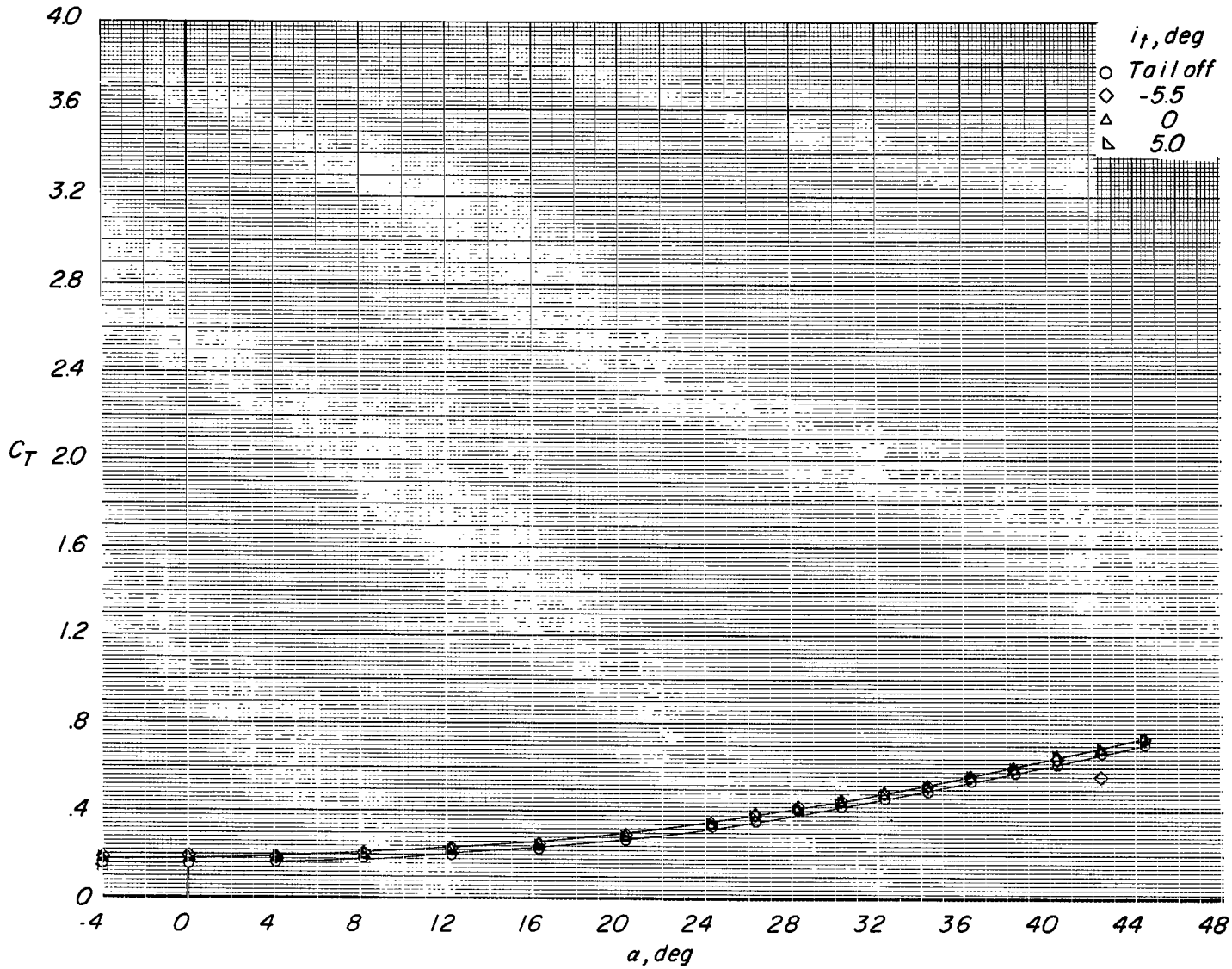

(e) Variation of C_T with α.

Figure 13.- Concluded.

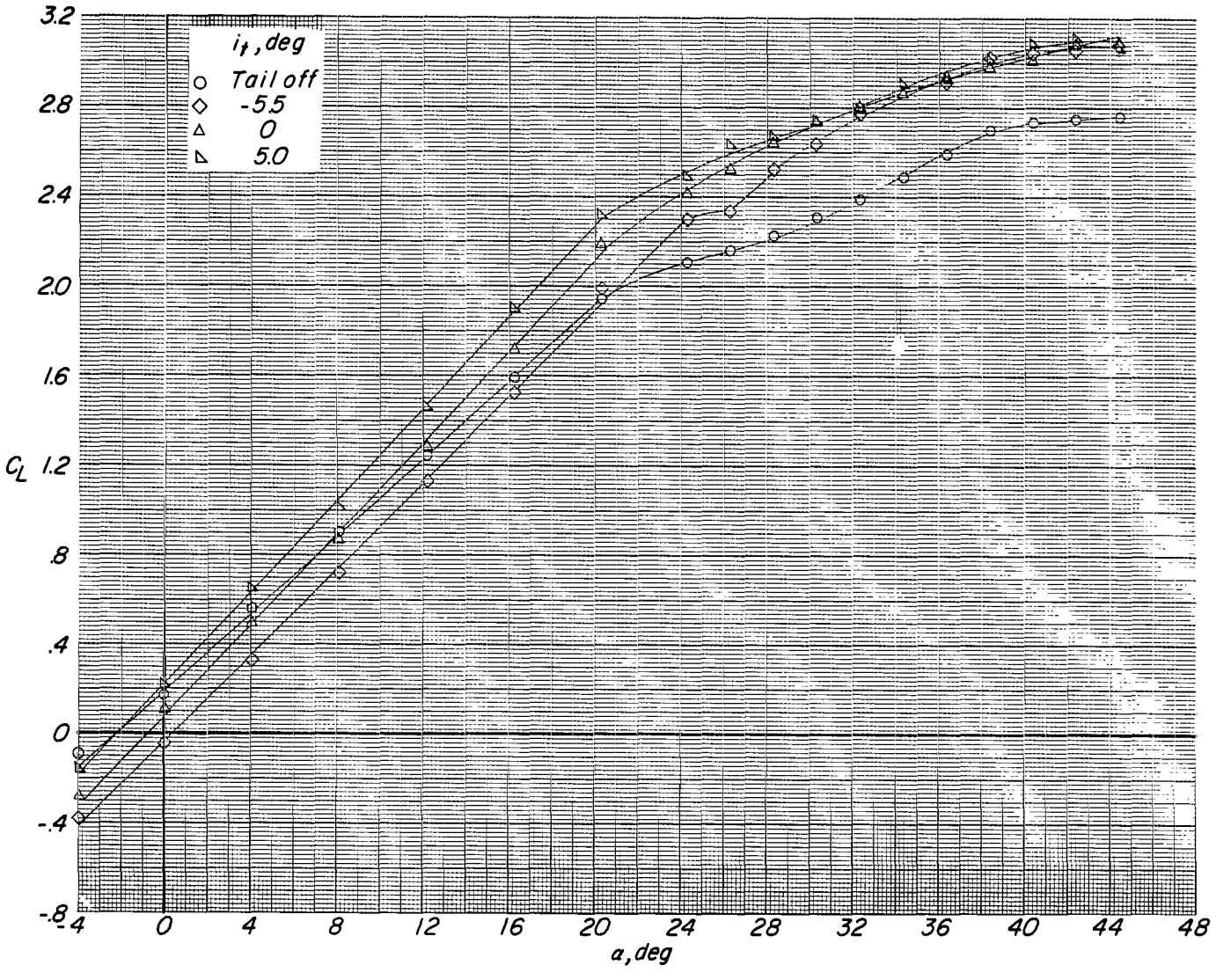

(a) Variation of C_L with α.

Figure 14.- Effect of tail incidence on longitudinal aerodynamic characteristics of configuration with large tail in low position. $\delta_f = 0^0$; reference $C_T = 0.44$.

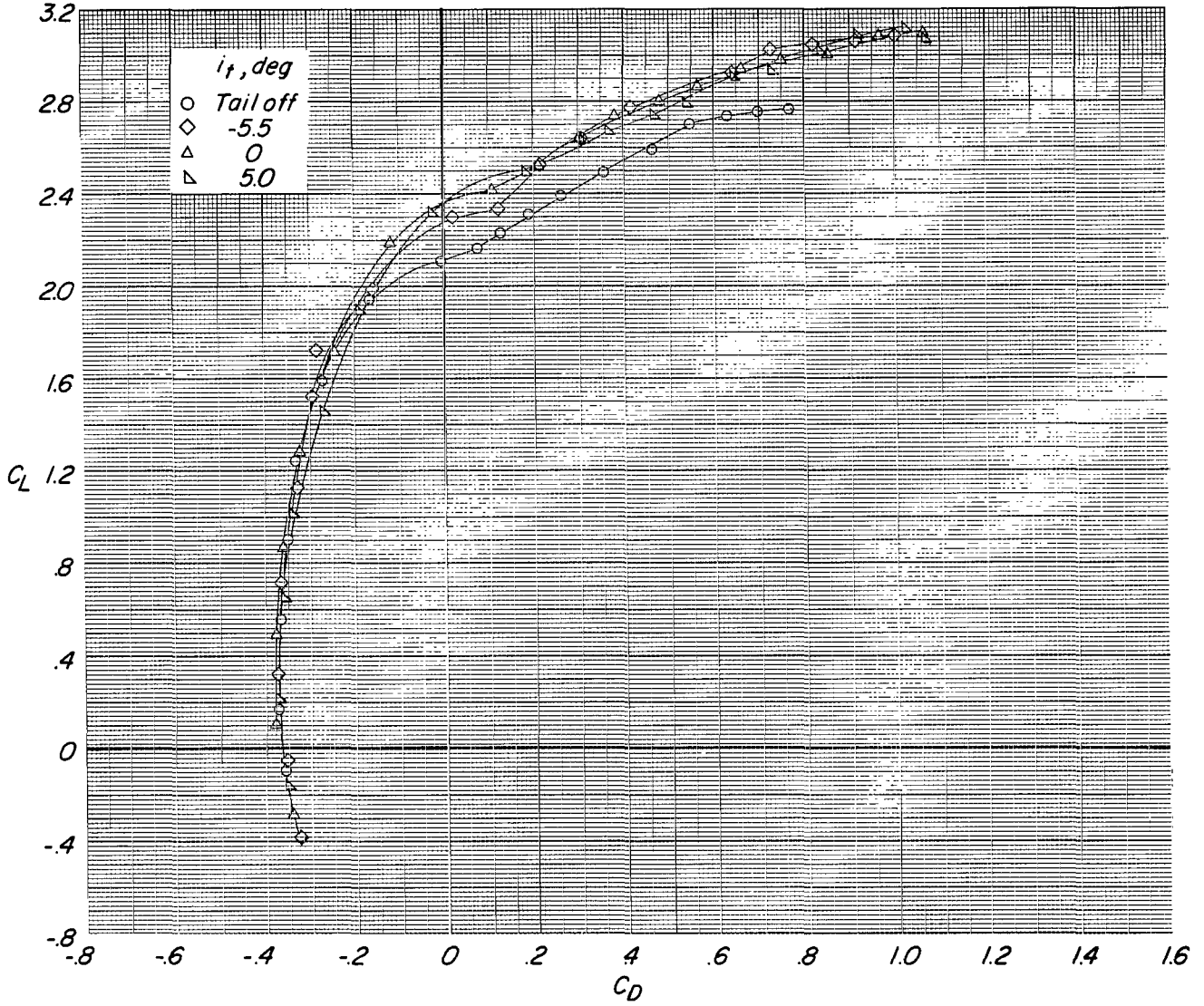

(b) Variation of C_L with C_D.

Figure 14.- Continued.

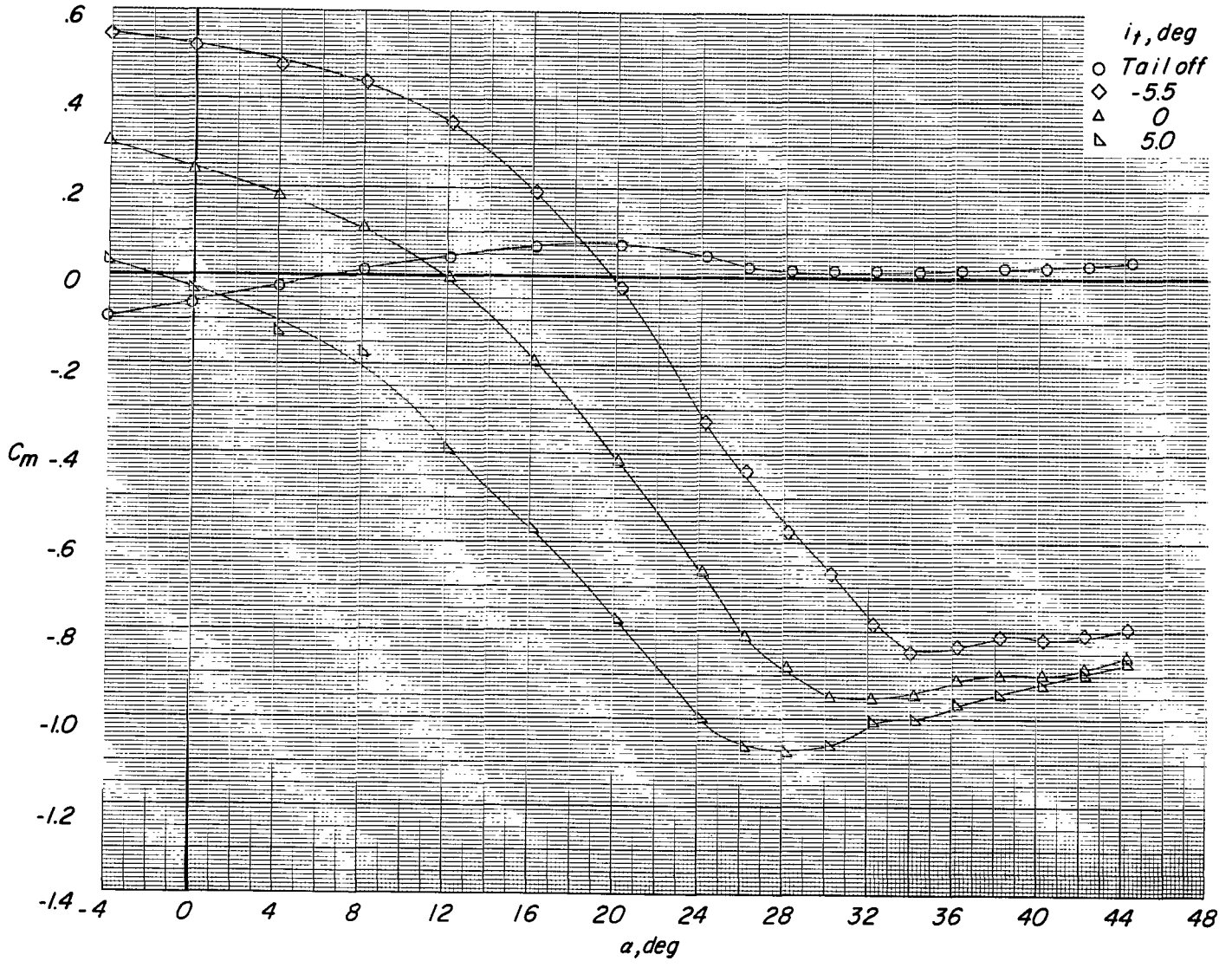

(c) Variation of C_m with α.

Figure 14.- Continued.

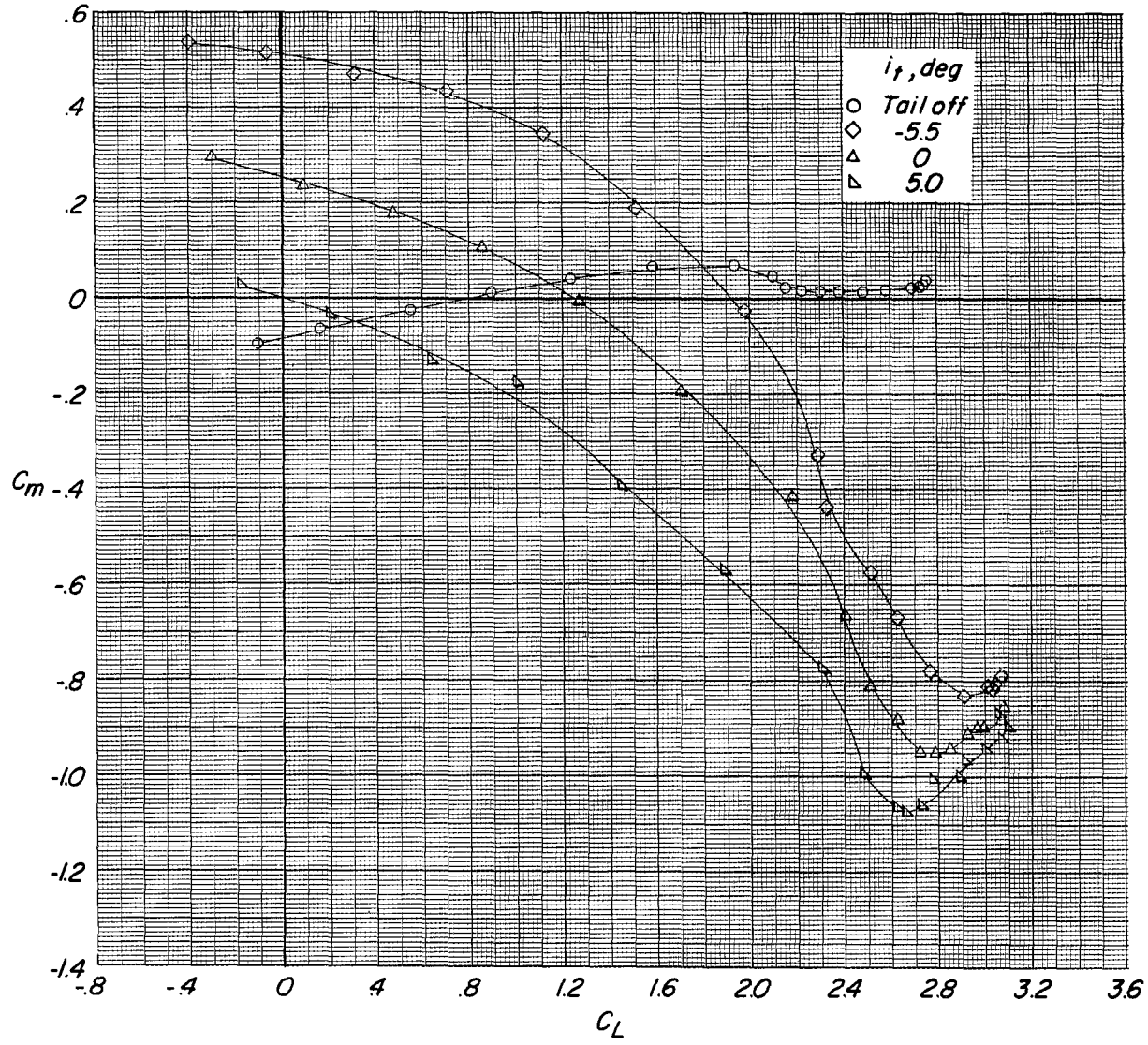

(d) Variation of C_m with C_L.

Figure 14.- Continued.

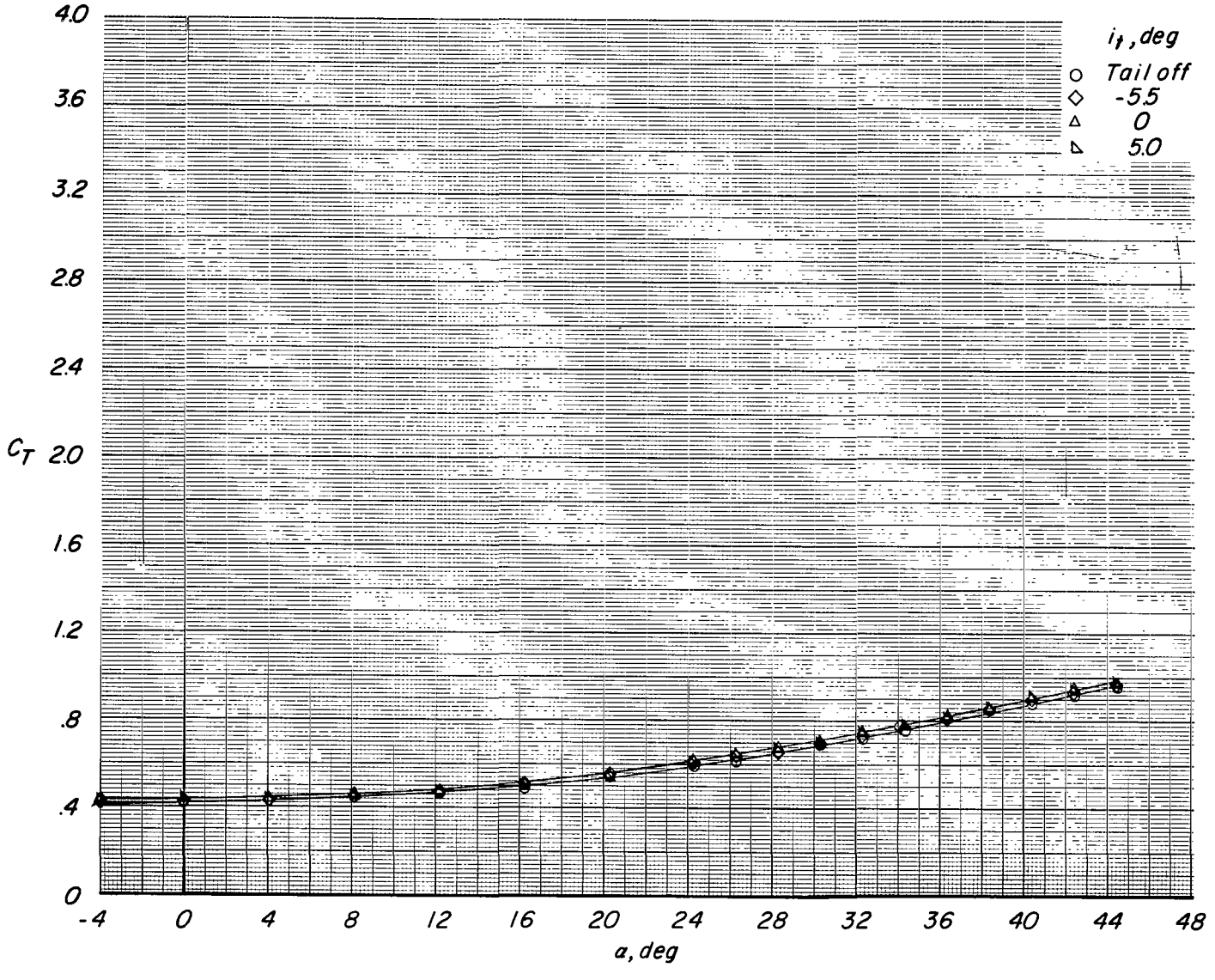

(e) Variation of C_T with α.

Figure 14.- Concluded.

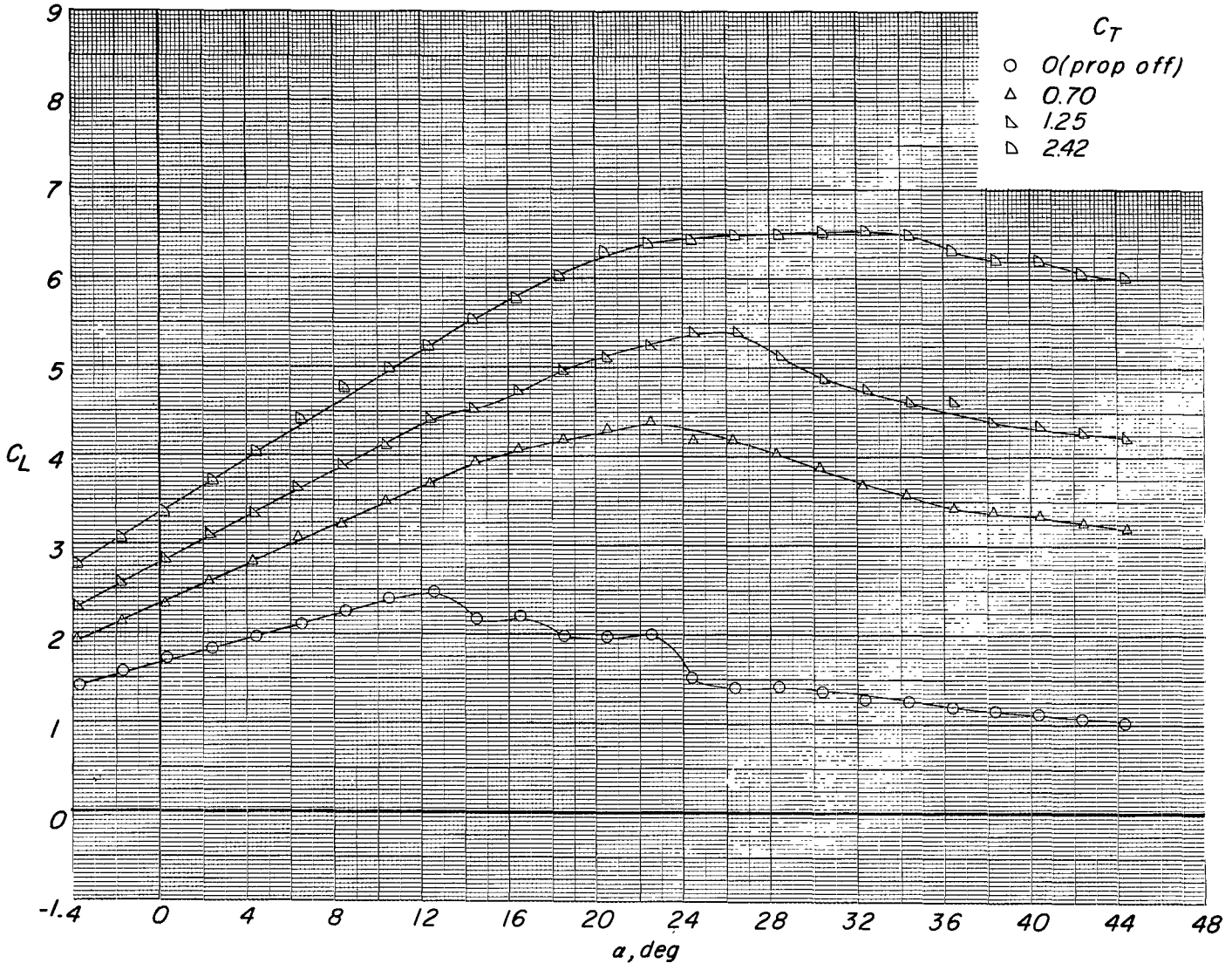

(a) Variation of C_L with α.

Figure 15.- Effect of propeller thrust coefficient (in terms of reference C_T) on longitudinal aerodynamic characteristics of flaps-deflected ($\delta_f = 45^0$) configuration with tail off.

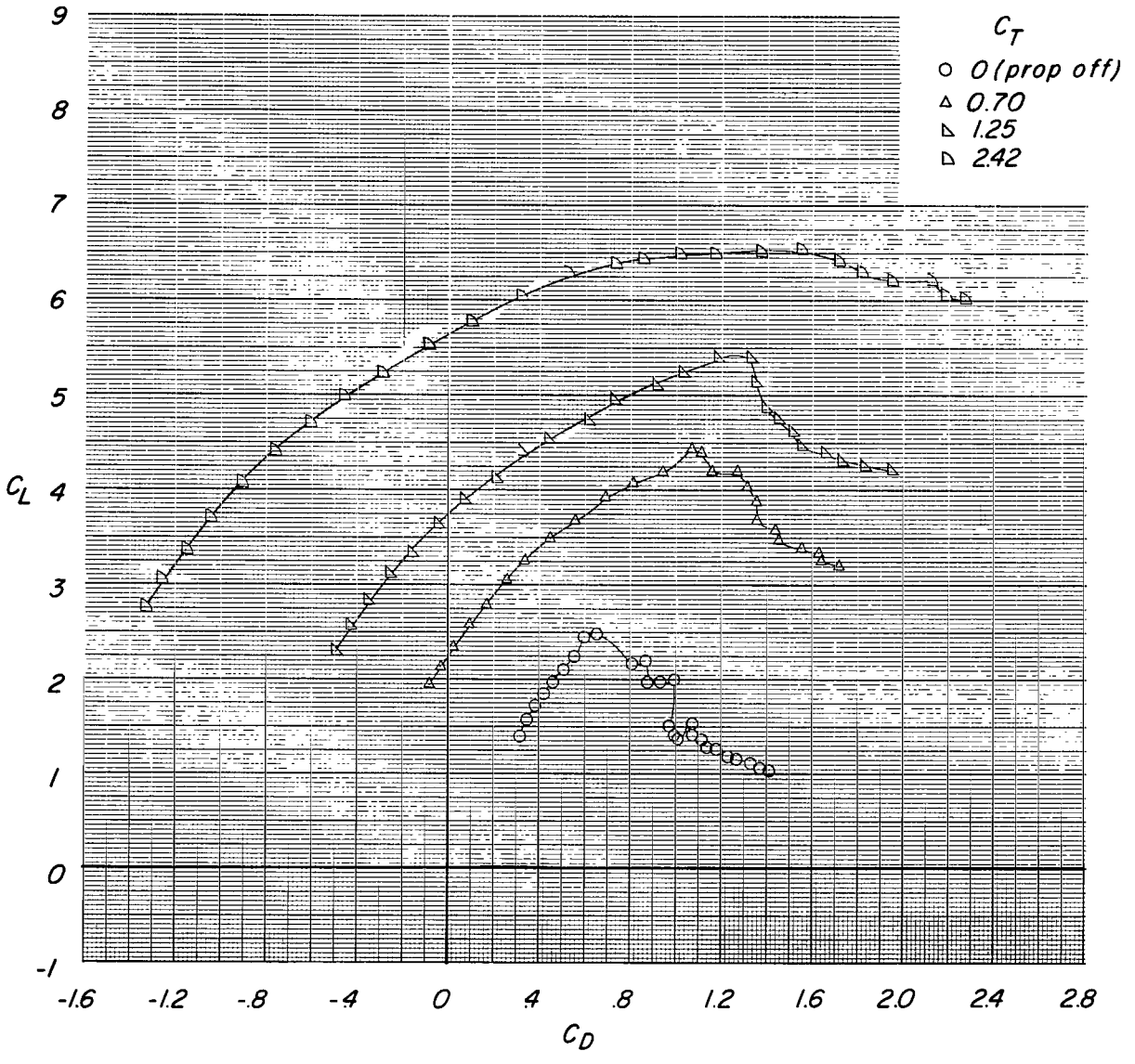

(b) Variation of C_L with C_D.

Figure 15.- Continued.

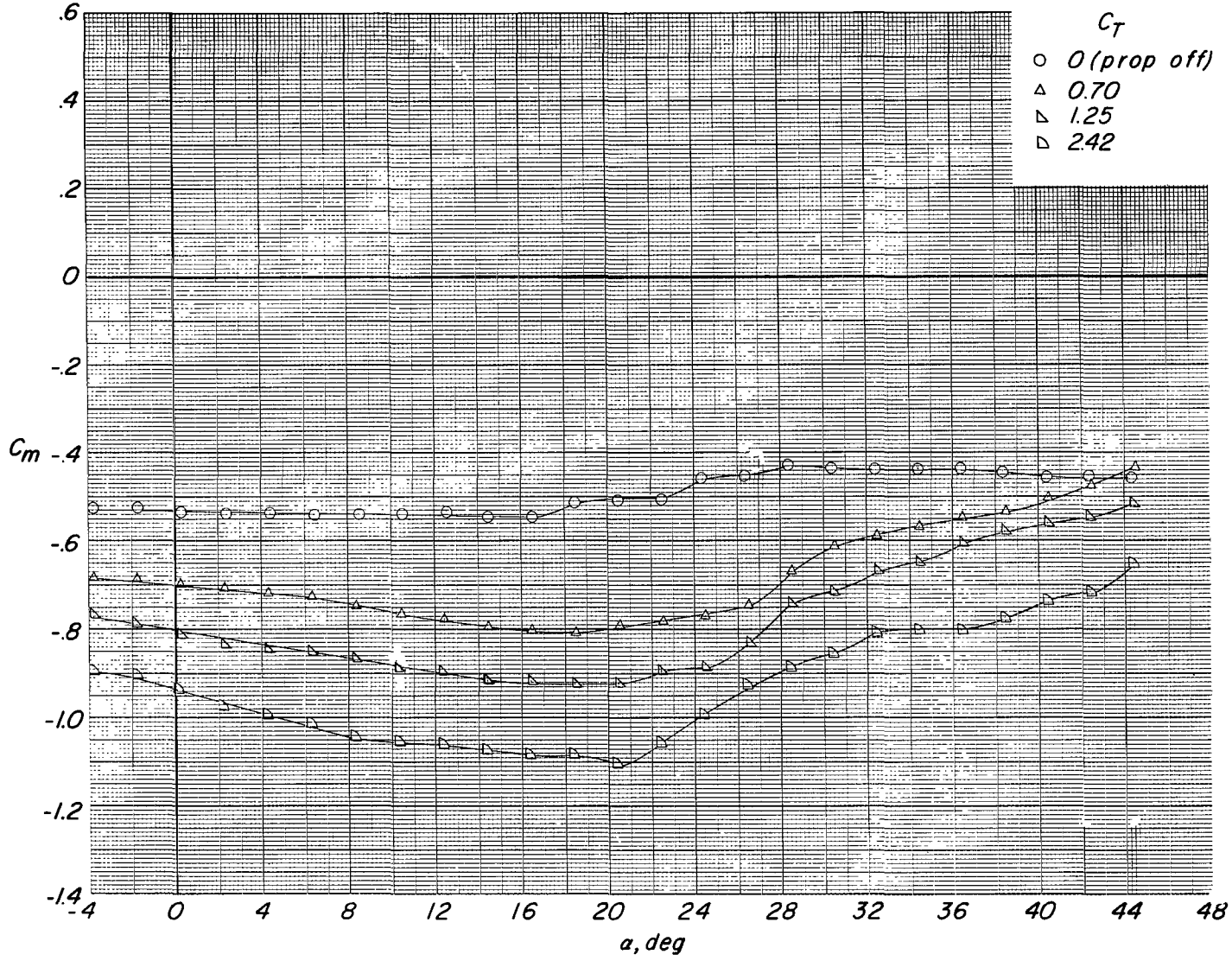

(c) Variation of C_m with α.

Figure 15.- Continued.

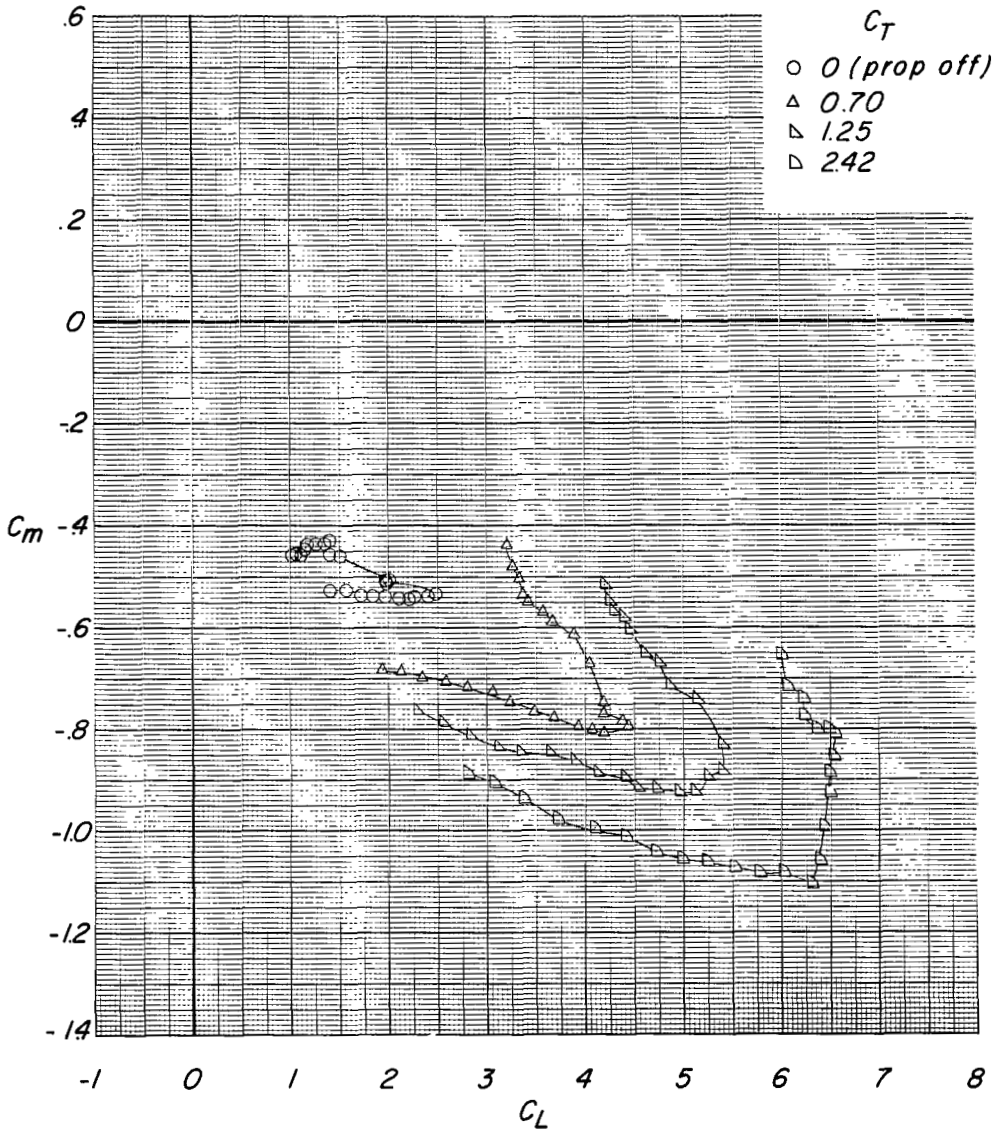

(d) Variation of C_m with C_L.

Figure 15.- Continued.

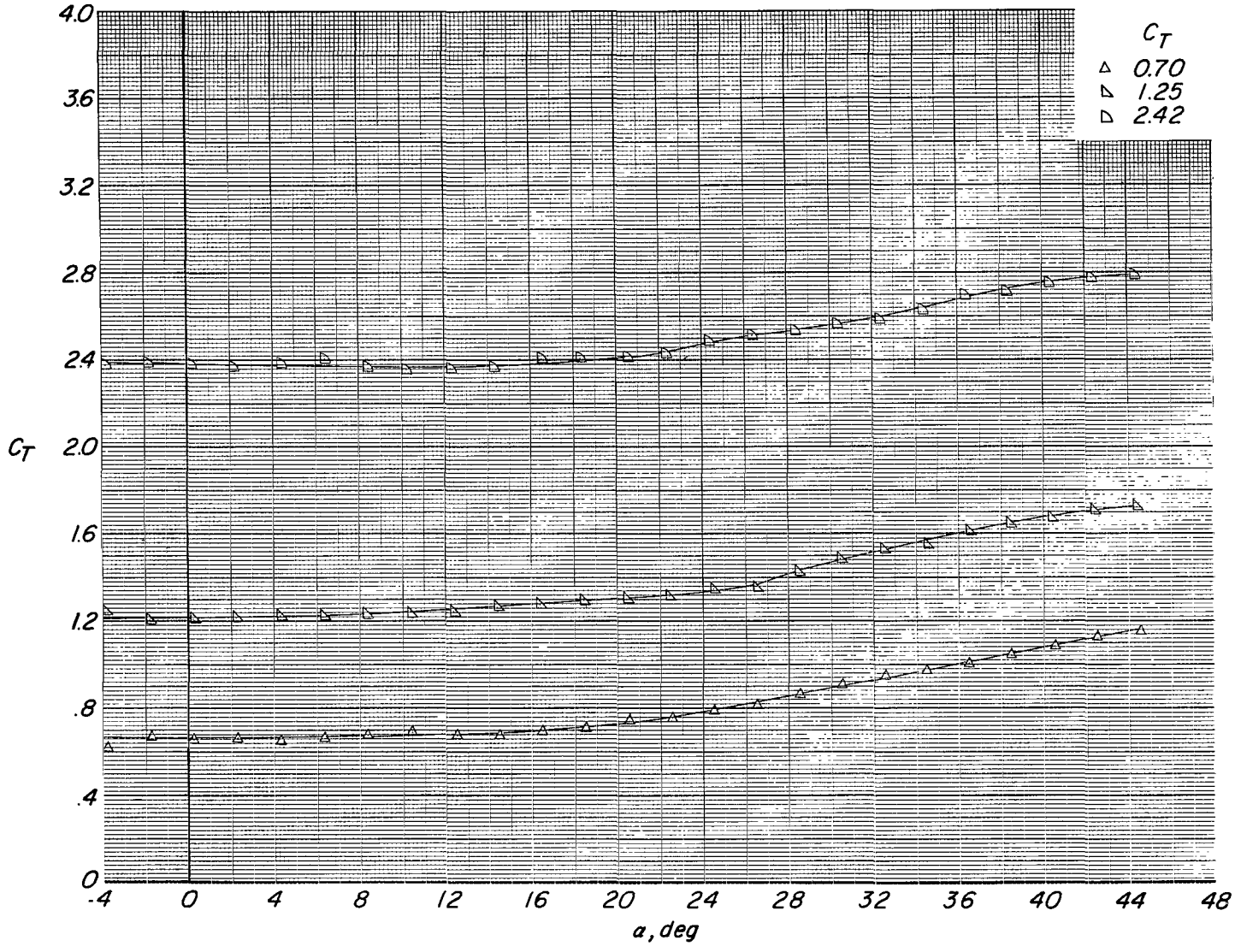

(e) Variation of C_T with α.

Figure 15.- Concluded.

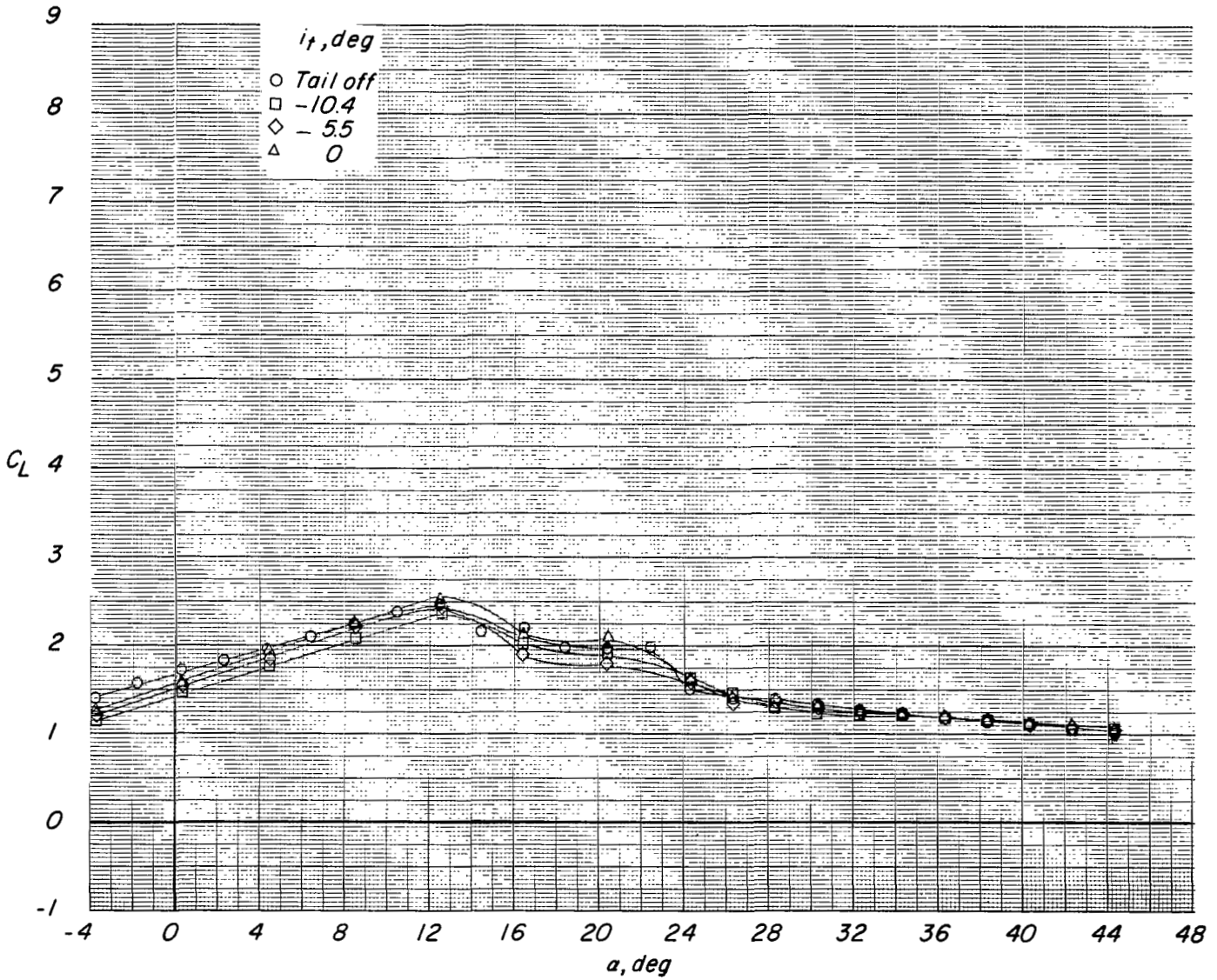

(a) Variation of C_L with α.

Figure 16.- Effect of tail incidence on longitudinal aerodynamic characteristics of configuration with small tail in high position. $\delta_f = 45^0$; $C_T = 0$.

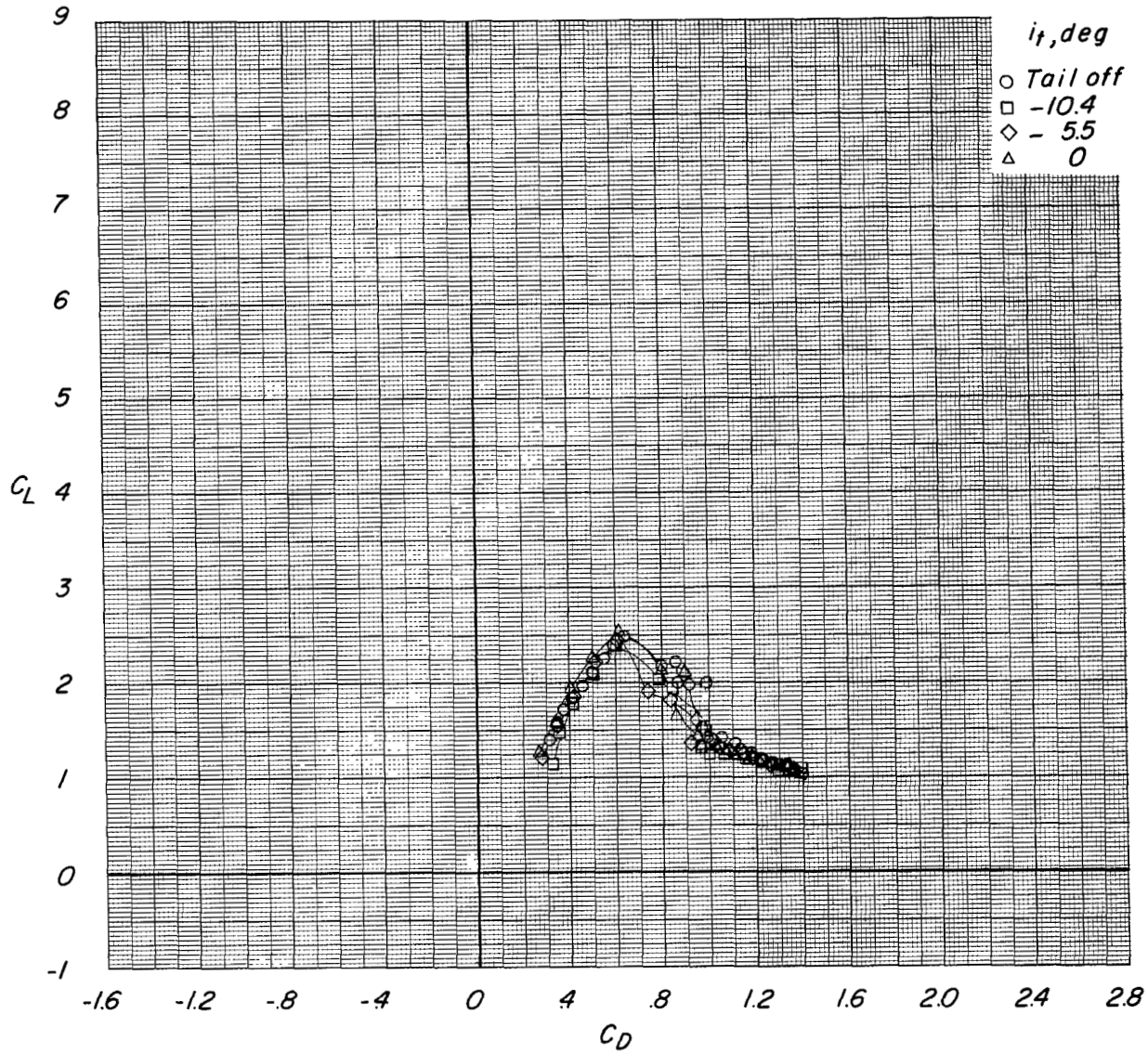

(b) Variation of C_L with C_D.

Figure 16.- Continued.

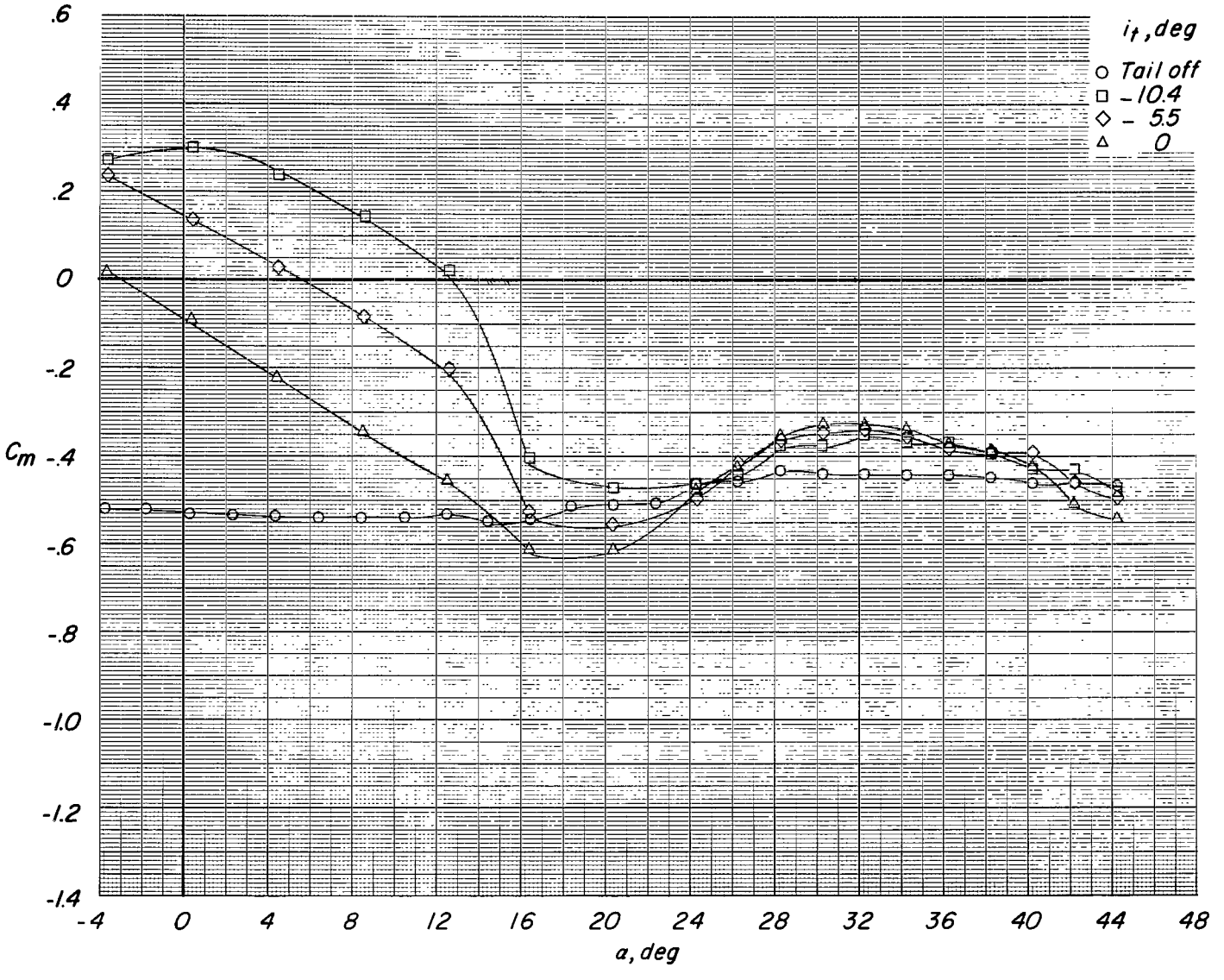

(c) Variation of C_m with α.

Figure 16.- Continued.

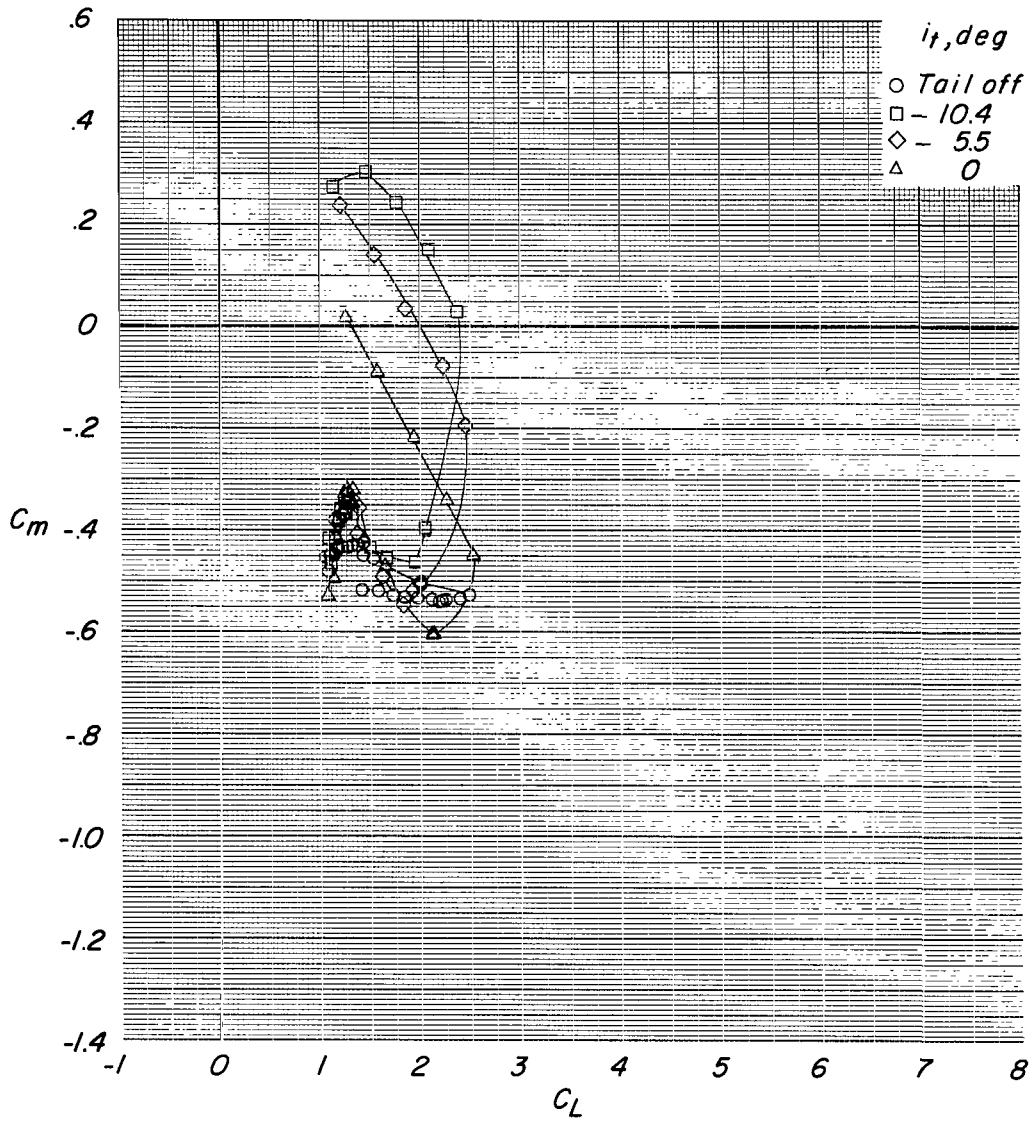

(d) Variation of C_m with C_L.

Figure 16.- Concluded.

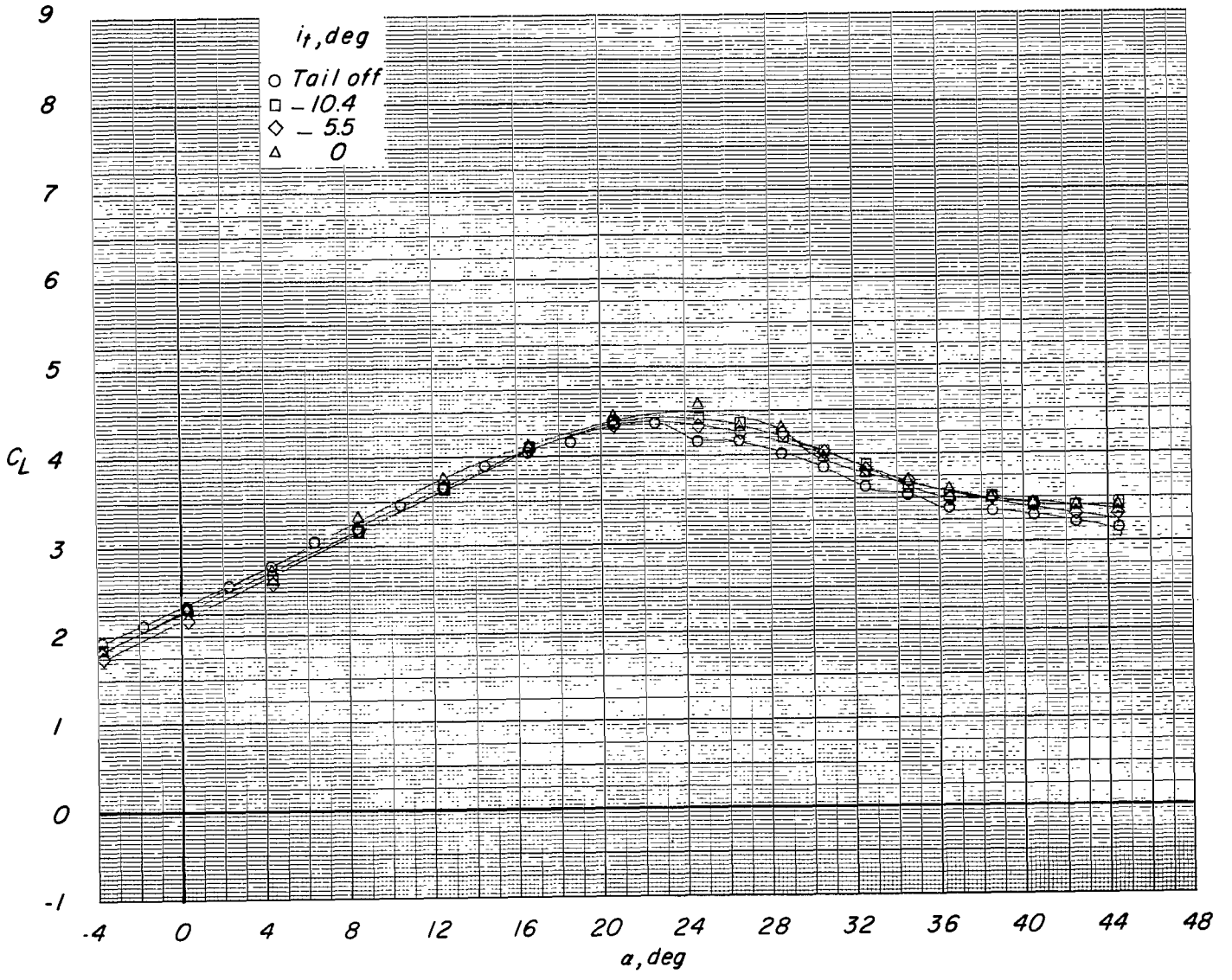

(a) Variation of C_L with α.

Figure 17.- Effect of tail incidence on longitudinal aerodynamic characteristics of configuration with small tail in high position. $\delta_f = 45^0$; reference $C_T = 0.70$.

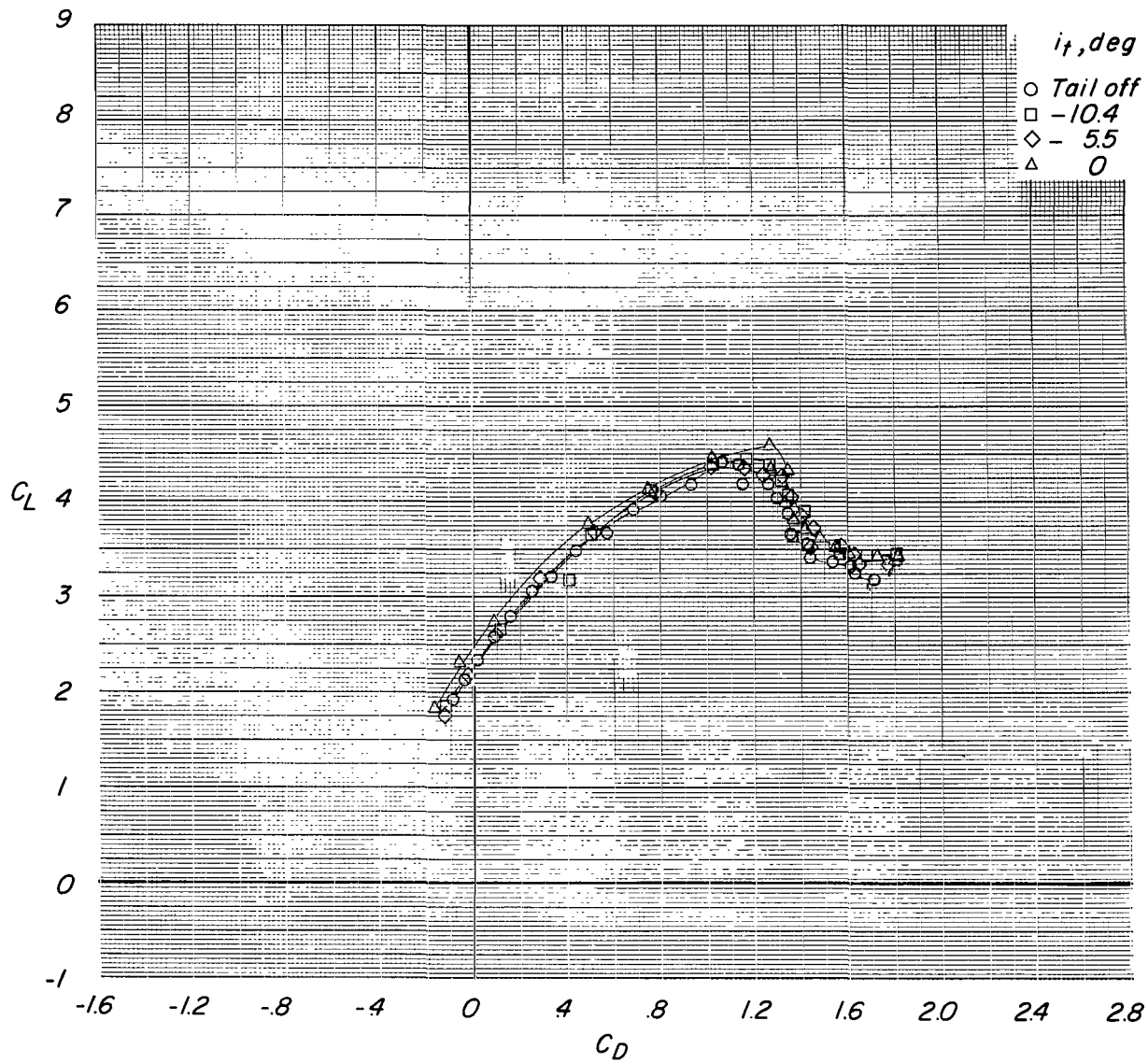

(b) Variation of C_L with C_D.

Figure 17.- Continued.

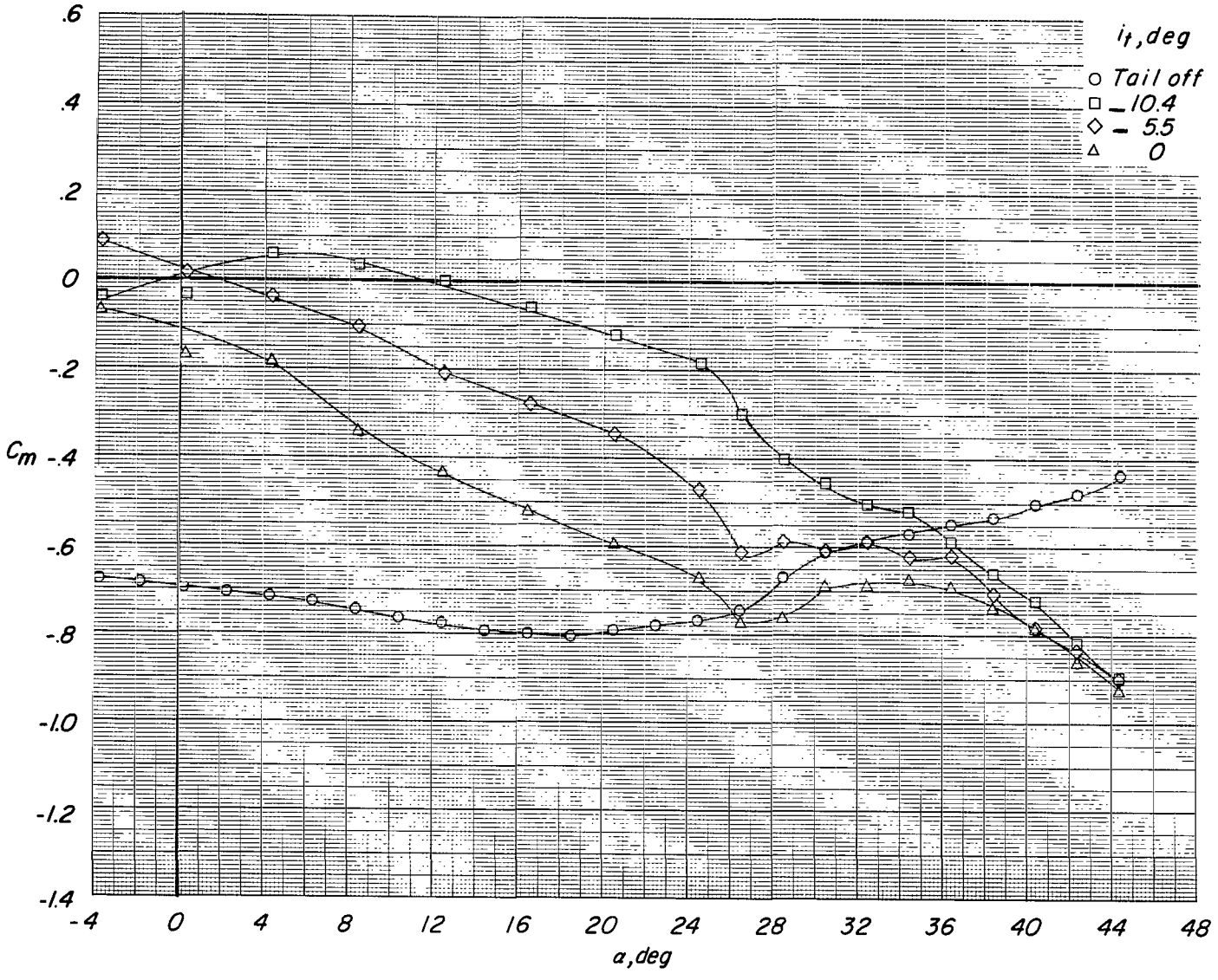

(c) Variation of C_m with α.

Figure 17.- Continued.

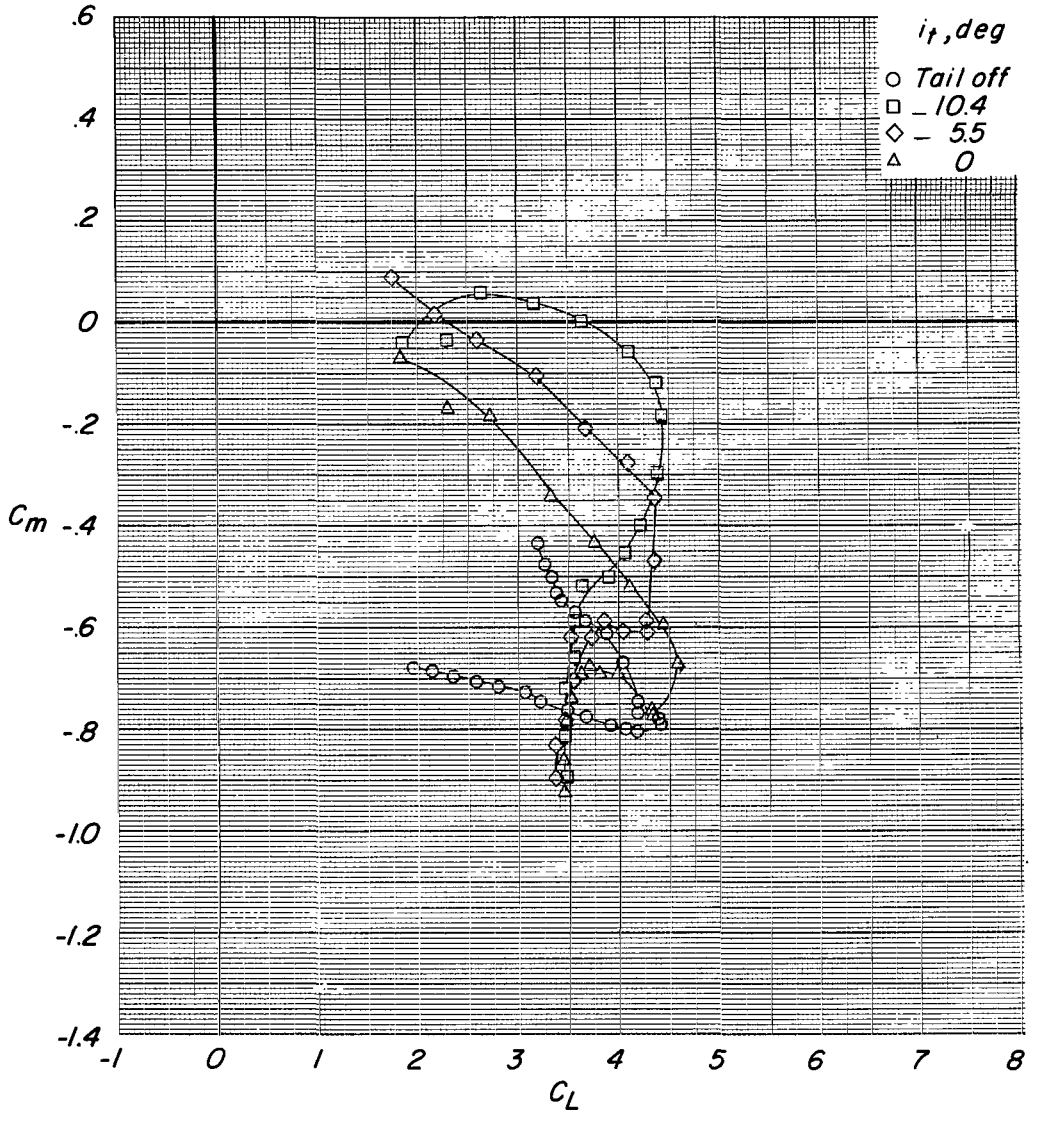

(d) Variation of C_m with C_L.

Figure 17.- Continued.

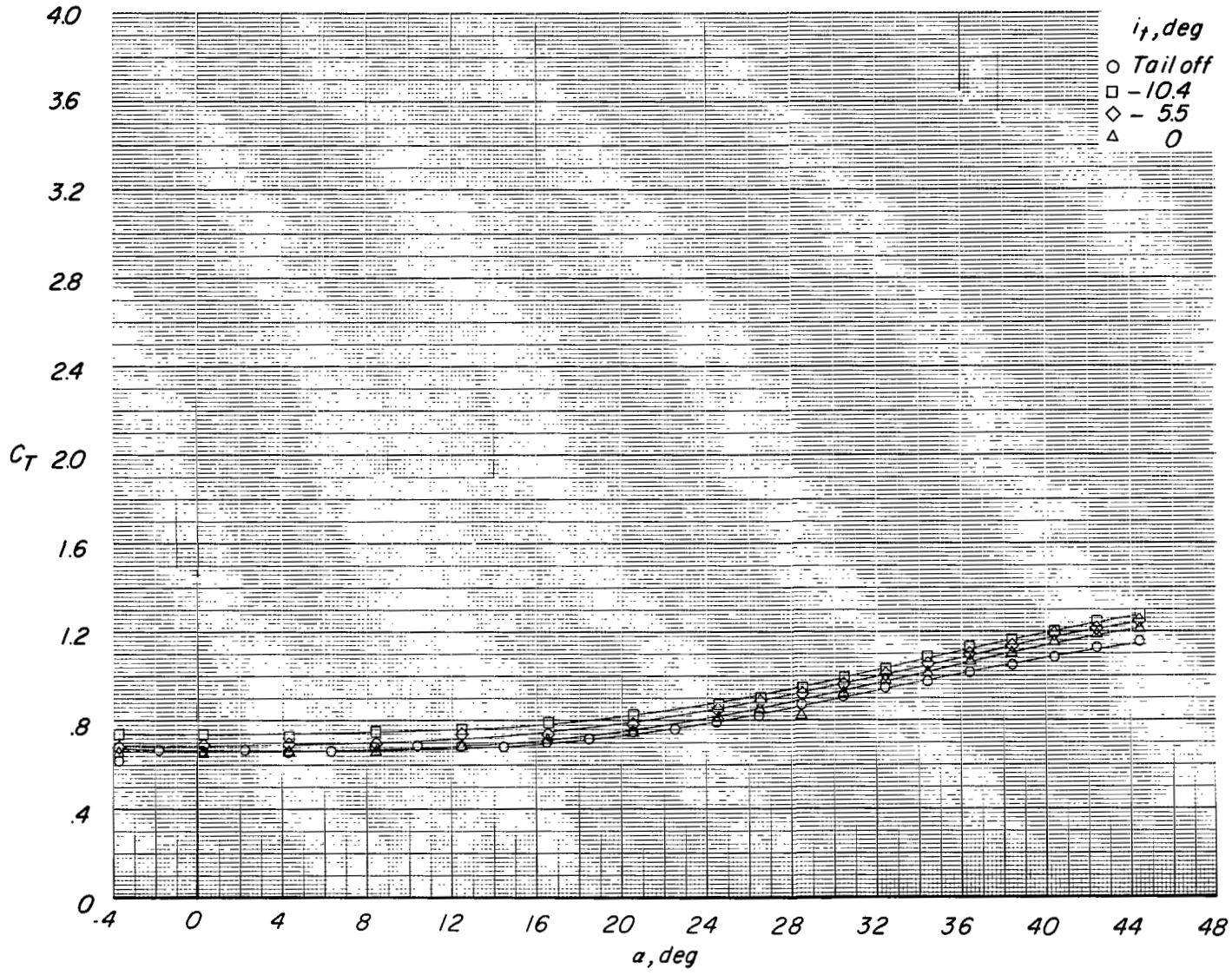

(e) Variation of C_T with α.

Figure 17.- Concluded.

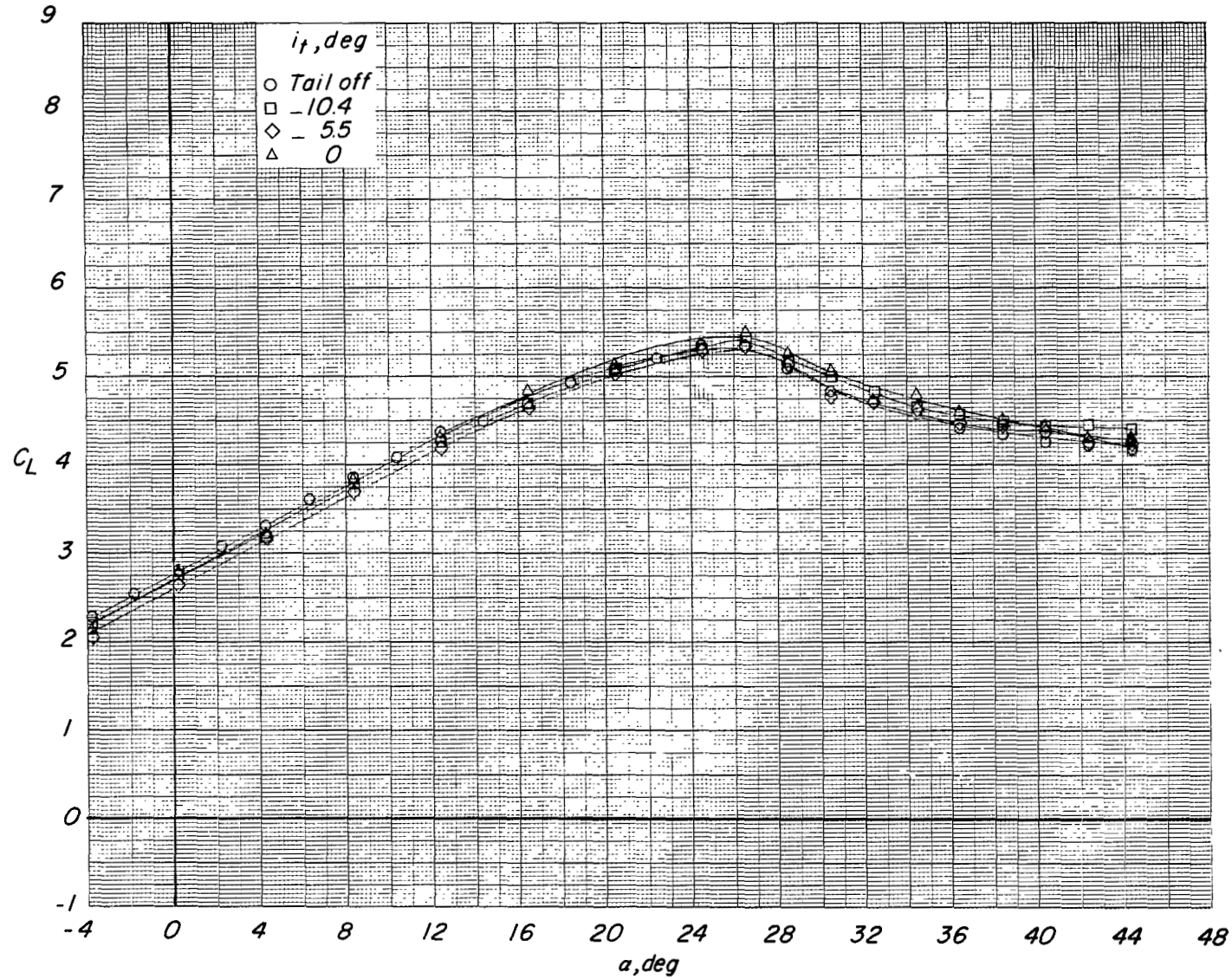

(a) Variation of C_L with α.

Figure 18.- Effect of tail incidence on longitudinal aerodynamic characteristics of configuration with small tail in high position. $\delta_f = 45^0$; reference $C_T = 1.25$.

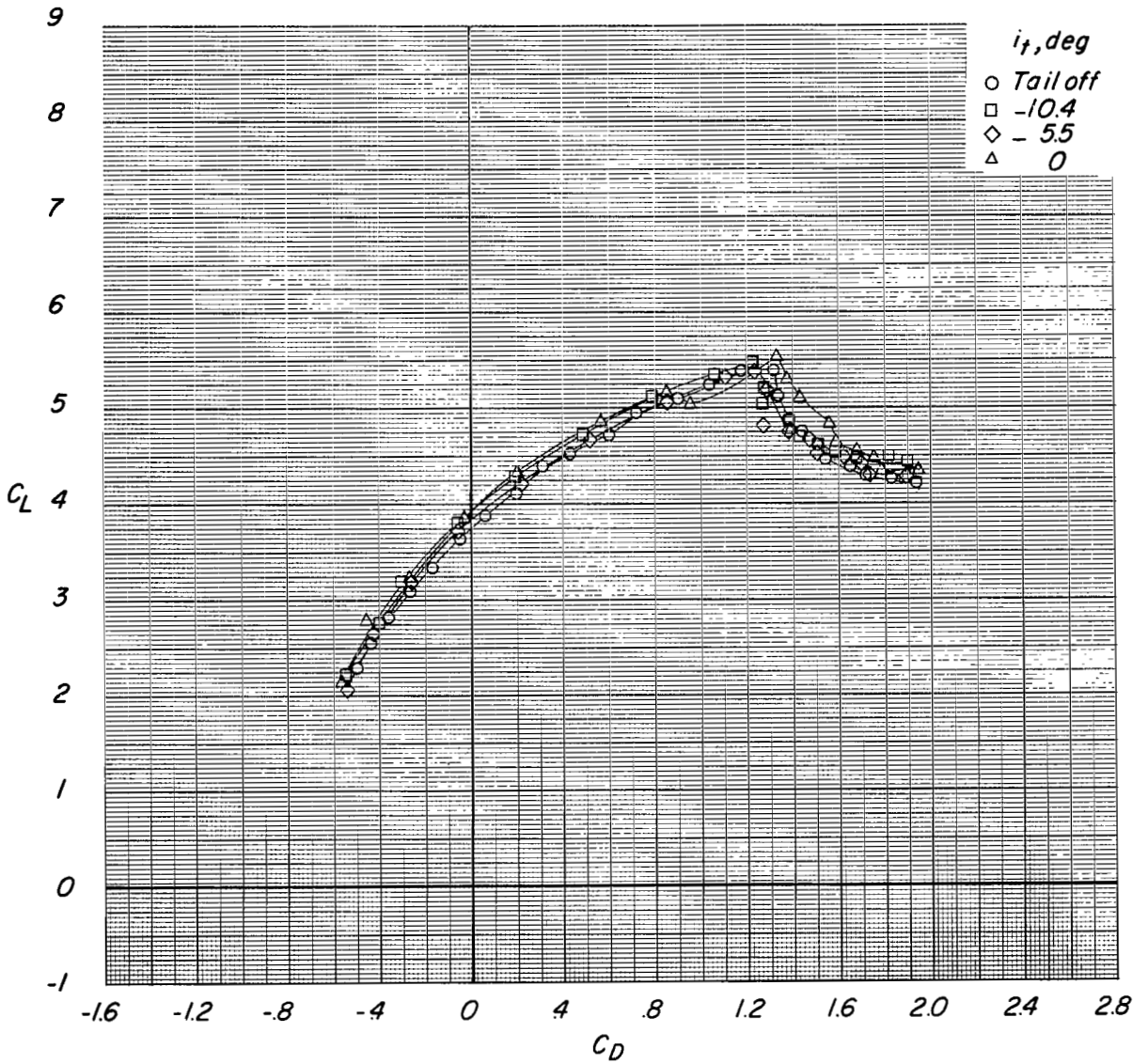

(b) Variation of C_L with C_D.

Figure 18.- Continued.

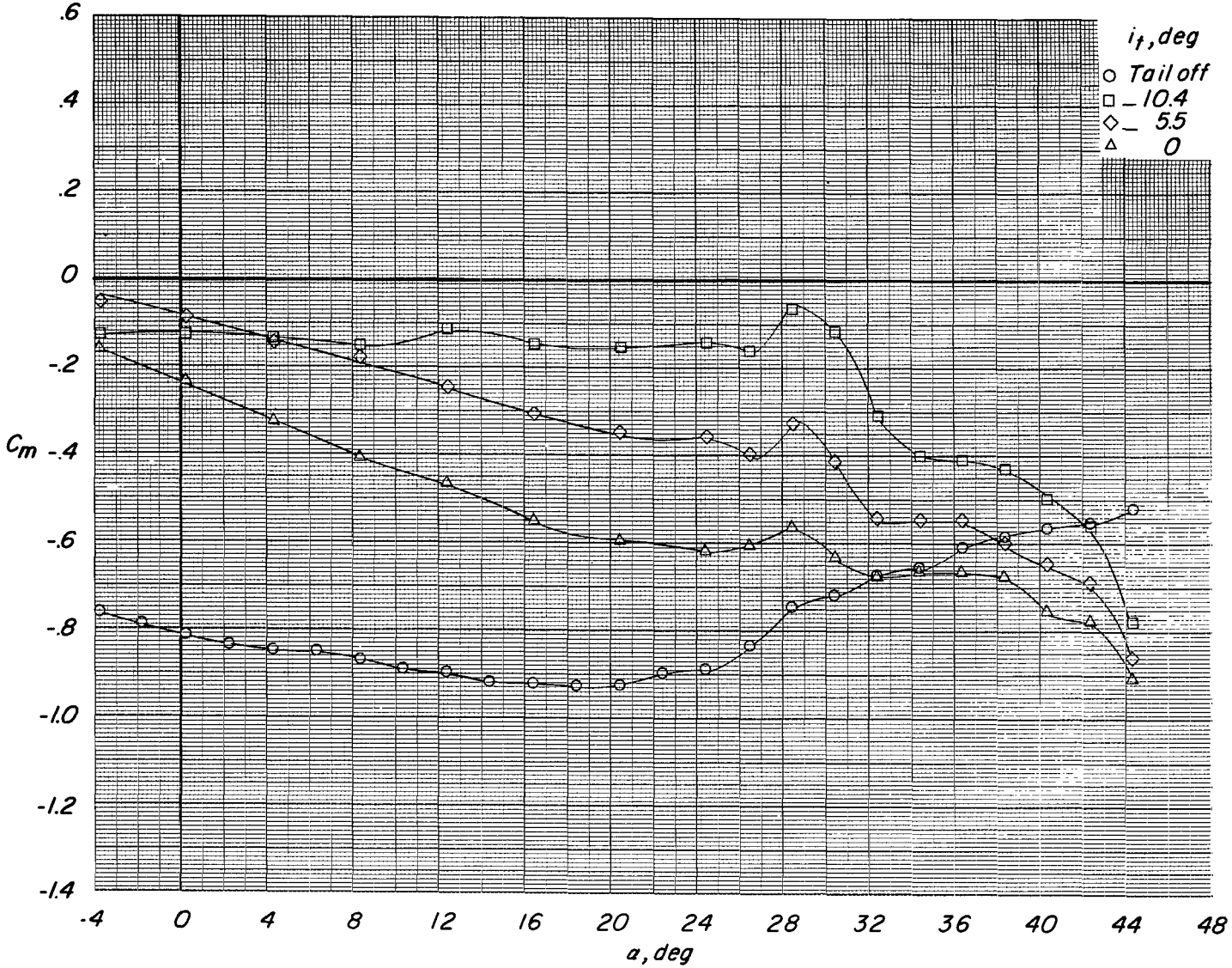

(c) Variation of C_m with α.

Figure 18.- Continued.

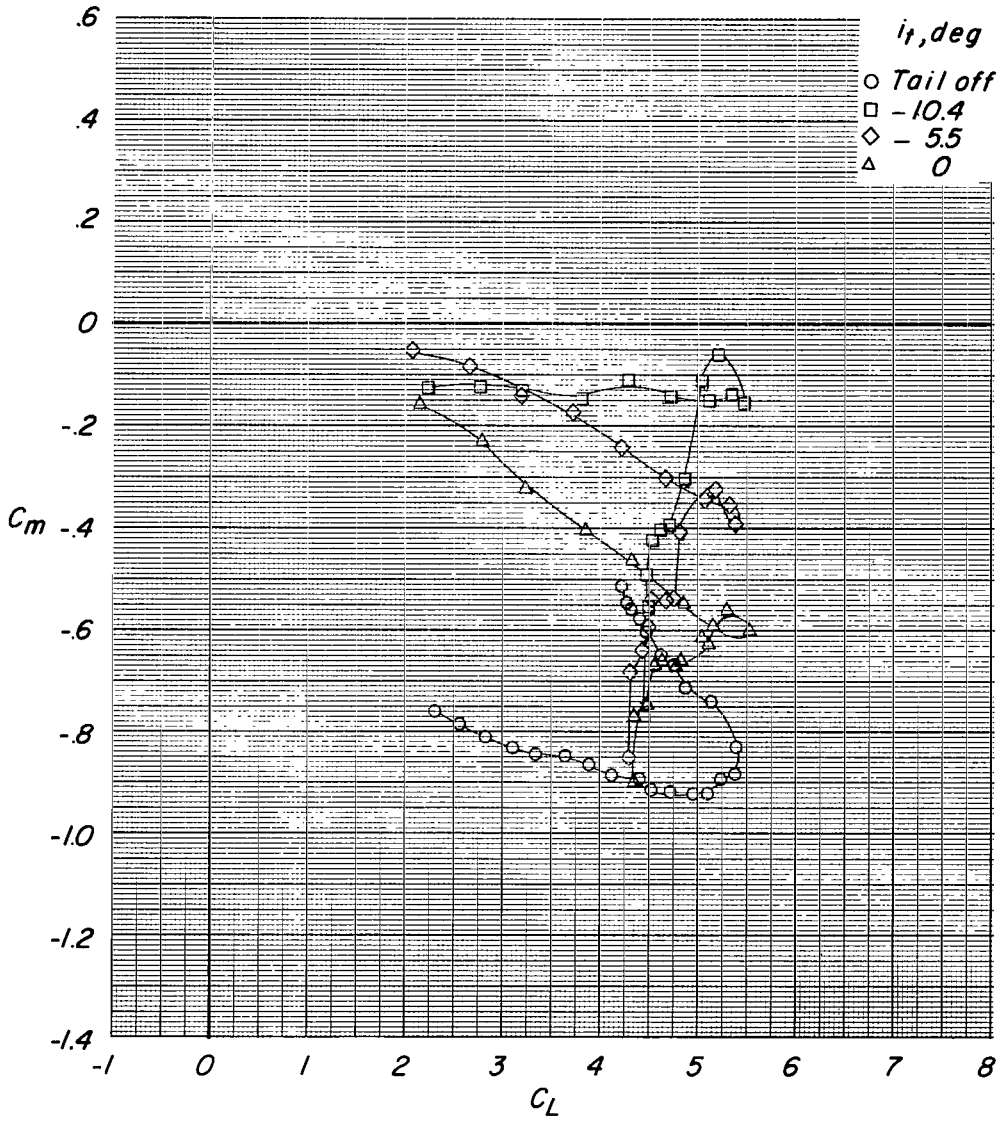

(d) Variation of C_m with C_L.

Figure 18.- Continued.

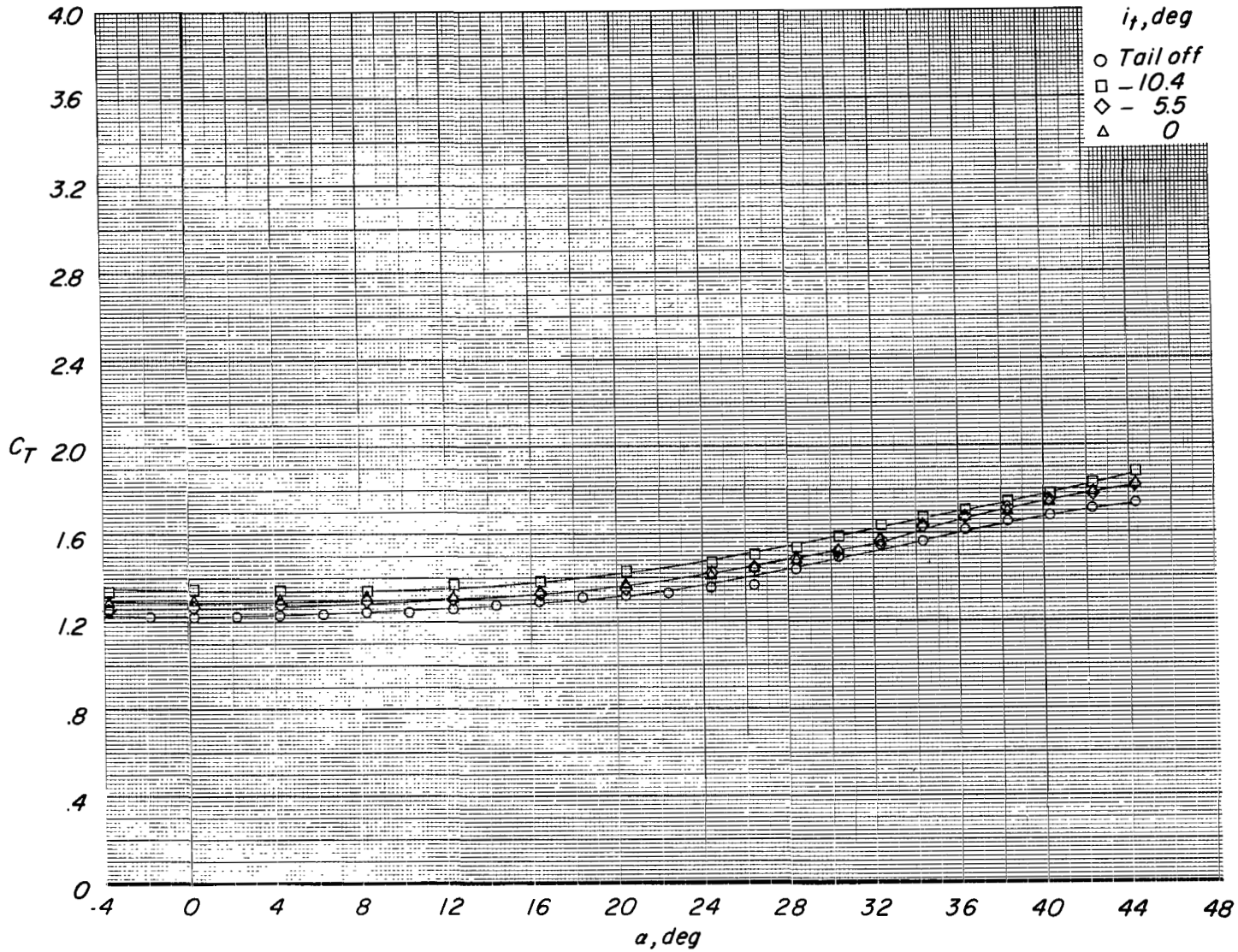

(e) Variation of C_T with α.

Figure 18.- Concluded.

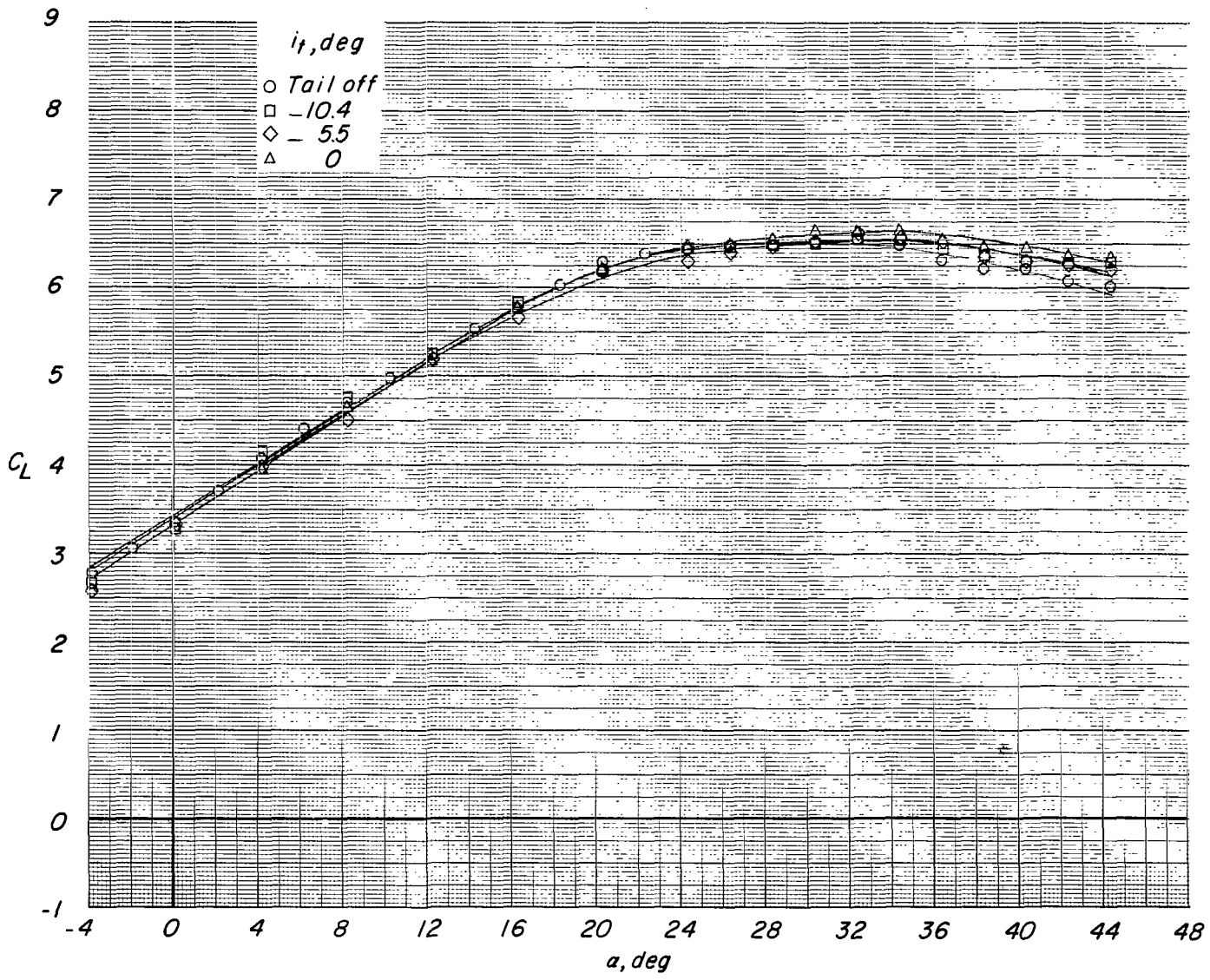

(a) Variation of C_L with α.

Figure 19.- Effect of tail incidence on longitudinal aerodynamic characteristics of configuration with small tail in high position. $\delta_f = 45^0$; reference $C_T = 2.42$.

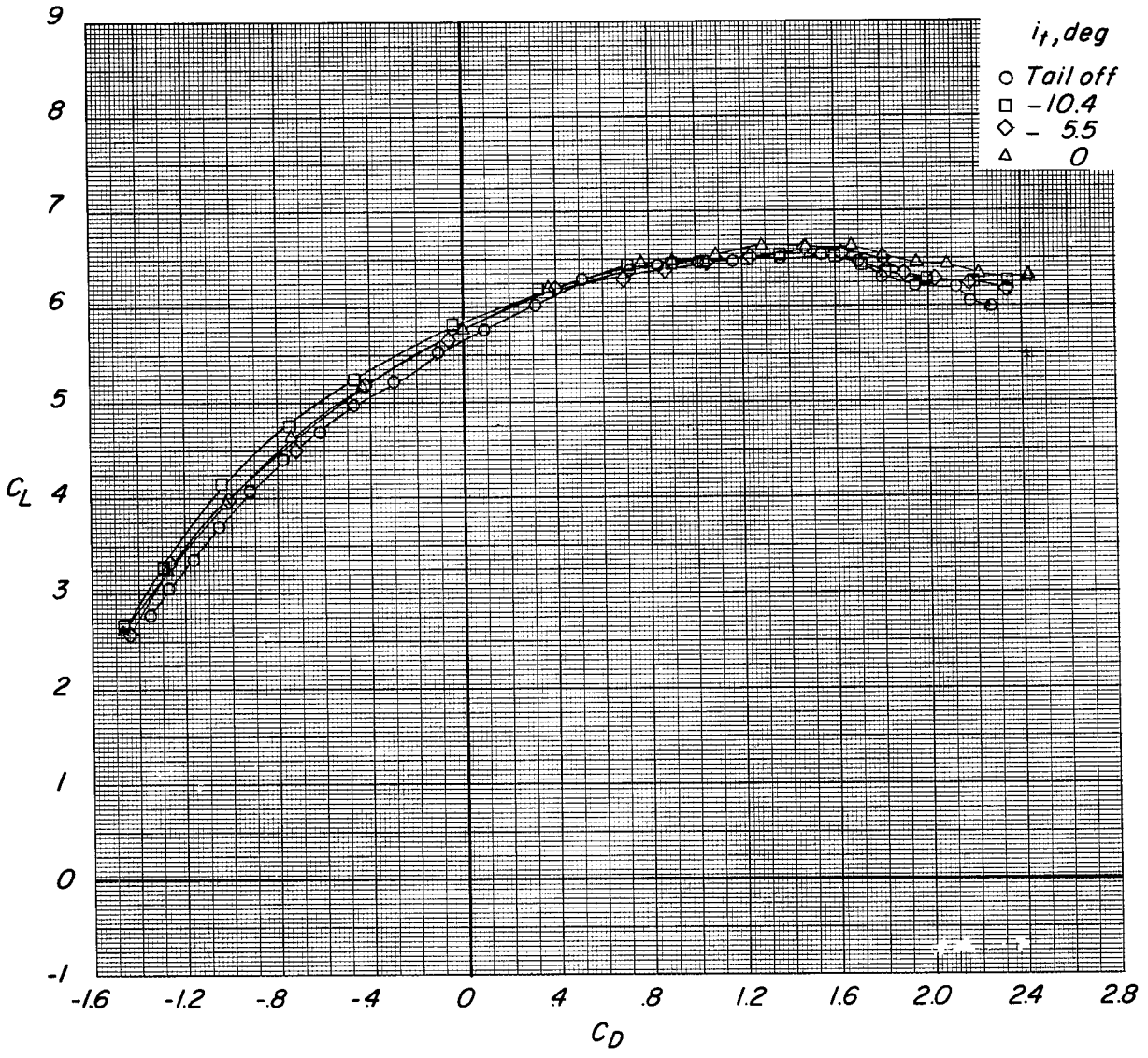

(b) Variation of C_L with C_D.

Figure 19.- Continued.

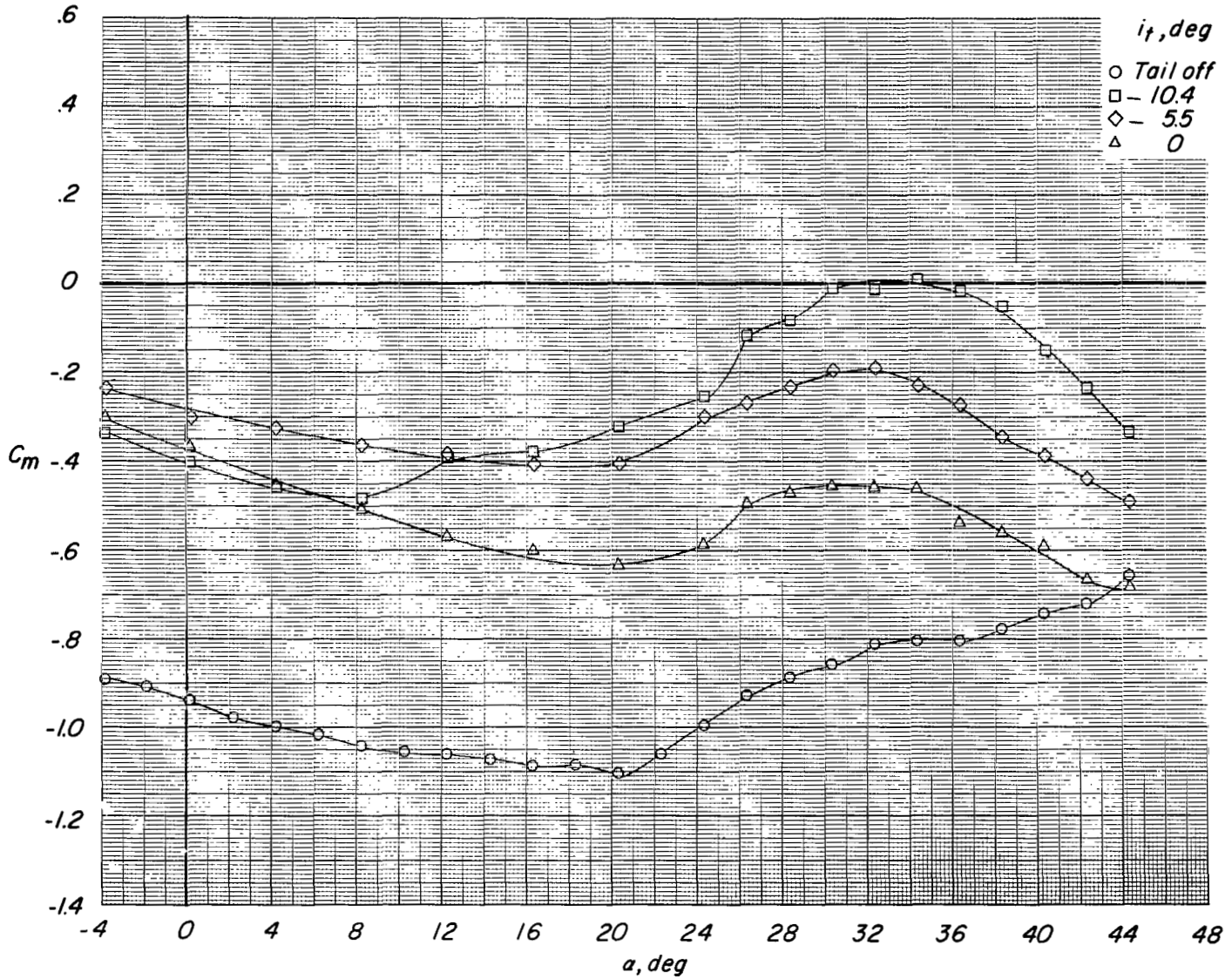

(c) Variation of C_m with α.

Figure 19.- Continued.

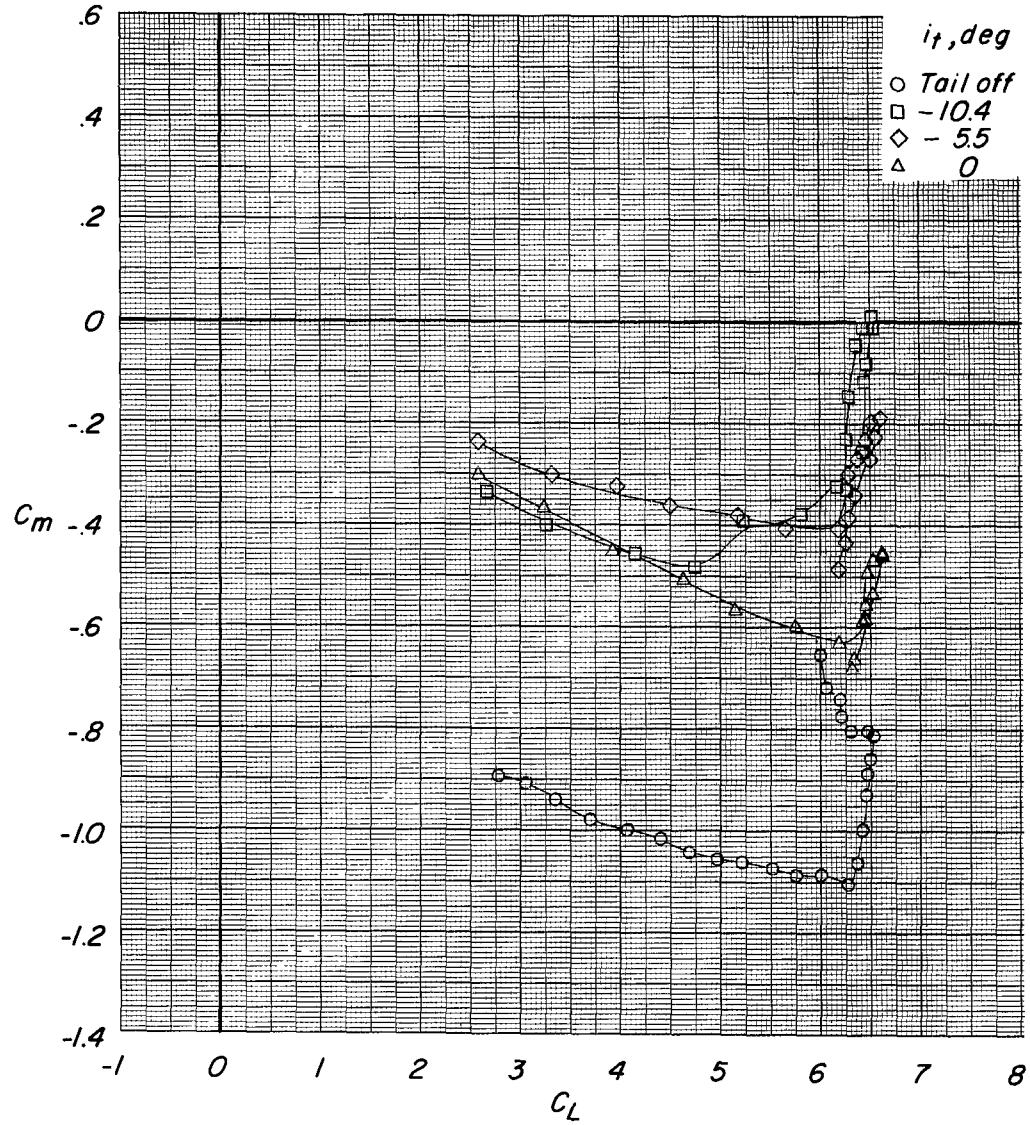

(d) Variation of C_m with C_L.

Figure 19.- Continued.

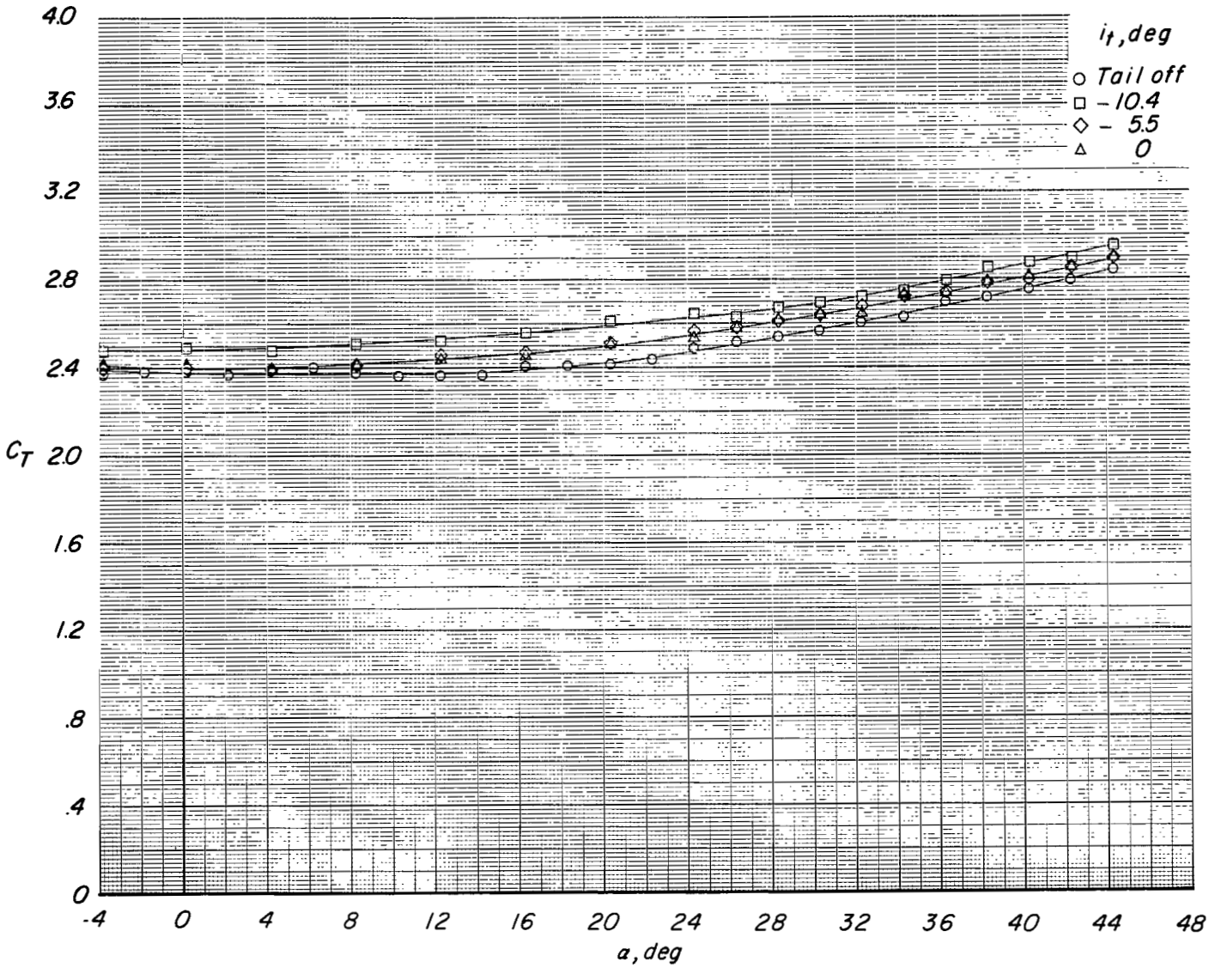

(e) Variation of C_T with α.

Figure 19.- Concluded.

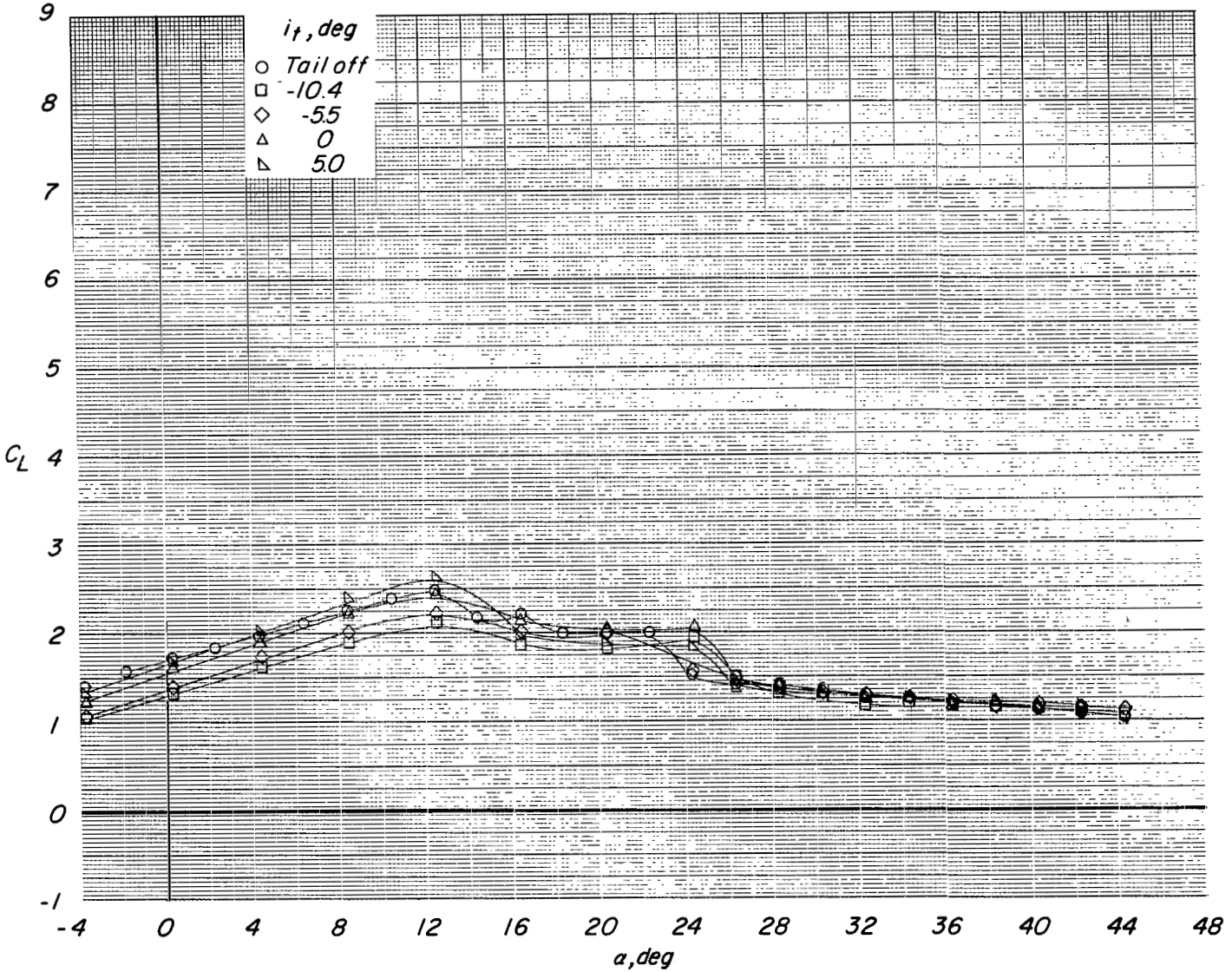

(a) Variation of C_L with α.

Figure 20.- Effect of tail incidence on longitudinal aerodynamic characteristics of configuration with large tail in high position. $\delta_f = 45^0$; $C_T = 0$.

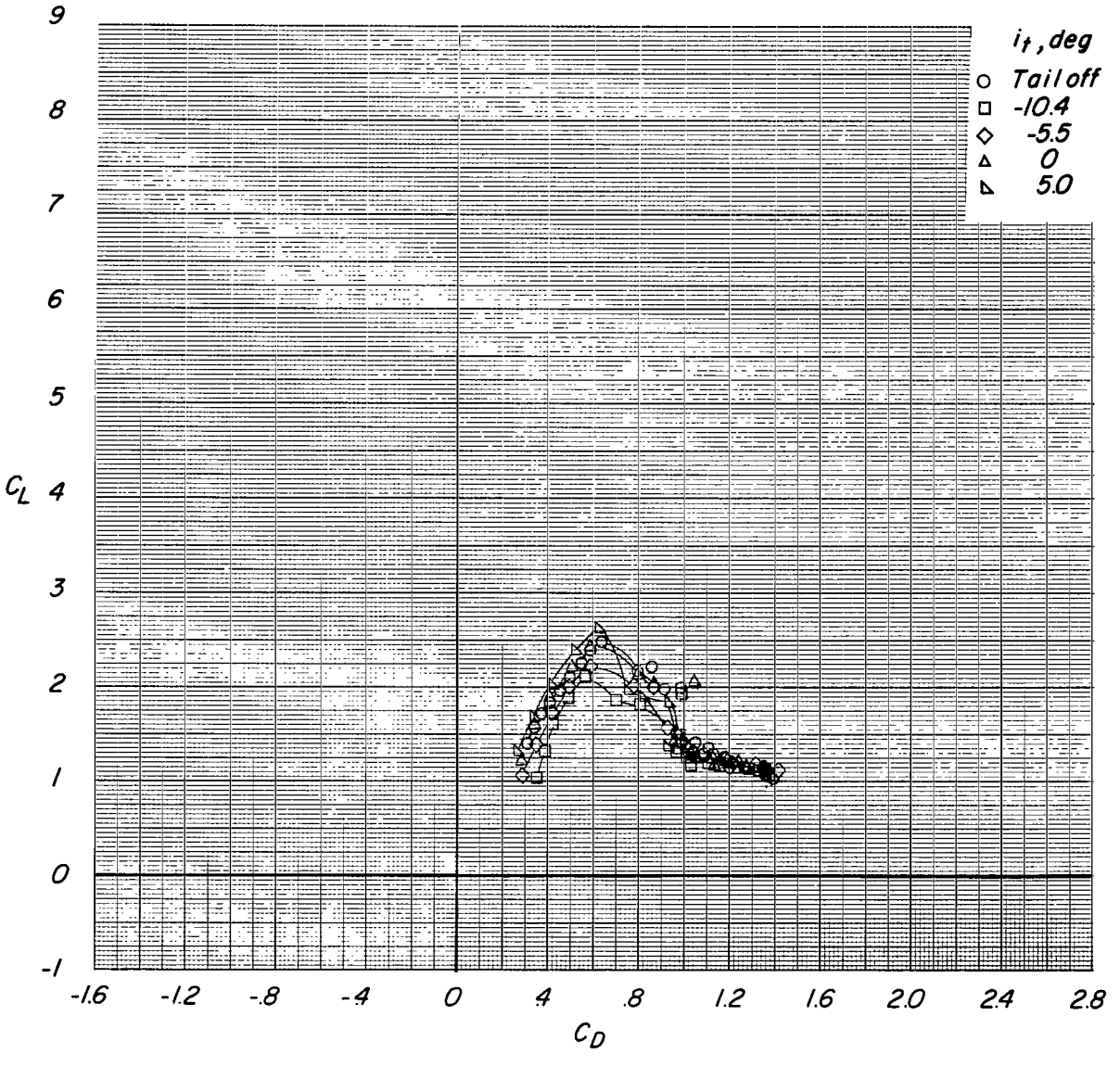

(b) Variation of C_L with C_D.

Figure 20.- Continued.

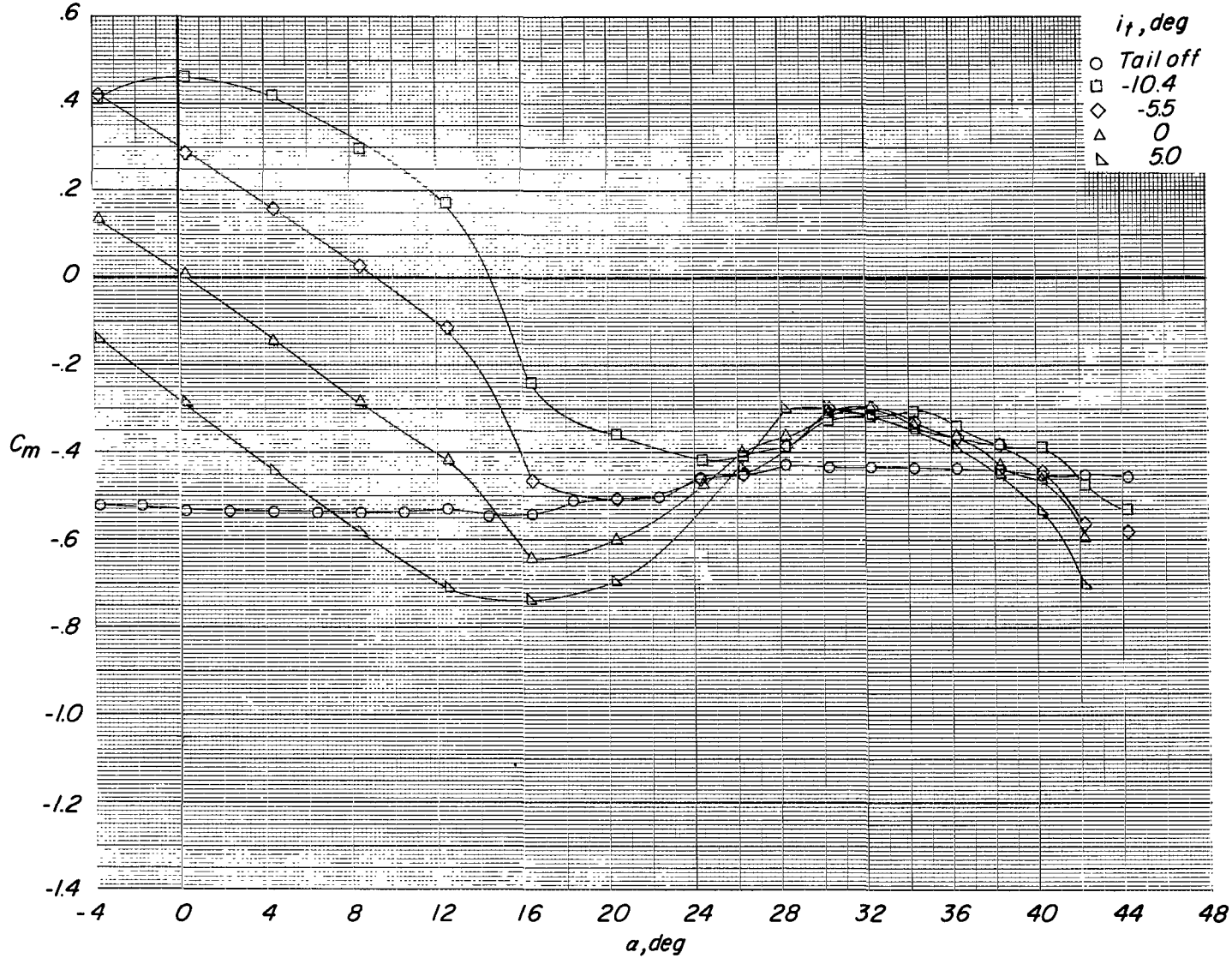

(c) Variation of C_m with α.

Figure 20.- Continued.

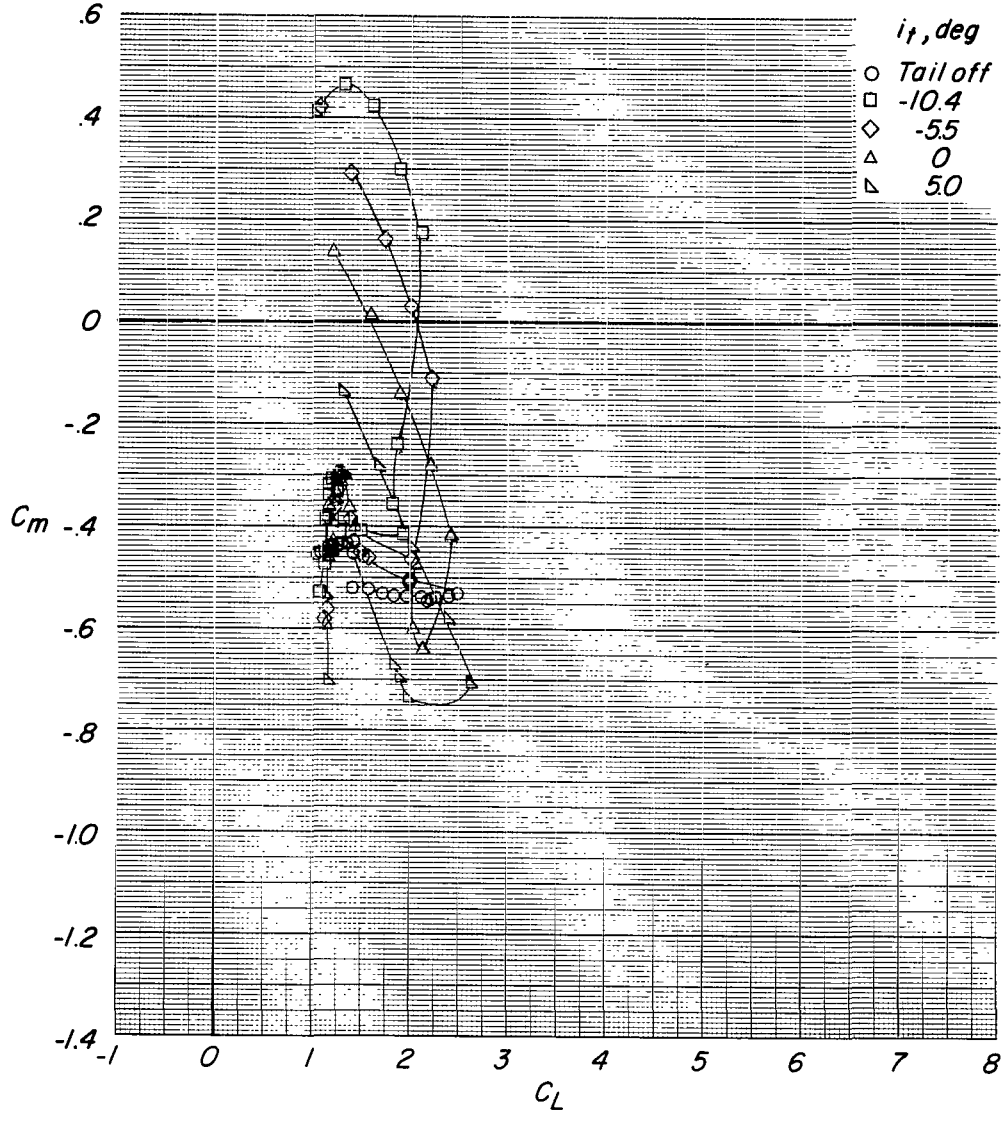

(d) Variation of C_m with C_L.

Figure 20.- Concluded.

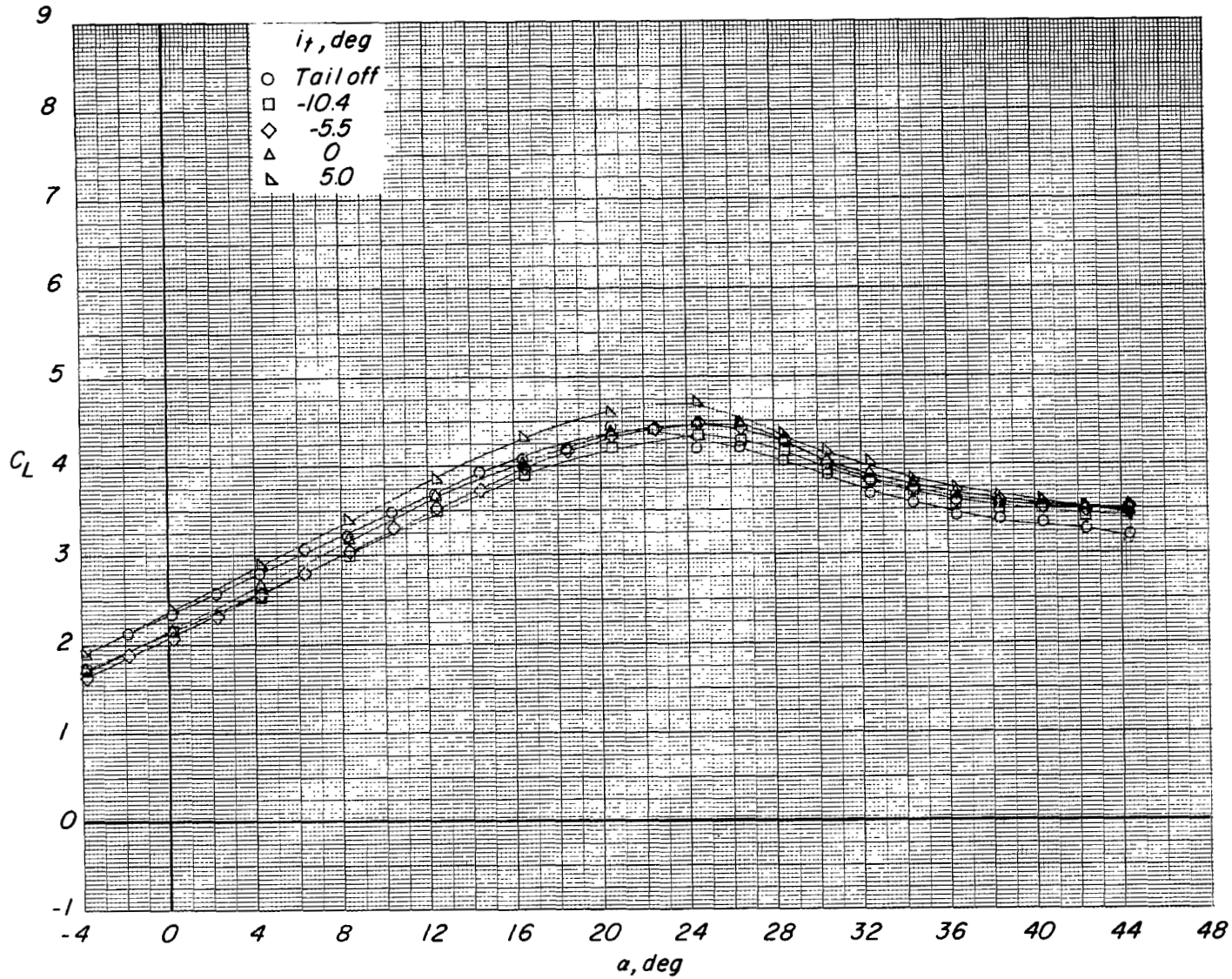

(a) Variation of C_L with α.

Figure 21.- Effect of tail incidence on longitudinal aerodynamic characteristics of configuration with large tail in high position. $\delta_f = 45^0$; reference $C_T = 0.70$.

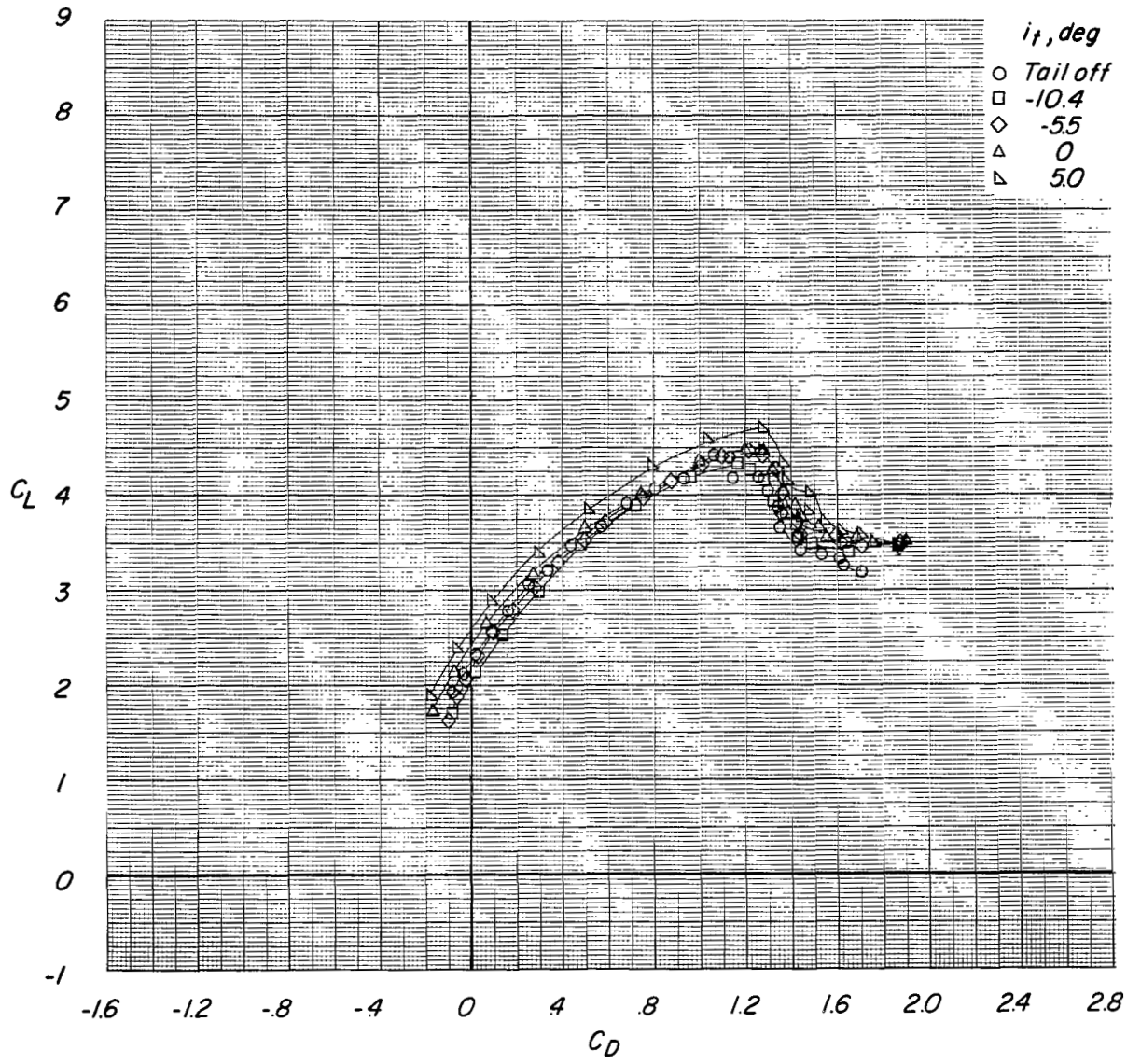

(b) Variation of C_L with C_D.

Figure 21.- Continued.

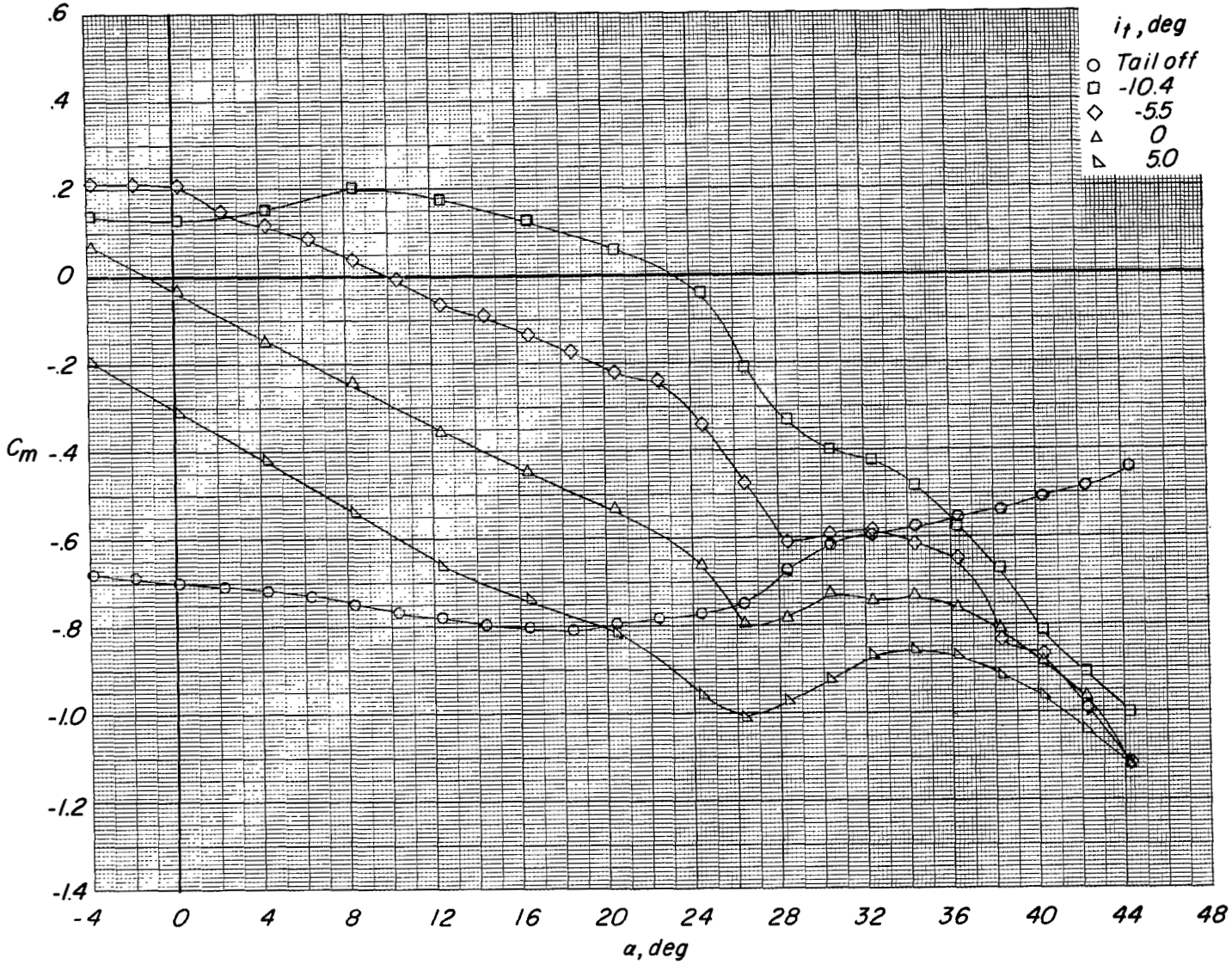

(c) Variation of C_m with α.

Figure 21.- Continued.

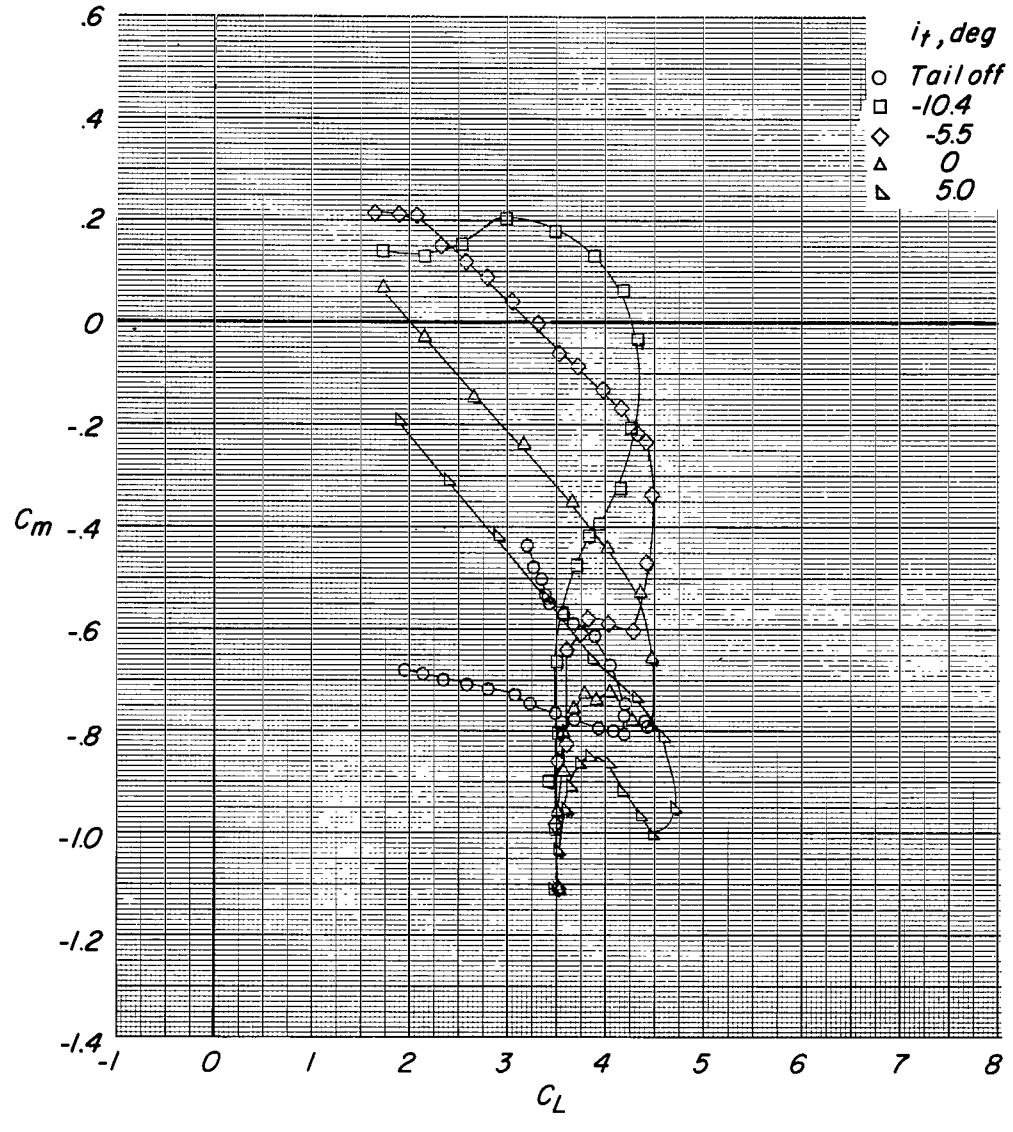

(d) Variation of C_m with C_L.

Figure 21.- Continued.

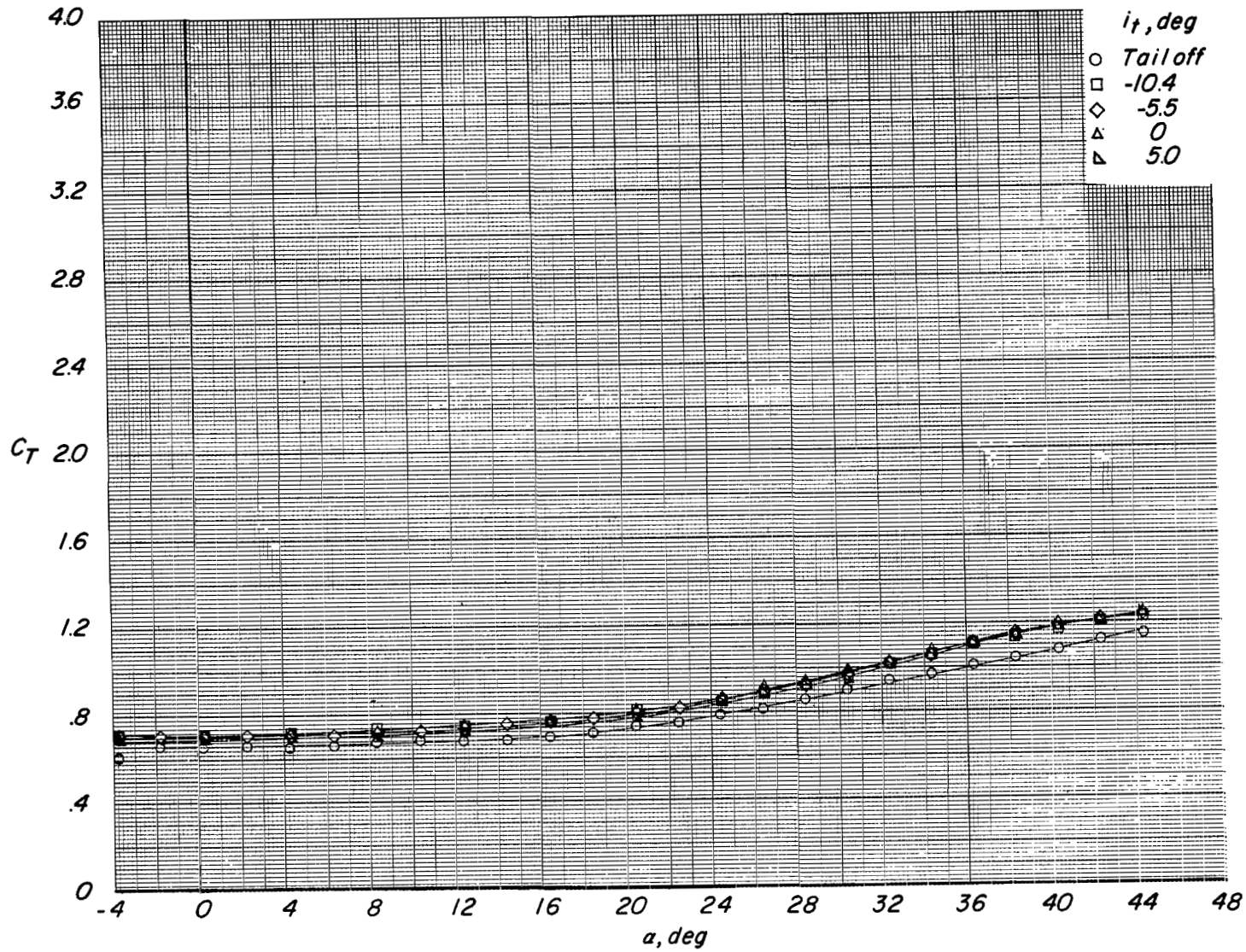

(e) Variation of C_T with α.

Figure 21.- Concluded.

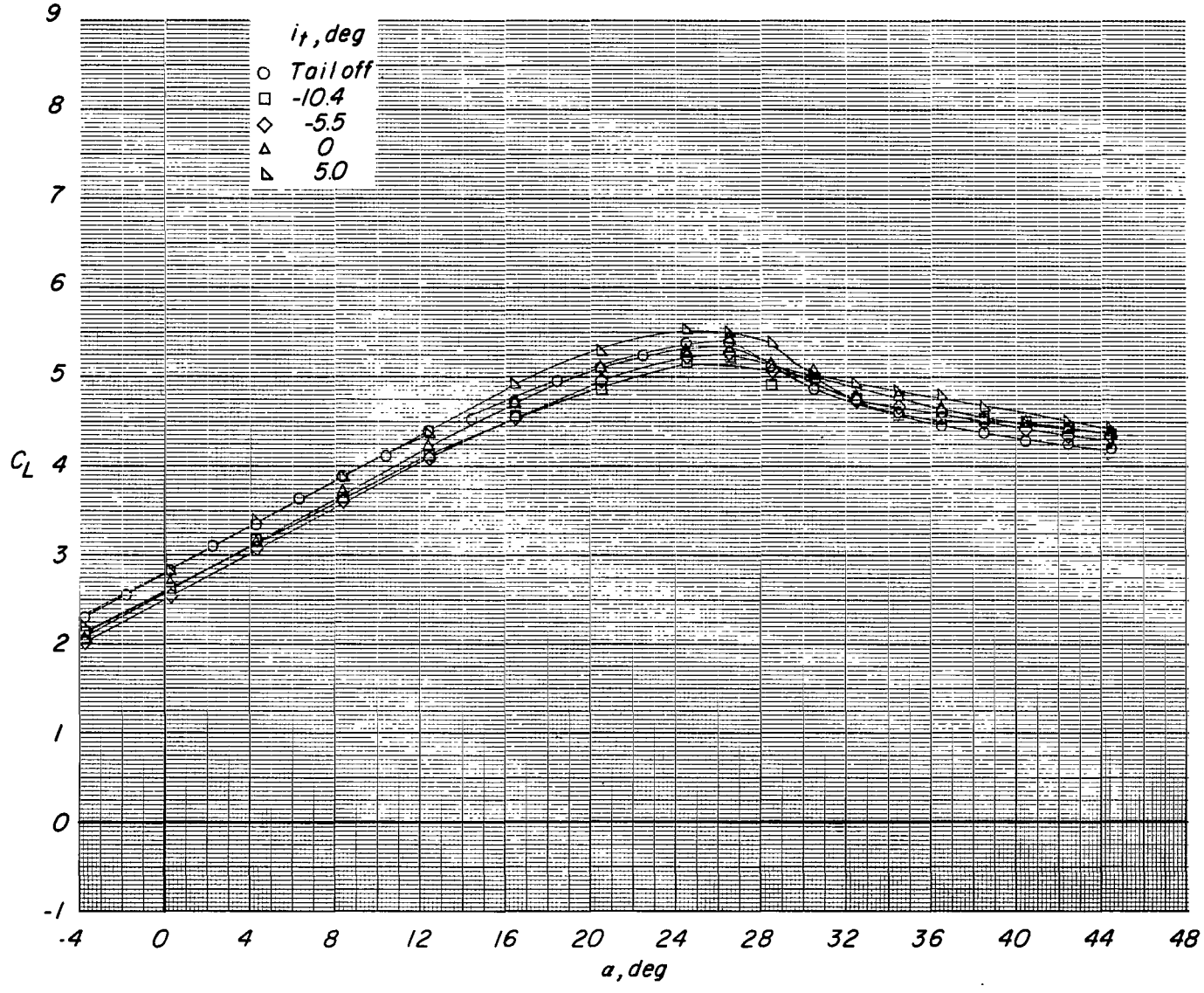

(a) Variation of C_L with α.

Figure 22.- Effect of tail incidence on longitudinal aerodynamic characteristics of configuration with large tail in high position. $\delta_f = 45^0$; reference $C_T = 1.25$.

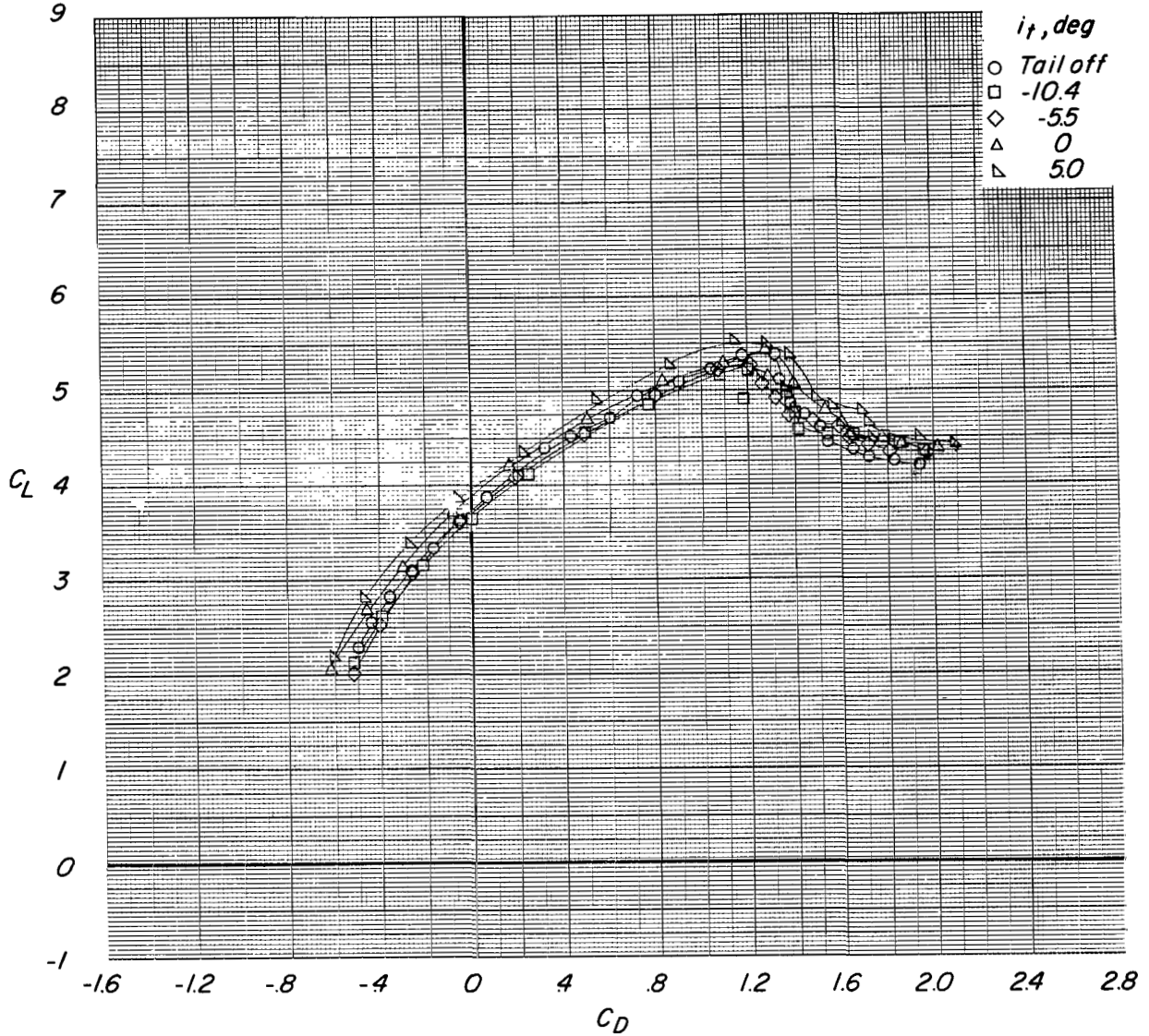

(b) Variation of C_L with C_D.

Figure 22.- Continued.

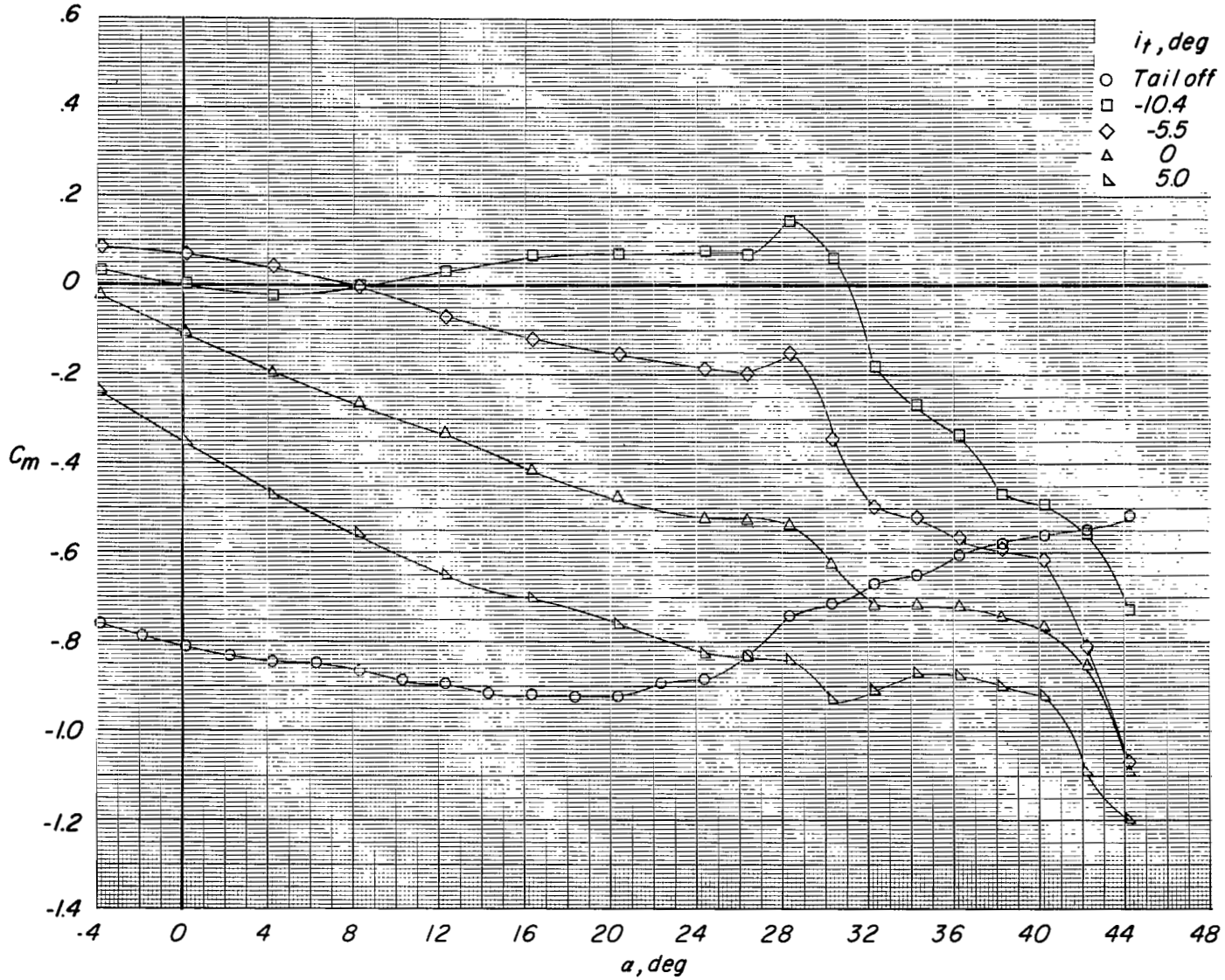

(c) Variation of C_m with α.

Figure 22.- Continued.

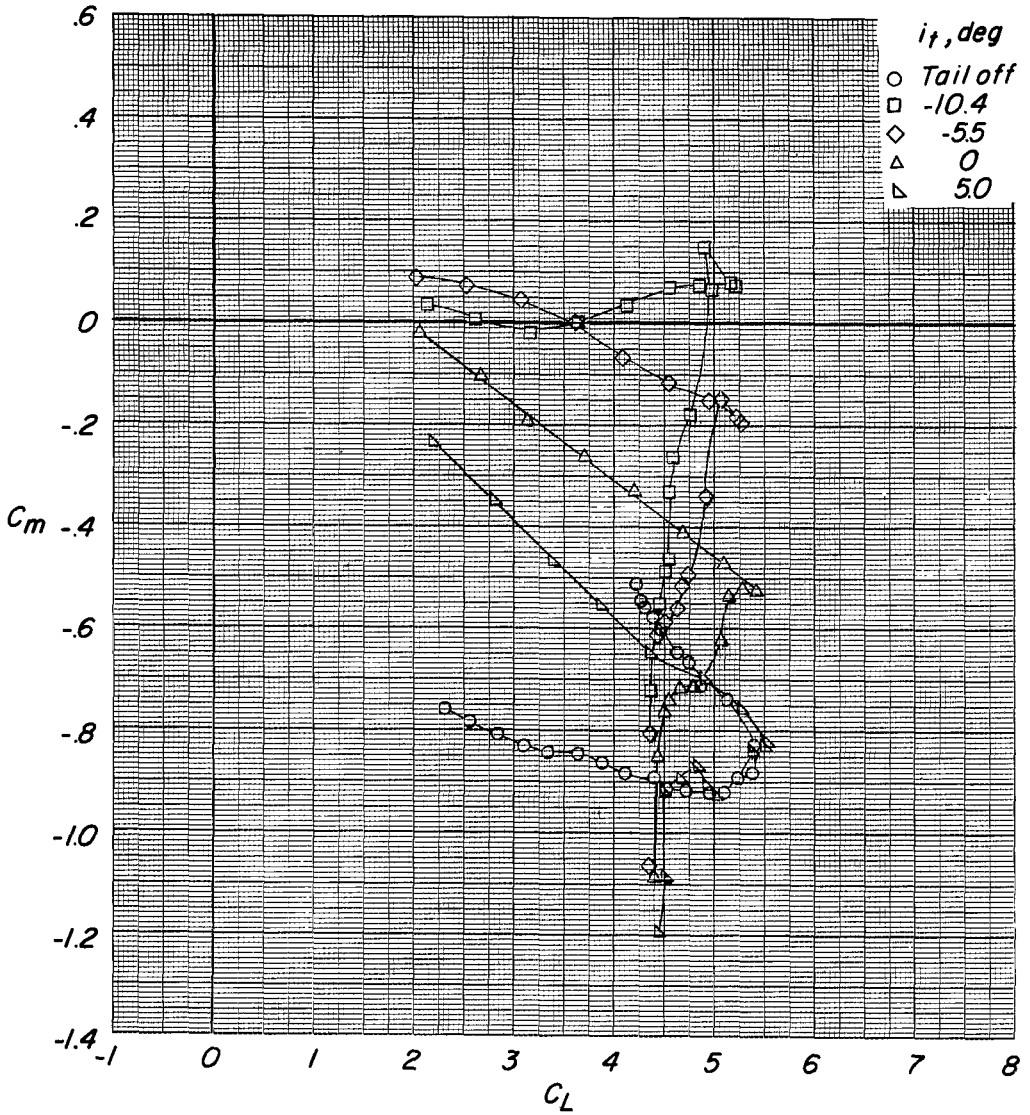

(d) Variation of C_m with C_L.

Figure 22.- Continued.

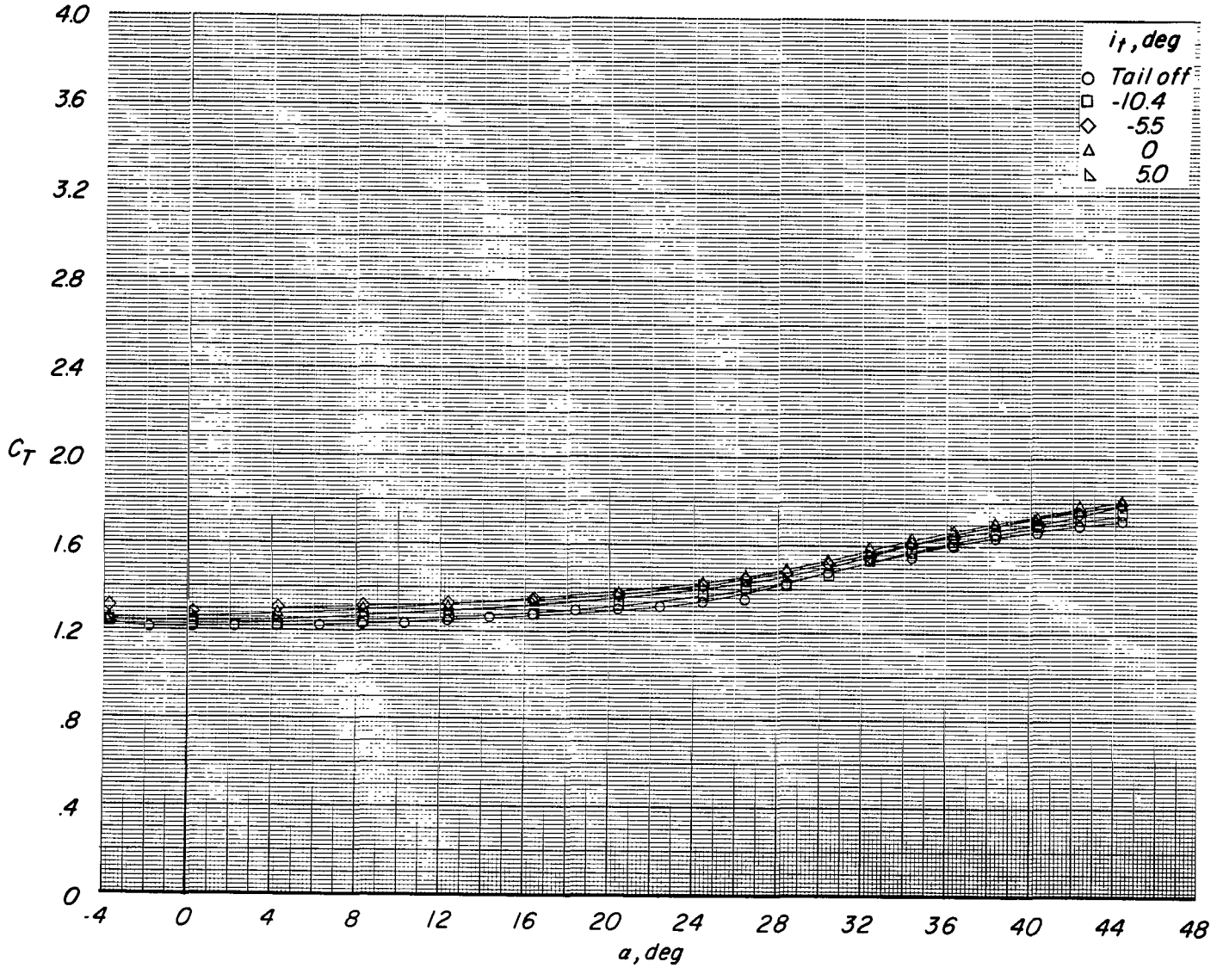

(e) Variation of C_T with α.

Figure 22.- Concluded.

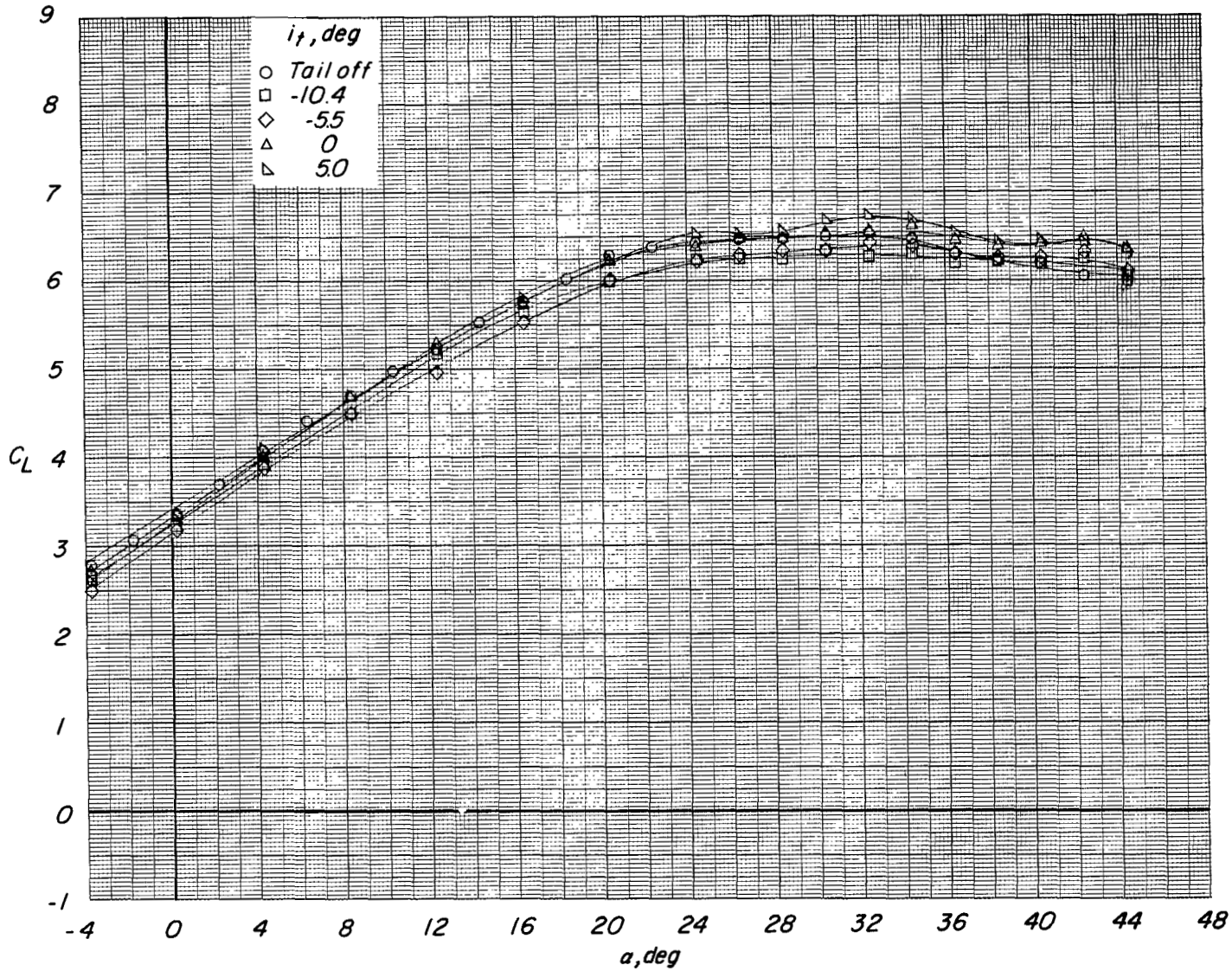

(a) Variation of C_L with α.

Figure 23.- Effect of tail incidence on longitudinal aerodynamic characteristics of configuration with large tail in high position. $\delta_f = 45^0$; reference $C_T = 2.42$.

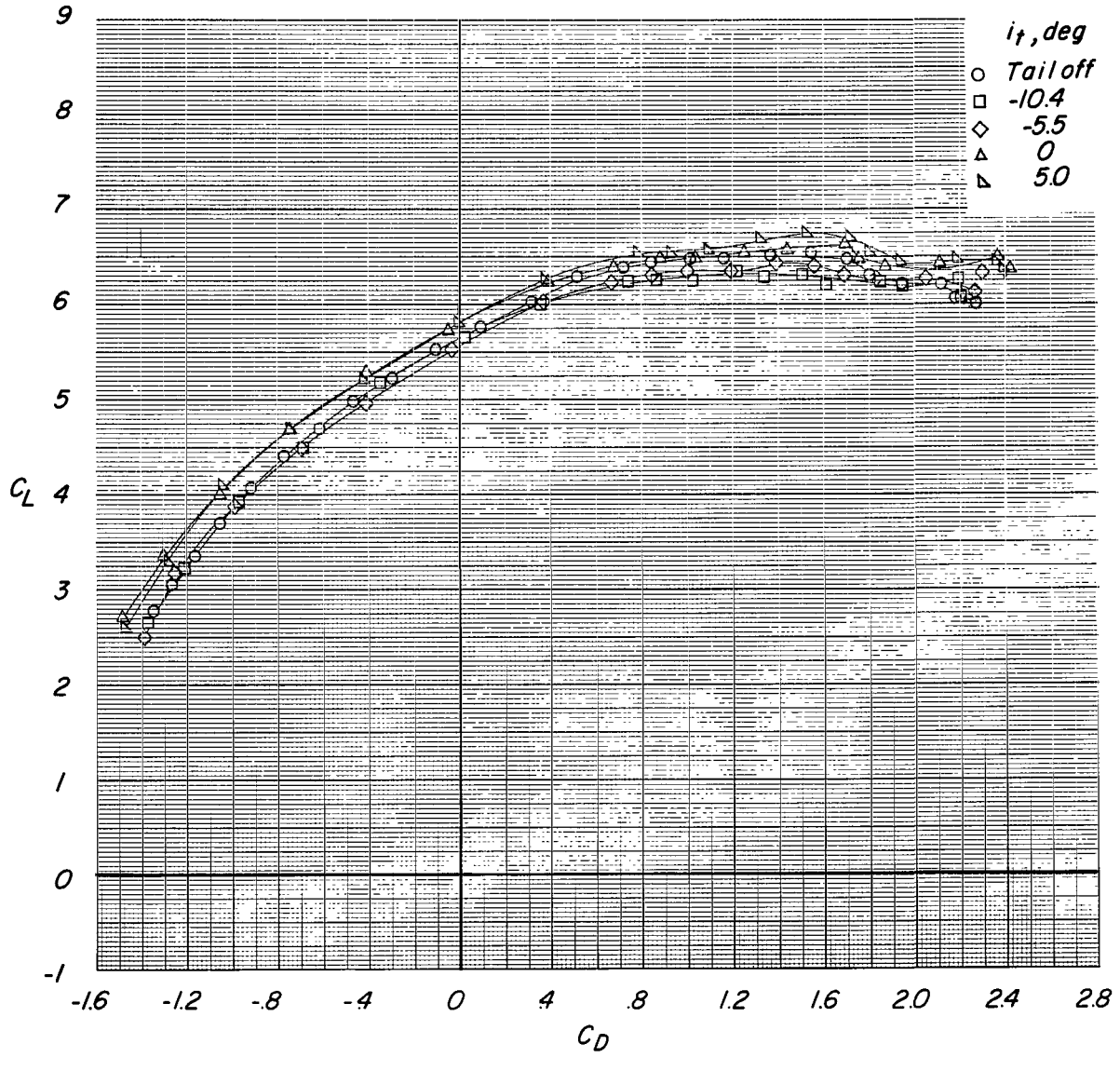

(b) Variation of C_L with C_D.

Figure 23.- Continued.

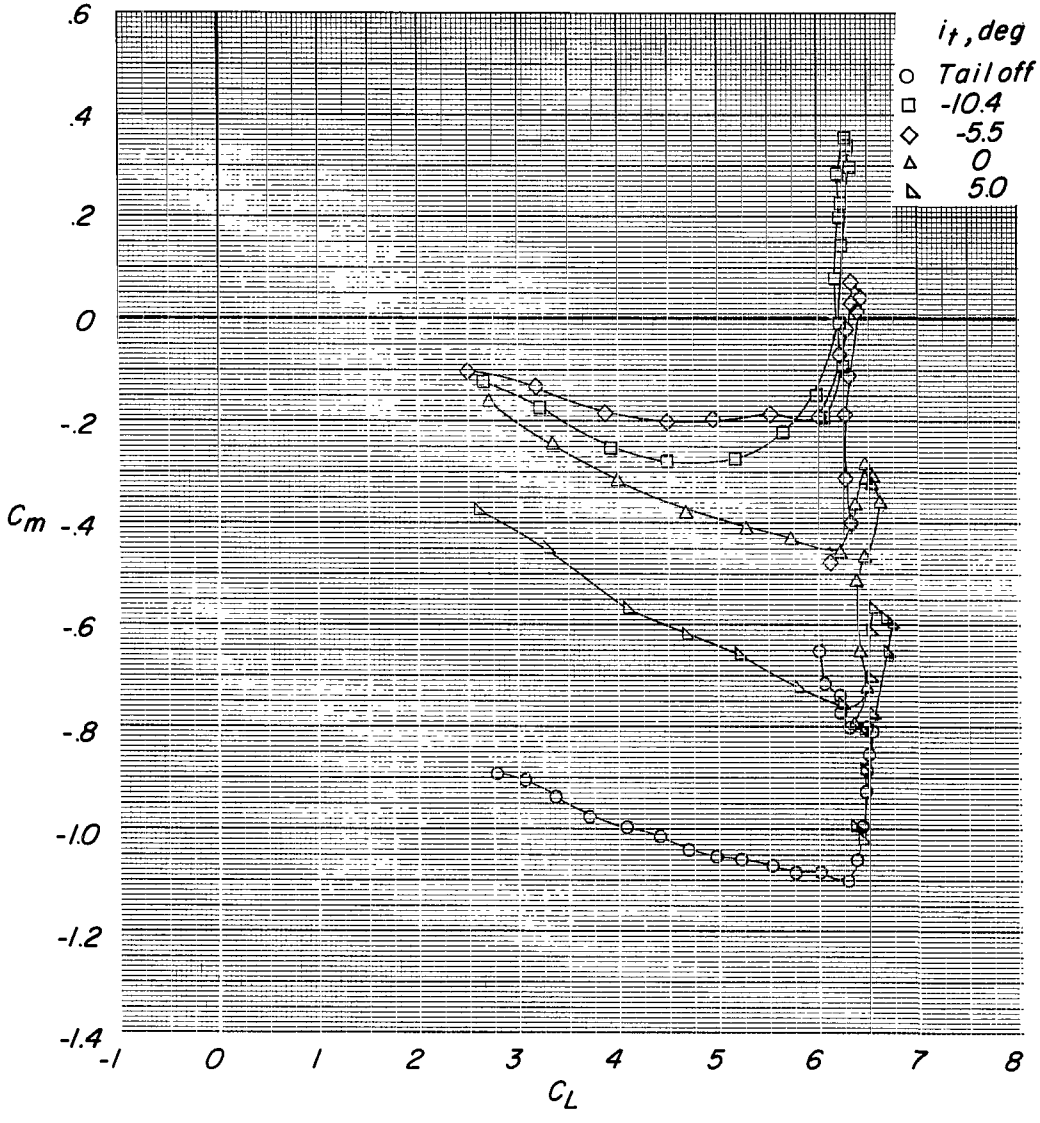

(c) Variation of C_m with C_L.

Figure 23.- Continued.

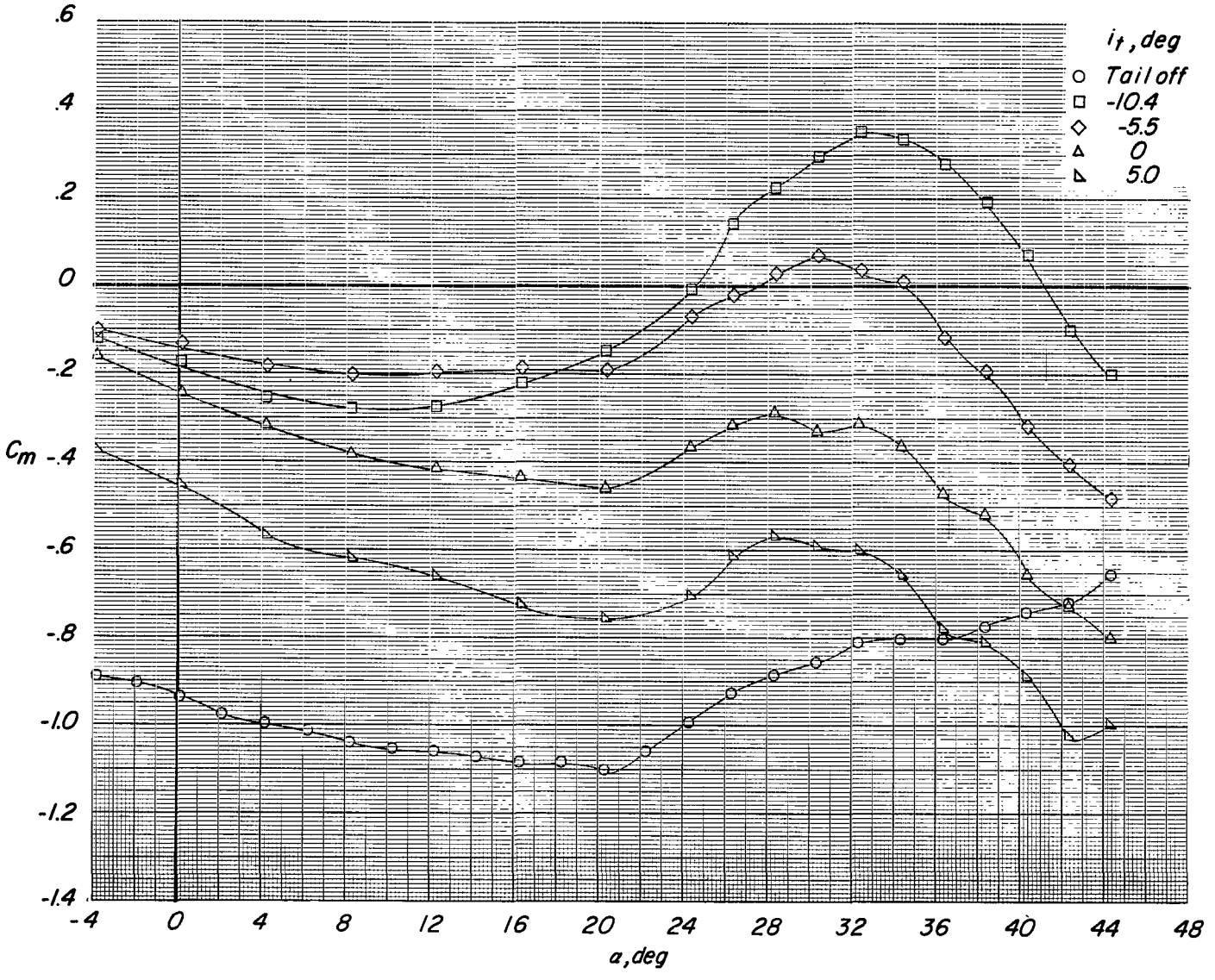

(d) Variation of C_m with α.

Figure 23.- Continued.

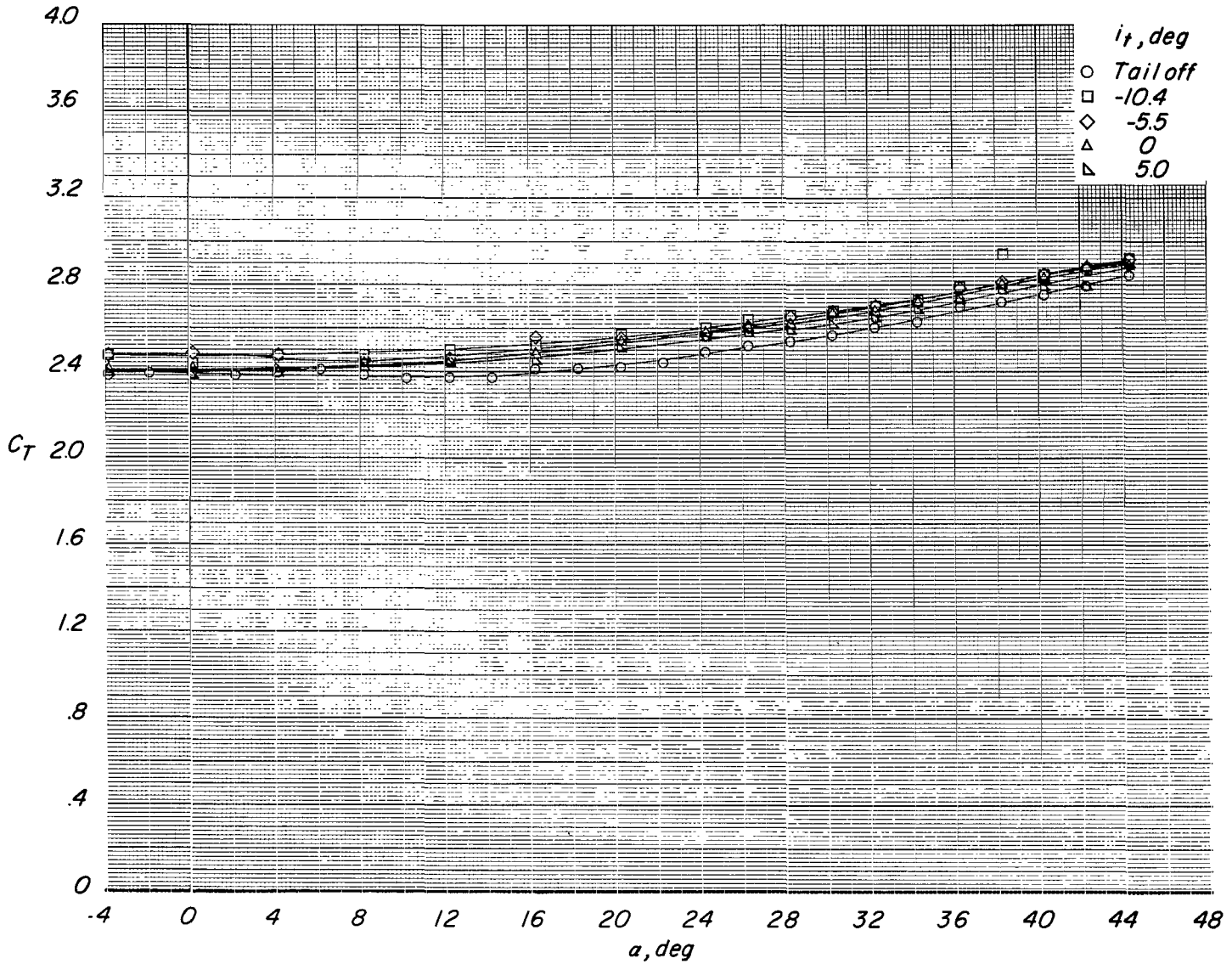

(e) Variation of C_T with α.

Figure 23.- Concluded.

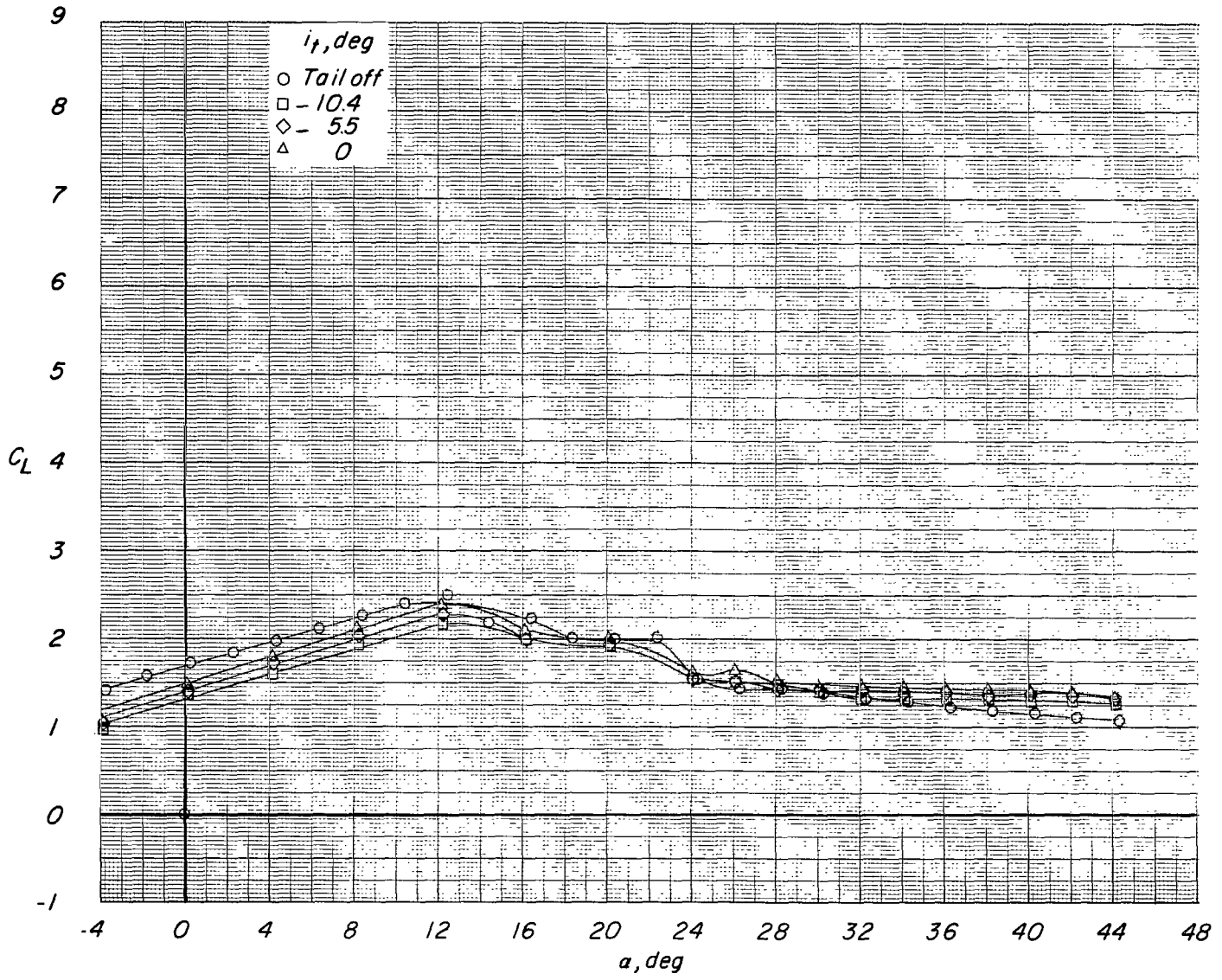

(a) Variation of C_L with α.

Figure 24.- Effect of tail incidence on longitudinal aerodynamic characteristics of configuration with large tail in low position. $\delta_f = 45^o$; $C_T = 0$.

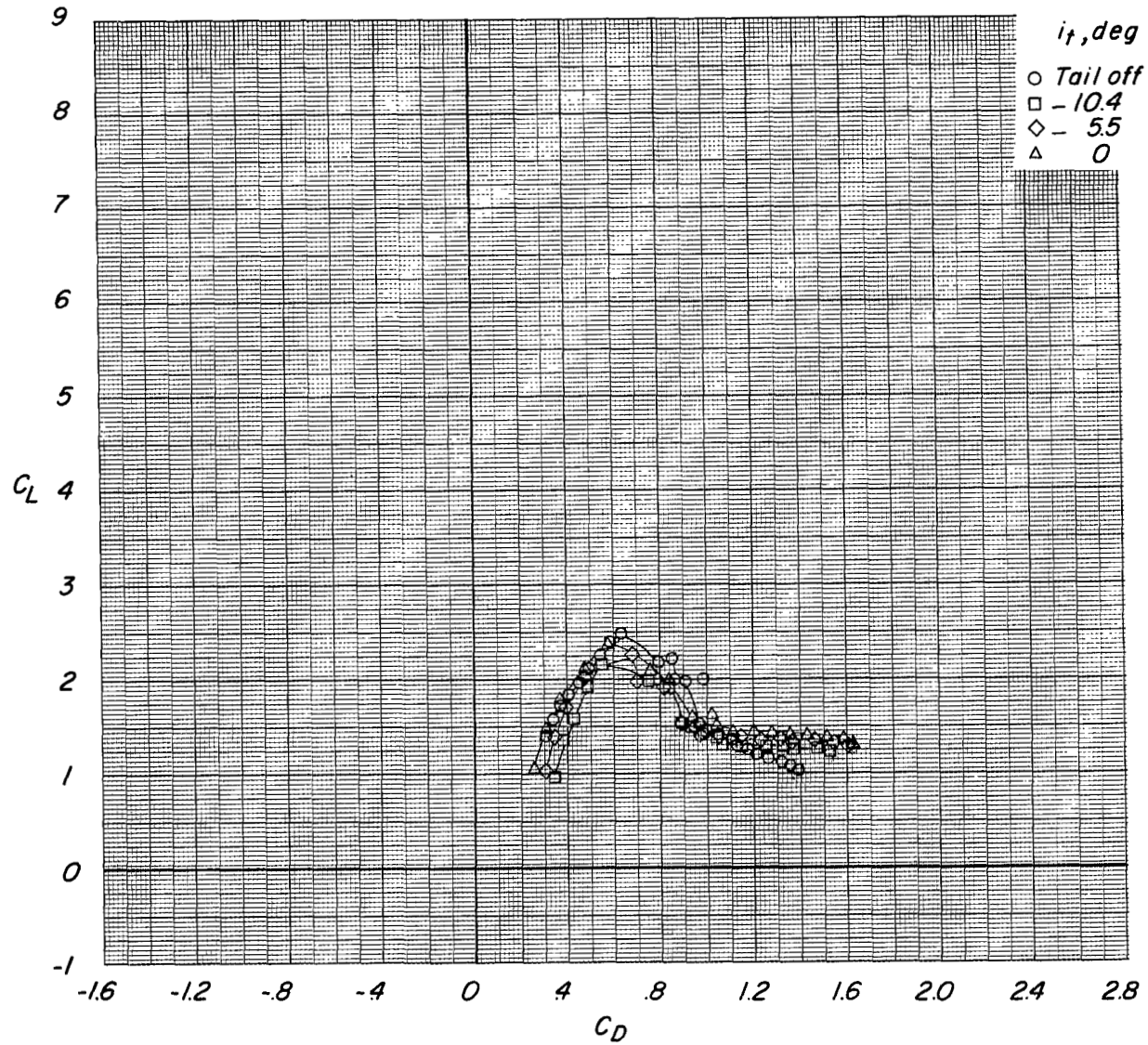

(b) Variation of C_L with C_D.

Figure 24.- Continued.

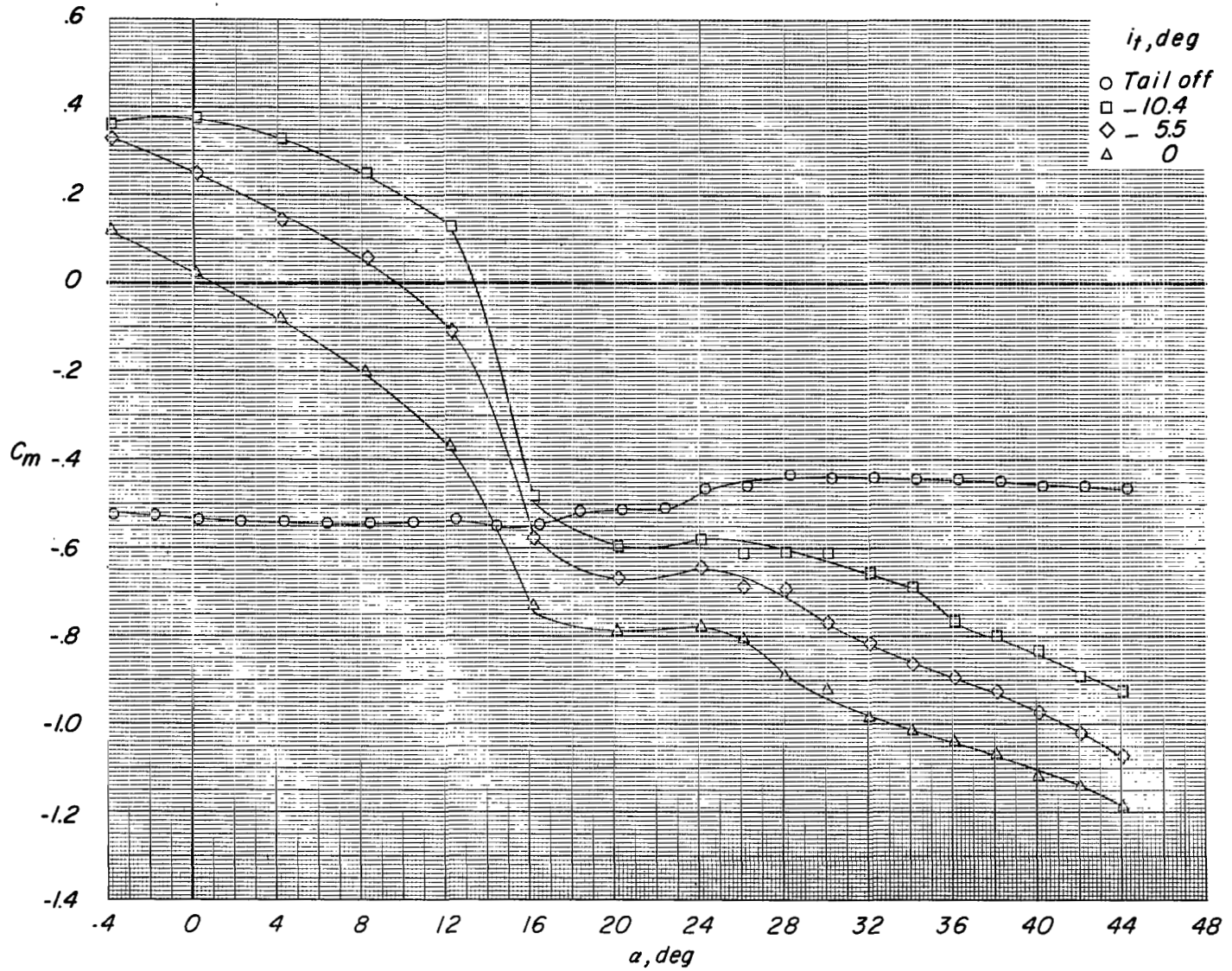

(c) Variation of C_m with α.

Figure 24.- Continued.

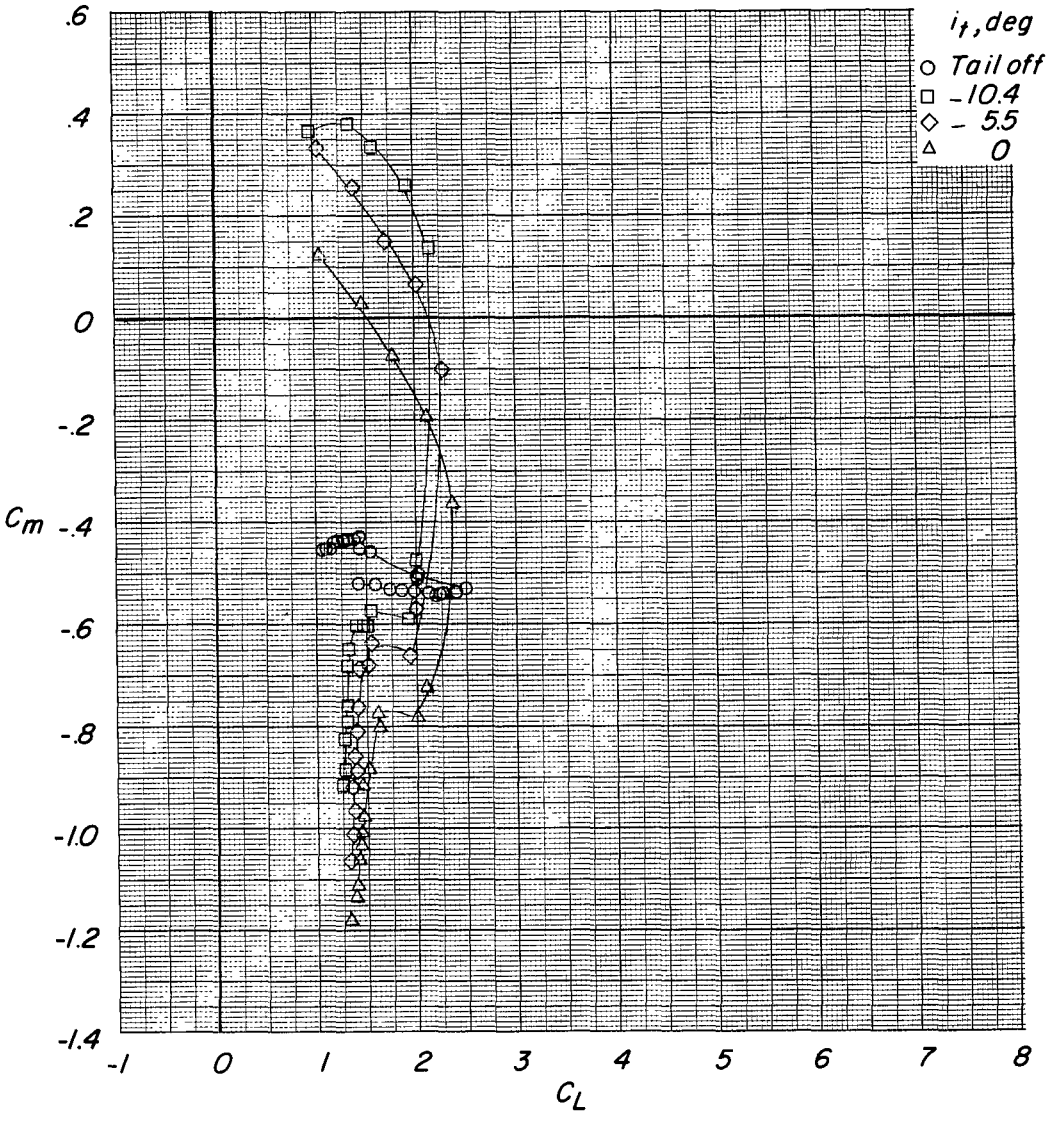

(d) Variation of C_m with C_L.

Figure 24.- Concluded.

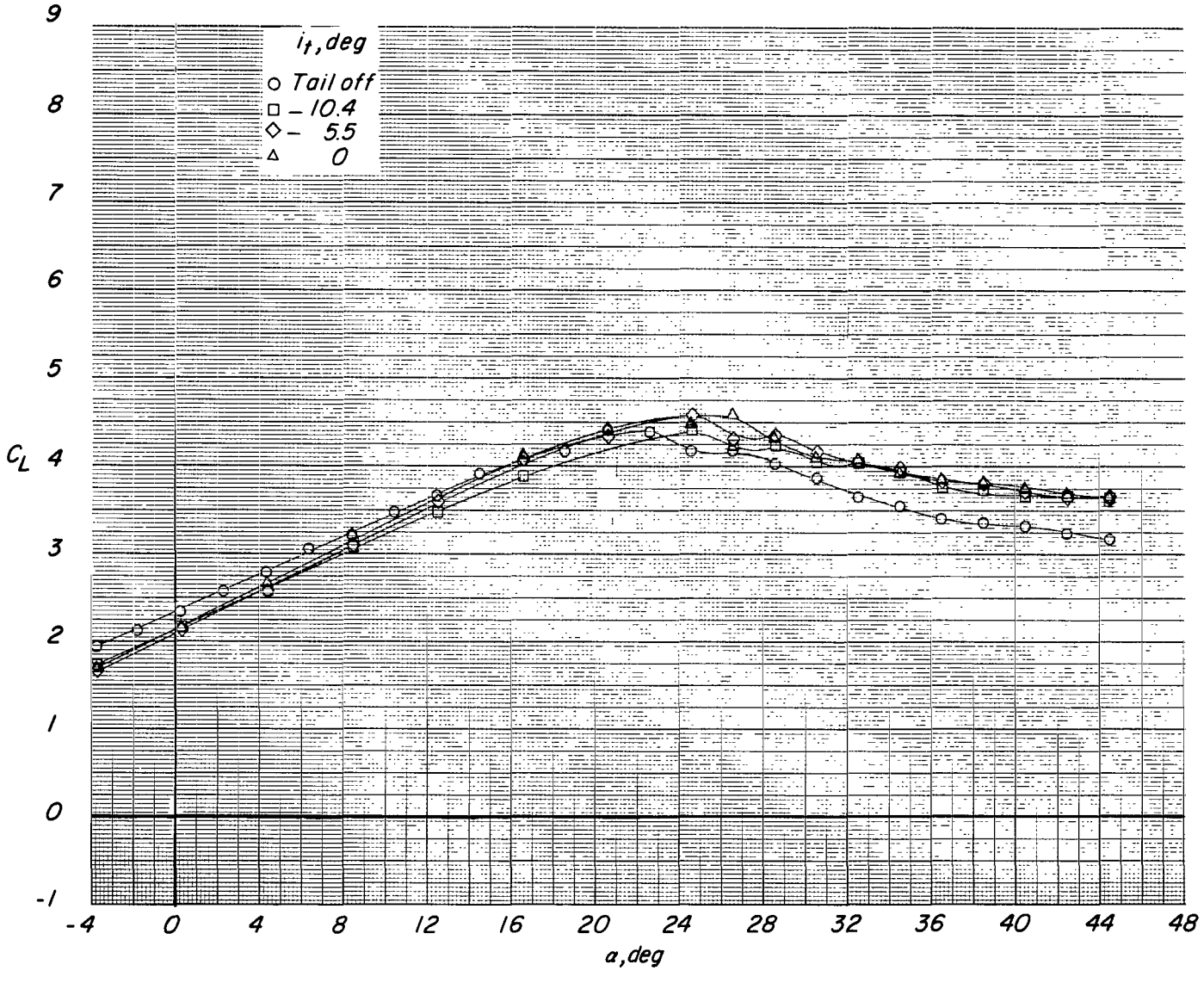

(a) Variation of C_L with α.

Figure 25.- Effect of tail incidence on longitudinal aerodynamic characteristics of configuration with large tail in low position. $\delta_f = 45^o$; reference $C_T = 0.70$.

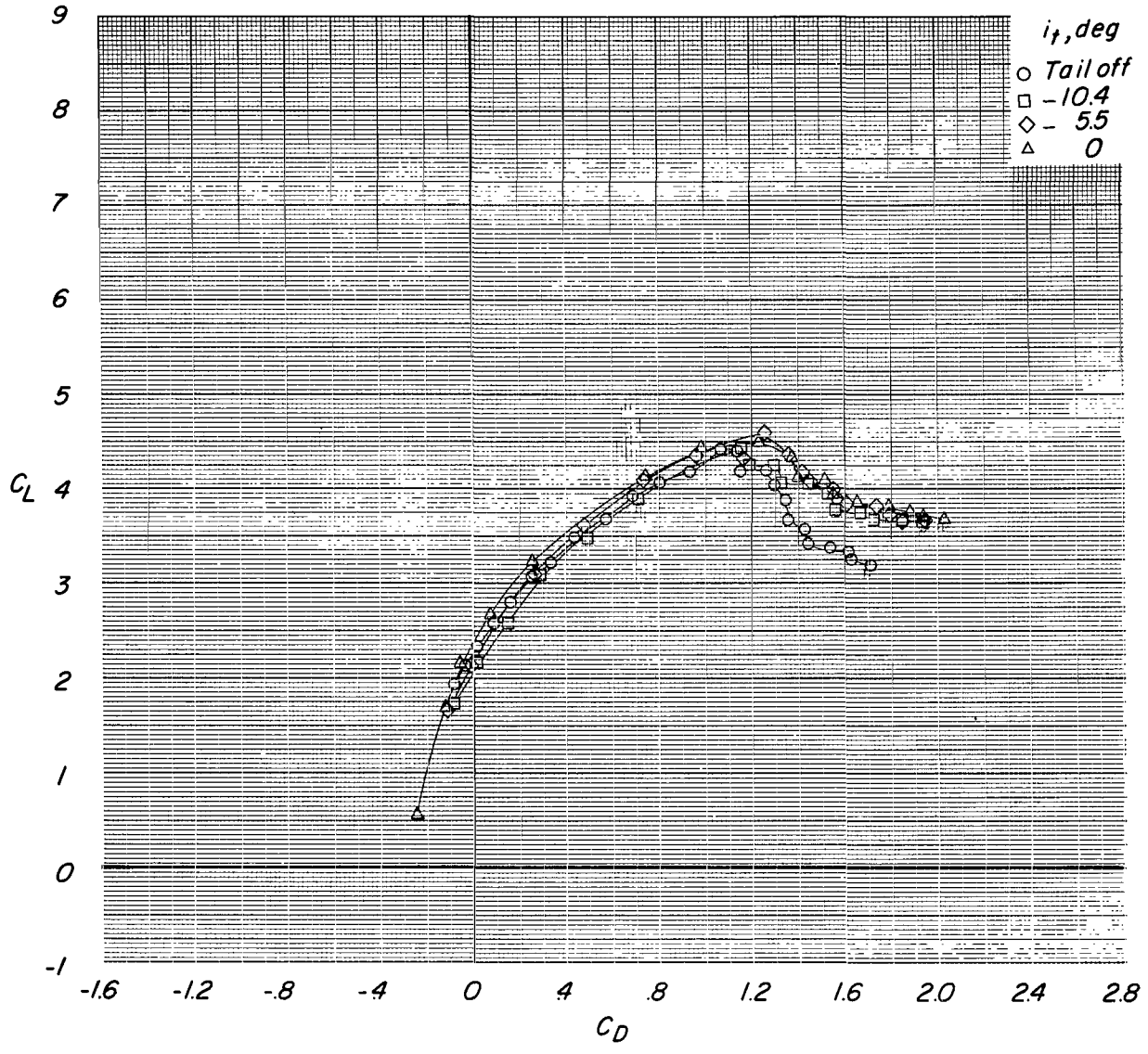

(b) Variation of C_L with C_D.

Figure 25.- Continued.

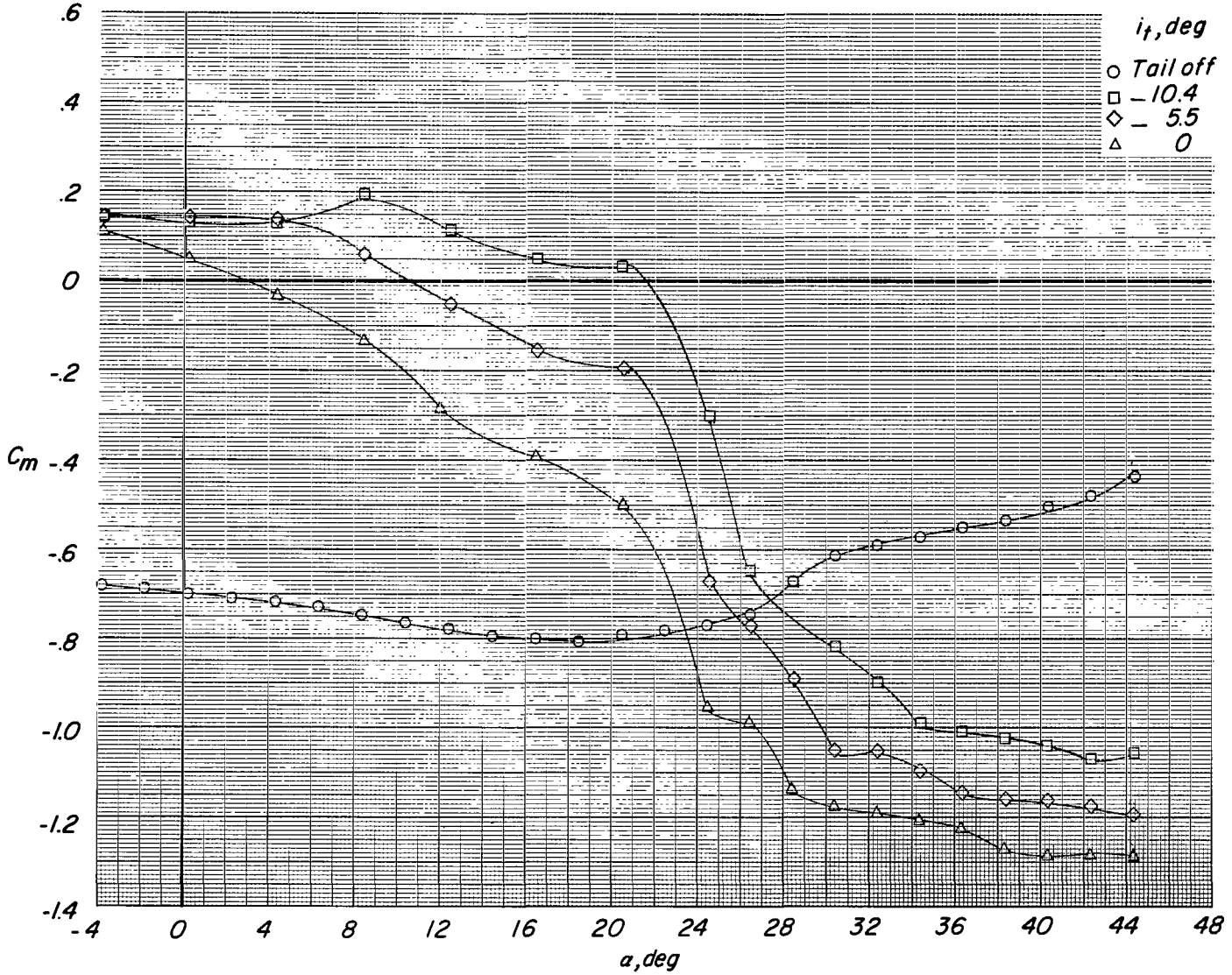

(c) Variation of C_m with α.

Figure 25.- Continued.

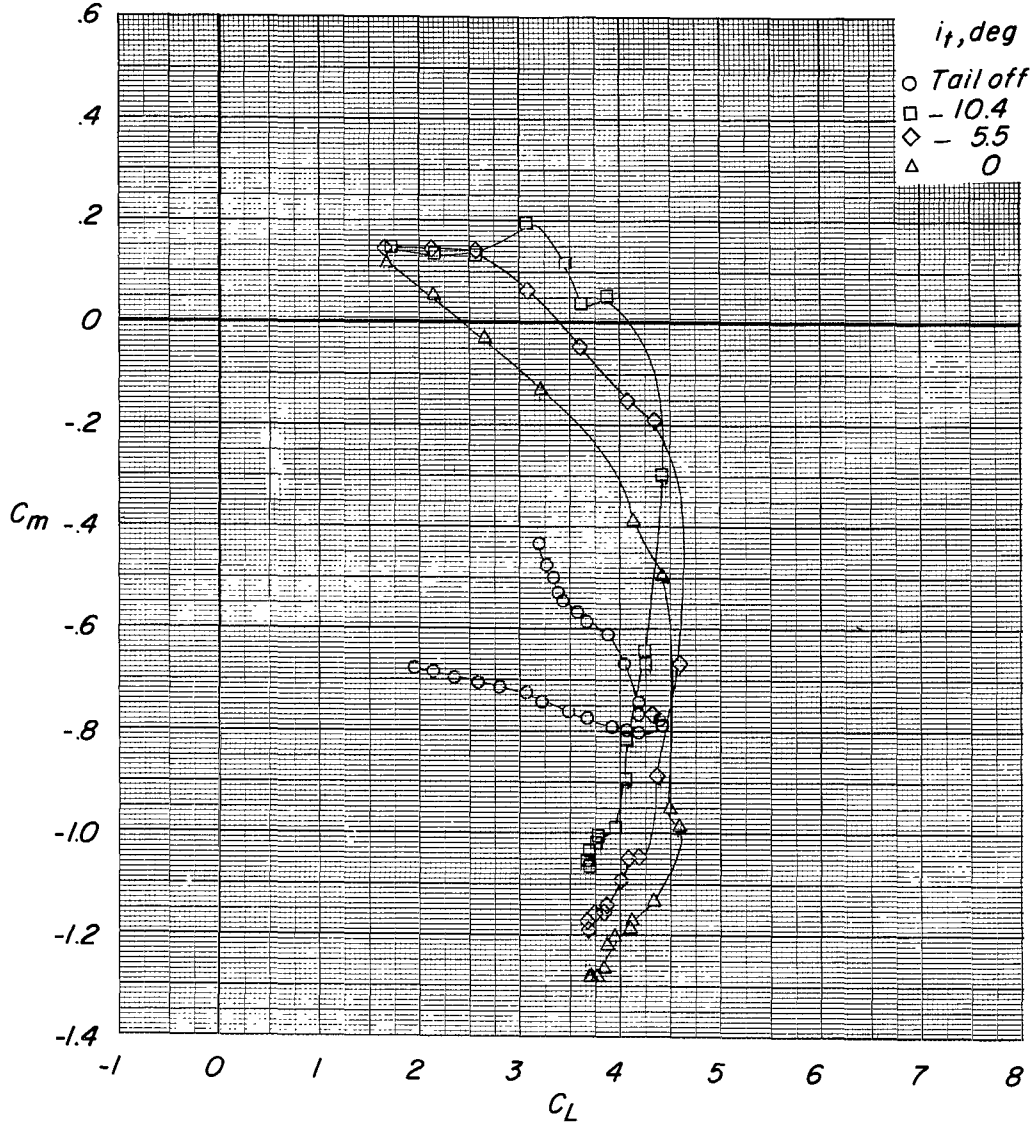

(d) Variation of C_m with C_L.

Figure 25.- Continued.

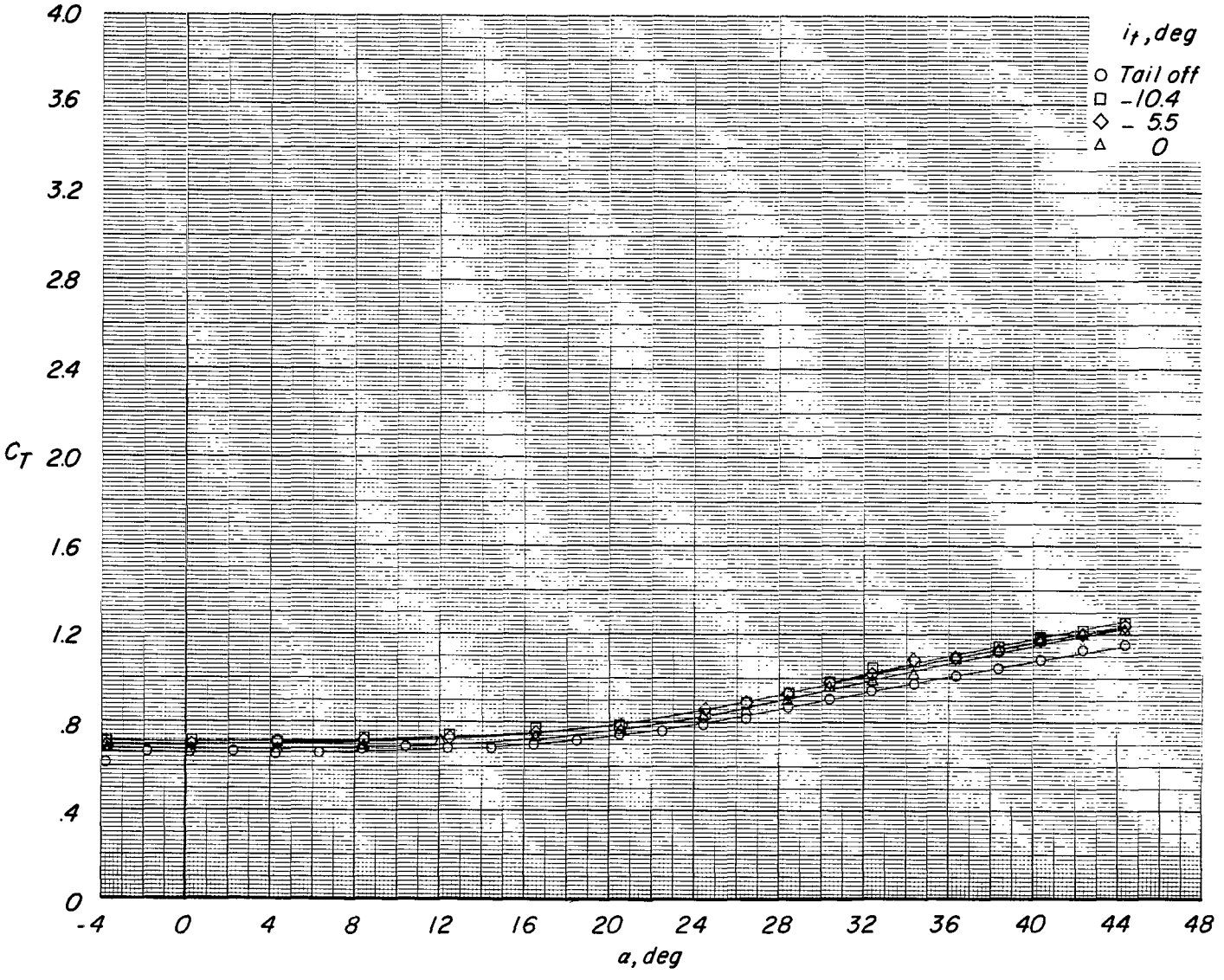

(e) Variation of C_T with α.

Figure 25.- Concluded.

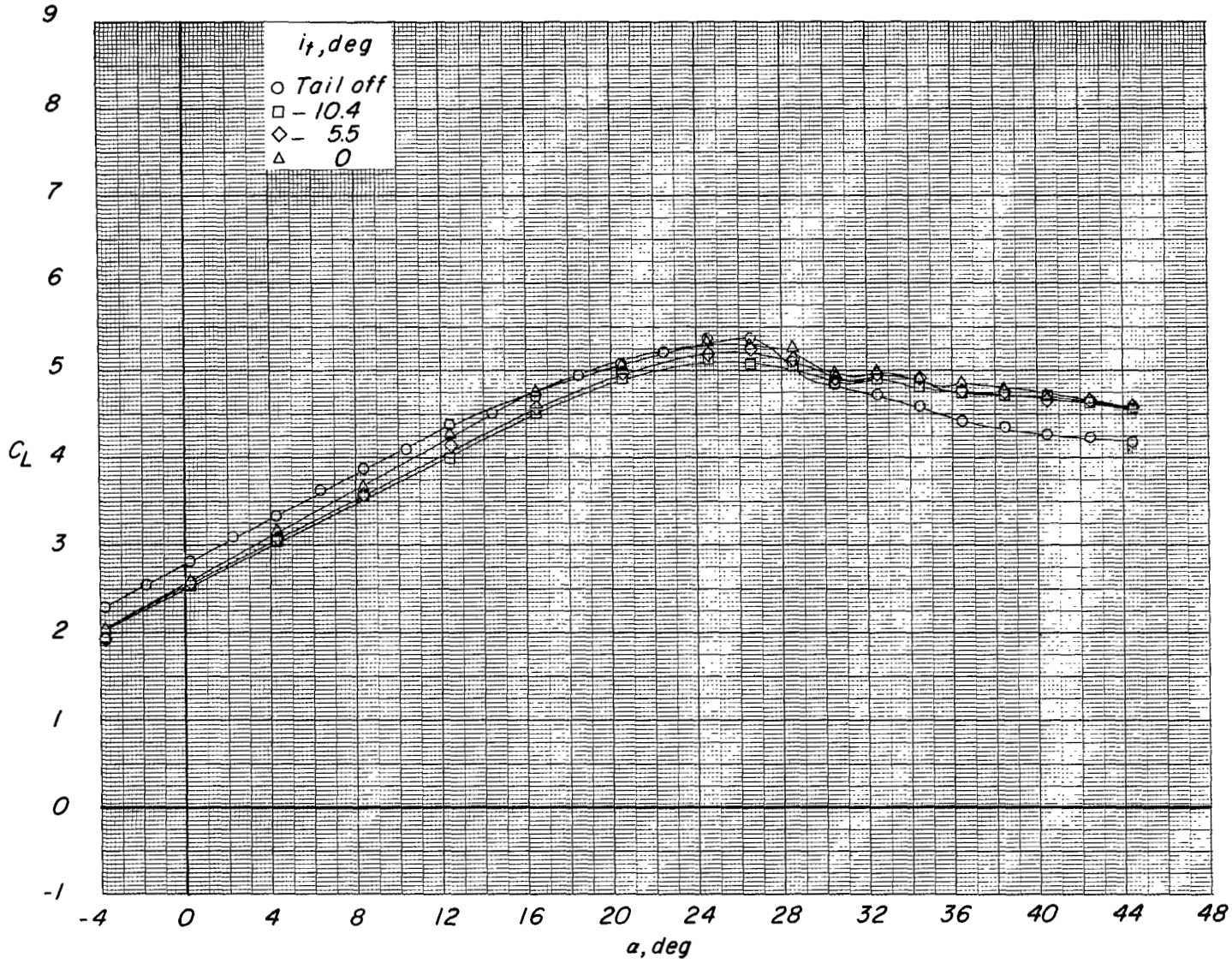

(a) Variation of C_L with α.

Figure 26.- Effect of tail incidence on longitudinal aerodynamic characteristics of configuration with large tail in low position. $\delta_f = 45^0$; reference $C_T = 1.25$.

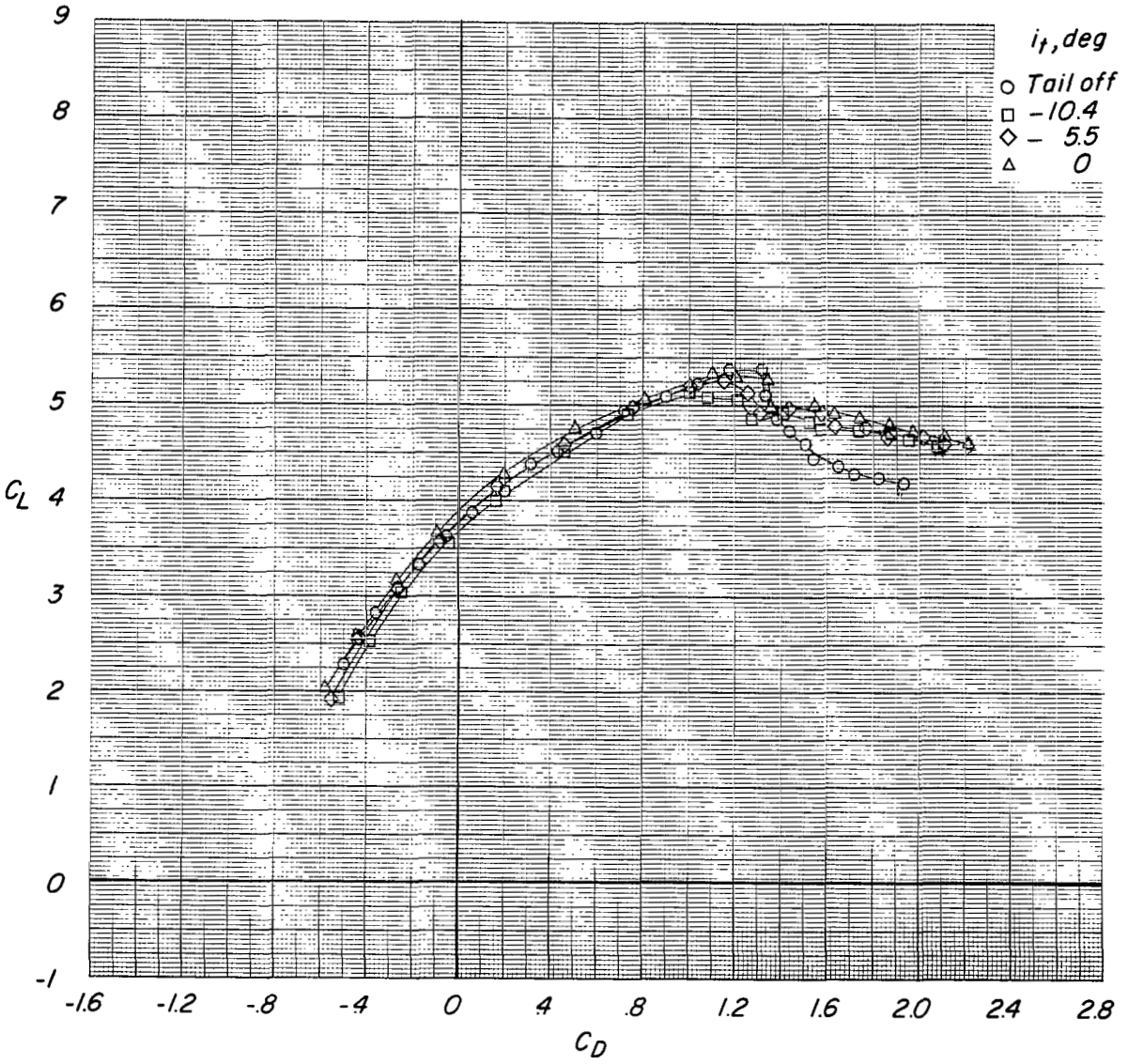

(b) Variation of C_L with C_D.

Figure 26.- Continued.

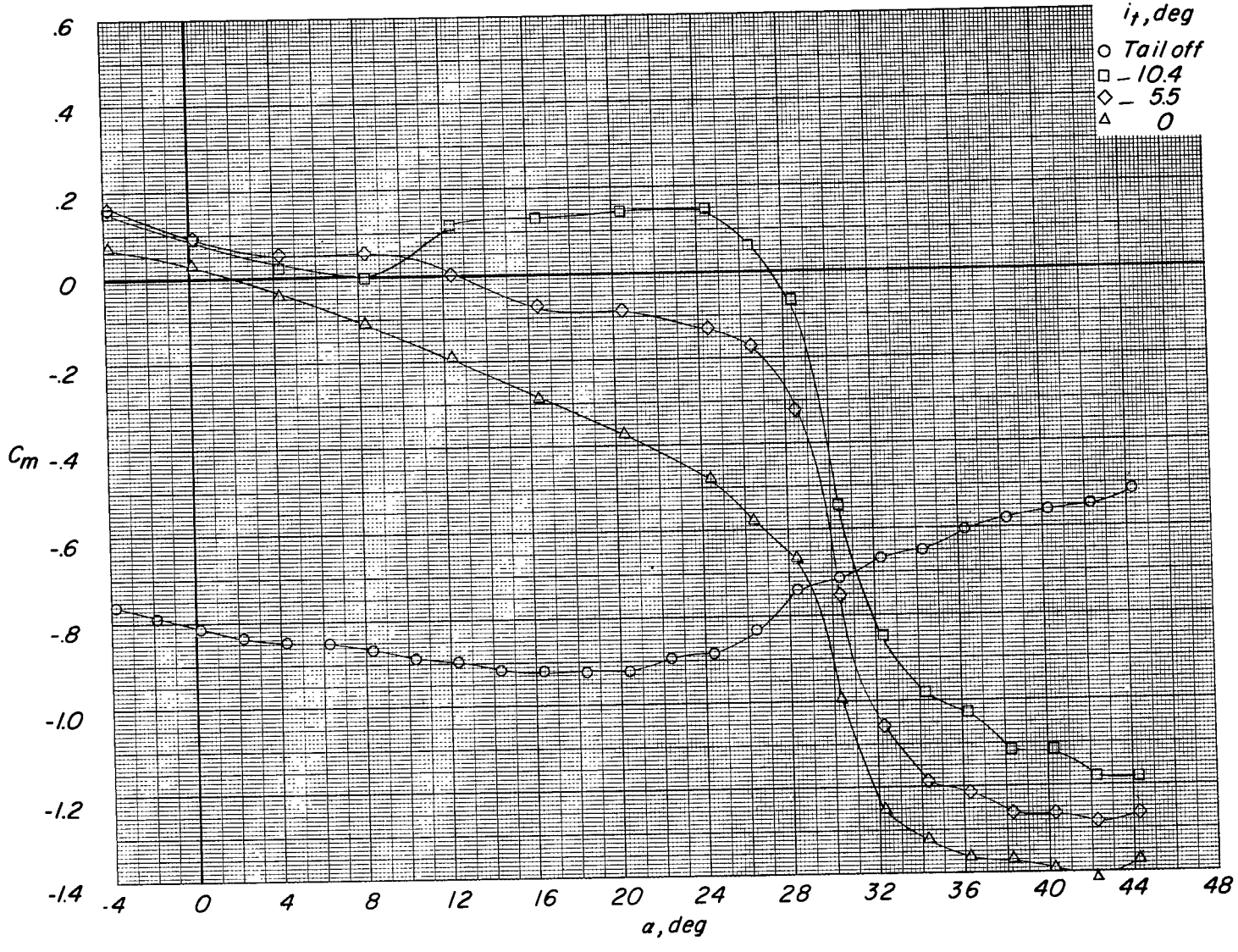

(c) Variation of C_m with α.

Figure 26.- Continued.

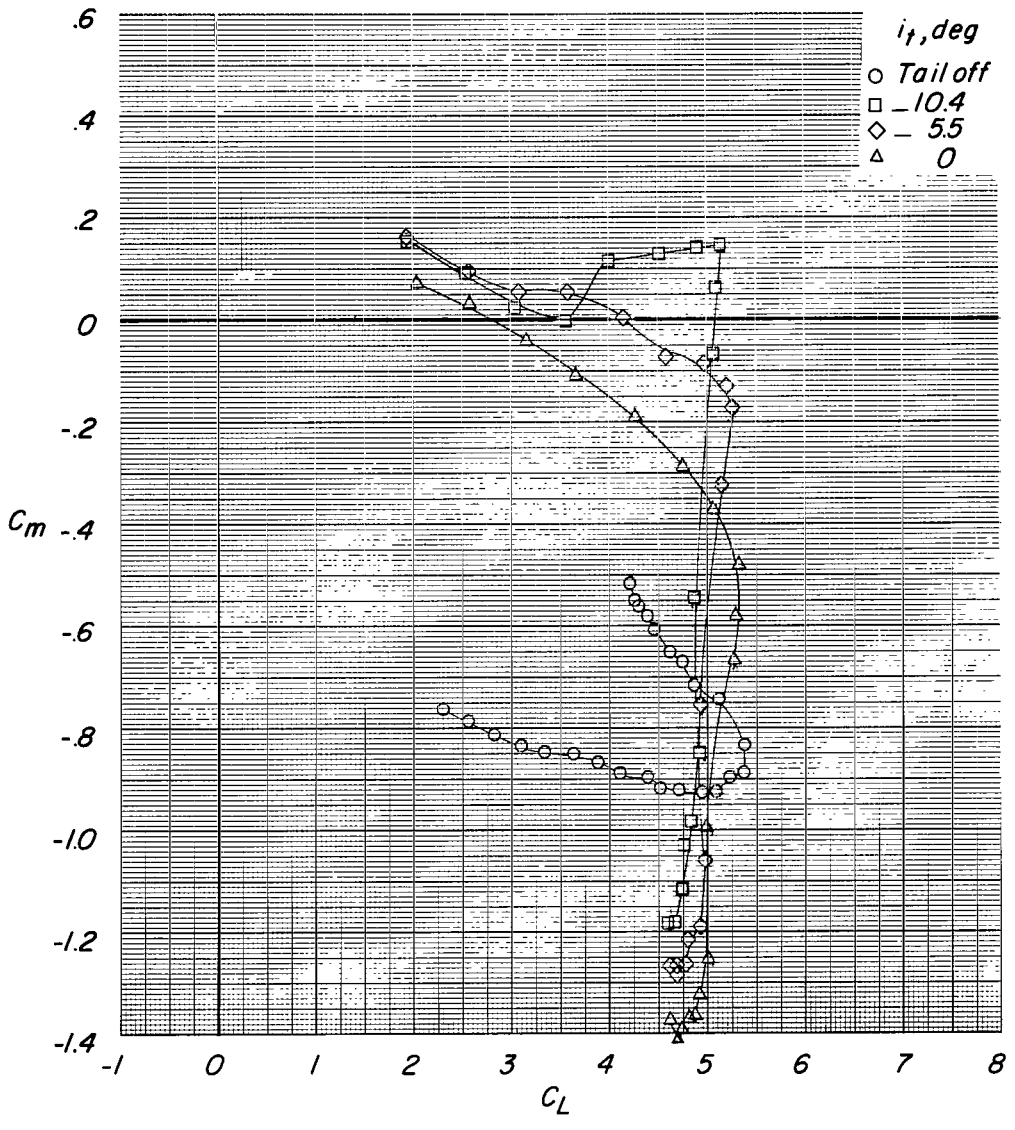

(d) Variation of C_m with C_L.

Figure 26.- Continued.

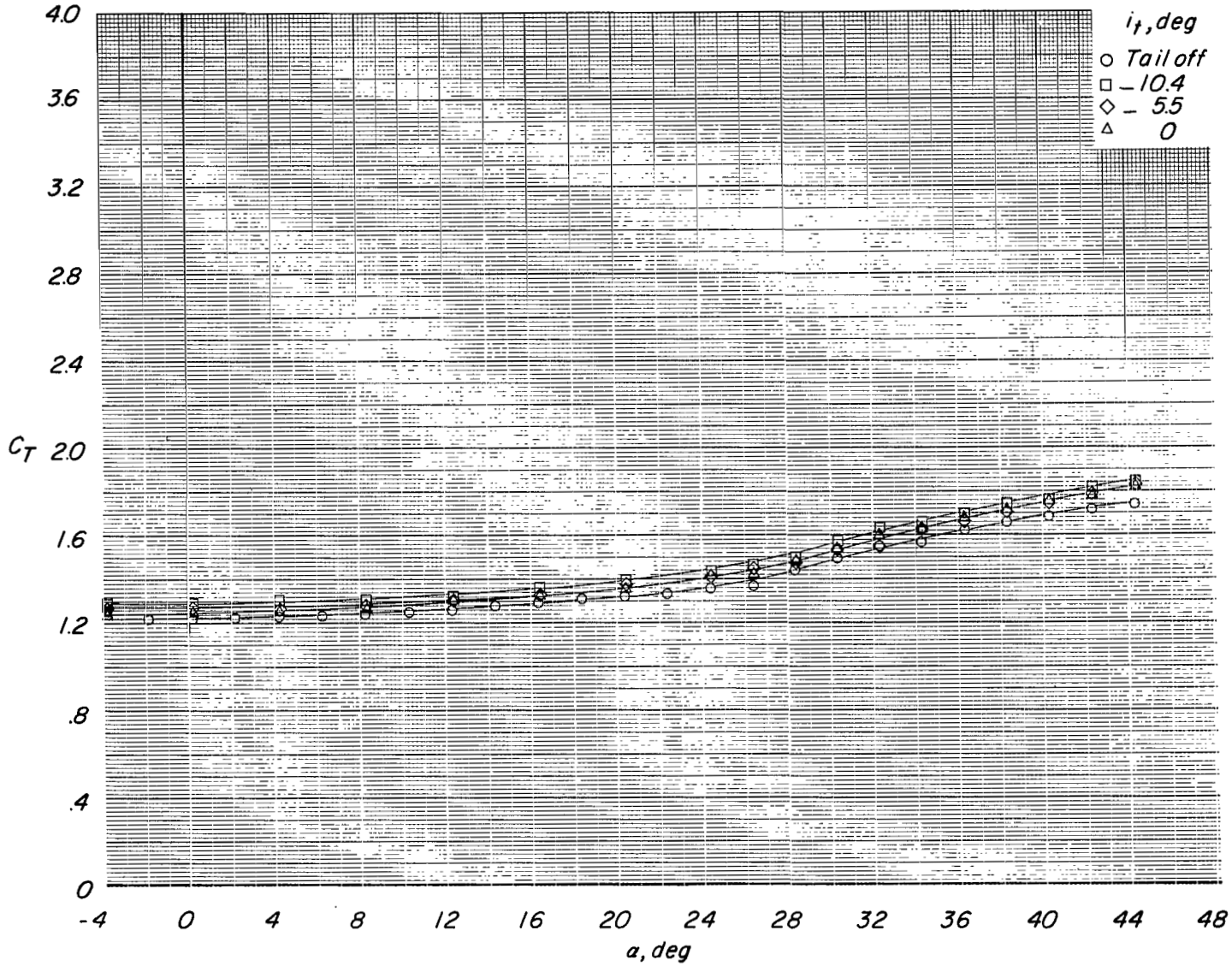

(e) Variation of C_T with α.

Figure 26.- Concluded.

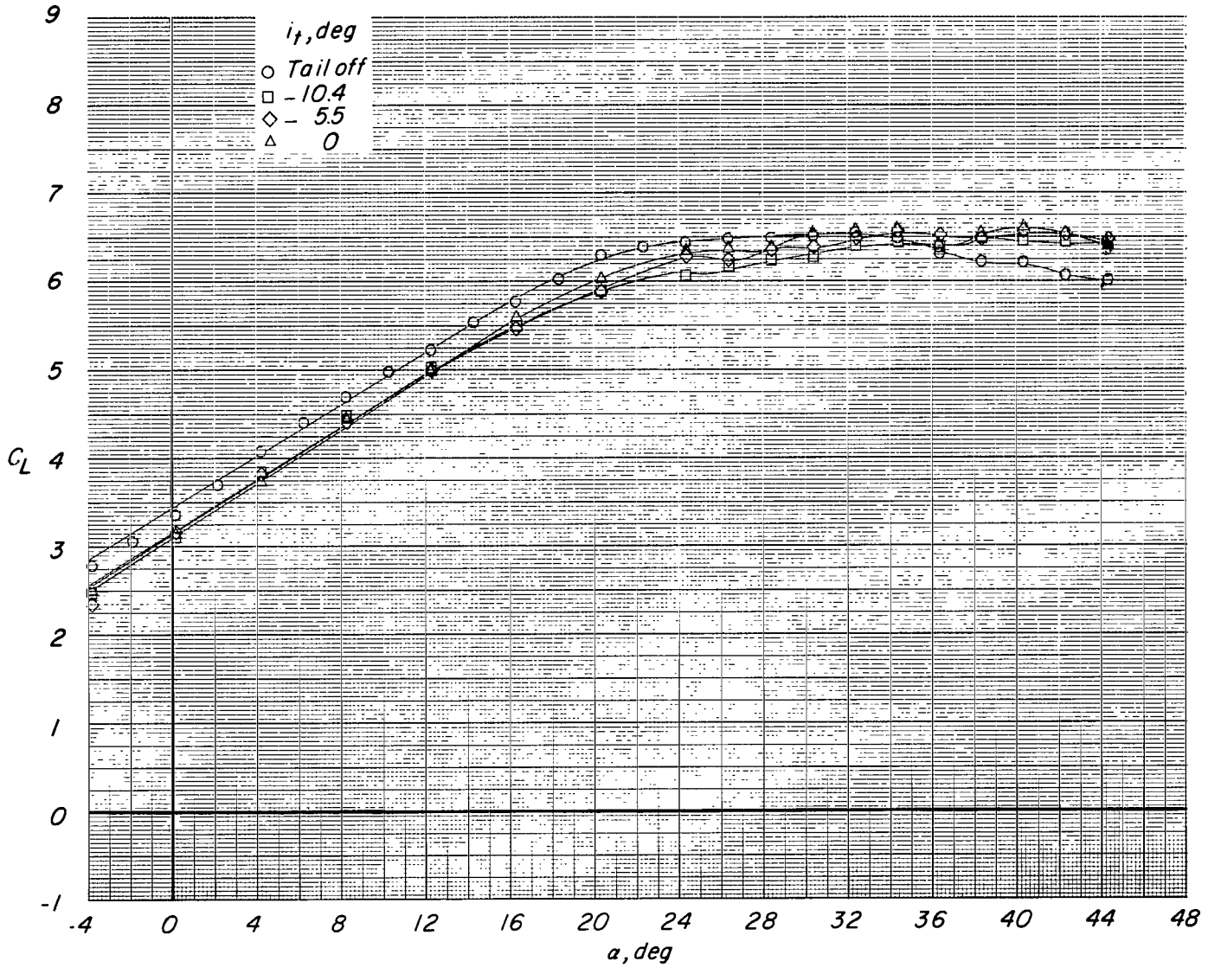

(a) Variation of C_L with α.

Figure 27.- Effect of tail incidence on longitudinal aerodynamic characteristics of configuration with large tail in low position. $\delta_f = 45^o$; reference $C_T = 2.42$.

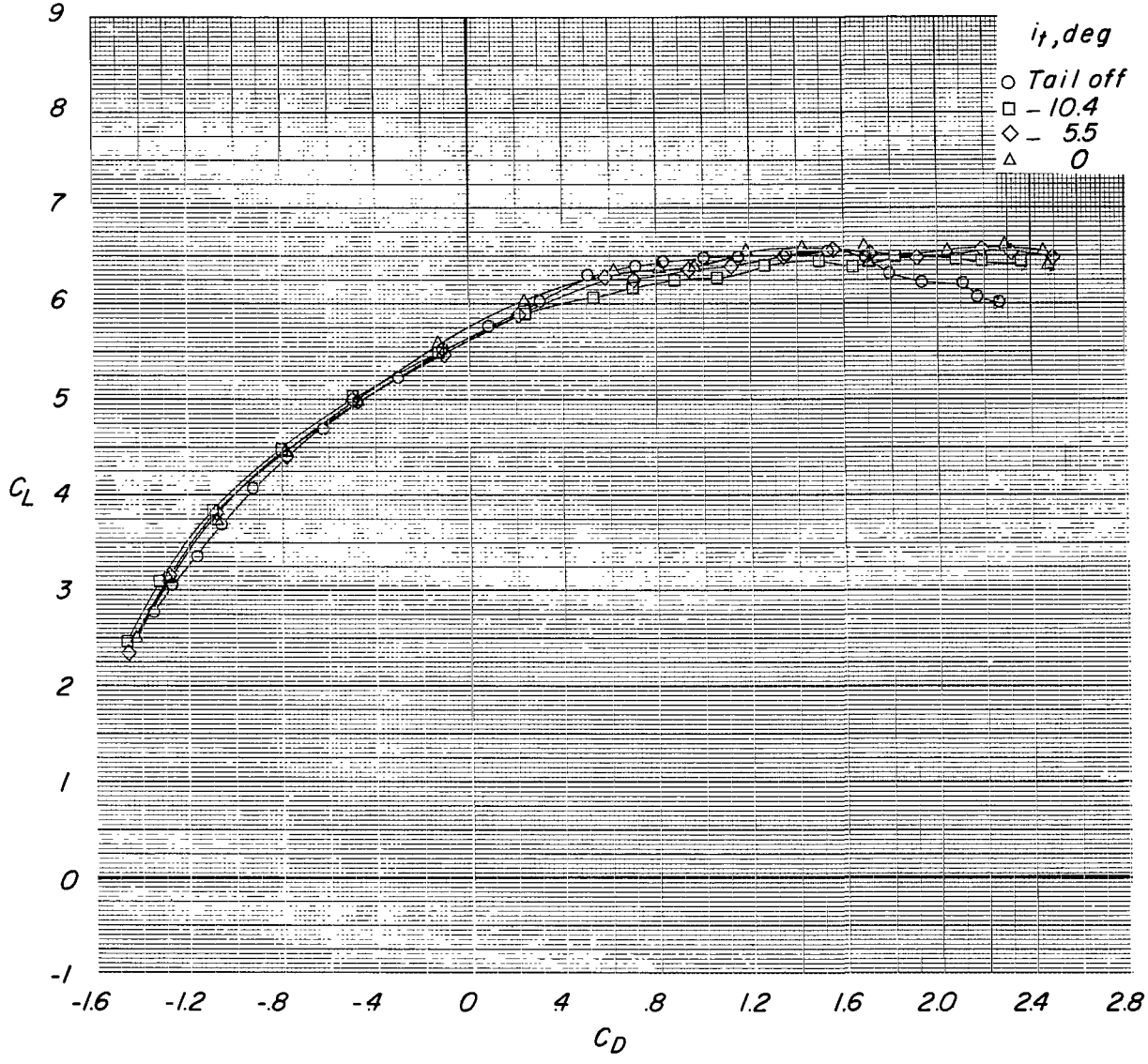

(b) Variation of C_L with C_D.

Figure 27.- Continued.

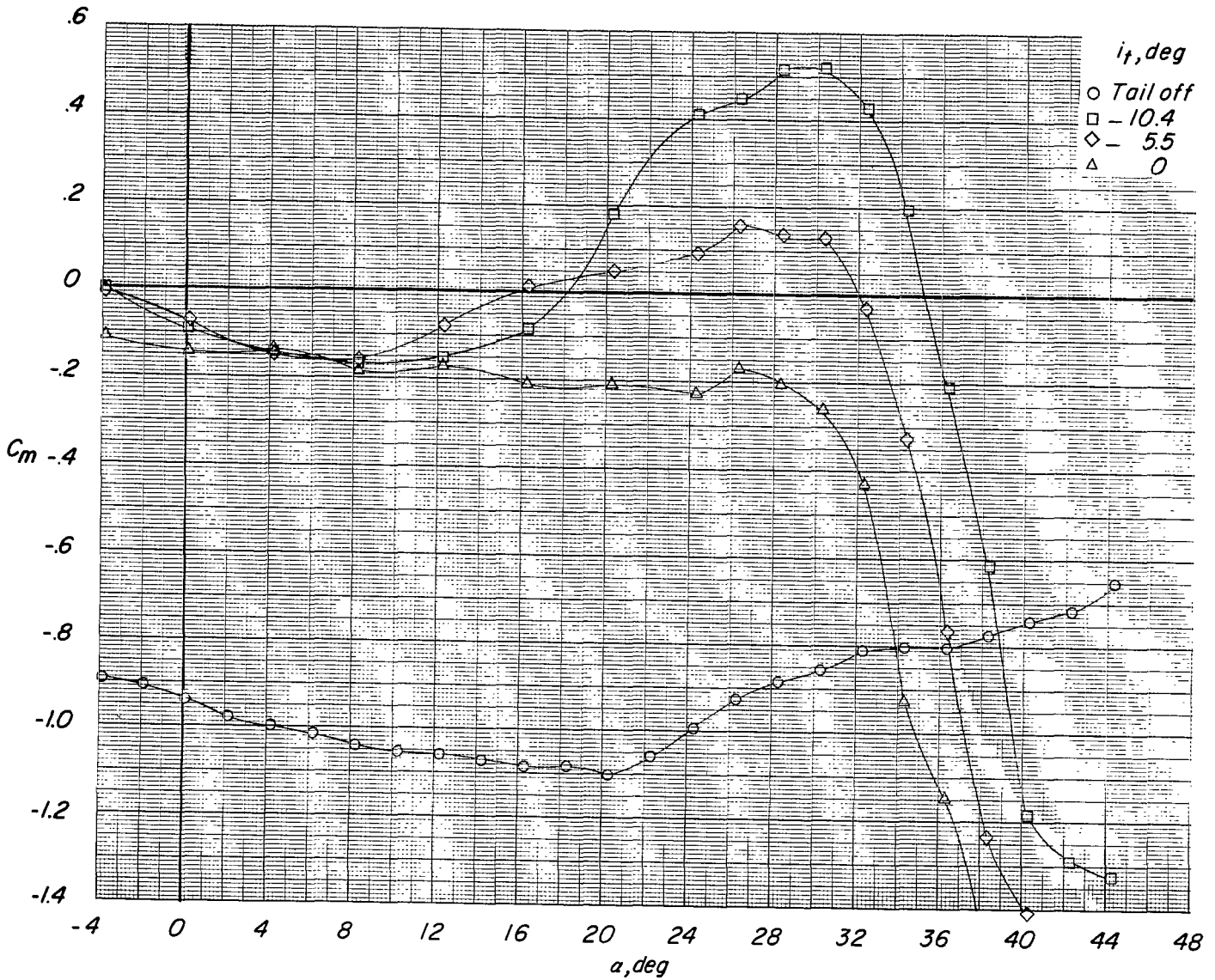

(c) Variation of C_m with α.

Figure 27.- Continued.

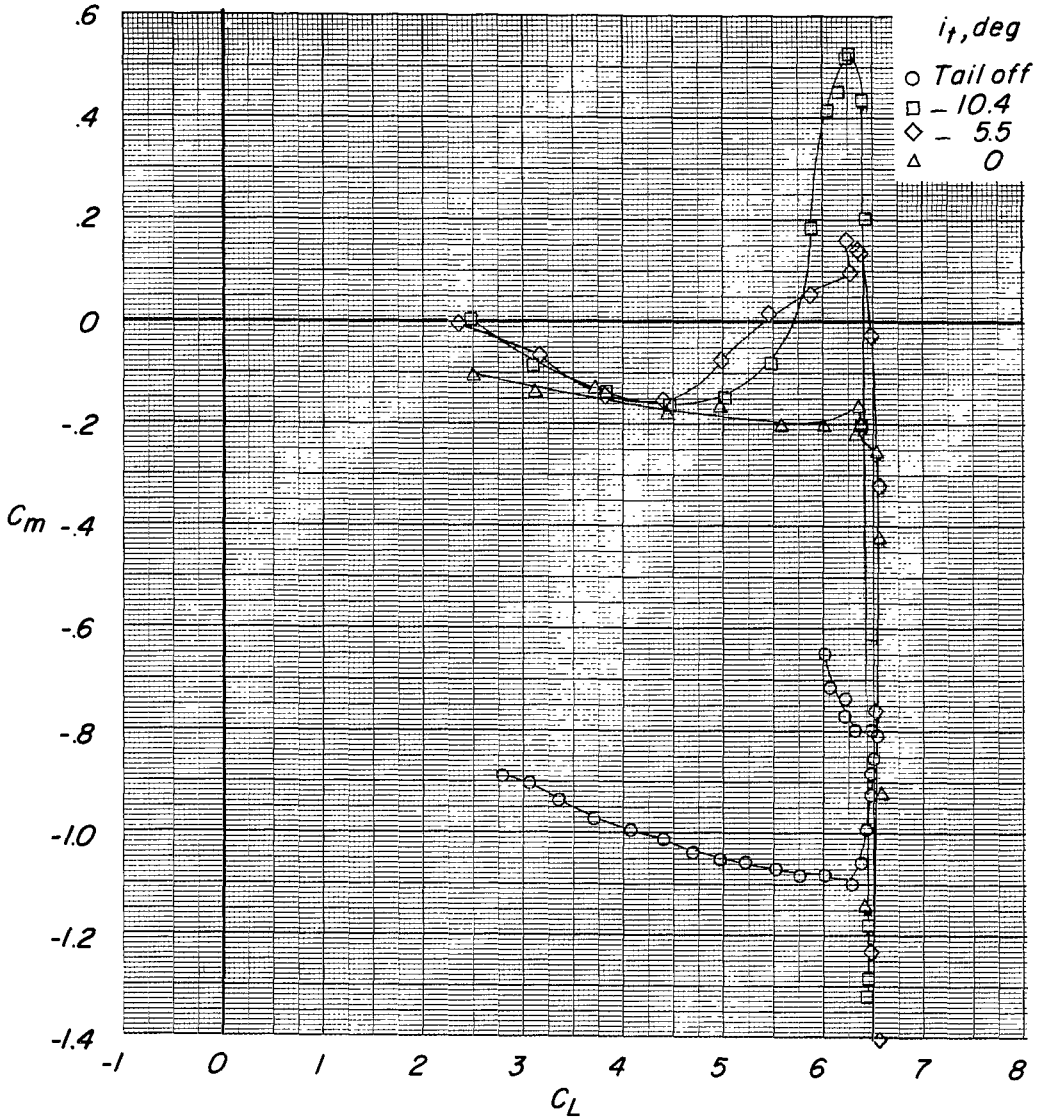

(d) Variation of C_m with C_L.

Figure 27.- Continued.

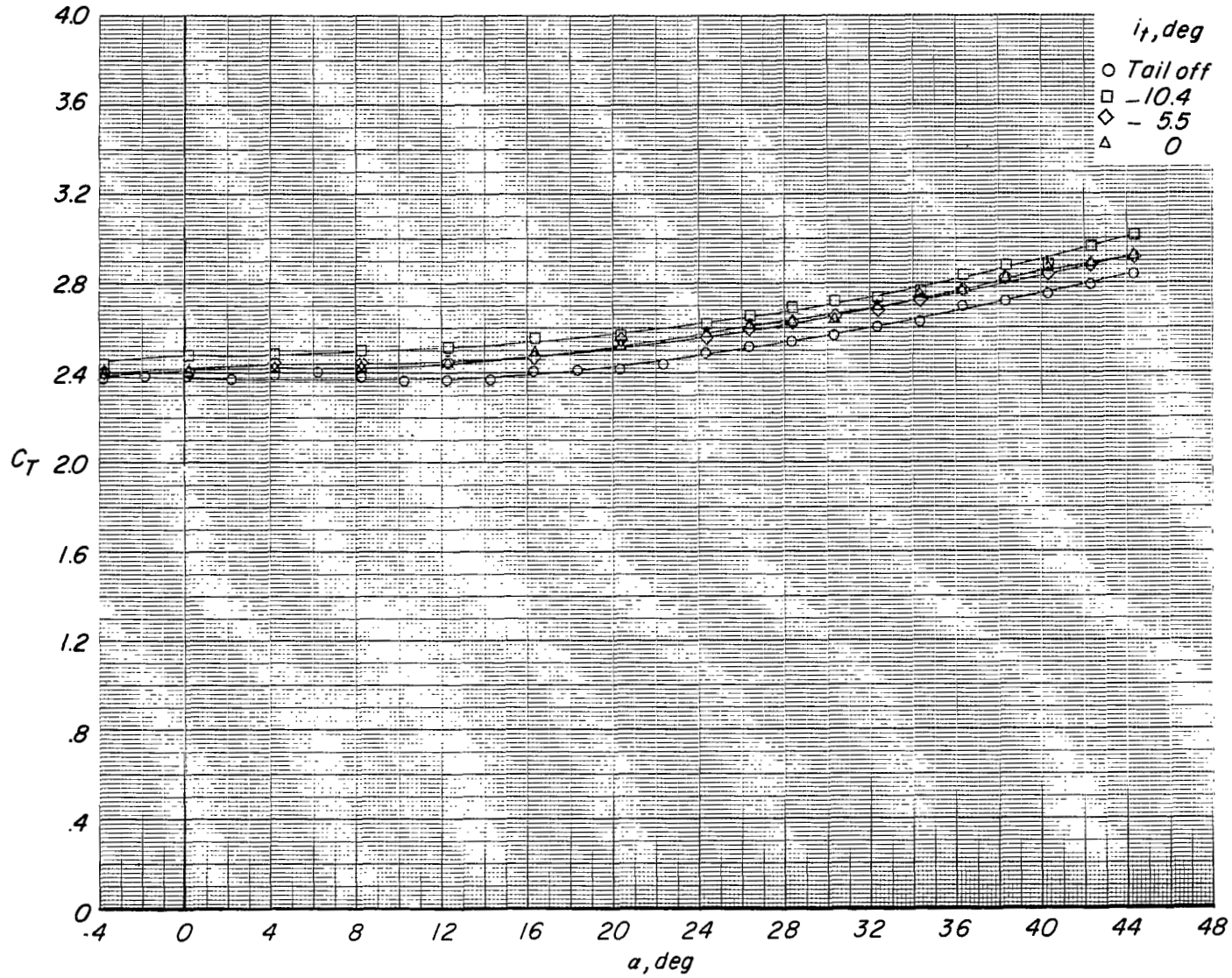

(e) Variation of C_T with α.

Figure 27.- Concluded.

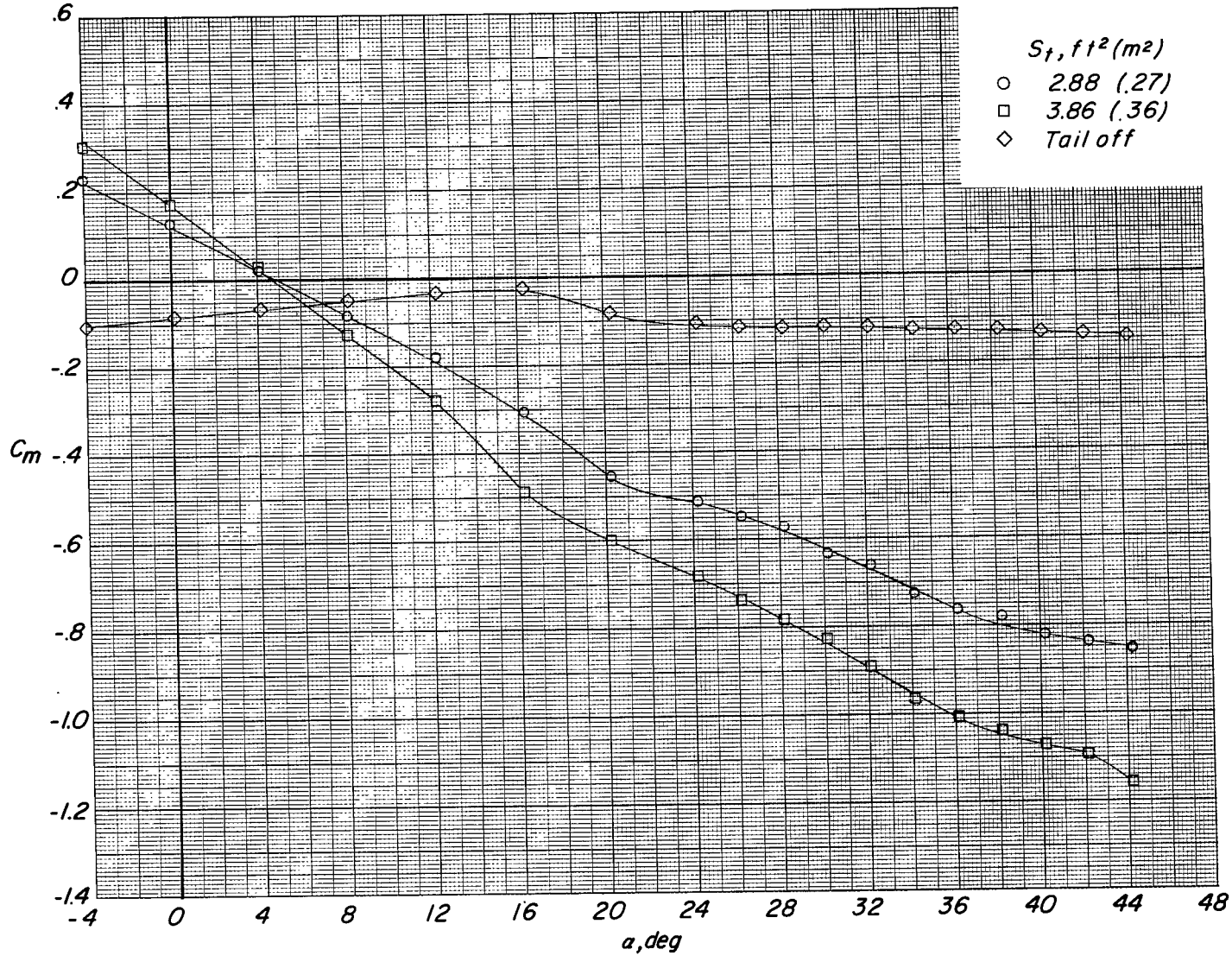

(a) $C_T = 0$ (propeller off).

Figure 28.- Effect of tail area for configuration with horizontal tail in high position. $i_t = 0^0$; $\delta_f = 0^0$.

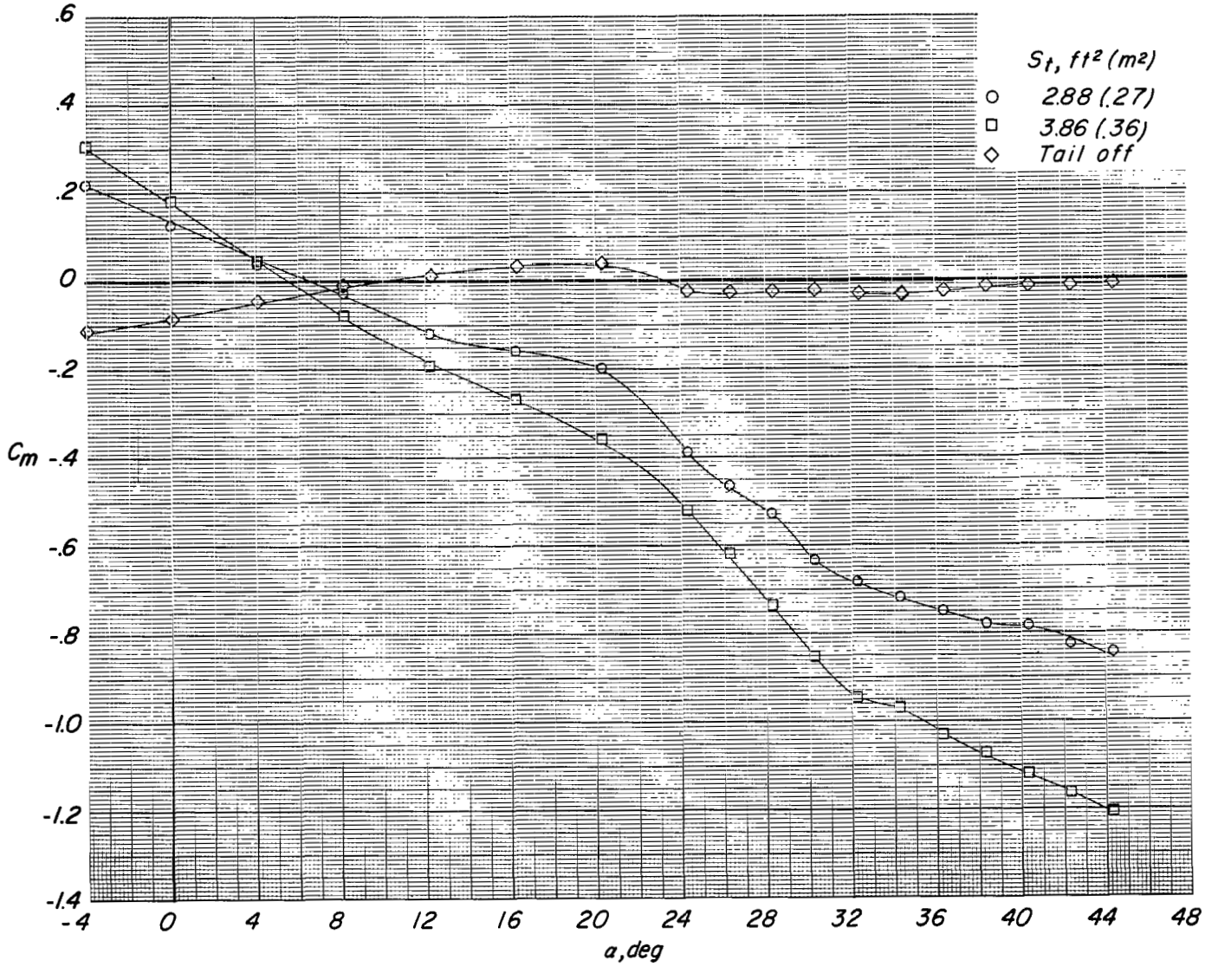

(b) Reference $C_T = 0.17$.

Figure 28.- Continued.

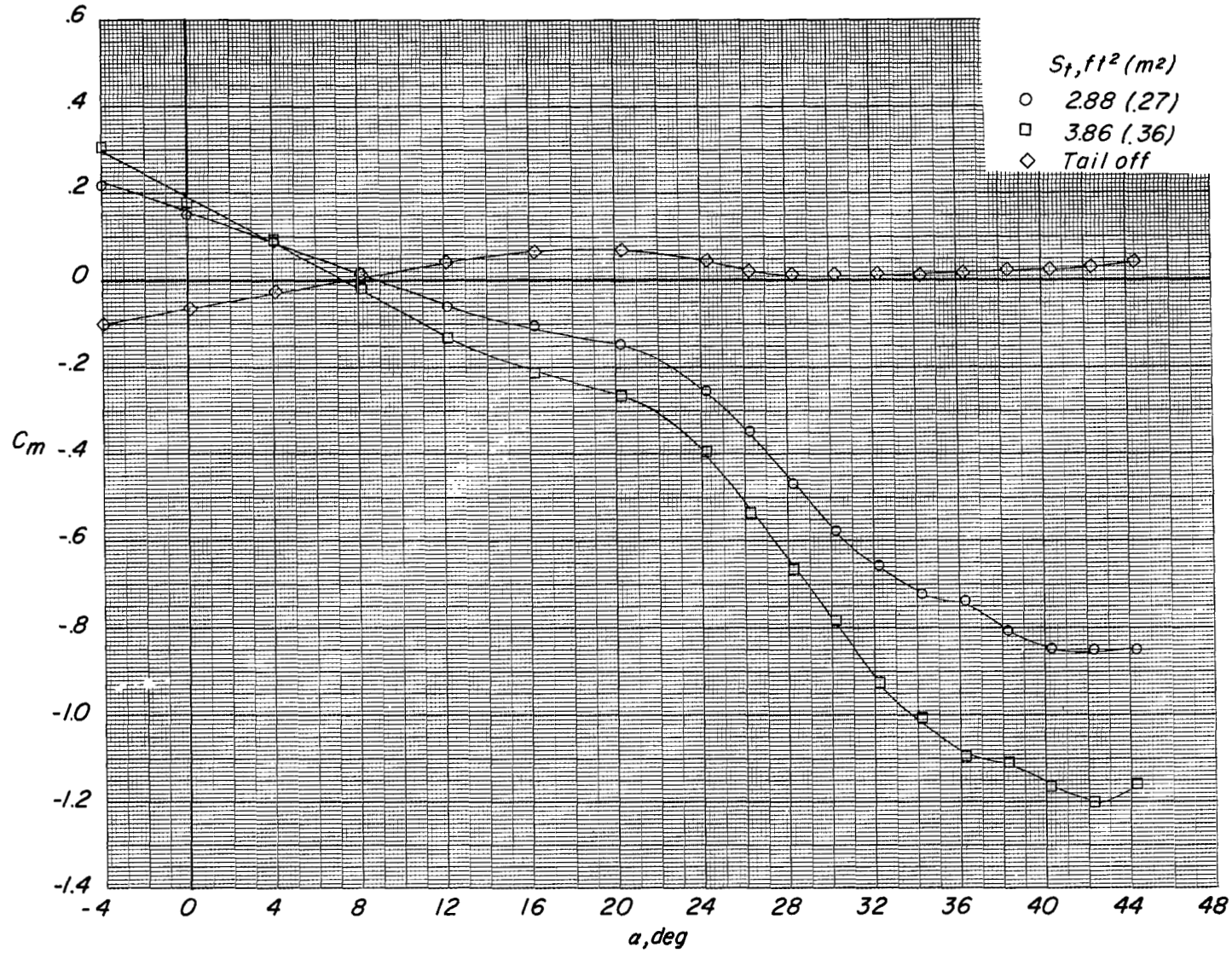

(c) Reference $C_T = 0.44$.

Figure 28.- Concluded.

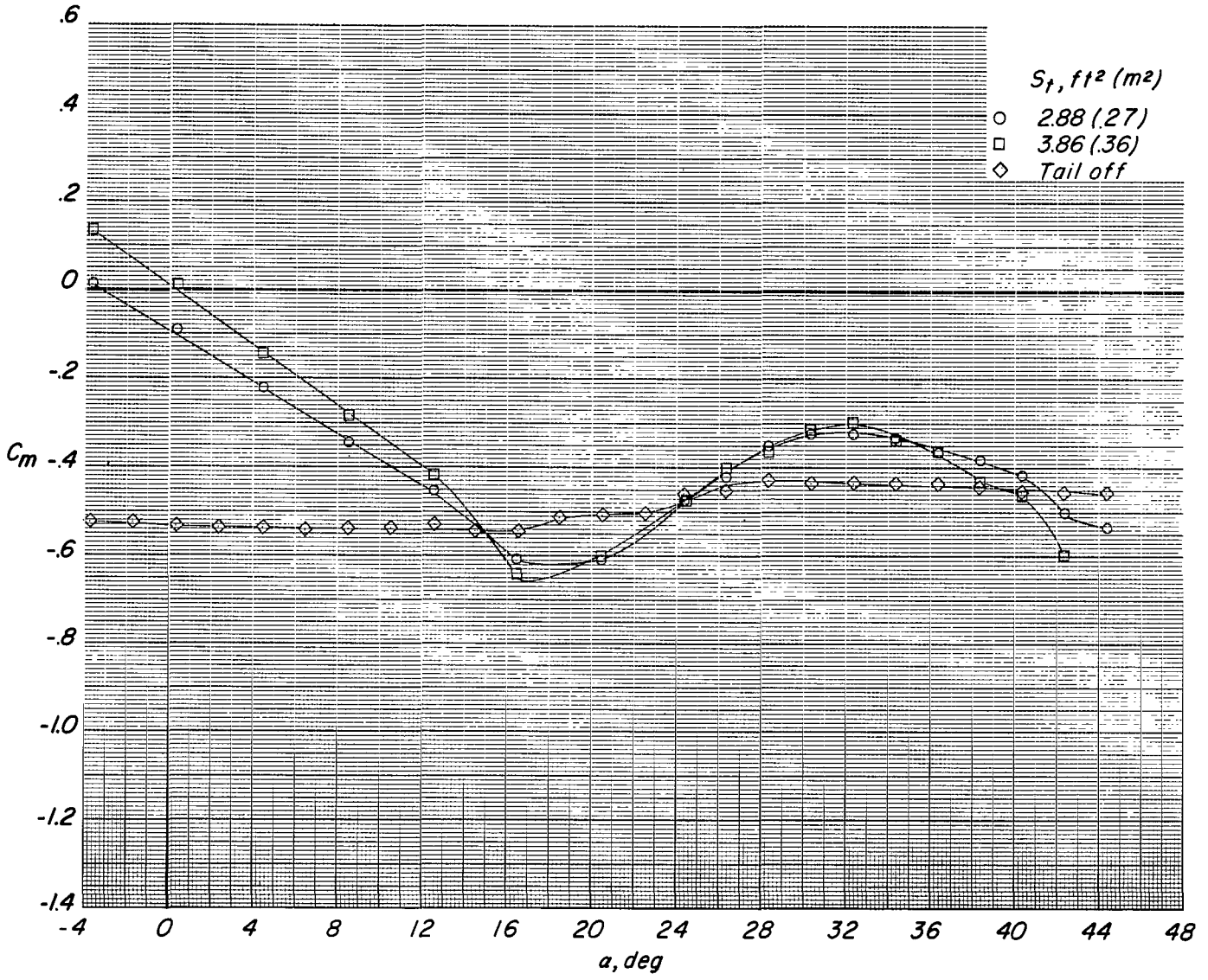

(a) $C_T = 0$ (propeller off).

Figure 29.- Effect of tail area for configuration with horizontal tail in high position. $i_t = 0^0$; $\delta_f = 45^0$.

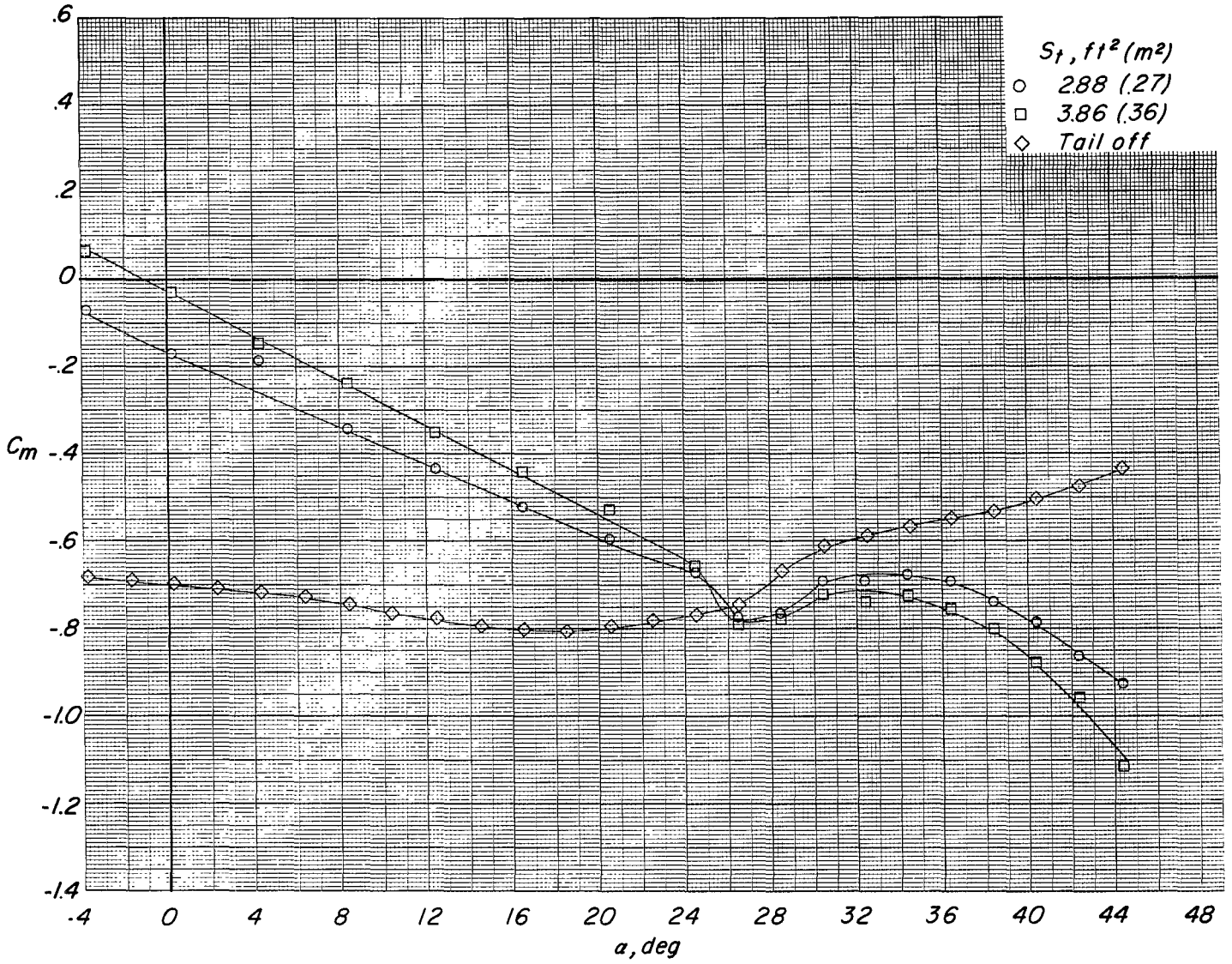

(b) Reference C_T = 0.70.

Figure 29.- Continued.

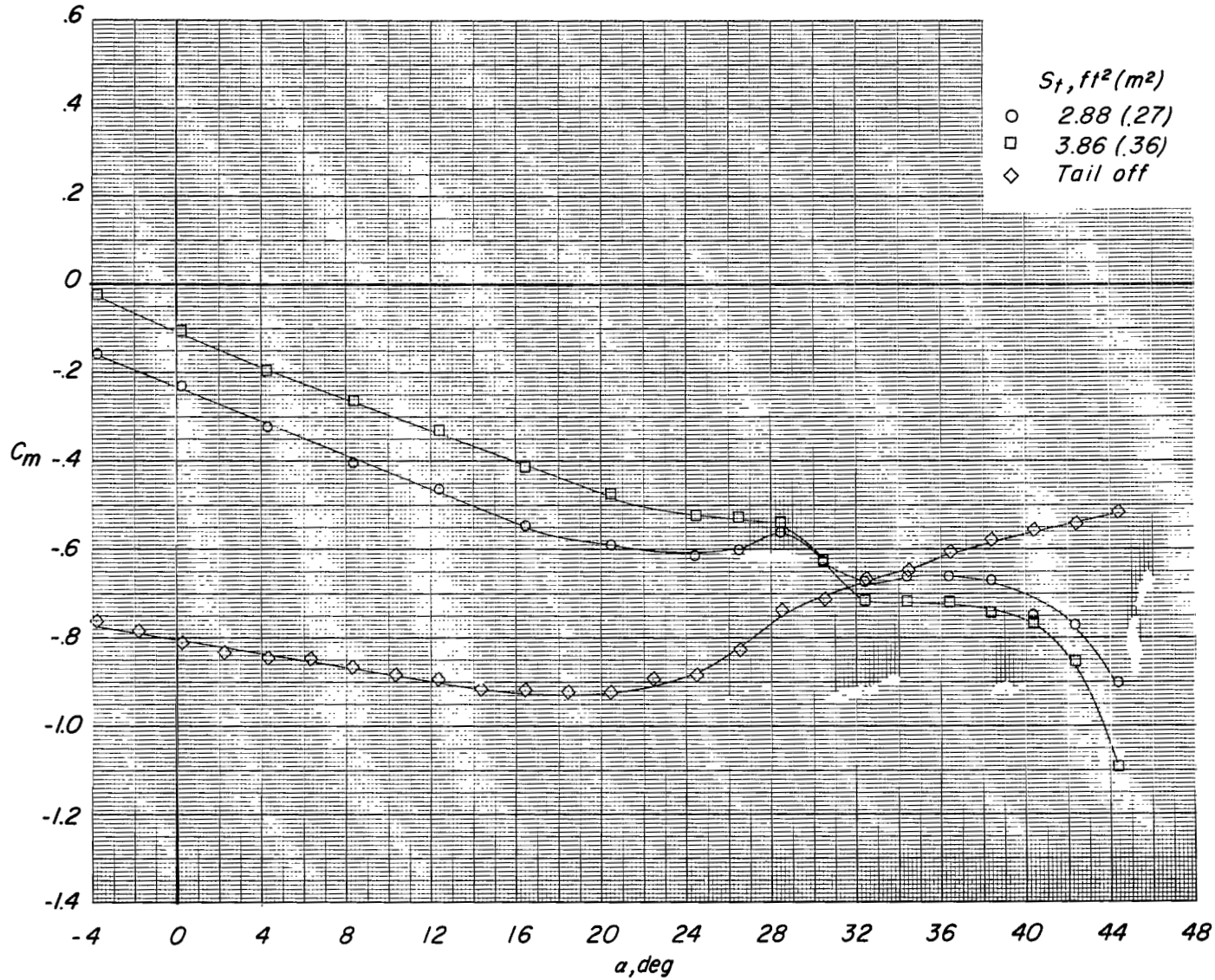

(c) Reference C_T = 1.25.

Figure 29.- Continued.

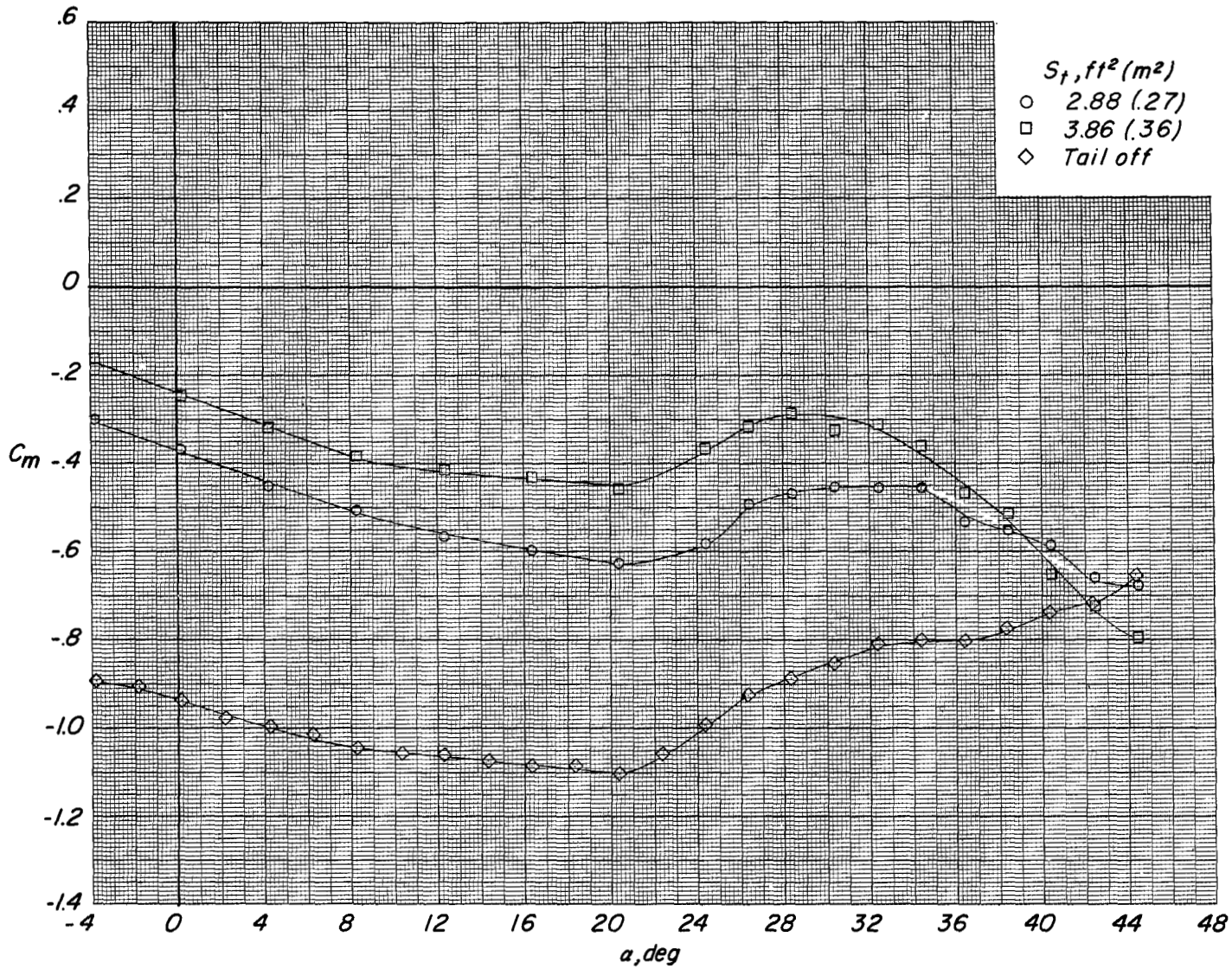

(d) Reference C_T = 2.42.

Figure 29.- Concluded.

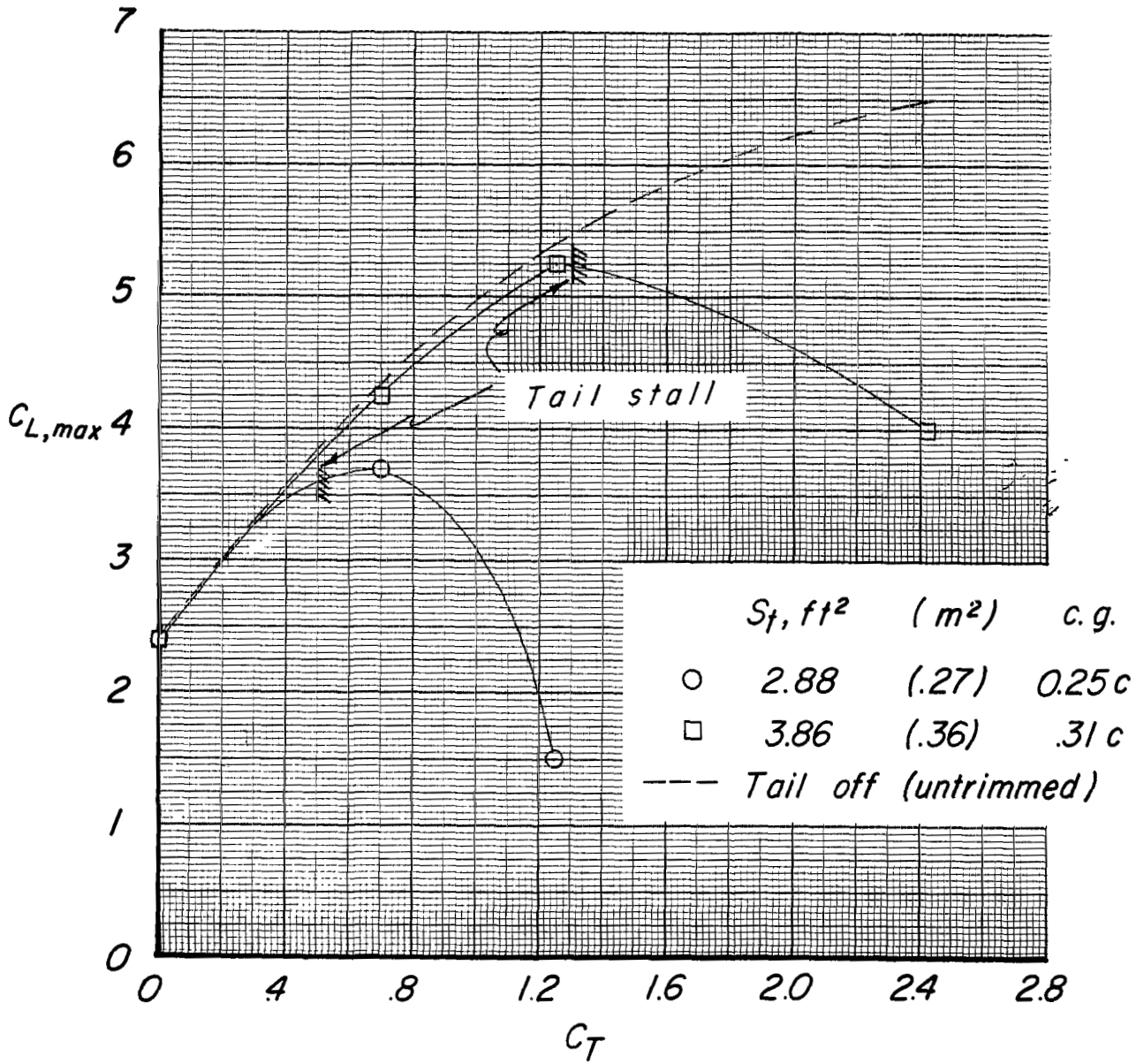

Figure 30.- Effect of tail area on maximum trimmed lift coefficient.

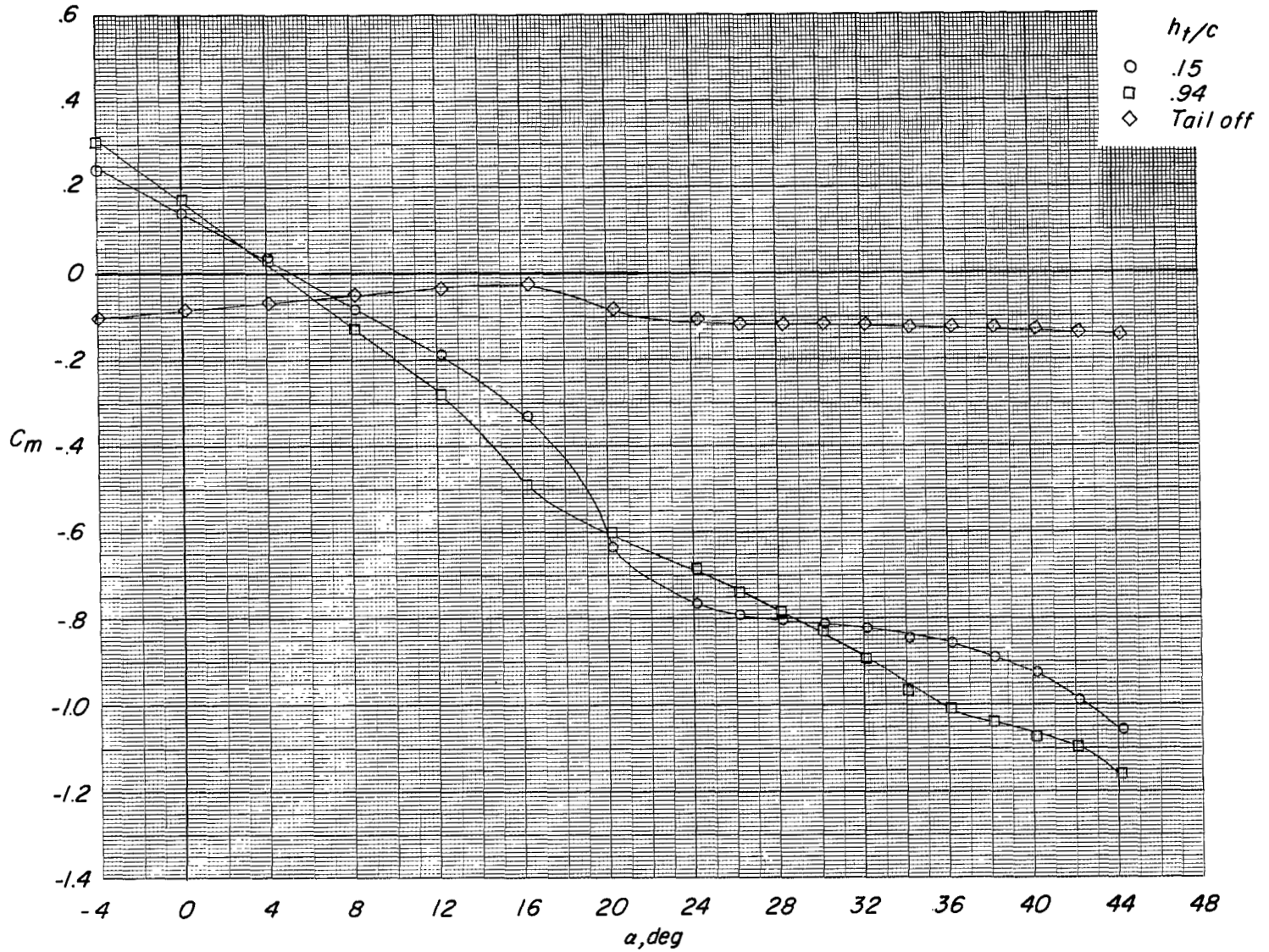

(a) $C_T = 0$ (propeller off).

Figure 31.- Effect of tail height for configuration with large tail. $i_t = 0^0$; $\delta_f = 0^0$.

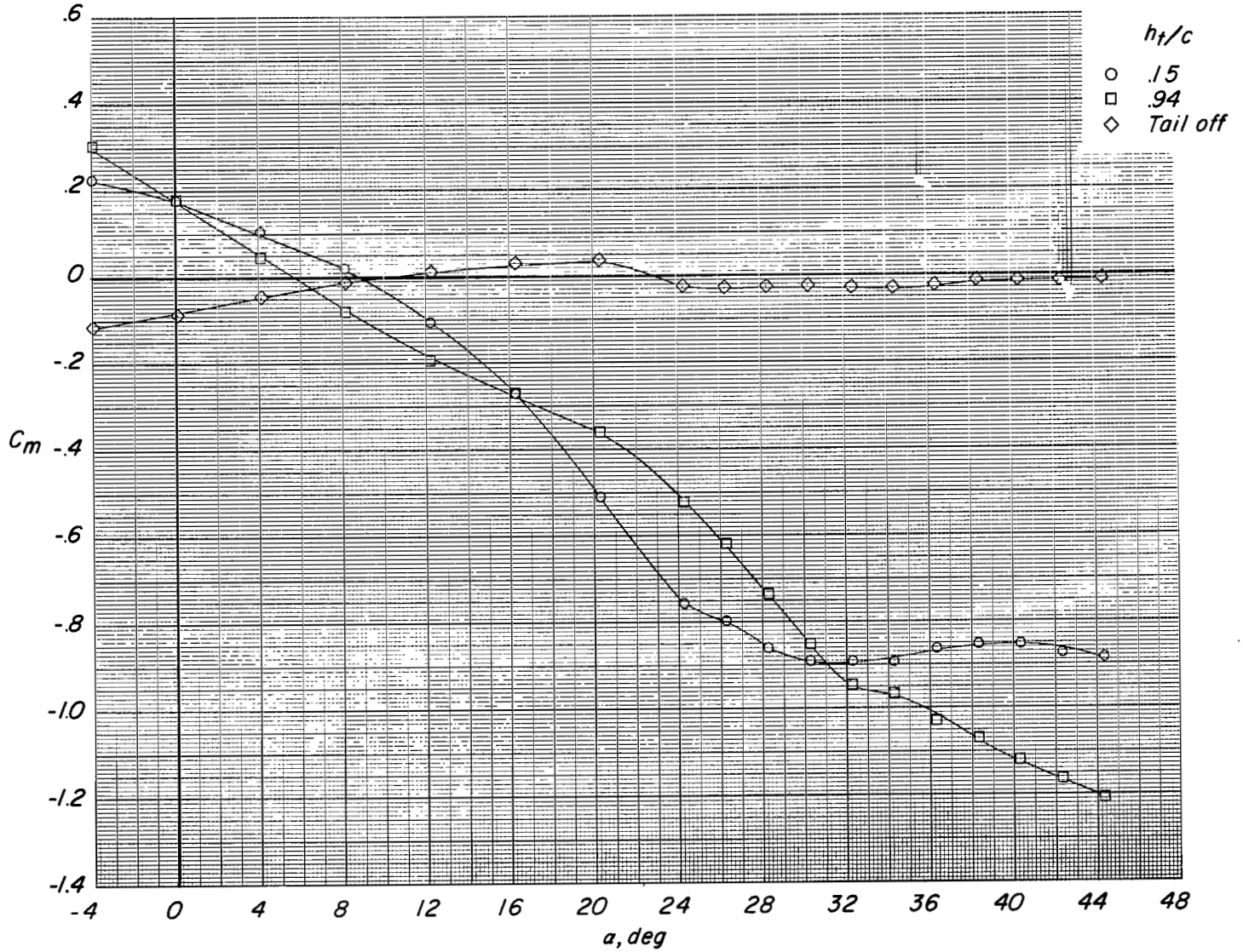

(b) Reference $C_T = 0.17$.

Figure 31.- Continued.

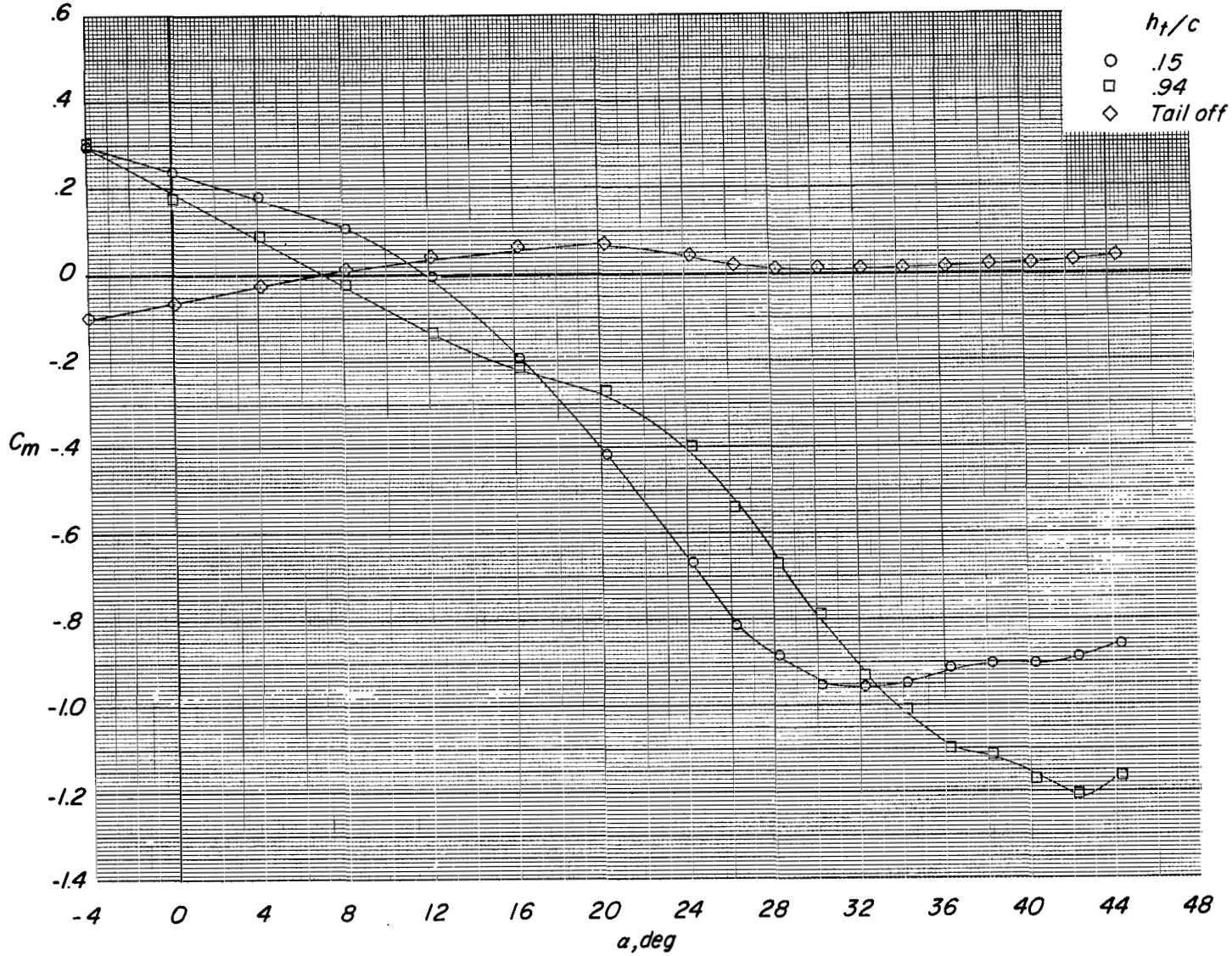

(c) Reference C_T = 0.44.

Figure 31.- Concluded.

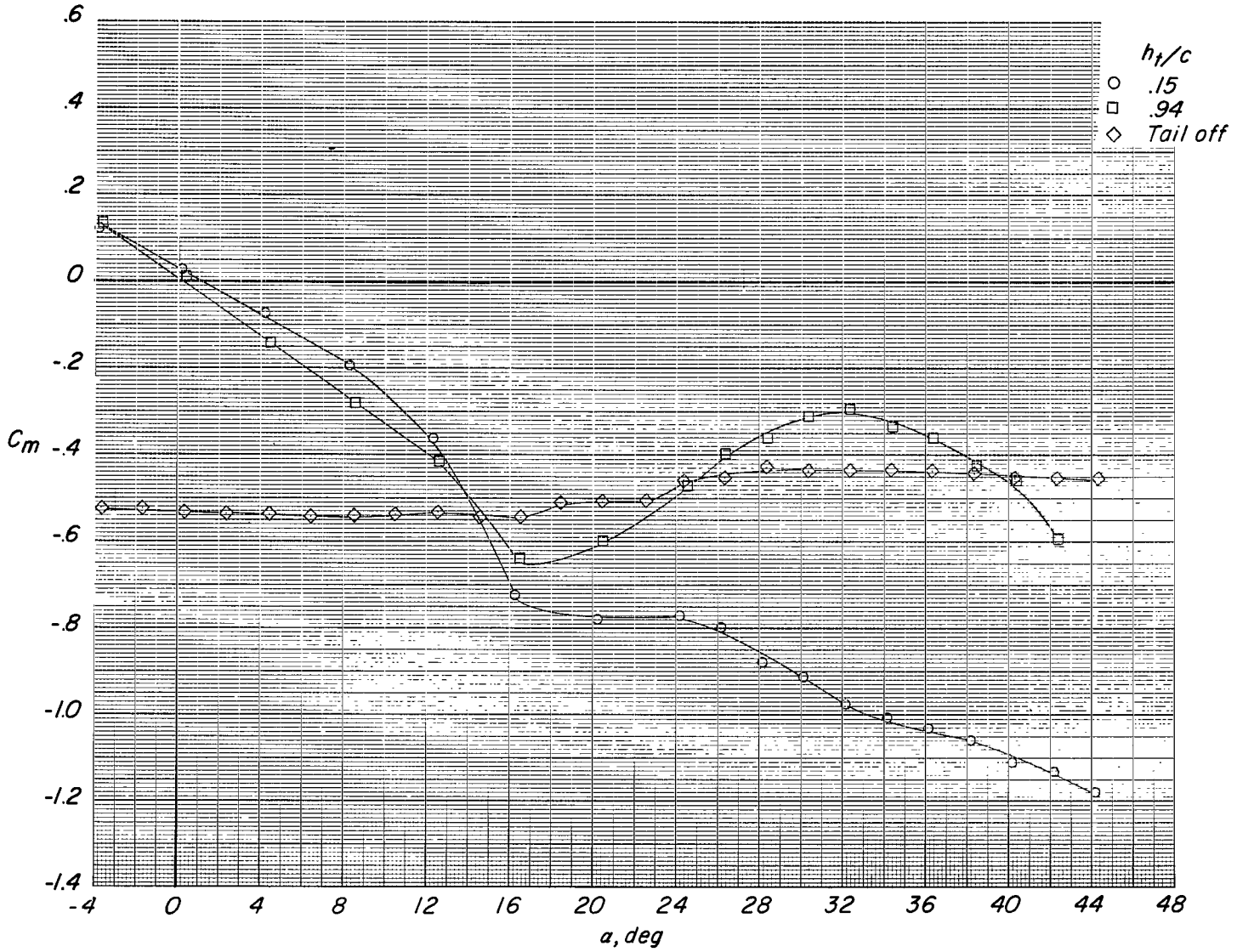

(a) $C_T = 0$ (propeller off).

Figure 32.- Effect of tail height for configuration with large tail. $i_t = 0^0$; $\delta_f = 45^0$.

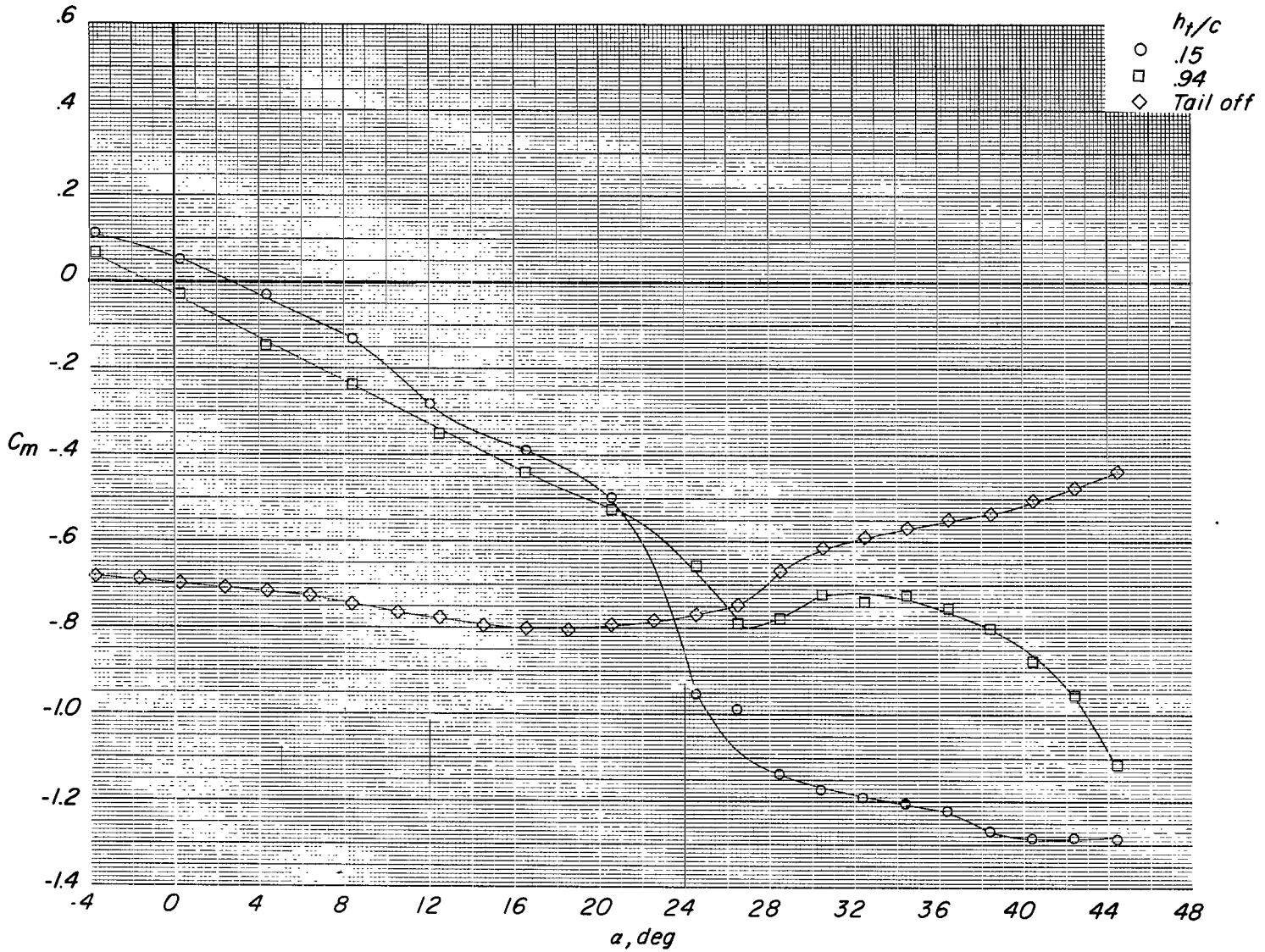

(b) Reference $C_T = 0.70$.

Figure 32.- Continued.

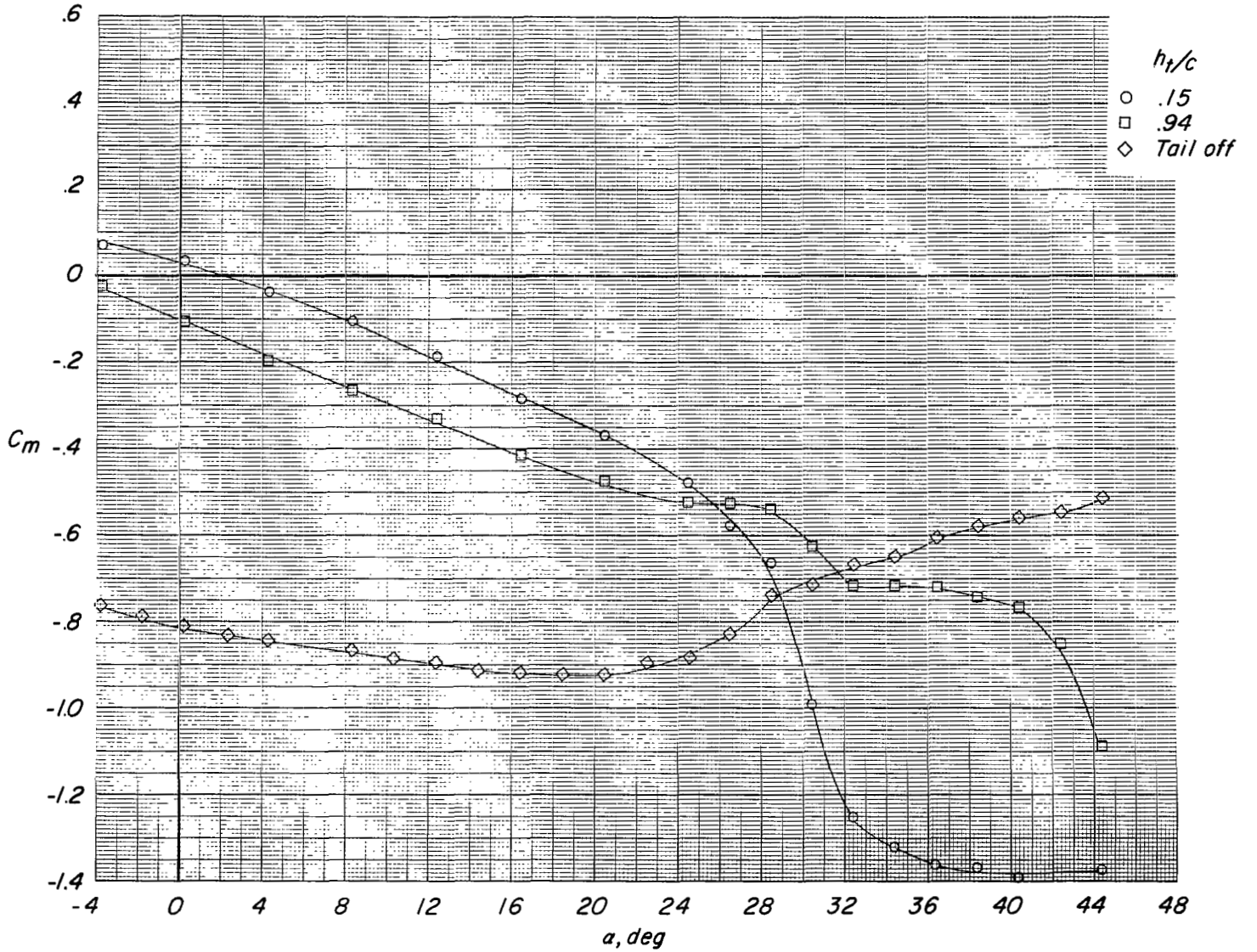

(c) Reference $C_T = 1.25$.

Figure 32.- Continued.

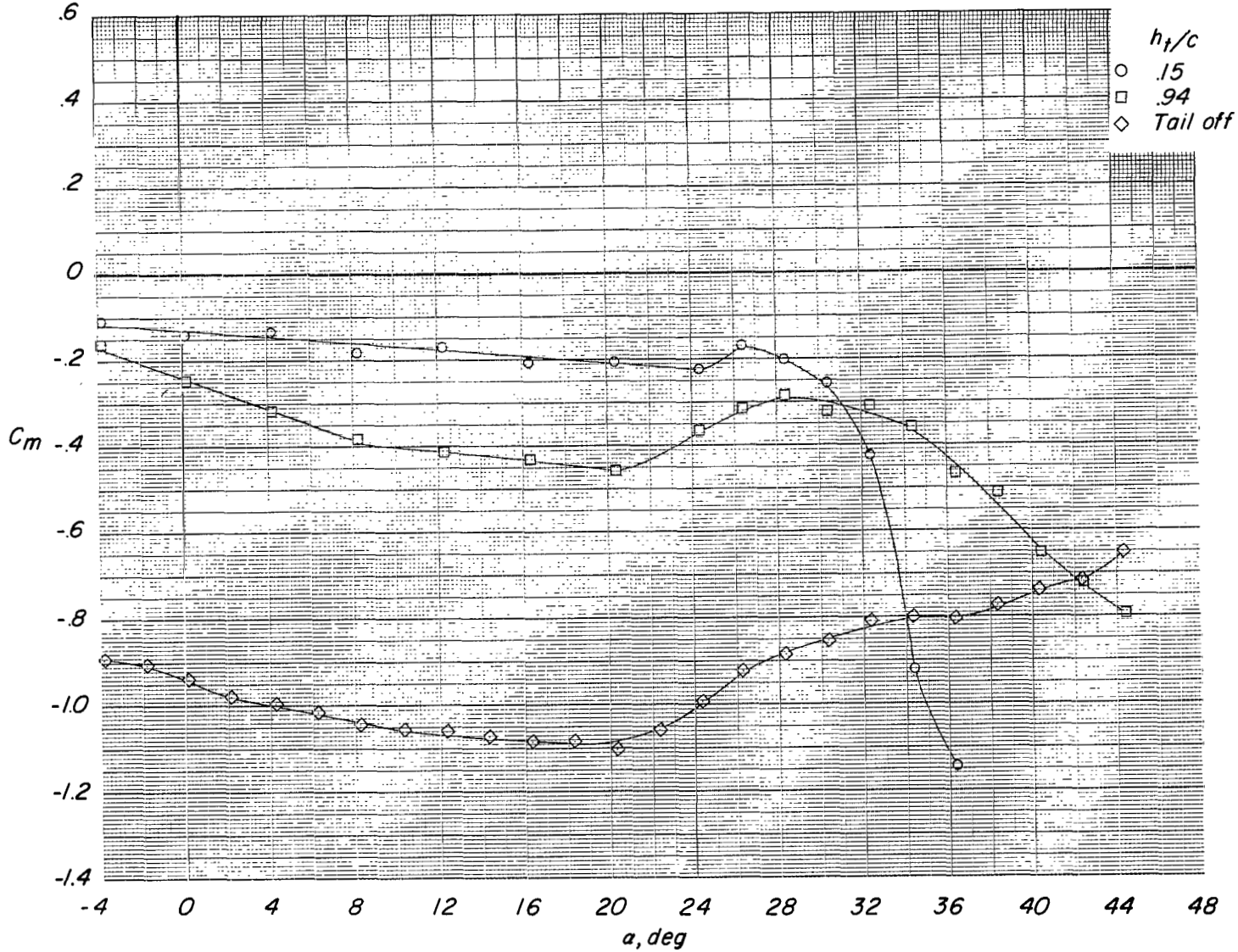

(d) Reference $C_T = 2.42$.

Figure 32.- Concluded.

"The aeronautical and space activities of the United States shall be conducted so as to contribute . . . to the expansion of human knowledge of phenomena in the atmosphere and space. The Administration shall provide for the widest practicable and appropriate dissemination of information concerning its activities and the results thereof."

—NATIONAL AERONAUTICS AND SPACE ACT OF 1958

NASA SCIENTIFIC AND TECHNICAL PUBLICATIONS

TECHNICAL REPORTS: Scientific and technical information considered important, complete, and a lasting contribution to existing knowledge.

TECHNICAL NOTES: Information less broad in scope but nevertheless of importance as a contribution to existing knowledge.

TECHNICAL MEMORANDUMS: Information receiving limited distribution because of preliminary data, security classification, or other reasons.

CONTRACTOR REPORTS: Technical information generated in connection with a NASA contract or grant and released under NASA auspices.

TECHNICAL TRANSLATIONS: Information published in a foreign language considered to merit NASA distribution in English.

SPECIAL PUBLICATIONS: Information derived from or of value to NASA activities. Publications include conference proceedings, monographs, data compilations, handbooks, sourcebooks, and special bibliographies.

TECHNOLOGY UTILIZATION PUBLICATIONS: Information on technology used by NASA that may be of particular interest in commercial and other nonaerospace applications. Publications include Tech Briefs; Technology Utilization Reports and Notes; and Technology Surveys.

Details on the availability of these publications may be obtained from:

SCIENTIFIC AND TECHNICAL INFORMATION DIVISION

NATIONAL AERONAUTICS AND SPACE ADMINISTRATION

Washington, D.C. 20546